HAL
open science

Importance of microtubule and F-actin architecture for proper chromosome alignment in mouse oocyte

Isma Bennabi

To cite this version:

Isma Bennabi. Importance of microtubule and F-actin architecture for proper chromosome alignment in mouse oocyte. Cellular Biology. Université Paris sciences et lettres, 2018. English. NNT : 2018PSLET013 . tel-02943886

HAL Id: tel-02943886

https://theses.hal.science/tel-02943886v1

Submitted on 21 Sep 2020

HAL is a multi-disciplinary open access archive for the deposit and dissemination of scientific research documents, whether they are published or not. The documents may come from teaching and research institutions in France or abroad, or from public or private research centers.

L'archive ouverte pluridisciplinaire **HAL**, est destinée au dépôt et à la diffusion de documents scientifiques de niveau recherche, publiés ou non, émanant des établissements d'enseignement et de recherche français ou étrangers, des laboratoires publics ou privés.

THÈSE DE DOCTORAT

de l'Université de recherche Paris Sciences et Lettres
PSL Research University

Préparée au CIRB, Collège de France
Laboratoire Terret & Verlhac

Importance of microtubule and F-actin architecture for proper chromosome alignment in mouse oocytes

Ecole doctorale Complexité du Vivant (ED515)

Spécialité Biologie Cellulaire

COMPOSITION DU JURY :

Mme. Sophie Louvet-Vallée
Présidente

Mme. Marie Delattre
Rapporteur

M. Péter Lénárt
Rapporteur

M. Benjamin Lacroix
Examinateur

M. Franck Perez
Examinateur

Mme. Marie-Emilie Terret
Examinateur

Mme. Marie-Hélène Verlhac
Membre invité

Soutenue par Isma Bennabi
le 20 septembre 2018

Dirigée par Marie-Emilie Terret

PSL RESEARCH UNIVERSITY PARIS · CIRB · COLLÈGE DE FRANCE 1530

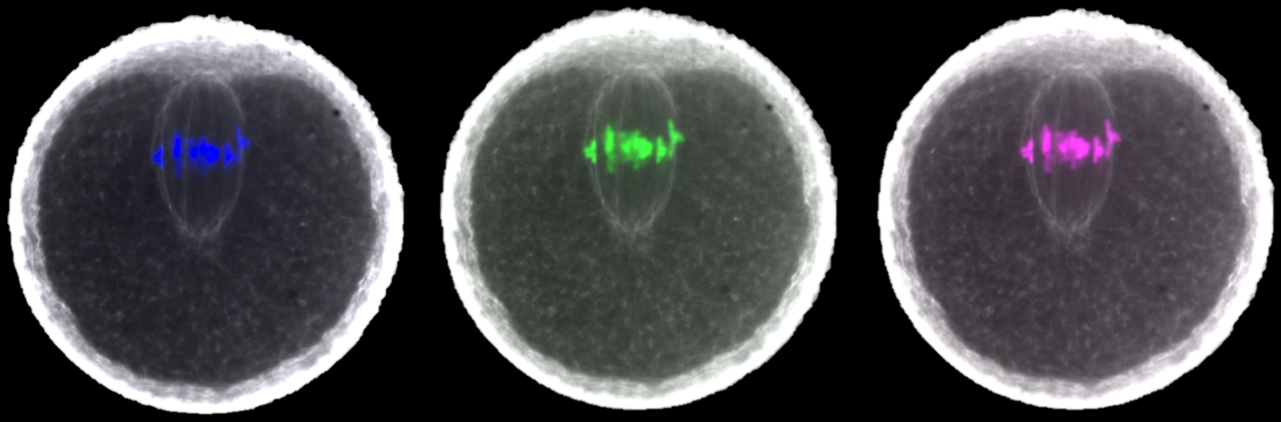

Importance of microtubule and F-actin architecture for proper chromosome alignment in mouse oocytes

Isma Bennabi

PhD thesis, 2018

Supervised by Marie-Emilie Terret

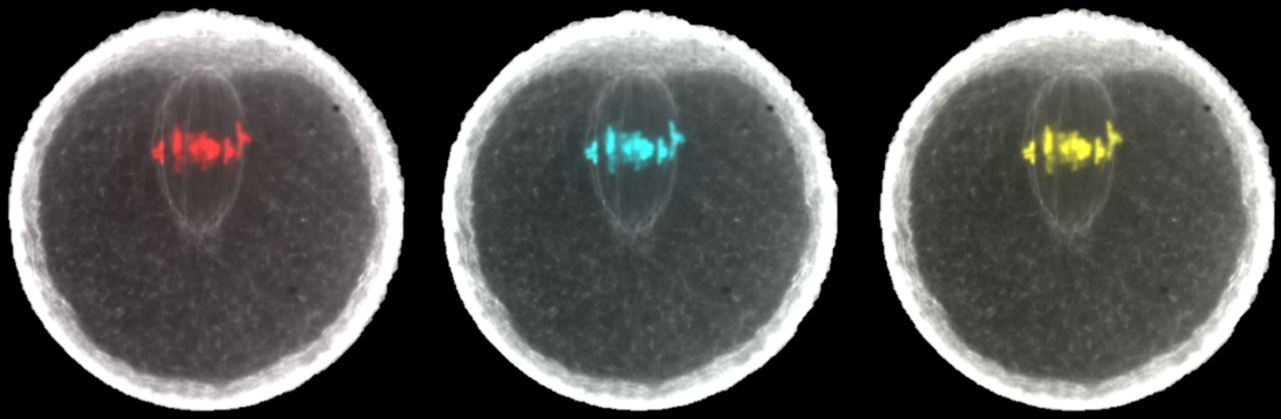

Abbreviations list

+ TIP: plus-end tracking protein

ADP: Adenosine diphosphate

AFM: Atomic Force Microscopy

Arp2/3: Actin related protein 2/3

ATP: Adenosine triphosphate

C.elegans: *Caenorhabditis elegans*

CDK1: Cyclin Dependent Kinase 1

CPC: Chromosomal Passenger Complex

dis1/TOG: Defect in sister chromatid disjoining 1/Tumor Overexpression Gene

D-TACC: *Drosophila* transforming acidic coiled-coil containing

EB1: End-Binding protein 1

Eg5: Egg5

ERK: Extracellular signal-regulated kinases

ERK1/2: Extracellular signal-regulated kinase 1 and 2

ERM: Ezrin, Radixin, Moesin

F-actin: Filamentous actin

FERM domain: Four-point one, Ezrin, Radixin, Moesin domain

FH1-FH2: Formin Homology domain 1 and 2

FMN1/2: Founding Mammalian Formin 1 and 2

G-actin: Globular actin

GDP: Guanosine diphosphate

GTP: Guanosine triphosphate

HSET: Human homologue of the KinC motor family

HURP: Hepatoma UpRegulated Protein

INCENP: Inner Centromeric Protein

K-fibers: kinetochore-microtubule attachments

MAP: Microtubule Associated Protein

MAPK: Mitogen Activated Protein Kinase

MCAK: Mitotic Centromere-Associated Kinesin

MEIKIN: MEIotic KINetochore factor

MEK: MAPK/ERK Kinase

Mos: Moloney murine Sarcoma virus

MPF: M-phase Promoting Factor

Msps: mini spindle

MT: microtubule

MTOC: MicroTubule Organizing Center

Ncd: Non-Claret Disjunctional

NEBD: Nuclear Envelope BreakDown

NPF: Nucleation Promoting Factor

NuMa: Nuclear Mitotic Apparatus

PB: Polar Body

PCM: Pericentriolar material

PLK1: Polo-like kinase 1

PLK4: Polo-like kinase 4

PP2A-B56: Protein Phosphatase 2A-B56

Ran: Ras-like nuclear protein

RCC1: Regulator of Chromosome Condensation 1

SAC: Spindle Assembly Checkpoint

SAF: Spindle Assembly Factor

SCAR: Suppressor of Cyclic AMP Repressor

Spire1/2: Spire 1 and 2

TACC3: Transforming Acidic Coiled Coil 3

TOG: Tumor Overexpressed Gene

TPX2: Targeting Protein for Xklp2

VCA (WCA) domain: (W) WASP-homology-2 (WH2 or W or verprolin-homology) domain, (C) Central (cofilin-homology or connector) domain, (A) Acidic domain

WASP: Wiskott-Aldrich Syndrome Protein

WAVE: WASP-family Verprolin-homologous protein

XMAP215: *Xenopus* Microtubule Associated Protein 215kDa

PROLOGUE 5

INTRODUCTION 6

I. CELL DIVISION AND MEIOTIC DIVISIONS 6

1. THE CELL CYCLE 6

2. MITOSIS 7

3. FEMALE MEIOSIS 7

3.1. Prophase I arrest 8

3.2. Overview of meiosis I and II in mouse oocytes 8

3.3. Centriole loss 9

3.4. Female meiosis is prone to chromosome segregation errors 10

II. SPINDLE ASSEMBLY AND CHROMOSOME SEGREGATION IN OOCYTES 11

1. THE MICROTUBULE CYTOSKELETON 11

1.1. Microtubule structure and dynamics 11

2. MICROTUBULE ASSOCIATED PROTEINS 12

2.1. MAPs 12

2.1.1. Stabilizing MAPs 12

2.1.2. Destabilizing MAPs 13

2.2. Non motor crosslinkers 13

2.3. Microtubule motors 13

2.3.1. Kinesin-5 14

2.3.2. Kinesin-14 14

3. MICROTUBULE NUCLEATION 15

3.1. Centrosome-dependent microtubule nucleation in mitosis 15

3.2. Centrosome-independent microtubule nucleation 15

3.2.1. The RanGTP pathway 15

3.2.2 The Augmin pathway 16

3.2.3. The CPC pathway 16

3.2.4. aMTOCs in mouse oocytes 17

4. SPINDLE BIPOLARIZATION 18

4.1. Centrosome-dependent spindle bipolarization in mitosis 18

4.2. Spindle bipolarization in the absence of centrosomes 18

4.2.1. Formation of a central microtubule array 18
a. Plus-end directed motors kinesin-5 and kinesin-6 19
b. aMTOCs organization in mouse oocytes 19
4.2.2. Microtubule nucleation 20
5. SPINDLE POLE FORMATION 20
5.1. Spindle pole formation by microtubule motors and MAPs 20
5.2. Spindle formation by aMTOCs 21
6. MODELING MEIOTIC SPINDLE ASSEMBLY 22
6.1. The slide and cluster model 22
6.2. Models integrating microtubule dynamics 23
7. CHROMOSOME ALIGNMENT 24
7.1. Chromosome alignment in oocytes 24
7.2. Kinetochore-microtubule attachments in mouse oocytes 25
7.3. Kinetochore-microtubule attachments in *Drosophila* oocytes 26
8. CHROMOSOME SEGREGATION 26
9. CONCLUSION ON MEIOTIC SPINDLE ASSEMBLY AND OPEN QUESTIONS 27
III. SPINDLE POSITIONING AND CHROMOSOME SEGREGATION IN OOCYTES 28
1. THE ACTIN CYTOSKELETON 28
1.1. Actin structure 28
1.2. Actin polymerization and dynamic 28
2. ACTIN ASSOCIATED PROTEINS 29
2.1. Actin nucleators 29
2.1.1. The Arp2/3 complex 29
a. A branching nucleator 29
b. Arp2/3 activation by NPFs 30
2.1.2. Formin 2 30
2.1.3. Spire 31
2.2. Actin motors 31
2.2.1. The conventional myosin II 32
2.2.2. The unconventional Myosin Vb and Myosin X 32
2.3. Actin regulators and organizing proteins 33
2.3.1. ERM proteins 33

2.3.2. The Mos/MAPK pathway 33
3. ACTIN IN MITOTIC CELL DIVISION 34
3.1. Mitotic spindle positioning 34
3.1.1. Cortical actin 34
a. Cortical tension 34
b. Polarized subcortical actin 35
c. Myosin X 36
3.1.2. Cytoplasmic actin 36
4. ACTIN IN FEMALE MEIOTIC DIVISION 37
4.1. Nucleus positioning 37
4.1.1 The F-actin meshwork in mouse oocytes 37
4.1.2 Mechanisms of actin-dependent nucleus positioning 38
4.2. Spindle positioning 38
4.2.1. Cytoplasmic actin 39
a. The actin cage 39
b. Myosin II 39
c. Myosin Vb 40
4.2.2. Cortical actin 40
a. Cortical actin thickening 40
b. Cortical myosin II 42
c. Measuring cortical tension in oocytes 42
d. Cortical tension 43
e. Cortical tension as a readout of oocyte quality 45
5. ACTIN IN SPINDLE ASSEMBLY AND CHROMOSOME ALIGNMENT 46
5.1. Mitotic cells 46
5.1.1. Cortical actin and cortical tension 46
5.1.2. Cytoplasmic actin 46
5.2. Actin and chromosomes in oocytes 47
5.2.1. The case of starfish oocytes 47
5.2.2. The case of mouse oocytes 48
6. FORMATION OF THE ACTIN CAP AND POLARIZATION OF THE OOCYTE 48
7. CONCLUSION ON MEIOTIC SPINDLE POSITIONING AND OPEN QUESTIONS 49

RESULTS 50

I. SHIFTING MEIOTIC TO MITOTIC SPINDLE ASSEMBLY IN OOCYTES DISRUPTS CHROMOSOME ALIGNMENT 51

II. ABERRANT LOW CORTICAL TENSION GENERATES CHROMOSOME MISALIGNMENT IN OOCYTE 72

DISCUSSION 118

I. PARTICULARITIES OF THE "INSIDE-OUT" SPINDLE ASSEMBLY IN OOCYTES 118

1. Are the effects of kinesin-14 on spindle assembly kinesin-5-dependent? 118

2. Is the microtubule ball stage important to prevent chromosome defects in oocytes? 119

II. SPINDLE POSITIONING BY F-ACTIN AND CONSEQUENCES ON CHROMOSOME BEHAVIOR 121

1. Forces generated by the actin networks in meiosis I oocytes 121

a. Forces within the cytoplasmic meshwork? 121

b. Influence of the cytoplasmic network architecture for force generation? 122

2. A link between F-actin and chromosomes/microtubules in chromosome segregation? 123

3. Myosin II activity and impact on chromosome behavior in meiosis I 124

a. Regulation of cortical myosin II activity in mouse oocytes? 125

b. Influence of myosin II on chromosome alignment? 125

4. Cortical tension: a new criterion of oocyte and embryo quality 126

INTRODUCTION

Prologue

Sexual reproduction relies on the fusion of two haploid gametes: the oocyte and sperm, leading to the formation of an embryo. These cells are created through meiosis, a specialized type of cell division that reduces the chromosome number by half and brings genetic diversity. Meiosis is opposed to mitosis that allows the renewal of somatic cells. Although essential for the propagation of species, female meiosis is highly prone to chromosome segregation errors. Indeed, at least 10 % of human pregnancies produce aneuploid embryos, the errors leading to aneuploidy almost always occurring in the oocyte (Nagaoka et al., 2012). Understanding the origin of these errors is therefore a major issue.

Chromosome segregation errors are attributable in part to the lack of centrioles in oocytes. In eukaryotes, the structure orchestrating chromosome alignment and segregation is the microtubule spindle. Whereas mitotic spindles assemble from two centrosomes that are major microtubule organizing centers (MTOCs) containing centrioles, meiotic spindles in oocytes lack centrioles. Thus, oocytes use alternative ways to assemble and position their spindle. In mouse oocytes, the spindle is not assembled by centrosomes but spindle microtubules are nucleated from multiple acentriolar MTOCs. Moreover, in mitosis centrosomes nucleate astral microtubules. Oocytes lack astral microtubules and thus meiotic spindle positioning depends only on F-actin. In particular, it relies on the nucleation of a cortical actin thickening leading to a decrease in cortical tension.

During my PhD I studied spindle assembly and spindle positioning in oocytes, two aspects of oocyte biology that could contribute to the high rate of aneuploidy observed in female meiosis. In the introduction, I will first introduce meiotic divisions. Next, I will discuss the atypical mechanisms of spindle assembly in oocytes and the consequences on chromosome alignment/segregation. At last, I will discuss the influence of spindle positioning by F-actin on chromosome alignment/segregation.

Introduction

I. Cell division and meiotic divisions

Cell division is the process by which a mother cell divides into two daughter cells. The challenge of cell division is to equally separate chromosomes between daughter cells. Indeed, errors during cell division can leads to aneuploidy. In eukaryotes, two types of cell division exist: mitosis and meiosis. Mitosis creates two daughter cells containing the same amount of DNA by the equal repartition of the genetic material. Whereas mitosis concerns somatic cells, meiosis allows the formation of haploid gametes. Meiosis consists of two successive divisions (meiosis I and II), without intervening DNA replication, which reduce the genetic content by half. In meiosis I, homologous chromosomes separate instead of sister chromatids in mitosis. However, meiosis II separates sister chromatids similarly to mitosis (Figure 1).
Many of the mechanisms at play during mitosis are conserved during meiotic divisions. However, some mechanisms and molecular players are strictly meiosis specific. Comparing the two types of cell division is crucial to understand how meiotic cells divide. Thus, mitosis and meiosis are often compared in the following chapters.

1. The cell cycle

Cell division is part of a larger cell cycle. In particular, it includes two alternating phases: interphase and M-phase (Mitotic or Meiotic division phase).
Interphase comprises three phases: G1, S and G2. The G1 phase corresponds to a growth phase during which cells synthesize RNA and proteins. Then, DNA is replicated during the S phase of the cell cycle. During the G2 phase, the replicated DNA is checked for possible replication errors and repaired. The genome is then separated in half during the M phase of the cell cycle, which is the phase where the cell physically separates into two daughter cells.
The entry in M-phase is regulated by the MPF (M-phase promoting factor). It is a two-subunit complex composed of CDK1 (Cyclin Dependent Kinase 1) and Cyclin B. The

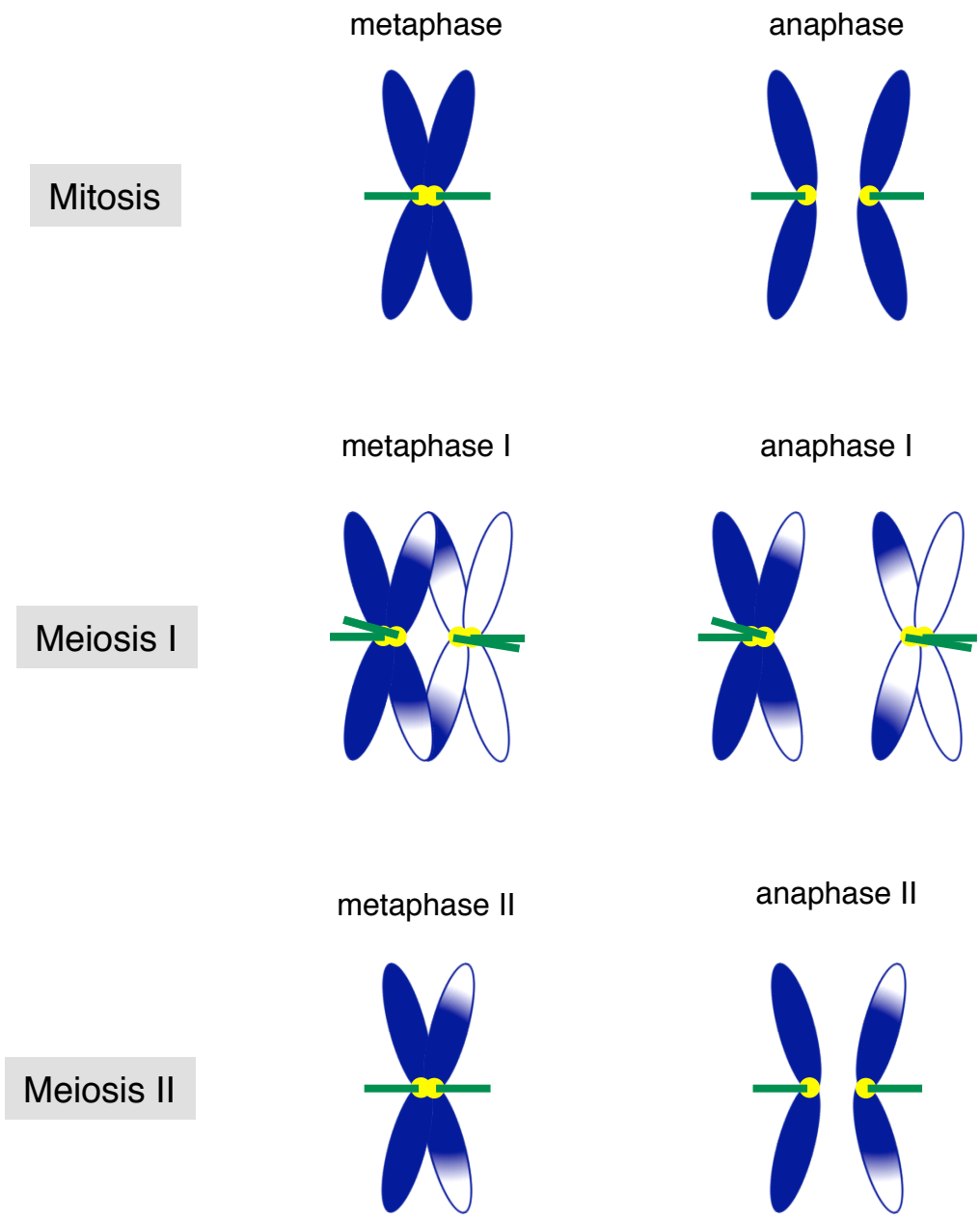

Figure 1: Chromosome segregation in mitosis versus meiosis

Chromosomes are in blue or white, microtubules in green and kinetochores in yellow.

MPF promotes the entry in M-phase (mitosis or meiosis) in all eukaryotic cells (for review see Brunet and Maro, 2005).

2. Mitosis

Mitosis comprises four phases: prophase, metaphase, anaphase, telophase (Figure 2). In prophase, the replicated DNA condenses into chromosomes that are each composed of two chromatids. Upon mitosis entry, the nuclear envelope disrupts in an event that is called NEBD (nuclear envelope breakdown).

In eukaryotes, the structure orchestrating chromosome alignment and segregation during cell division is the microtubule spindle. In mitotic cells, the microtubules that compose the spindle are mostly nucleated from centrosomes acting as major microtubule organizing centers (MTOCs). Canonical centrosomes are composed of a pair of centrioles surrounded by pericentriolar material (PCM) that possesses the microtubule nucleation activity. The microtubule slow growing end (- end) is tethered to the PCM of the centrosome while the fast growing (+ end) is directed towards chromosomes. The centrosomes are replicated during the S phase of the cell cycle.

Centrosomes nucleate kinetochore microtubules (k-fibers) that attach chromosomes to the spindle poles by their kinetochores. Kinetochores are multiprotein complexes localized at the centromeric region of chromosomes in most cells. Chromosomes attached by their kinetochores progressively align on the metaphase plate during prometaphase. Once all chromosomes are aligned on the metaphase plate and under tension, anaphase can occur and chromosomes separate. Cytokinesis physically separates the cytoplasms into two so that two new daughter cells form. Eventually, after completing mitosis, cells enter interphase of the next cell cycle.

3. Female meiosis

Sexual reproduction relies on the fusion of paternal and maternal haploid gametes, respectively the sperm and the extremely large oocyte, forming a new diploid organism. Meiotic divisions (meiosis I and II) contribute solely to the formation of haploid gametes.

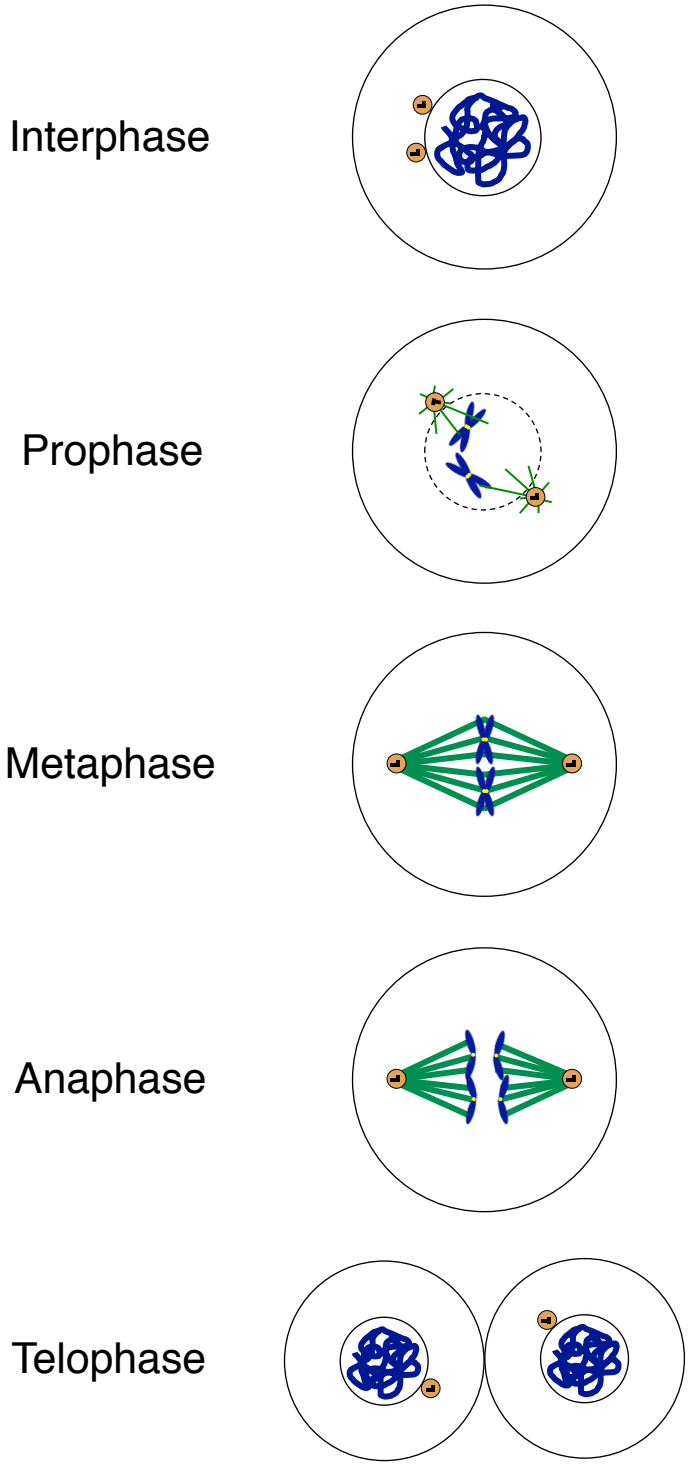

Figure 2: Mitosis
DNA is in dark blue, microtubules in green, kinetochores in yellow, pericentriolar material in brown and centrioles in black.

In mammals, the process of oocyte formation starts during fetal life. Oocytes enter meiosis before birth and then rapidly block in prophase of the first meiotic division (prophase I).

3.1. Prophase I arrest

Oocytes are blocked in prophase I for many years, starting in the embryo and finishing when meiosis resumes in the adult. The events of DNA recombination between homologous chromosomes occur in prophase I. At puberty, oocytes are periodically recruited for growth while still arrested in prophase I (Eppig and O'Brien, 1996). During this so-called "growth phase", oocytes accumulate a huge amount of protein and RNA stores. After the growth phase, oocytes have grown enormous, from 20 μm to 80 μm in diameter, and are competent to resume meiosis. MPF activity controls prophase I arrest and subsequent meiosis resumption (for review see Brunet and Maro, 2005).

3.2. Overview of meiosis I and II in mouse oocytes

The two meiotic divisions (meiosis I and II) are very asymmetric in size, leading to the formation of a large oocyte and two small polar bodies (PB) that will degenerate (Figure 3). Half of the genomic content is extruded in the small polar bodies while the huge oocyte retains the other half of the genomic information as well as maternal stores accumulated during the growth phase.

After oocytes resume meiosis, the rupture of the nuclear envelope (NEBD) is the first noticeable event (Figure 3). Then, the first meiotic spindle assembles and spindle bipolarization occurs 3-4 hours after NEBD. The meiosis I spindle forms at the center of the oocyte, where the nucleus was just before meiosis resumption. Then, the spindle progressively migrates from the center to the cell cortex, leading to a division very asymmetric in size (Verlhac et al., 2000). Anaphase I and the extrusion of the first polar body occur around 8 hours after NEBD. Then the meiosis II spindle forms parallel to the cortex and oocytes undergo a second arrest in metaphase II. Oocytes

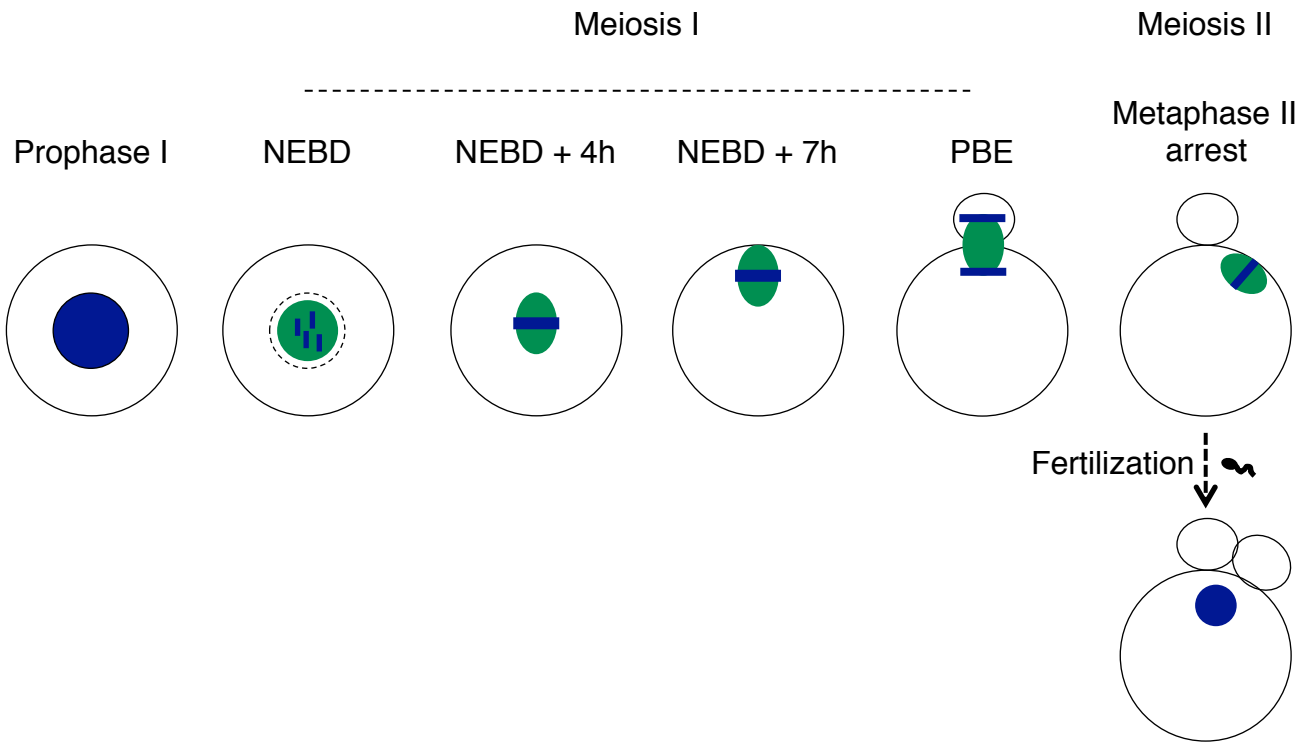

Figure 3: Mouse meiotic divisions

DNA is in dark blue, microtubules in green. NEBD stands for nuclear envelope breakdown. PBE stands for polar body extrusion.

are released from this second block only by fertilization, leading to anaphase II followed by the extrusion of the second polar body.

3.3. Centriole loss

Surprisingly, whereas the majority of male gametes retain centrosomes containing centrioles, centrioles are eliminated before meiotic divisions in oocytes of most metazoan species (Szollosi et al., 1972; Manandhar et al., 2005).

A puzzling observation is that whereas centrioles and PCM are lost in oocytes of most metazoan species, mouse oocytes still retain multiple discrete PCM or aMTOCs (acentriolar MTOCs) that can participate in spindle formation (Maro et al., 1985). In contrast to most species, sperm centrioles degenerate in rodents during spermatogenesis and thus are not contributed by the sperm at fertilization (Woolley and Fawcett, 1973; Manandhar et al., 1998). Instead, centrioles progressively assemble de novo in early embryos (Gueth-Hallonet et al., 1993). How centrioles are generated in rodent early embryos is not known. Nevertheless these discrete PCM could serve as templates for later generation of centriole-containing centrosomes in the embryo.

Still, very little is known about why and how centrioles are eliminated in oocytes of most species. One hypothesis is that centriole elimination prevents multipolar spindle formation in the first embryonic division after introduction of the sperm centriole(s) upon fertilization. However, in rodents the sperm does not contribute with a centriole. Another hypothesis would be that it prevents parthenogenesis (egg activation in the absence of fertilization) since injection of centrosomes in *Xenopus* eggs induces activation without fertilization (Tournier et al., 1989). Recent studies have started to unravel how centrioles are removed in oocytes. In starfish, meiotic divisions take place in the presence of centriole-containing centrosomes. Mother centrioles are eliminated by extrusion into polar bodies and the remaining daughter centriole is degraded in the cytoplasm (Borrego-Pinto et al., 2016). However, even if centrosomes are retained, they do not nucleate microtubules able to capture chromosomes in the huge volume of the cell. In these oocytes, centriole-containing centrosomes only participate in chromosome capture once chromosomes are close

enough to be reached by microtubules. Chromosome gathering is however achieved by a contractile actin mesh that delivers chromosomes to the spindle (Lénàrt et al., 2005; Mori et al., 2011; Bun et al., 2018 and see chapter III.5.2.1.). In the fruit fly, centriole elimination is a progressive process that ends up just prior meiotic spindle assembly. Centriole maintenance by perturbing this process results in spindle assembly defects in oocytes and early embryos, and thus to female sterility (Pimenta-Marques et al., 2016).

The absence of canonical centrosomes constitutes one of the many factors that could contribute to the innate susceptibility of oocyte to produce errors in chromosome segregation (see chapter 3.3. below). However, despite its contribution to oocyte aneuploidy, centriole elimination must likely be crucial for gamete fitness of most metazoan species.

3.4. Female meiosis is prone to chromosome segregation errors

As mentioned above, it has been known for over a decade that female meiosis is highly prone to chromosome segregation errors, especially in humans (Hassold and Hunt, 2001; Hassold et al., 2007; Nagaoka et al., 2012). At least 10 % of human pregnancies produce aneuploid embryos (presenting a gain or loss of entire chromosomes), inducing spontaneous abortions and congenital defects such as trisomies whose incidence increases with maternal age (Nagaoka et al., 2012). These defects are attributable in part to the atypical modes of spindle assembly and spindle positioning imposed by the lack of centrioles in oocytes and a weaker spindle assembly checkpoint (SAC). The SAC will not be addressed here, for review see (Etemad and Kops. 2016; Touati and Wassmann, 2016). In the next chapters, the mechanisms of spindle assembly and spindle positioning and the consequences on chromosome alignment/segregation are reviewed in details.

II. Spindle assembly and chromosome segregation in oocytes

1. The microtubule cytoskeleton

In eukaryotes, the structure orchestrating chromosome alignment and segregation during cell division is the spindle. The spindle is a highly organized and dense structure composed of microtubules and microtubule associated proteins (MAPs). First, we will discuss the structure and dynamics of microtubules, then the assembly of a microtubule spindle and the consequences on chromosome alignment/segregation.

1.1. Microtubule structure and dynamics

Protofilaments are linear polymers made of heterodimers of two isoforms of tubulin: α- and β-tubulin (Figure 4). The parallel association of protofilaments forms microtubules lattices (Figure 4). Thirteen protofilaments associate in a hollow cylinder of 25 nm in diameter to form one microtubule (Desai and Mitchison, 1997). Microtubules are polarized with one end presenting β-tubulin and the other presenting α-tubulin. They are respectively called the plus- and minus-ends. Polymerization is fast at the growing plus-end and slow at the minus-end (Figure 4 and 5).

Microtubules are extremely dynamic, switching rapidly between growing and shrinking states. This process is based on GTP hydrolysis by the tubulin subunits. Both α- and β-tubulin monomers can bind GTP. GTP binding to the α-tubulin monomer is irreversible and can be considered as part of the α-tubulin structure. On the contrary, GTP binding to a β-tubulin monomer is reversible. Indeed, during microtubule polymerization, a GTP-bound tubulin subunit is added to the plus-end of a growing microtubule. Then GTP hydrolysis occurs, which changes the conformation of tubulin subunits, the protofilaments dissociate and the microtubule shrinks (Figure 5). This combination of polymerization, depolymerization and transitions between the two states is known as “dynamic instability” (Mitchison and Kirschner, 1984). The

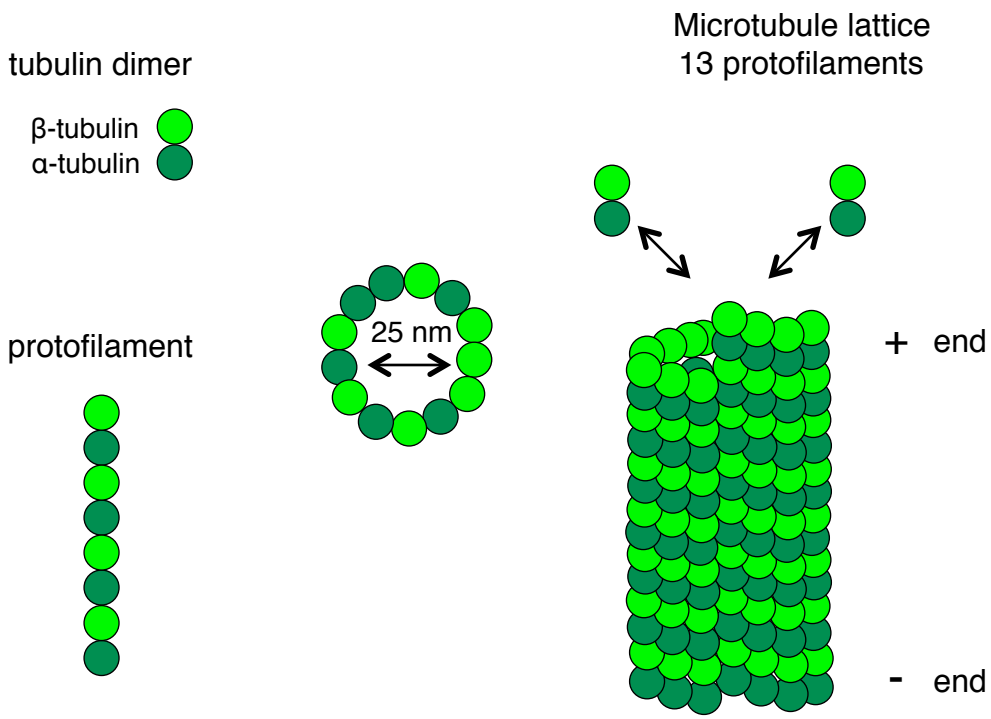

Figure 4: Microtubule structure

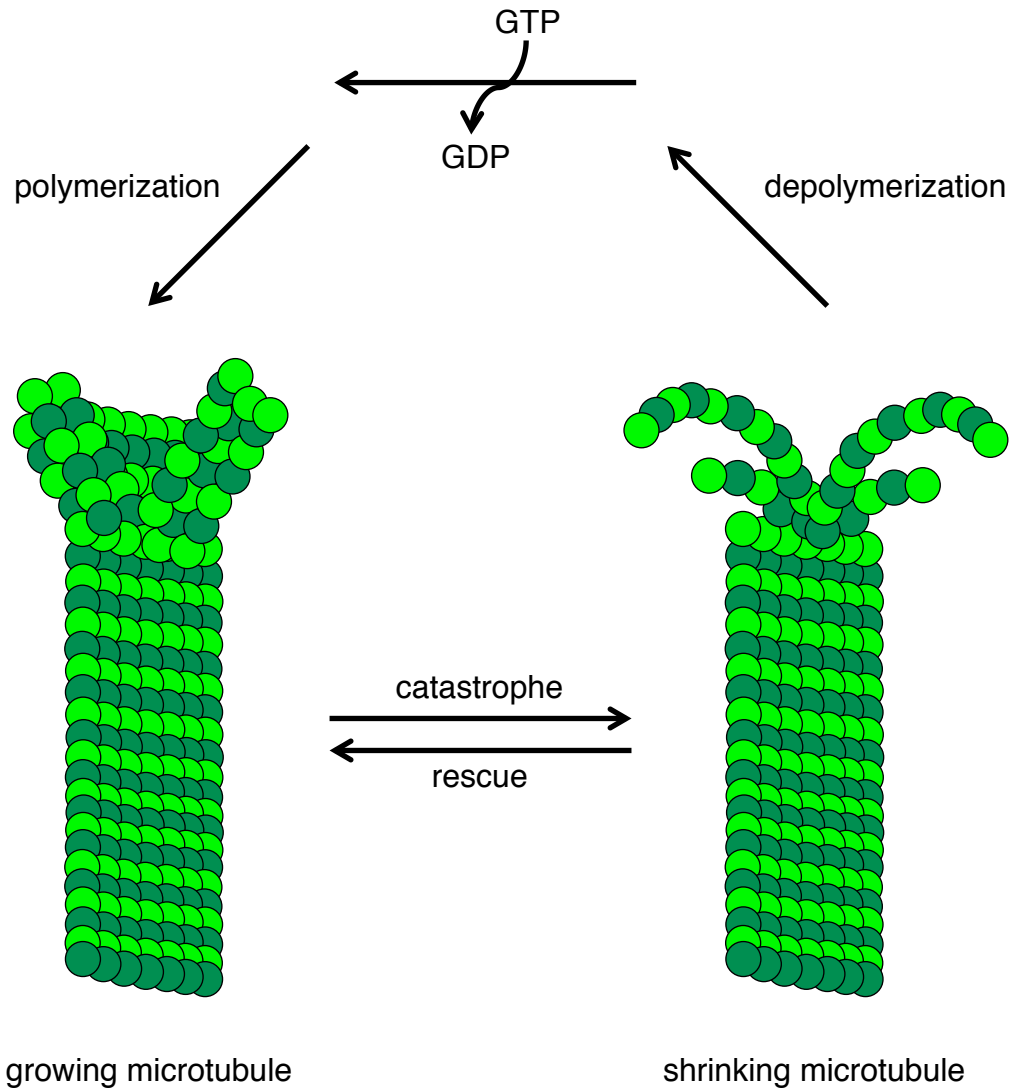

Figure 5: Microtubule dynamics

transition from growth to shrinkage is known as catastrophe, the transition from shrinkage to growth is known as rescue.
The regulation of microtubule formation also depends on the transcription of different tubulin isoforms, tubulin post-translational modifications and the interaction of microtubules with diverse associated proteins (MAPs), on which I will focus.

2. Microtubule associated proteins

2.1. MAPs

In vivo, numerous proteins interact with microtubules. These proteins are called Microtubule Associated Proteins (MAPs). Below, we are only reviewing in detail the proteins that will be addressed in the following chapters.

2.1.1. Stabilizing MAPs

The +TIPs are a large family of microtubule plus-ends proteins. The majority of +TIPs are stabilizing MAPs, influencing microtubule polymerization or promoting microtubule rescue over catastrophe. Their localization at the growing plus-end of microtubules is called “tracking”.
The End-binding proteins (EB1, 2 and 3) belong to the +TIPs family (for review see Lansbergen and Akhmanova, 2006). The EB-family member EB3 tagged with GFP can be expressed in mouse oocytes to detect microtubules and microtubule growth (see results).
The highly conserved Dis1/TOG-family also belongs to the +TIPs proteins. Its conserved members are Msps in *Drosophila* (see chapter II.5.1.) and XMAP215 in *Xenopus*. It is thought to be a tubulin polymerase, as it highly increases microtubule polymerization.

2.1.2. Destabilizing MAPs

Several kinesin motors have been described for their microtubule destabilizing activity. Among them, the kinesin-13 MCAK is the best characterized for its high microtubule depolymerization activity (see chapter II.6.). MCAK was shown to regulate mitotic spindle length (Walczak et al., 1996; Goshima and Vale, 2003).
Microtubule severing enzymes such as Katanin are another example of destabilizing MAPs. Katanin is able to transform long microtubules into shorter ones. In *C.elegans* oocytes, Katanin increases the density of small microtubules by severing pre-existing ones and could thus contribute to increase microtubule number by amplifying microtubule nucleation (Srayko et al., 2006).

2.2. Non motor crosslinkers

Microtubule crosslinkers bridge adjacent microtubules and can organize microtubules into bundles with specific polarity patterns.
In vitro, HURP is able to stimulate microtubule bundling (Koffa et al., 2006). During mitosis, HURP stabilizes kinetochore-microtubule attachments (Silljé et al., 2006). In mouse oocytes, HURP is recruited to the central spindle by kinesin-5 where it stabilizes the microtubule central array (see II.4.2.1.).
NuMA crosslinks microtubule minus-ends at spindle poles composed of centrosomes. Remarkably, the function of NuMA in tethering microtubule minus-ends is conserved in acentriolar spindles (see II.5.1.). Indeed, NuMA accumulates at spindle poles in rabbit, human and mouse oocytes (Yan et al., 2006; Alvarez Sedó et al., 2011; Kolano et al., 2012).

2.3. Microtubule motors

Microtubule motors are MAPs that move along microtubules. They create force and movement by using energy from ATP hydrolysis. Motor proteins can transport cargos within the cell and sort and orient microtubules relative to each other. They can be divided in two main groups: 1) minus-end directed motors that walk towards

microtubule minus-ends such as Dynein and kinesin-14, 2) plus-end directed motors that walk towards microtubule plus-ends such as most kinesins.

The minus-end directed motor Dynein works in a complex with Dynactin and NuMA to cross-link parallel microtubules in the same orientation (Kardon and Vale, 2009). The Dynein complex is essential to tether together microtubule minus-ends at mitotic and meiotic spindle poles (see II.5.1.).

The kinesin class of motors contains 14 family of mostly plus-end directed motors with the exception of the minus-end directed kinesin-14 (Lawrence et al., 2004). Several kinesins are involved in spindle assembly. Below, we are only addressing in details the kinesin-5 and kinesin-14. Their function in spindle assembly will be developed in the following chapters.

2.3.1. Kinesin-5

The kinesin-5 is a plus-end-directed motor, also called Eg5 in vertebrates. Kinesin-5 is a dimer and complexes to form a homotetramer with two motor domains at each end (Kashina et al., 1996). Kinesin-5 crosslinks antiparallel microtubules and slides them apart (Figure 6; Kapitein et al., 2005). A pair of parallel microtubules presents their minus- and plus-ends in the same orientation, whereas antiparallel microtubules present their minus- and plus-ends in opposite orientations. Kinesin-5 is essential for spindle bipolarity establishment during mitosis and meiosis (see II.4.1 and II.4.2.1).

2.3.2. Kinesin-14

The kinesin-14 is a minus-end-directed microtubule motor. Its homologues are Ncd in *Drosophila*, XCTK2 in *Xenopus* and HSET in human. Kinesin-14 comprises a C-terminal motor domain and a N-terminal tail domain capable of binding microtubules (Cai et al., 2009). Kinesin-14 is important for regulating spindle assembly, spindle length, and pole organization (Walczak et al., 1997; Mountain et al., 1999; Sharp et al., 1999; Hepperla et al., 2014; Syrovatkina et al., 2015; Molodtsov et al., 2016; Braun et al., 2017). During mitosis, HSET can slide anti-parallel microtubules apart and sort them into parallel bundles (Fink et al., 2009; Braun et al., 2009; Hentrich and

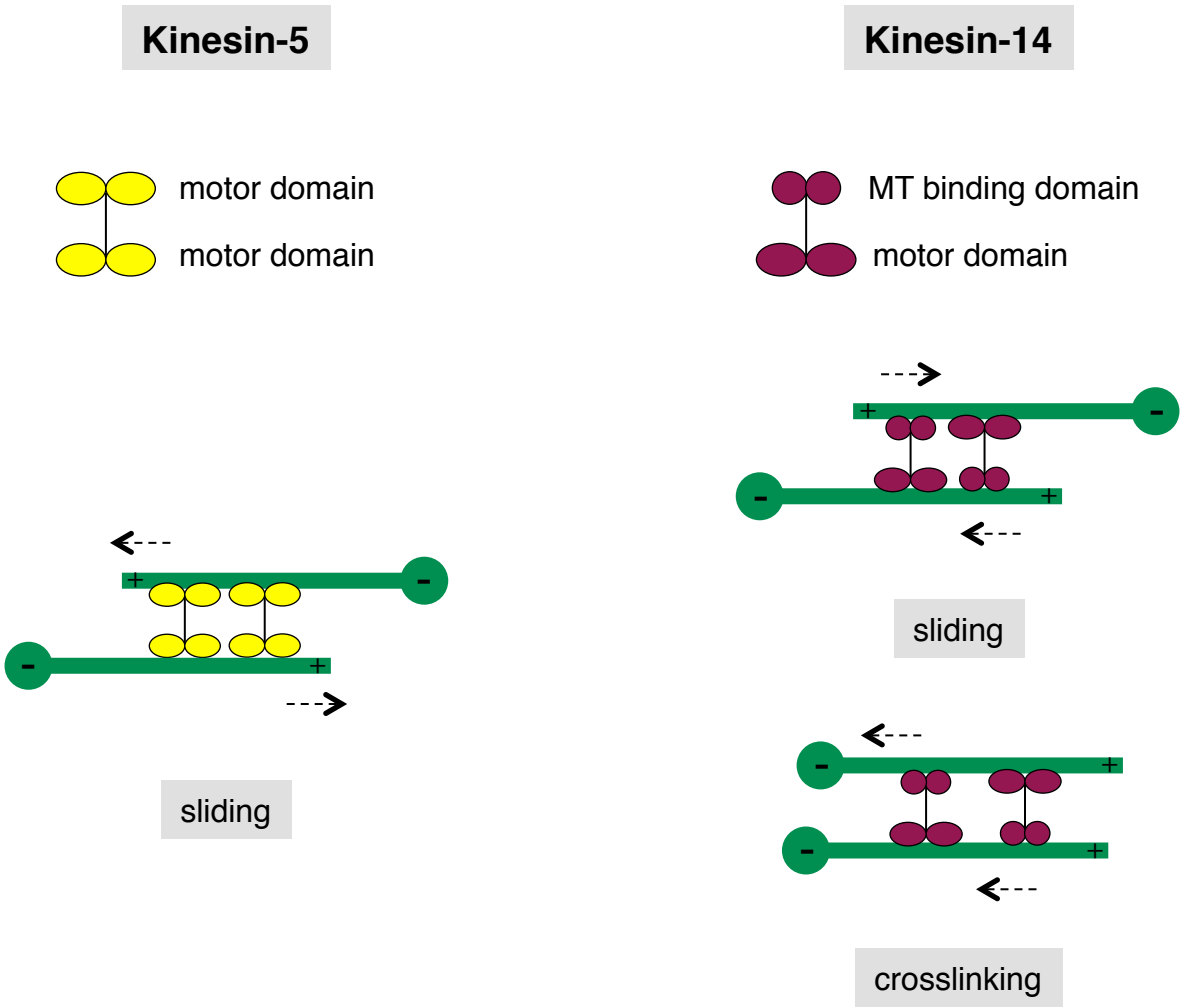

Figure 6: Microtubule motors
Microtubules are in green, green circles represent minus ends.

Surrey, 2010). In contrast, when the orientation of two opposing microtubules is parallel, HSET cross-links them and transports them to the poles (Figure 6).

3. Microtubule nucleation

3.1. Centrosome-dependent microtubule nucleation in mitosis

In mitosis, the spindle is formed by microtubules that are nucleated from canonical centrosomes (Figure 7B). Although centrosome-mediated spindle formation is dominant in most mitotic cells, mitosis can still take place in the absence of centrosomes, showing that other centrosome-independent pathways can participate in spindle formation (Khodjakov et al., 2000; Basto et al., 2006; Azimzadeh et al., 2012; Bazzi and Anderson, 2014). These centrosome-independent pathways become dominant in cells lacking centrosomes such as oocytes.

3.2. Centrosome-independent microtubule nucleation

Since most oocytes lack canonical centrosomes, they use alternative pathways to nucleate microtubules (Figure 7).

3.2.1. The RanGTP pathway

The small Ran GTPase is present in a gradient around chromosomes both in mitotic and meiotic cells (Figure 7A). The RanGTP active form is produced by the Ran guanosine exchange factor RCC1 that is localized on chromosomes (Kalab et al., 1999). This gradient of active Ran locally activates Spindle Assembly Factors (SAFs) that participate in microtubule nucleation, interaction and stabilization as well as motor activities (for review see Meunier and Vernos, 2016). These Spindle Assembly factors interact with importins via their nuclear localization sequences (NLS) and are kept inhibited. RanGTP promotes the dissociation of SAFs from their inhibitory binding to importins, causing their local activation and release (Gruss et al., 2001; Nachury et al., 2001). In human oocytes, RanGTP inhibition seems to delay

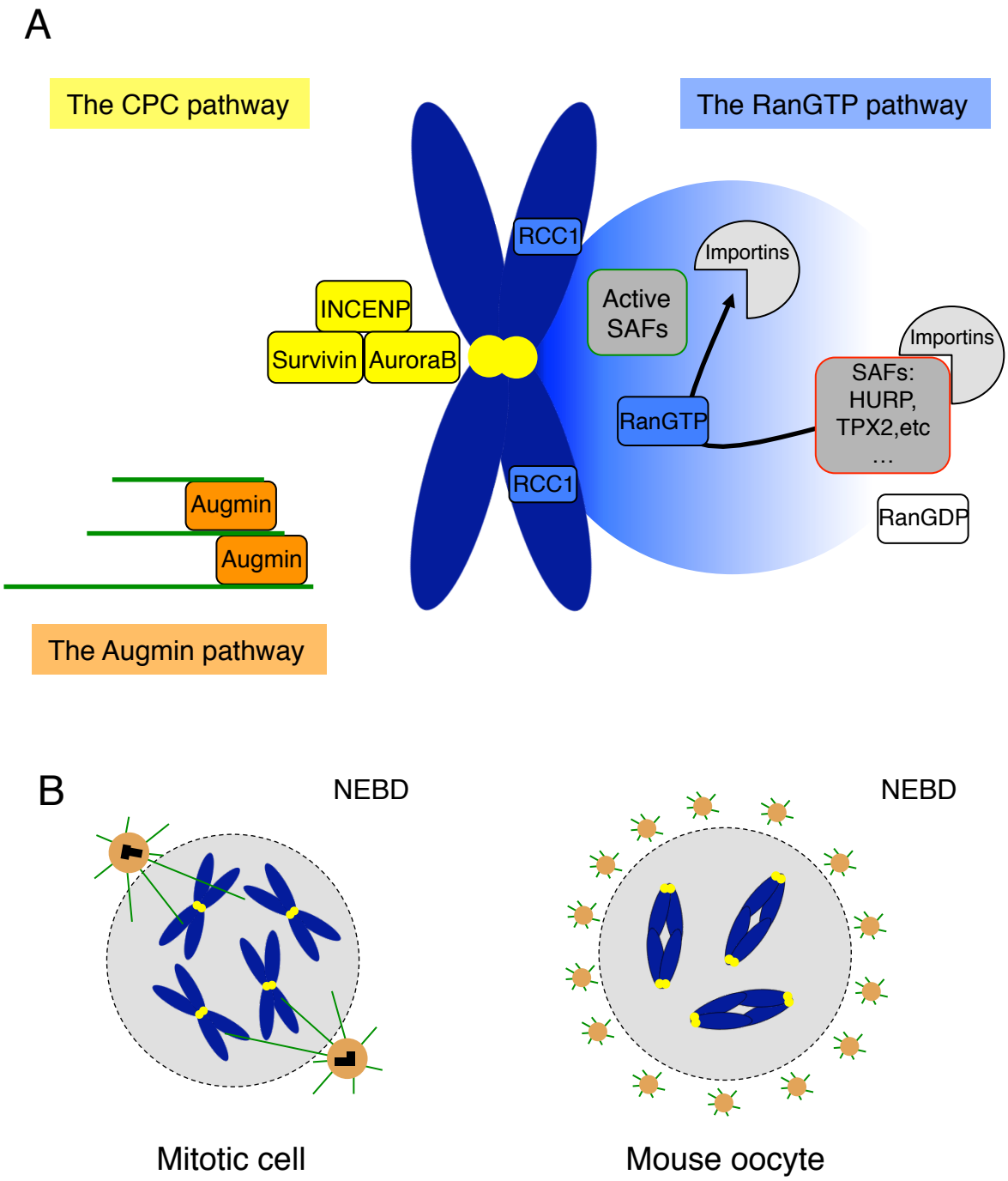

Figure 7: Pathways replacing centrosomes for microtubule nucleation in oocytes

NEBD stands for nuclear envelope breakdown. DNA is in dark blue, microtubules in green, kinetochores in yellow, pericentriolar material in brown and centrioles in black.

microtubule nucleation and impair spindle formation (Holubcová et al., 2015). Differently, inhibition of RanGTP delays but does not impair spindle assembly in meiosis I in mouse and *Drosophila* oocytes, whereas it does in meiosis II (Dumont et al., 2007; Cesario and McKim, 2011). This suggests that although the RanGTP pathway is involved in microtubule nucleation for spindle assembly in the absence of centrosomes, other pathways are important.

3.2.2 The Augmin pathway

Among these, the Augmin pathway generates new microtubules along pre-existing microtubules (Figure 7A and for review see Sánchez-Huertas and Lüders, 2015). The Augmin complex is composed of eight proteins (named HAUS 1 to 8) able to recruit γ-tubulin to the sides of microtubules within the spindle (Goshima et al., 2008; Lawo et al., 2009; Uehara et al., 2009). In *Xenopus* egg extracts, Augmin depletion results in reduced microtubule nucleation and multipolar spindle formation suggesting a role of the Augmin complex in spindle bipolarization (Petry et al., 2011). In fruit flies, Augmin compensates for the lack of centrosomes by promoting microtubules nucleation at meiotic spindle poles (Colombié et al., 2013).

3.2.3. The CPC pathway

Similarly, the Chromosomal Passenger Complex (CPC) pathway is also involved in microtubule stabilization and spindle assembly in *Xenopus* egg extracts and *Drosophila* oocytes (Figure 7A and Sampath et al., 2004; Kelly et al., 2007; Tseng et al., 2010; Radford et al., 2012; Das et al., 2016). The CPC is associated with kinetochores and is composed of the Aurora B/C kinase, the inner centromere protein INCENP, Survivin and Borealin (for review see Dumont and Desai, 2012).
Interestingly, it was recently shown that an Aurora B/14-3-3 dependent process spatially restricts the activity of kinesin-14 Ncd to spindle microtubules in *Drosophila* oocytes (Beaven et al., 2017). 14-3-3 family members bind phosphoproteins and regulate their activity and localization. 14-3-3 prevents Ncd from binding to microtubules. The chromosome associated Aurora B kinase phosophorylates Ncd,

thus releasing Ncd from its inhibitory binding to 14-3-3. Similarly to the RanGTP pathway, this mechanism provides a spatial regulation to the activation of a kinesin crucial for bipolar spindle assembly in the large volume of oocytes. The role of the kinesin-14 Ncd in bipolarity establishment is described below (see part 4.2.)

3.2.4. aMTOCs in mouse oocytes

In addition to these microtubules nucleation pathways, mouse oocytes contain acentriolar MTOCs (aMTOCs) capable of nucleating microtubules (Figure 7B and Maro et al., 1985). At NEBD the nucleation capacity of these aMTOCs is low but it increases throughout meiosis I. Indeed, levels of the RanGTPase effector TPX2 (Wittmann et al., 2000) rise progressively during meiosis I (Brunet et al., 2008), which intensifies the extent of phosphorylation of the aMTOC protein TACC3 and increases microtubule nucleation activity at aMTOCS (Still et al., 1999; Eyers et al., 2003; Tsai et al., 2003; Bayliss et al., 2003; Kinoshita et al., 2005; Brunet et al., 2008). These aMTOCs are perinuclear before meiotic divisions so that they can be readily distributed around the chromatin when NEBD occurs (Luksza et al., 2013). Although the exact composition of these structures is not exhaustively known, they contain classical pericentriolar components (PCM) such as γ-tubulin and pericentrin and are likely bona fide PCM (Gueth-Hallonet et al., 1993; Carabatsos et al., 2000). In mitotic cells, the PCM size is regulated by centrioles such that microtubule nucleation is carefully tuned (Kirkham et al., 2003; Conduit and Raff, 2010; Gopalakrishnan et al., 2012; Woodruff et al., 2015). In mouse oocytes, the size of the PCM seems to scale with the cell volume but the regulatory mechanisms at play are unknown (Luksza et al., 2013). Surprisingly, such acentriolar MTOCs are not detected on the nuclear envelope in prophase I or at later stages in spindle poles from *Xenopus*, C. elegans, *Drosophila* and human oocytes (Gard et al., 1991; Srayko et al., 2006; Matthies et al., 1996; Holubcová et al., 2015).

Although all these microtubule nucleation pathways are essential for spindle assembly in the absence of nucleation by centrosomes, little is known about their relative contribution in oocytes and how they interact together.

4. Spindle bipolarization

Once microtubules are formed, the spindle must assemble in a bipolar fashion in order to accurately segregate chromosomes in two distinct groups.

4.1. Centrosome-dependent spindle bipolarization in mitosis

In mitotic cells, centrosomes are duplicated during interphase of the cell cycle and cells enter mitosis with two centrosomes. At the onset of mitosis, centrosome separation is driven by the microtubule sliding activity of kinesin-5. Duplicated centrosomes thus form the spindle axis and promote rapid spindle bipolarization (Toso et al., 2009, Tanenbaum and Medema, 2010).

4.2. Spindle bipolarization in the absence of centrosomes

In oocytes, spindle bipolarization does not rely on a bipolar axis predefined by the two separated centrosomes. Instead, spindle bipolarization is a sequential and slow process. It can take up to 12 minutes in *C.elegans*, 4 hours in mouse and 6.5 hours in human oocytes, which corresponds to around half the transition time from NEBD to anaphase in these species (Dumont et al., 2007; Schuh and Ellenberg, 2007; Holubcová et al., 2015; Sumiyoshi et al., 2015) and 40 minutes in *Drosophila* oocytes (Sköld et al., 2005).

4.2.1. Formation of a central microtubule array

In the absence of centrosomes, the establishment of a bipolar spindle depends on the sorting and stabilization of microtubules into a central array via microtubule motors and microtubule associated proteins (Heald et al., 1996; Walczak et al., 1998). A crucial step in this process is the transformation of an unorganized ball of microtubules into a bipolar array presenting anti-parallel microtubules in opposite orientations (Schuh and Ellenberg, 2007; Kitajima et al., 2011). This is achieved via

the sorting and bundling of microtubules by plus-end directed microtubule motors (Figure 8 and 9).

a. Plus-end directed motors kinesin-5 and kinesin-6

Kinesin-5 (Eg5) was shown to be essential for the establishment and maintenance of spindle bipolarity in *Xenopus* extracts and mouse oocytes (Figure 9) since its inhibition results in monopolar spindles (Walczak et al., 1998; Kapoor et al., 2000; Mailhes et al., 2004; Schuh and Ellenberg, 2007; Fitzharris et al., 2009). In *Drosophila*, the kinesin-6 family member Subito facilitates spindle bipolarization (Figure 9) by promoting the formation of a central microtubule array (Jang et al., 2005; Jang et al., 2007). In particular, CPC central spindle proteins such as Incenp and Aurora B fail to localize to this central region in subito mutants.

b. aMTOCs organization in mouse oocytes

In mice, where oocytes assemble a meiotic spindle in the presence of multiple aMTOCs, these aMTOCs have to be properly organized in order to ensure correct spindle bipolarization (Figure 8). Before NEBD, aMTOCs are decondensed by PLK1. Upon NEBD they are spread along the nuclear envelope by a microtubule- and dynein-dependent mechanism, and following NEBD, aMTOCs are fragmented in smaller structures by kinesin-5 (Luksza et al., 2013; Clift and Schuh, 2015). This fragmentation process is essential for bipolar spindle formation as a failure to fragment aMTOCs induces defects in bipolar spindle assembly and chromosome alignment (Clift and Schuh, 2015). Next, concomitant to the formation of a central microtubule array, aMTOCs are progressively sorted along the central spindle into distinct poles between NEBD and 4 hours after (Schuh and Ellenberg, 2007; Breuer et al., 2010). A key player in this process is the microtubule associated protein and RanGTPase factor HURP which has a role very comparable to the one of Subito in *Drosophila* (Tsou et al., 2003). HURP is recruited by kinesin-5 to the central spindle (Figure 9) and permits aMTOCs sorting by facilitating microtubule stability in this region (Breuer et al., 2010). The stabilization of microtubules in the region of overlap

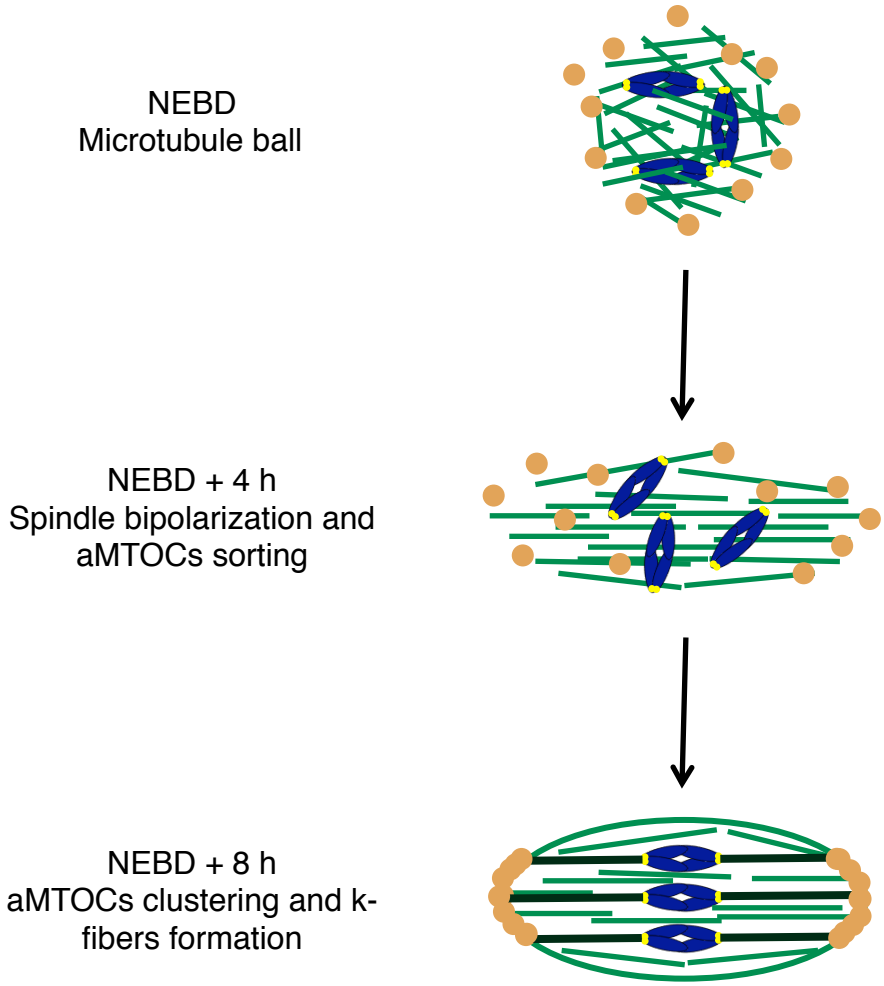

Figure 8: Spindle assembly in mouse oocytes
DNA is in blue, microtubules in green, kinetochores in yellow, k-fibers in dark green and aMTOCs in brown.

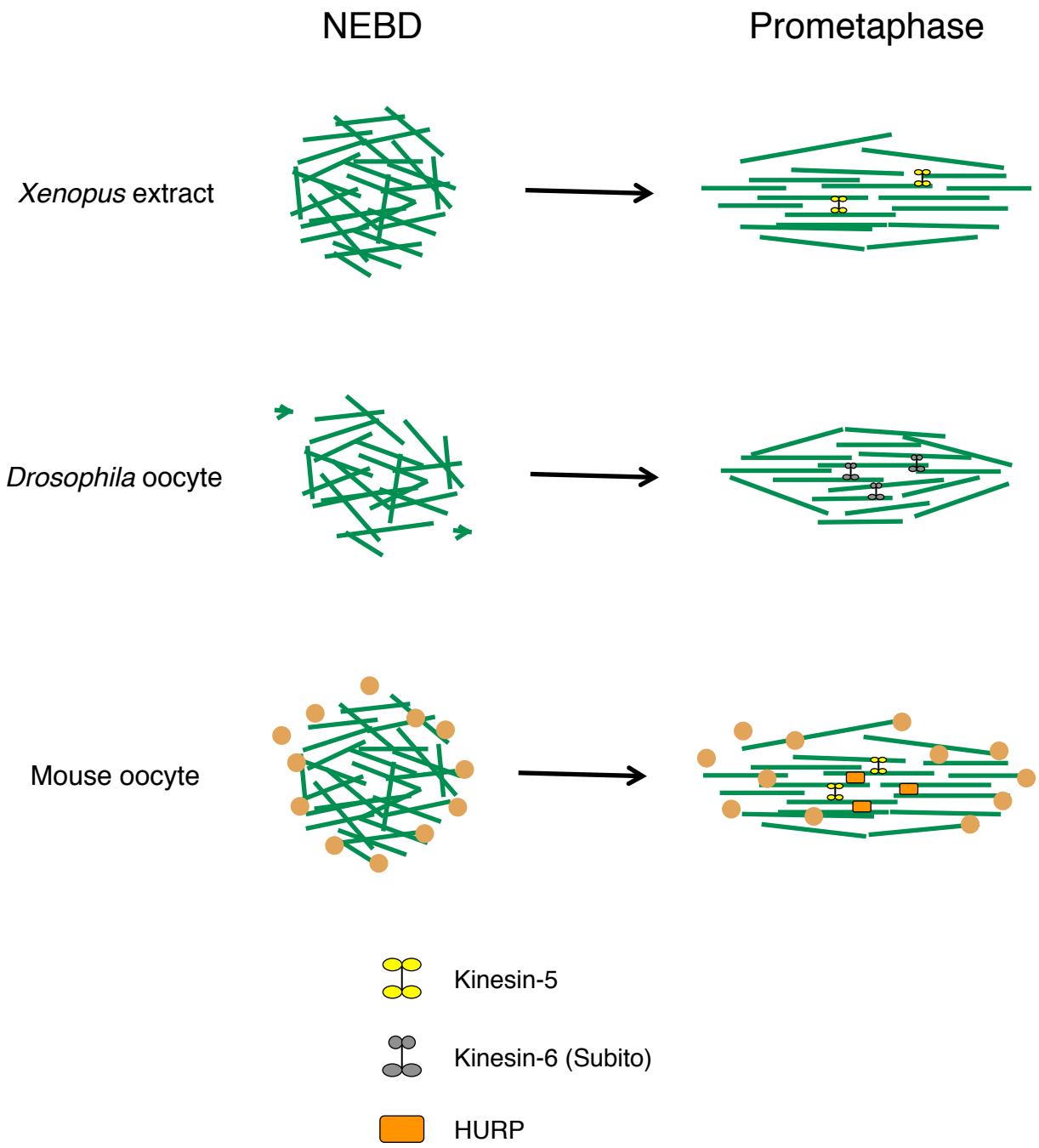

Figure 9: Spindle bipolarization in the absence of centrosomes
Organization of microtubules into a bipolar array via microtubule motors and microtubule-associated proteins. Microtubules are in green, aMTOCs in brown.

of anti-parallel microtubules provides tracks on which motors can bind aMTOCs as their cargos and transport them to spindle poles.

Interestingly, in human oocytes where spindle bipolarization is extremely slow, most spindles fail to maintain a bipolar shape but instead go through phases of multipolarity (Holubcová et al., 2015). Such unstable spindles are rarely observed in mitotic spindles or meiotic spindles from other species, except in oocytes from the hurp-/- strain (Breuer et al., 2010), thus raising the question of the nature of the regulatory mechanisms at play in human oocytes favoring this instability.

4.2.2. Microtubule nucleation

Microtubule nucleation can also affect spindle bipolarization. Although the RanGTP pathway is not strictly required for bipolar spindle assembly in mouse oocytes, the expression of Ran dominant-negative or gain-of-function mutants can respectively decrease or increase the timing of spindle bipolarization (Dumont et al., 2007). In addition, it was recently shown that Aurora A and Plk4 kinases cooperate to initiate bipolar spindle formation in mouse oocyte by amplifying microtubule growth (Bury et al., 2017). The inhibition of Aurora B and Plk4 decreases microtubule nucleation thus leading to a delay in the timing of spindle bipolarization. All these results suggest that a critical mass of microtubules must be reached to establish spindle bipolarity.

5. Spindle pole formation

Spindle poles in mitosis are organized by a single centrosome (Figure 10). Pole formation in oocytes is different, since it is not organized by a single entity. *Drosophila* excepted, most oocytes present spindle poles that are less focused than in mitosis, having a barrel-shape aspect.

5.1. Spindle pole formation by microtubule motors and MAPs

The formation of spindle poles, which is the region where microtubule minus-ends are converging, relies on the activity of microtubule motors and microtubule

associated proteins (Figure 10). Studies in *Xenopus* egg extracts have shown that Dynein and kinesin-14 minus-end motors shape the poles by focusing microtubule minus-ends in these regions (Heald et al., 1996; Walczak et al., 1998). In *Drosophila* oocytes, Ncd (kinesin-14) prevents pole splitting and multipolar spindle formation (Endow and Komma, 1997; Sköld et al., 2005). Furthermore, Dynein in a complex with Dynactin and NuMA is essential to tether microtubule minus-ends at meiotic spindle poles in *Xenopus* egg extracts (Merdes et al., 1996). Acentrosomal poles in *Drosophila* oocytes contain the microtubule-associated protein Msps, which is a member of the dis1/TOG family. Msps is recruited to spindle poles by kinesin-14 (Ncd) and D-TACC where it prevents loss of bipolarity possibly by stabilization of microtubules ends (Cullen and Okhura, 2001). The *C.elegans* homolog ZYG-9 is also enriched at spindle poles and is required for spindle assembly (Matthews et al., 1998). In mouse oocytes, NuMA is required for the formation of barrel-shaped spindle poles as well as microtubule minus-end cohesion since its impairment causes hyper-focused poles that often lose microtubule connection (Kolano et al., 2012).

5.2. Spindle formation by aMTOCs

In mouse oocytes, the discrete aMTOCs organize spindle poles (Figure 8 and 10). Following their bipolar sorting, aMTOCs progressively cluster together between 4 and 7 hours after NEBD, and will contribute to the cohesion and integrity of spindle poles (Kolano et al., 2012). Even though not addressed so far properly, if the sorting of aMTOCs fails to be optimal, the number of aMTOCs at each pole might not be identical and could thus favor force imbalance within the meiotic spindle compared to mitotic spindles where the poles are formed by equivalent centrosomes. This would resemble the process of clustering of extra-centrosomes in cancer cells in which unbalanced poles favor chromosome mis-segregation (Kwon et al., 2008; Breuer et al., 2010). In *C.elegans*, *Drosophila*, *Xenopus* and humans, microtubule minus-ends do not seem to be anchored to discrete aMTOCs entities (Figure 10). Although they are not anchored to detectable structures, their poles are shaped by a combination of factors as described above. In addition, most meiotic spindle poles, with the exception of *Drosophila*, have a broad shape compared to the more focused mitotic

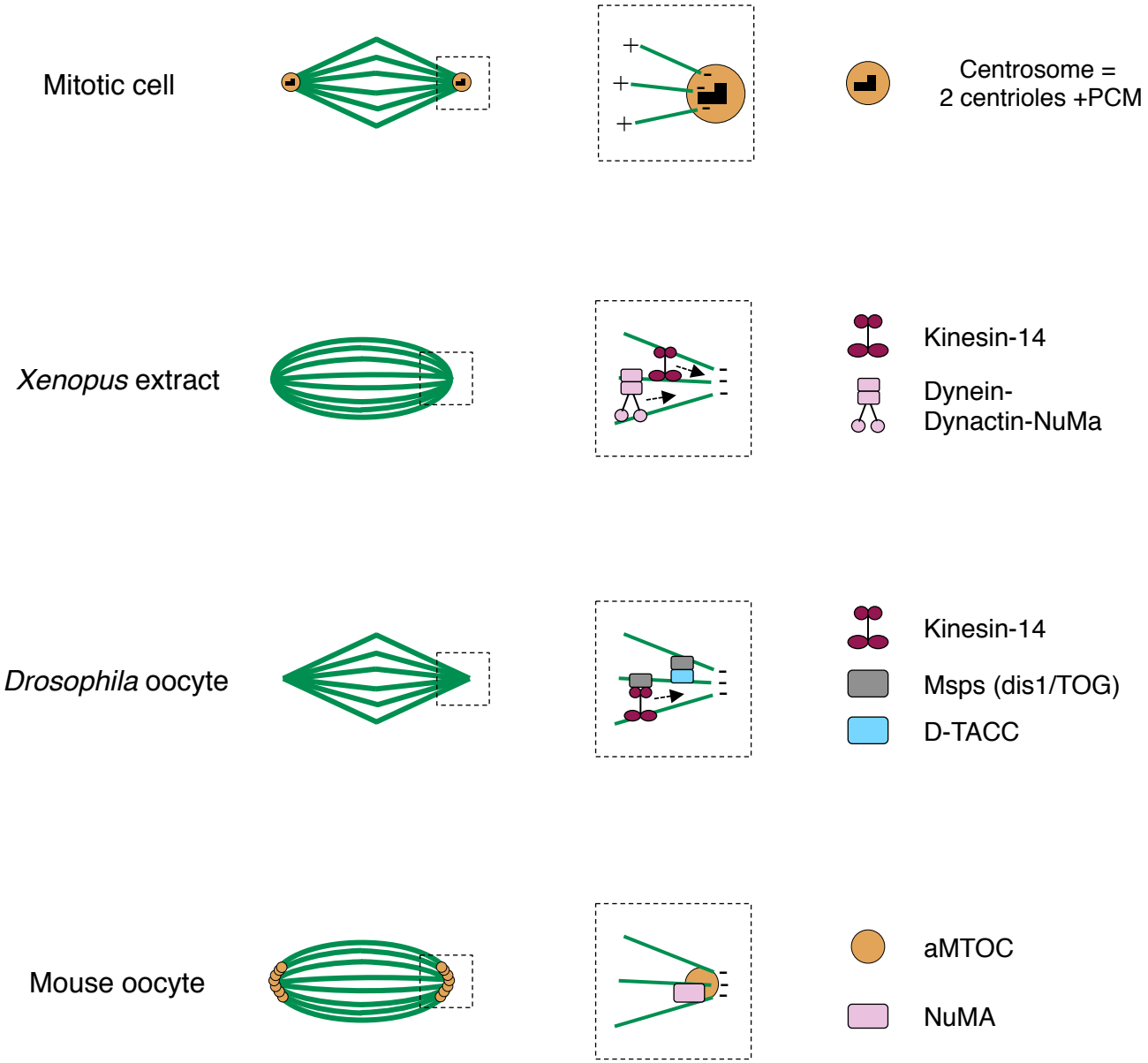

Figure 10: Spindle pole formation

The dashed square shows magnification of the spindle pole where microtubule motors and microtubule associated proteins organize microtubule minus ends.

spindle poles, which could be related to the lack of tight organizers, the centrosomes. Thus meiotic spindle poles could possibly be less robust than the mitotic ones that are anchored to distinct centrosomes.

6. Modeling meiotic spindle assembly

Because the spindle is an extremely complex system, models with intermediate levels of complexity can be very informative. These models focus on simple mechanisms in isolation and thus allow understanding their effects in a broader biological context. Several models based on mathematical analysis or computer simulation have been developed to study spindle assembly (Cytrynbaum et al., 2005; Goshima et al., 2005; Schaffner and José, 2006; Loughlin et al., 2011). Notably, the modeling of 2 asters (~centrosomes) showed that the interplay between motors of opposite polarity can give rise to stable anti-parallel structures, similar to mitotic spindles (Surrey et al., 2001; Nédélec, 2002; Nédélec et al., 2003). Although this approach is relevant in mitotic cells where centrosome-dependent microtubule nucleation predominates, it is less informative for meiotic spindles lacking canonical centrosomes.

Among the few modeling studies dedicated to meiotic spindle assembly, two studies that I will review below are of particular importance.

6.1. The slide and cluster model

Burbank and colleagues showed that a “slide-and-cluster” model could create steady-state bipolar spindles with defined poles (Burbank et al., 2007). This model is based on the following activities: (1) microtubules are nucleated in the spindle midzone near chromosomes, (2) a plus-end-directed motor slides new nucleated microtubules poleward, (3) a minus-end-directed motor clusters microtubule minus ends and (4) microtubules are lost by dynamic instability (Figure 11). The coordination of all these activities forms a spindle of stable steady-state length exhibiting “poleward microtubule flux” (Dumont and Mitchison, 2009). In this model, two types of motors control microtubule motion: a “sliding motor” representing the plus-end-directed motor

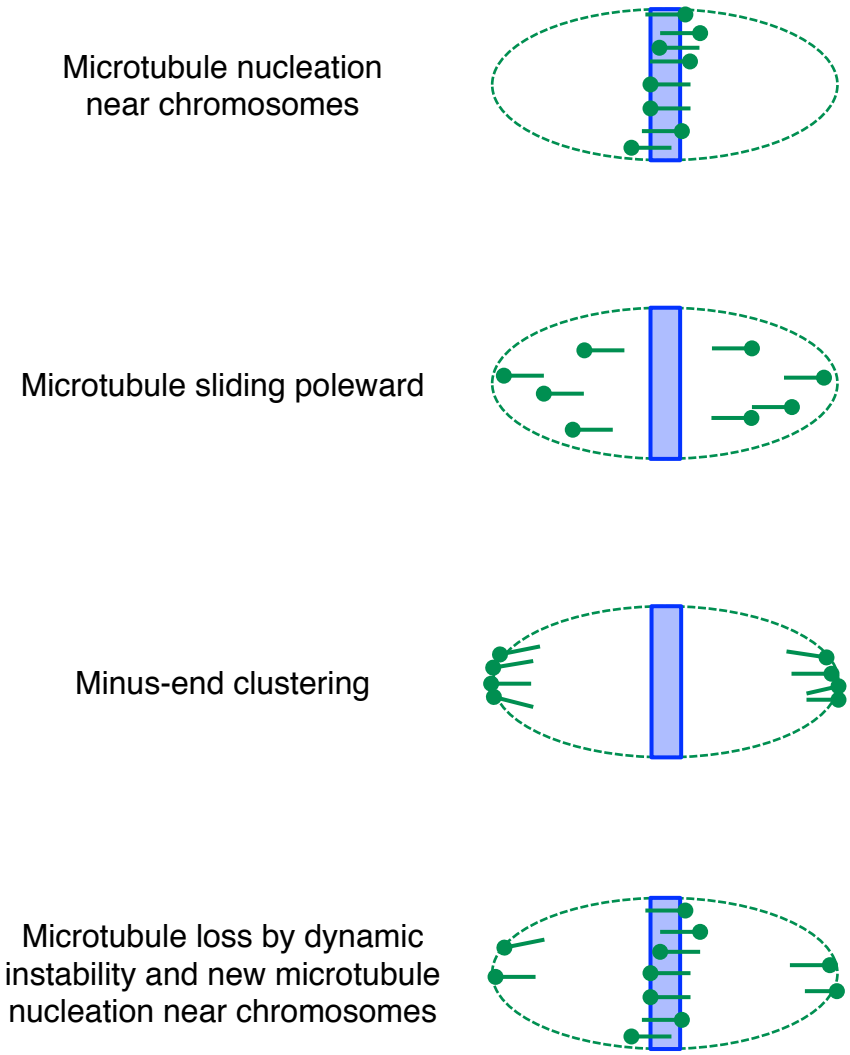

Figure 11: Modeling spindle assembly

The “slide-and-cluster” model. Microtubules are in green, green circles represent minus ends, the spindle midzone containing chromosomes is is blue.

kinesin-5 and a “clustering motor” representing the minus-end-directed motors dynein or kinesin-14. Near the chromosomes, both types of motors work together to slide microtubules outward. Near the poles, both motors are antagonistic because the clustering motor pulls microtubules inward. Thus, microtubules slow down, stop and are clustered to form poles. This gradient of microtubules sliding velocity is the primary prediction of the model. This prediction was confirmed by fluorescent speckle microscopy in *Xenopus* extract spindles, thus supporting this model.

6.2. Models integrating microtubule dynamics

The “slide-and-cluster” model does not take into account microtubule dynamic instability. Indeed, all microtubules are of constant length and have a specified lifetime but their plus ends are not dynamic. However, plus-end dynamics are important to incorporate in a model of bipolar spindle assembly because plus-end growth is a lot faster than microtubule sliding towards the pole. In a model similar to the “slide-and-cluster” in which all microtubules are nucleated at the spindle midzone, plus-ends would grow poleward three times faster than minus-ends slide poleward. As a result, it would assemble into a microtubule structure where plus-ends point outward. Loughlin and colleagues solved this problem by simulating nucleation of dynamic microtubules throughout the spindle (Loughlin et al., 2010). In their model, the number of microtubules is kept constant by two nucleation mechanisms: microtubule nucleation at the spindle midzone near chromosomes and microtubule amplification generating new microtubules along the side of pre-existing microtubules. With this model, a steady-state bipolar spindle can be obtained by using microtubule minus-end cross-linking and a “sliding motor” but without a “clustering motor”. Instead, the formation of well-defined poles requires a minus-end cross-linker (NuMA-like) and microtubule depolymerization activity toward minus-ends (kinesin-13-like). Interestingly, this model also reproduces features of Xenopus egg extract spindle bipolarization.

Although these two models are based on different hypothesis, they both propose a coherent picture of meiotic spindle assembly. They rely on the interplay between a

sliding plus end motor and a minus-end clustering protein (either a crosslinker or a motor). Both models highlight the importance of a fine-tuned balance between plus-end and minus-end directed activities. Indeed, disrupting this balance by changing the concentration of one of those actors could affect the steady-state spindle length or even disrupt the bipolarization process.

Finally, comparing these models shows the complexity and the importance of including microtubule dynamics in meiotic spindle modeling. However, both models start with already aligned filaments and assume a fixed central chromosome plate, as their focus was on the establishment of a steady-state bipolar structure. It would be interesting to extend such models to also address earlier steps of spindle assembly, when microtubule are not aligned, and to include the contribution of other activities such as microtubule nucleation by chromosomes or aMTOCs.

7. Chromosome alignment

After a bipolar spindle is formed, chromosomes align in the spindle equator.

In mitosis, the “search and capture” model states that microtubules growing toward the chromosomes are rapidly captured and stabilized by the kinetochores, establishing stable kinetochore-microtubule attachments (Kirschner and Mitchison, 1986; Wollman et al., 2005).

7.1. Chromosome alignment in oocytes

In oocytes, chromosome alignment is a much slower and progressive process that depends on the interaction of microtubules with chromosome arms and kinetochores. The interaction of chromosome arms with microtubules and microtubule motors, which also exist in the short prometaphase of mitotic cells, are thought to generate forces pushing chromosomes toward the spindle equator (Brunet et al., 1999; Mazumdar and Misteli, 2005; Cai et al., 2009; Cheeseman and Desai, 2008; Wandke et al., 2012). In *C.elegans*, the kinesin-like protein KPL-19 localizes to a non-kinetochore chromatin region where microtubules contact chromosomes and could

promote the motion of chromosomes toward the equator (Wignall and Villeneuve, 2009).

7.2. Kinetochore-microtubule attachments in mouse oocytes

An electron microscopy study has suggested that mouse oocytes establish extremely delayed kinetochore-microtubule attachments (k-fibers), 1 to 2 hours prior to anaphase (Brunet et al., 1999). However, even though stable k-fibers appear to be formed late in mouse oocytes, this does not exclude the possibility that microtubules could establish earlier contacts with kinetochores. Indeed, kinetochore-microtubule attachments are observed after calcium or cold treatment 3 to 4 hours before anaphase (Lane et al., 2012). Yet k-fiber stability varies until late metaphase I. A study at high resolution using live microscopy revealed that almost all kinetochores undergo multiple steps of error correction before engaging into stable bipolar attachments (Kitajima et al., 2011). Thus k-fibers may not have been well preserved during electron microscopy fixation procedures and failed to be detected at earlier stages (Brunet et al., 1999). It may be interesting to re-analyze in more details the timing of apparition of k-fibers by electron microscopy. The delay in k-fiber formation depends on CDK1 activity, which increases very gradually throughout meiosis I (Davydenko et al., 2013). A precocious increase in CDK1 activity leads to premature stable kinetochore-microtubule attachments and lagging chromosomes at anaphase. Aurora B/C phosphorylation activity destabilizes the attachments whereas PP2A-B56, recruited at kinetochores by an increase in CDK1 activity, stabilizes kinetochore-microtubule attachments (Yoshida et al., 2015). Using a genetic approach it has been shown in mouse oocytes that Aurora C corrects erroneous kinetochore attachments (Balboula and Schindler, 2014). In addition, kinetochore microtubule stability is regulated by their position within the spindle as they can undergo Aurora A-dependent destabilization near spindle poles (Chmátal et al., 2015). It is thought that a delay in k-fiber formation would prevent the stabilization of erroneous attachments before bipolar spindle formation, a very slow and unsteady process in meiosis I.

7.3. Kinetochore-microtubule attachments in *Drosophila* oocytes

A recent study has shown that stable k-fibers formation is also slow in *Drosophila* oocytes (Gluszek et al., 2015) but depends on an alternative mechanism. The catastrophe-promoting complex Sentin-EB1 is responsible for delaying stable k-fibers attachments by regulating microtubule ends dynamics. Mutant oocytes for sentin present more stable k-fibers early on in meiosis I, which is deleterious for bivalent segregation. Thus one could speculate that slow k-fiber formation might be beneficial in the context of spindles organized from multiple aMTOCs or from chromosomes which might produce more merotelic attachments (in which one kinetochore is attached to both spindle poles) than spindles organized from centrosomes.

8. Chromosome segregation

Once chromosomes are aligned on the spindle equator, pulling by k-fibers drives chromosome separation. In mitotic cells, chromosome separation is driven first by shortening of the kinetochore-microtubule attachments (anaphase A) and then by spindle elongation (anaphase B).

In mouse oocytes, the opposite happens: first, the spindle elongates by a kinesin-5 dependent mechanism, and then kinetochore-microtubule attachments shorten (Fitzharris 2012). Interestingly, in nematodes, k-fibers align chromosomes but are not required for chromosome separation at anaphase (Dumont et al., 2010). Instead, it is proposed that microtubule assembly between chromosomes promotes their separation. During anaphase, central spindle microtubules located between the segregating chromosomes push chromosomes apart (Laband et al., 2017). Spindle poles almost completely disappear at anaphase in this species, they are dispensable for chromosome segregation and even brake chromosome separation. In addition, *C.elegans* chromosomes are holocentric presenting kinetochores ensheathing the entire chromosome length (Oegema et al., 2001). Although the presence of holocentric chromosomes could favor microtubule nucleation between chromosomes at anaphase it could also promote the formation of merotelic attachments. Whether this kinetochore-independent separation mechanism is conserved in mammalian

oocytes is still unknown, even though spindles lacking k-fibers are still able to undergo anaphase in mouse oocytes (Deng et al., 2009).

In mitosis, sister kinetochores are attached to opposite poles before segregation (bi-oriented) and cohesins (protein complexes holding the sister chromatid together) are cleaved at anaphase leading to separation (Figure 1). In meiosis I, sister kinetochores are attached to the same pole (mono-orientation) whereas homologous chromosomes are attached to opposite poles (Figure 1, for review see Watanabe, 2012). At anaphase I, the meiotic-specific cohesin Rec8 is protected from cleavage at centromeres, permitting the separation of homologous chromosomes but not the separation of sister chromatids (for review see Wassmann, 2013).

9. Conclusion on meiotic spindle assembly and open questions

In conclusion, spindle morphogenesis in oocytes is different from mitotic cells. In particular, spindle assembly in oocytes of most species starts with the formation of a microtubule ball, followed by the slow organization of a bipolar spindle and ends with the formation of barrel-shaped meiotic poles that are often less focused than mitotic ones. Interestingly, all these processes are extremely slow. It mirrors the long duration of the first meiotic division, as meiosis I requires 8–12 h in mice and more than 20 h in humans. The question of why meiosis I spindle organization is so unusual remains open. In particular, it is far from clear if this unique “inside out” mode of spindle assembly is required for meiotic spindle function that is segregating chromosomes.

III. Spindle positioning and chromosome segregation in oocytes

We have seen above that the lack of centrioles in oocytes imposes very original modes of spindle assembly and chromosome behavior. The next chapters address how the lack of centrioles also imposes very atypical modes of spindle positioning that have consequences on chromosome segregation in the large size of oocytes.

1. The actin cytoskeleton

In eukaryotic cells, actin is one of the most abundant proteins. Actin is highly conserved and involved in numerous cellular processes such as migration, morphogenesis or cell division. In the next chapters, we will focus on the role of actin in mitotic and meiotic cell division.

1.1. Actin structure

Actin filaments (F-actin) polymers are composed of actin monomers, or globular actin (G-actin), arranged in an helix (Figure 12). Similar to microtubules, actin filaments are polarized with fast polymerization at the “plus-end” or “barbed-end” as opposed to the “minus-end” or “pointed-end” (Figure 12). However, actin and microtubule filaments have different properties. For example, actin filaments are more flexible and have a smaller diameter than microtubules.

1.2. Actin polymerization and dynamic

The G-actin to F-actin transition is based on ATP hydrolysis by the actin subunits. Actin monomers can bind ATP and hydrolyze ATP in ADP + Pi. Actin filaments can polymerize at their plus ends while depolymerizing at the minus-end. During this steady-state process called “treadmilling”, actin filaments can remain at a constant length (Figure 12, for review see Pollard, 2016).
A critical concentration of G-actin must be reached in order for F-actin filaments to start polymerization. Polymerization comprises two steps: nucleation and elongation.

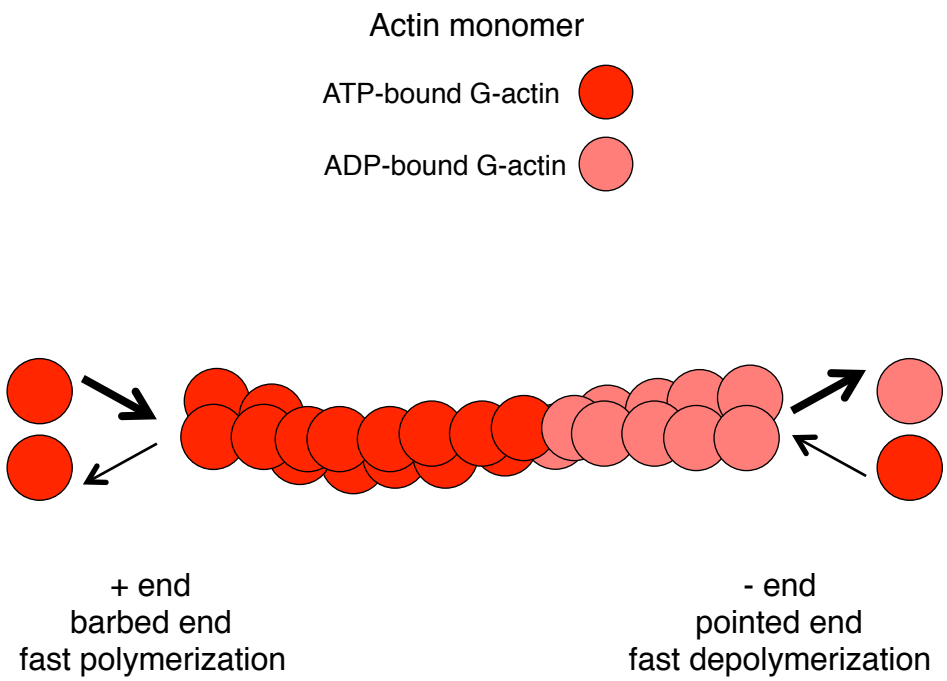

Figure 12: Actin filaments

However, spontaneous actin nucleation is not kinetically favorable. *In vivo*, this obstacle is overcome by actin nucleators (see below) which are proteins promoting actin nucleation.

2. Actin associated proteins

Many proteins interact with actin in living cells such as actin nucleators, actin stabilizing/destabilizing proteins and motors. Below, we are only reviewing in details the proteins that will be addressed in the following chapters.

2.1. Actin nucleators

As mentioned above, the process of actin nucleation is a slow and unfavorable process. *In vivo*, actin nucleation occurs with the help of actin nucleators.

2.1.1. The Arp2/3 complex

a. A branching nucleator

Arp2/3 was the first major actin nucleator identified. The Arp2/3 complex is highly conserved in almost all eukaryotes and involved in numerous cellular processes (for review see Campellone and Welch, 2010; Rotty et al., 2013; Pollard., 2016). Arp2/3 localizes at the cell cortex and plays a major role in mitotic divisions and mouse meiotic divisions (see following chapters).

Arp2/3 is a large complex composed of seven subunits, including two actin-related proteins: Arp2 and Arp3. The Arp2/3 complex binds existing actin mother filaments and nucleates branches at a 70° angle (Figure 13). Arp2 and Arp3 are structurally similar to G-actin and can bind to the pointed-end of actin filaments, thus providing the first two subunits of the new filament and allowing further elongation (Machesky et al., 1994; Welch et al., 1997).

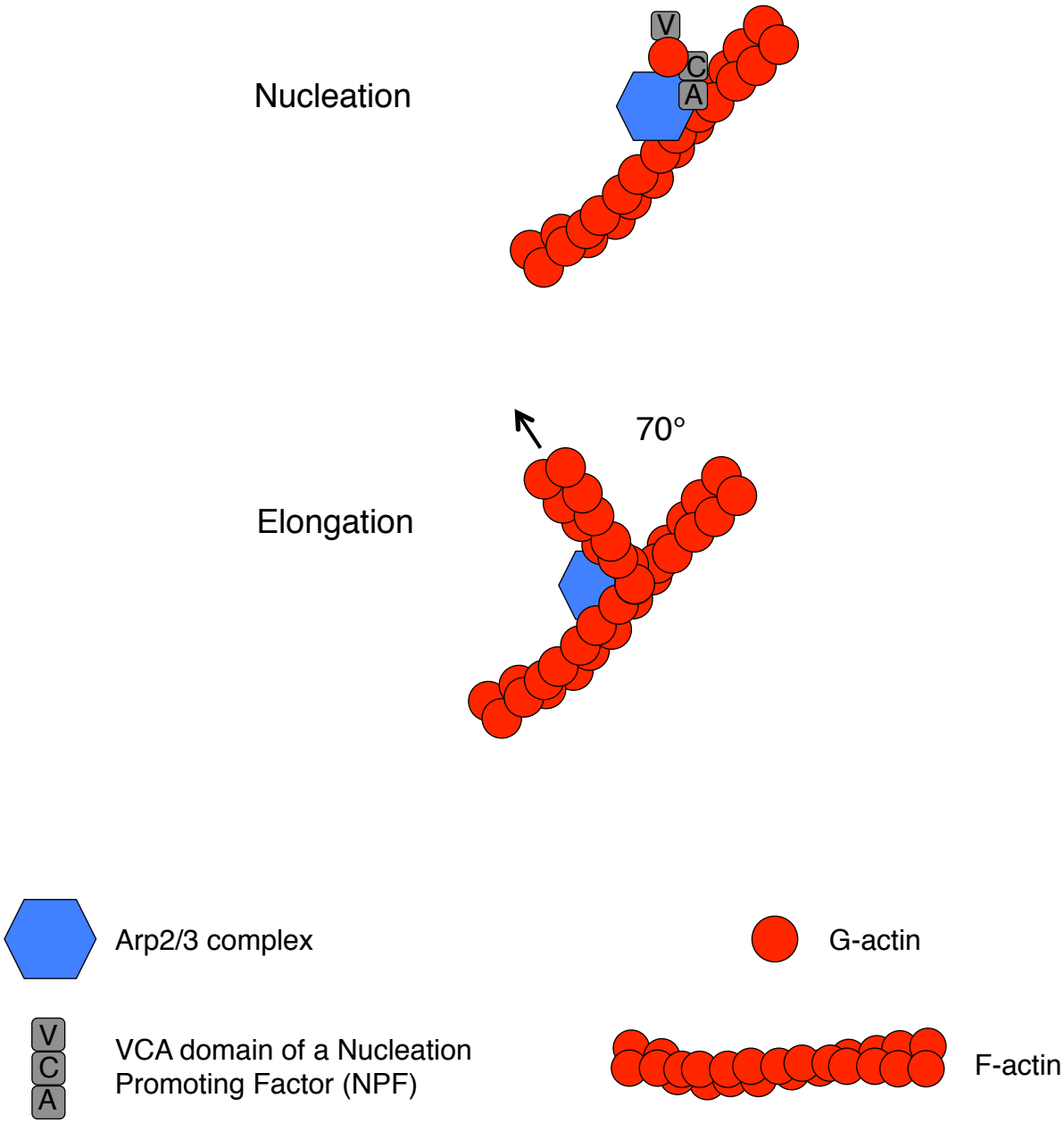

Figure 13: Branched actin nucleation by Arp2/3

b. Arp2/3 activation by NPFs

To nucleate actin, the Arp2/3 complex must be activated by nucleation-promoting factors (NPFs). NPFs form a very broad family of proteins that will not fully be addressed in details here (for review see Rotty et al., 2013). A large group of NPFs, called class I NPFs, activate Arp2/3 using a “VCA domain”. This domain is composed of a WH2 domain (also called V or VH2 for Verpolin Homology domain 2), a connector domain (C) and an acidic domain (A). It binds actin monomers via its V motif and binds Arp2/3 through the CA connector motif, thus allowing actin nucleation by Arp2/3 (Figure 13). Class I NPFs include the SCAR/WAVE (Suppressor of Cyclic AMP Repressor/WASP-family Verprolin-homologous protein) family, which comprise three mammalian isoforms: Wave1, 2 and 3 (for review see Rotty et al., 2013). In particular, Wave2 is an upstream regulator of Arp2/3 in mouse oocytes and is essential for normal oocyte asymmetric division (Sun et al., 2011; Liu et al., 2012; Chaigne et al., 2013 and see chapter 4.2.2.b).

2.1.2. Formin 2

Proteins of the Formin family are conserved in almost all eukaryotes. Formins are involved in cell migration, cell polarity and cytokinesis (for review see Campellone and Welch, 2010 and Chesarone et al., 2010). Unlike Arp2/3, Formins nucleate linear actin filaments instead of branched F-actin. Formins are multidomain proteins that all share C-terminal formin homology (FH) domains: FH1 and FH2, which possess the actin nucleation activity.

The FH2 domain is sufficient to trigger actin nucleation *in vitro* (Sagot et al., 2002; Pring et al., 2003). It is highly conserved and forms a ring-shaped dimer that binds to barbed ends of elongating filaments (Figure 14 and for review see Campellone and Welch, 2010, Chesarone et al., 2010 and Pollard, 2016). The FH1 domain binds to G-actin in a complex with Profilin, which is a protein that associates with G-actin monomers in cells. FH1 binding to G-actin-Profilin complexes accelerates F-actin elongation, presumably by promoting G-actin delivery to the barbed end (Figure 14

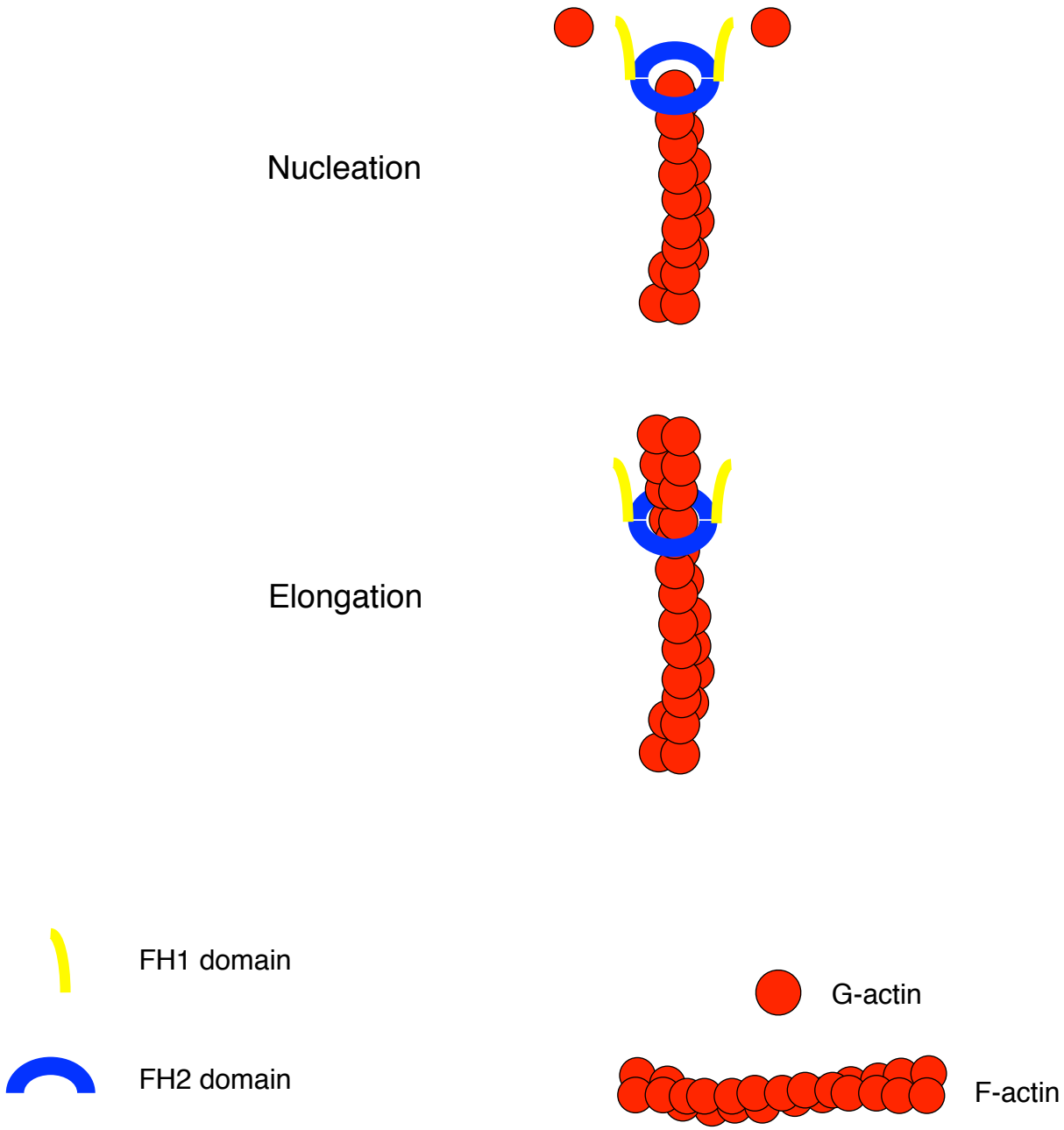

Figure 14: Linear actin nucleation by Formin 2

and Romero et al., 2004; Kovar et al., 2006; Vavylonis et al., 2006; Paul and Pollard, 2008).

There are 15 mammalian formins distributed in seven different classes. Among them, Formin 2, which belongs to the FMN class, is expressed in mouse oocytes and is crucial for mouse meiotic divisions (Dumont et al., 2007; Azoury et al., 2008; Schuh and Ellenberg, 2008; Pfender et al., 2011; Almonacid et al., 2015 and see chapter III.4. for a review of this process).

2.1.3. Spire

Spire is another type of actin nucleator, which produces unbranched actin filaments. Spire proteins use actin monomer-binding domains to nucleate linear F-actin. However, the mechanism of actin nucleation by Spire1/2 is still unclear (see review Campellone and Welch, 2010). Interestingly, Spire 1 and 2 (Spire1/2) can bind Formin 1 and 2. Spire1/2 cooperates with Formin 2 in mouse oocytes and is crucial for F-actin polymerization and asymmetric division (see chapter III.4.1.1 and Pfender et al., 2011; Montaville et al., 2014).

2.2. Actin motors

Myosin motors are proteins that bind and move along actin filaments. They create force and movement by using energy from ATP hydrolysis. The myosin family of proteins contains 35 members, which are divided in many groups and involved in numerous cellular processes such as vesicle transport and cytokinesis (Bloemink and Geeves., 2011).

Myosins share a conserved N-terminal head motor domain, which has been shown to bind actin filaments. The C-terminal tail motor domain is quite variable between classes and can bind to a wide range of partners. Myosins are all plus-end directed motors with the exception of myosin VI. Myosin II is the first myosin class discovered and is considered conventional whereas all other myosin classes are considered unconventional. Among all these classes, myosin II and Vb play a key role during mouse meiotic divisions, which is addressed in the following chapters.

2.2.1. The conventional myosin II

Myosin II is the first myosin class discovered and it has been very well studied especially for its role in muscle contraction. Myosin II is composed of two heavy chains and four light chains (see review Vicente-Manzanares et al., 2009). The long heavy chain tails are supercoiled and dimerize to form myosin II minifilaments (Figure 15). Myosin II is the only myosin capable of dimerizing in bipolar minifilaments. Myosin II minifilaments crosslink and slide actin filaments, thus generating contractile or tensile forces within actin networks (Figure 15). Interestingly, *in vitro* studies showed that actin network architecture can determine myosin II activity (Reymann et al., 2012; Ennomani et al., 2016). In addition, myosin II activity can be regulated by its phosphorylation at several sites. For example, phosphorylation of the light chain by MLCK (Myosin Light Chain Kinase) activates myosin II by allowing its interaction with F-actin (for review see Vicente-Manzanares et al., 2009).

2.2.2. The unconventional Myosin Vb and Myosin X

Unlike the conventional myosin II, unconventional myosins do not form minifilaments but rather bind their partner via their tails.

Myosin V motors move along actin filaments and can transport cargos (for review see Hammer and Sellers, 2012). Myosin Vb is crucial for actin vesicle and cytoplasmic movement in mouse oocytes, a process that is detailed later in this chapter. In particular, myosin Vb was shown to bind to Rab11 proteins of the Rab GTPase family thus participating in the dynamics of recycling endosomes (Hammer and Sellers, 2012).

Eventually, the atypical myosin X can bind both actin and microtubule filaments (Divito and Cheney., 2008). In particular, Myosin X is able to bind microtubules through its MyTH4-FERM C-terminal domain. Myosin X is crucial for spindle morphogenesis and positioning in mammalian cultured cell and *Xenopus* oocytes and embryos (see 3.1.1.c.).

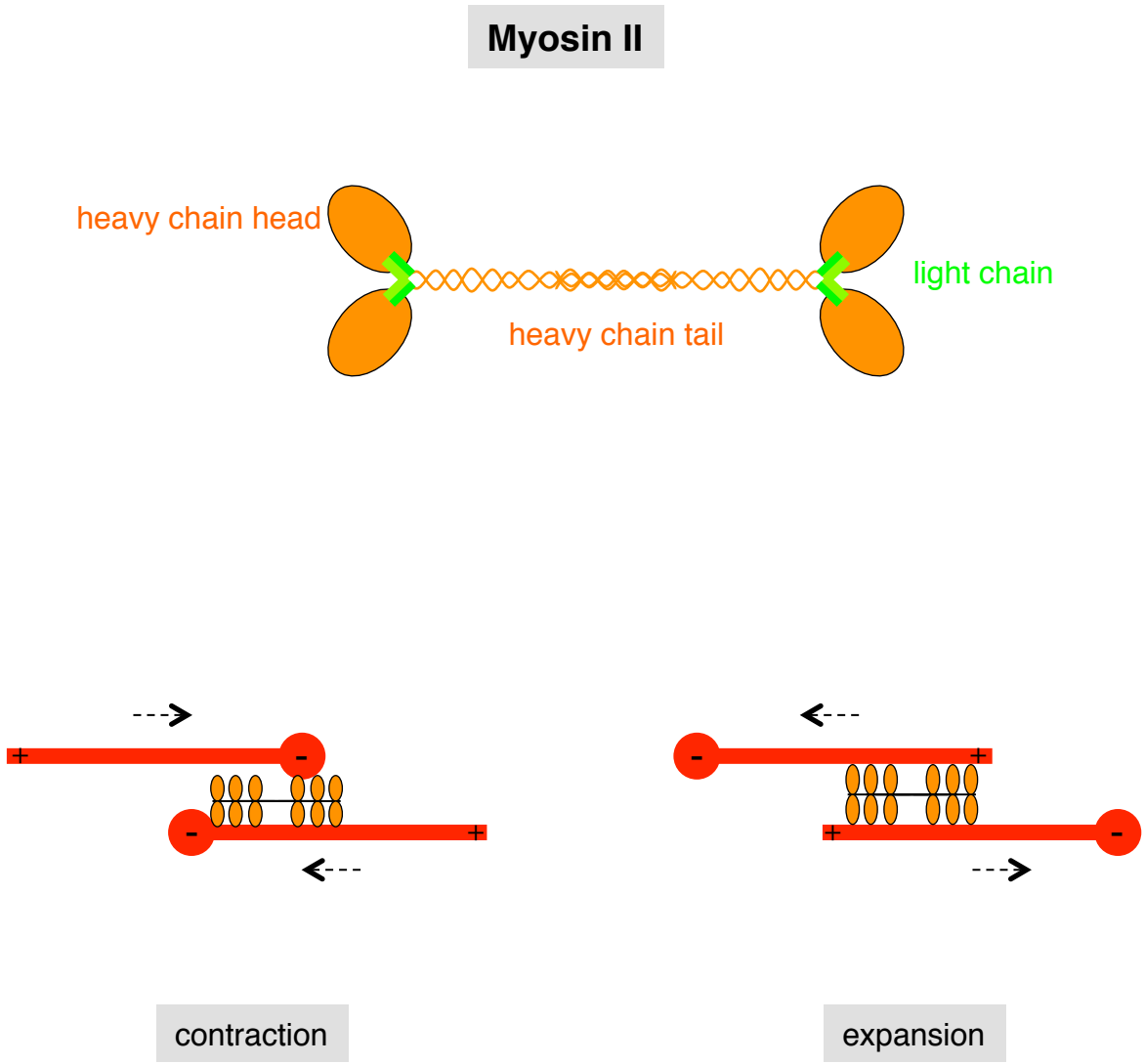

Figure 15: Myosin II motors
Actin is in red, red circles represent minus ends.

2.3. Actin regulators and organizing proteins

2.3.1. ERM proteins

Ezrin, Radixin and Moesin constitute the ERM proteins. ERM proteins organize the cell cortex in many cell types and can interact with both the plasma membrane and filamentous actin (for review see Fehon et al., 2010). ERM proteins all have a N-terminal FERM domain and a C-terminal domain containing the F-actin binding site. The C-terminal domain can bind the FERM domain in a closed conformation. Its unbinding triggers the activation of ERM proteins and allows connection of the membrane to the actin network underneath. In the next chapters, the role of ERM proteins in cell cortex mechanics in mitotic cells and mouse oocytes is reviewed in details.

2.3.2. The Mos/MAPK pathway

The MAPK (Mitogen-activated protein kinase) pathway constitutes a cascade of phosphorylation proteins. Upstream of the pathway, a MAPKKK (MAP Kinase Kinase Kinase) phosphorylates a MAPKK (MAP Kinase Kinase), which in turn phosphorylates the downstream Serine/Threonine kinase MAPK (MAP Kinase). These kinases respectively correspond to Mos, MEK and ERK1/2 in mouse oocytes. It has been shown that the MAPK pathway plays a crucial role in actin cytoskeleton regulation in many cells. In particular, the Mos/MAPK pathway triggers actin nucleation by Arp2/3 at the cortex in mouse oocytes (Chaigne et al., 2013 and see chapter III.4.2.2.). This is thought to be mediated by MAPK-dependent phosphorylation of Wave2, a NPF of Arp2/3, similar to what was observed in migrating cells (Mendoza et al., 2011).

3. Actin in mitotic cell division

3.1. Mitotic spindle positioning

Once the spindle is formed, it must be correctly positioned within the cell to control the division geometry. In mitosis, centrosomes nucleate the microtubules composing the spindle but also astral microtubules. These microtubules emanating from the poles connect the spindle to the cell cortex and exert forces allowing spindle positioning (Figure 16). Astral microtubules interact at the cell cortex with dynein, which produces pulling forces that power spindle positioning (for review see McNally, 2013). In addition to astral microtubules, actin also plays an important role in mitotic spindle positioning. Several studies revealed that F-actin is required for spindle orientation in mammalian cultured cells, since treatment with F-actin depolymerization drugs induces randomization of spindle orientation (Théry et al., 2005; Toyoshima and Nishida, 2007). Below, we discuss the implication of actin in this process.

3.1.1. Cortical actin

The mitotic cortex acts as a foundation for spindle orientation.

a. Cortical tension

At the interface between a cell and its environment, surface tension primarily governs cell shape and plays a role in mitotic spindle positioning. Surface tension is defined as energy per unit area or force per unit length. Considering the interface between a liquid and its environment, surface tension tends to minimize the surface of contact between the liquid and its environment. For example, surface tension causes the almost spherical shape of liquid drops. Importantly, in isolated cells surface tension is dominated by cortical tension.

The cell cortex contains a thin network of crosslinked actin filaments together with myosin II underneath the plasma membrane (for review see Salbreux et al., 2012).

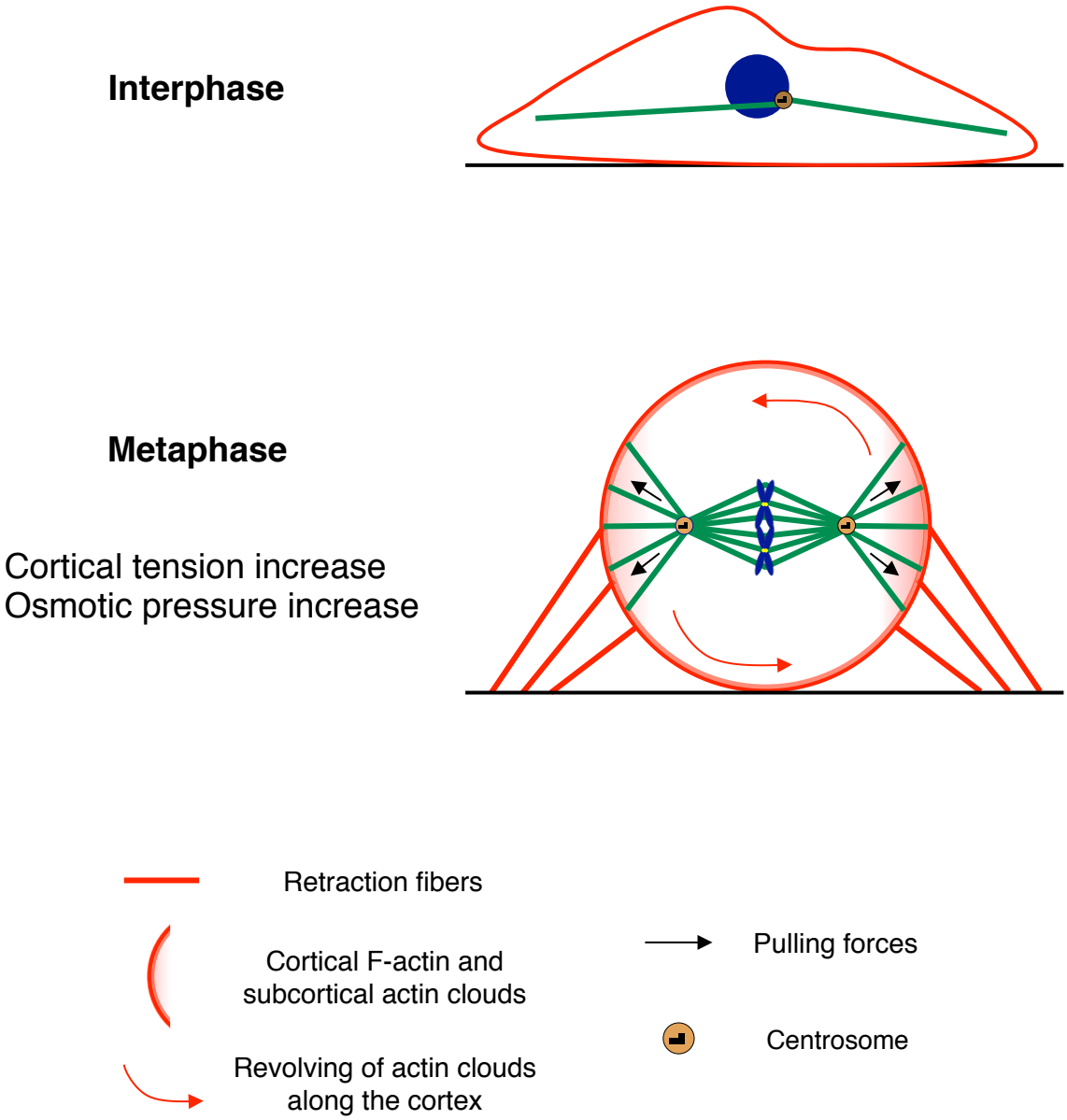

Figure 16: Mitotic rounding and spindle positioning
DNA is in dark blue, microtubules in green, actin in red, kinetochores in yellow, pericentriolar material in brown and centrioles in black.

Cortical tension is a tensile force exerted on a portion of the cortex by the surrounding cortical network. Cortical tension is primarily generated by myosin II motors, which create contractile stresses by sliding actin filaments (Figure 15, for review see Clark et al., 2014; Toyoda et al., 2017). In addition, *in vitro* studies using a micropatterning method enabling spatial control of actin assembly showed that actin network architecture can influence myosin II activity and regulate myosin-induced contractility (Reymann et al., 2012; Ennomani et al., 2016). A recent study in mammalian cultured cells also revealed that cortical actin architecture is important to regulate cortical tension (Chugh et al., 2017). The authors showed that cortical thickness is reduced in mitotic cells with increased cortical tension compared to interphase. In mitotic HeLa cells, cortex thickness is around 200 nm, versus 400 nm approximately in interphase. Measuring cortical thickness in live mitotic cells is challenging because it is below the resolution limit of conventional light microscopes. To overcome this issue, cortical thickness was measured by combining confocal imaging and theoretical modeling of the cortex (Clark et al., 2013). In particular, this method relies on the differential labeling of the actin cortex and the plasma membrane above it. Moreover, their computational model identified that maximal cortical tension is achieved at intermediate actin filament length. However, Chugh et al. did not take into account cortical actin dynamics, which could also play a key role in this process (see Clark et al., 2014). At mitosis onset, mitotic cells round up in a Cdk1-dependent manner (Figure 16). The rounding force depends on an increase in cortical tension driven by the actin cytoskeleton and ERM proteins (Carreno et al., 2008; Kunda et al., 2008; Fink et al., 2011), together with an increase in osmotic pressure (Stewart et al., 2011). Mitotic cell rounding is necessary for correct spindle positioning (Kunda et al., 2008), probably because astral microtubules must be anchored on a stiff cortex in order to efficiently exert forces positioning the spindle.

b. Polarized subcortical actin

During mitotic rounding, cells maintain contacts with their adhesive substrate through F-actin rich membrane tubes called retraction fibers (Figure 16). In response to

extracellular cues, these retraction fibers control spindle positioning by recruiting polarizing factors to the cortex. In particular, laser ablation of retraction fibers facing the spindle poles in cells dividing on cross-shaped micro-patterns leads to spindle reorientation with the remaining retraction fibers (Fink et al., 2011). This demonstrates that retraction fibers participate in mitotic spindle orientation. In addition, retraction fibers control the localization of dynamic subcortical actin clouds nucleated by Arp2/3 in mammalian cells (Mitsushima et al., 2010; Fink et al., 2011). These subcortical actin clouds revolve periodically along the cell cortex and provide pulling forces, which position the spindle relative to the cells adhesion pattern (Figure 16).

c. Myosin X

A recent study showed that the unconventional myosin X orients centrosomes toward retraction fibers and subcortical actin clouds via its microtubule binding activity in mammalian cells (Kwon et al., 2015). Moreover, in the epithelium of *Xenopus* embryos, myosin X localizes at mitotic spindle poles where it is essential for spindle morphogenesis, orientation and anchoring to the cortex (Woolner et al., 2008).

3.1.2. Cytoplasmic actin

Whereas most studies focused on the role of cortical actin in mitotic spindle positioning, the role of cytoplasmic actin remains unclear. In yeast, F-actin cables are essential for spindle positioning and extend from the cortex to the cytoplasm where they interact with microtubules emanating from the spindle pole bodies (for review see Sandquist et al., 2011). In *Xenopus* embryos, F-actin cables surround the mitotic spindle and extend toward the cortex (Woolner et al., 2008) but their precise role and whether or not they are conserved in mammalian mitotic cells is not known.

4. Actin in female meiotic division

In female meiotic division, F-actin plays an important role in various processes such as nucleus and spindle positioning. In particular, the role of cytoplasmic and cortical F-actin has been very well described in mouse oocytes lacking centrioles and astral microtubules.

4.1. Nucleus positioning

In mouse, nucleus positioning occurs during the growth phase of prophase I arrested oocytes (see chapter I.3.). Before growth, the nucleus is close to the cortex. During growth, the nucleus moves from an off-centered position to the center of the oocyte (Figure 17). Interestingly, nucleus centering is conserved in mouse and human oocytes and correlates with the ability of the oocyte to undergo meiotic divisions (Brunet and Maro, 2007; Levi et al., 2013). In mitotic cells (for review see Gundersen and Worman, 2013) and in oocytes of most species studied so far (Miyazaki et al., 2000; Miyazaki et al., 2005; McNally et al., 2010; Tissot et al., 2017), nucleus positioning is microtubule-dependent. Mouse oocytes are an exception to this rule, since nucleus positioning is actin-dependent only.

4.1.1 The F-actin meshwork in mouse oocytes

Before meiosis resumption, the fully-grown prophase I oocyte is filled with a very dense F-actin meshwork (Figure 17). This meshwork is very similar to the F-actin meshwork that is required for spindle positioning and asymmetric division in meiosis I (see chapter III.4.2.1). Formin 2 and Spire1/2 cooperate at the surface of actin-coated vesicles to nucleate the straight actin filaments that compose the meshwork. Indeed, the invalidation or inhibition of both nucleators results in oocytes lacking the F-actin cytoplasmic meshwork (Azoury et al., 2008; Schuh and Ellenberg, 2008; Pfender et al., 2011; Almonacid et al., 2015). Moreover, the actin-coated vesicles are positive for the Rab GTPase member Rab11a and move in a myosin Vb-dependent manner (Schuh, 2011; Holubcova et al., 2013).

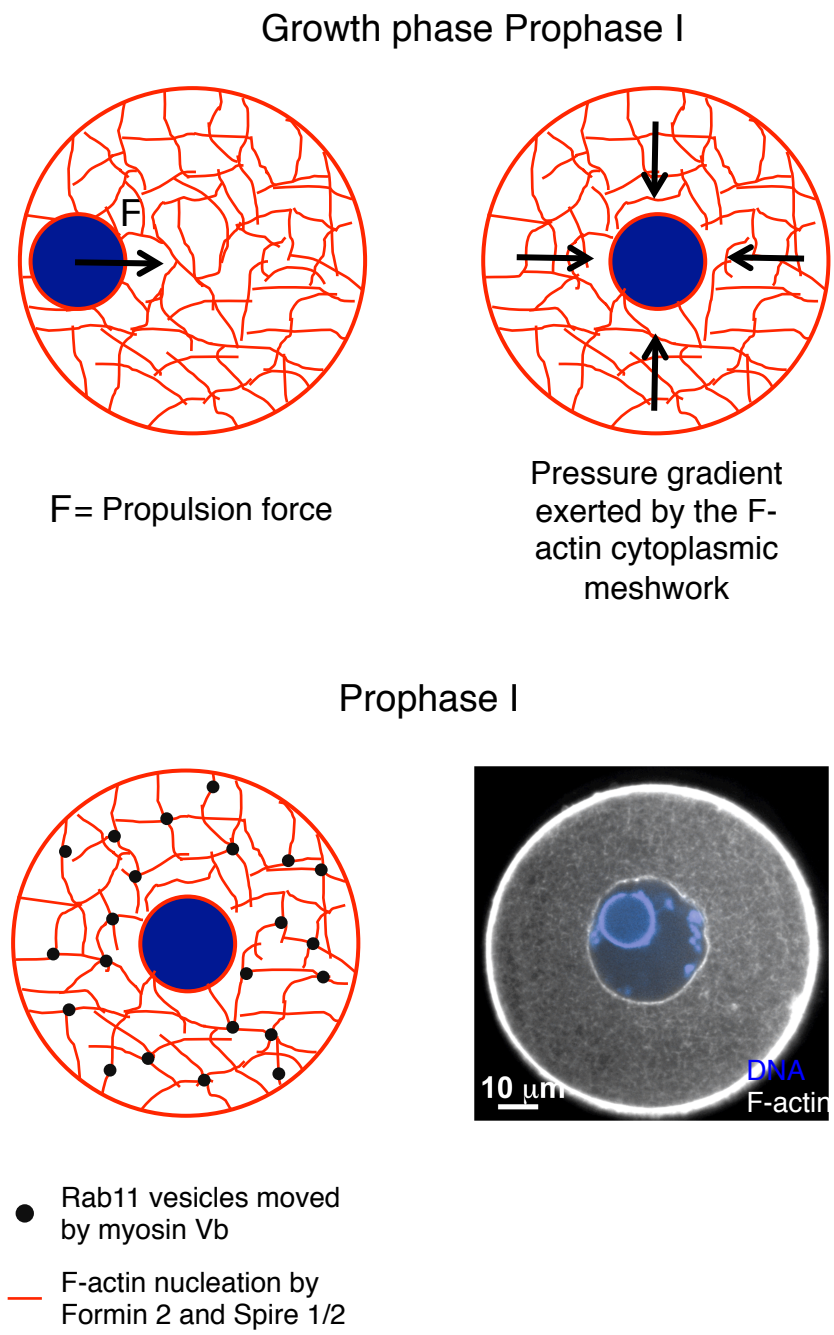

Figure 17: Nucleus positioning in mouse oocytes
Spinning disk image from the review Almonacid et al., 2017.

4.1.2 Mechanisms of actin-dependent nucleus positioning

It was shown that oocytes invalidated for Formin 2 (*Fmn2-/-*) have off-centered nuclei. The reintroduction of Formin 2 in these oocytes allows the reappearance of the actin mesh and recentering of the nucleus within 5 hours (Almonacid et al., 2015). This is because actin vesicles move in the cytoplasm with a velocity gradient and are biased towards the cortex in their directionality: they move fast towards the cortex from 10 μm below it and slow and randomly close to the oocyte center. This generates a pressure gradient and a propulsion force sufficient to center the nucleus (Figure 17). Interestingly, this centering mechanism is not nucleus-specific, meaning that any big object, such as oil droplets or beads, can be centered in oocytes via this mechanism (Almonacid et al., 2015; Colin et al., *In Preparation*). The motor for actin vesicle movement is myosin Vb, since the expression of a dominant-negative tail of myosin Vb impairs actin network dynamics (Holubcova et al., 2013). Myosin Vb is also responsible for fluidizing the cytoplasm by moving it around the actin vesicles, allowing the movement of big objects. Indeed, the expression of the dominant-negative tail of myosin Vb increases cytoplasmic viscosity as measured using optical tweezers, blocking cytoplasmic activity (Almonacid et al., 2015). As a consequence, the nucleus stays off-centered in these oocytes suggesting that myosin Vb favors nucleus movement by putting actin vesicles in motion and fluidizing the cytoplasm.

4.2. Spindle positioning

After centering of the nucleus during growth of prophase I arrested oocytes, meiosis resumption occurs. The first meiotic spindle forms where the nucleus was, at the approximate oocyte center, and organizes chromosomes. Interestingly, the genome is then off-centered with the progressive migration of the spindle from the center of the oocyte to the closest cortex.

4.2.1. Cytoplasmic actin

When oocytes enter meiosis, the actin meshwork is dismantled at NEBD and reforms progressively during meiosis I, mirroring Formin 2 regulation (degradation at NEBD and re-accumulation). This actin meshwork dismantlement is necessary for proper spindle migration since maintaining it impairs spindle movement, probably by exerting too much centripetal forces on the spindle, placing it at the exact geometrical center of the oocyte (Azoury et al., 2011). Thus spindle formation needs to be free of any constraints in order to break symmetry and allow the spindle to migrate.

a. The actin cage

The meiosis I meshwork appears to be quite similar to the prophase I meshwork and is composed of the same major players: Formin 2 and Spire1/2 at the surface of Rab11a/myosin Vb vesicles (Figure 18). However, after its reformation in meiosis I the cytoplasmic actin meshwork also comprises an actin cage surrounding the microtubule spindle, with actin filaments running along microtubules and penetrating within the spindle (Azoury et al., 2008; Schuh and Ellenberg, 2008; Mogessie and Schuh, 2017). This cytoplasmic actin cage is connected to the actin-rich cortex (Figure 18).

b. Myosin II

Although these meshes are comparable, they complete extremely different functions. The prophase I meshwork centers the nucleus, whereas the meiosis I cytoplasmic actin meshwork off-centers the spindle and chromosomes towards the cortex. In addition, meiosis I spindle movement takes 2-3 hours with a mean velocity of 0.12 μm/min (Verlhac et al., 2000). This is much faster than nucleus positioning occurring within 5 hours with a mean velocity of 0.07 μm/min (Almonacid et al., 2015).
This difference can be explained by the specific effect of myosin II on spindle migration. Indeed, the migration of the meiosis I spindle from the cell center to the cortex requires myosin II activity (Figure 18). Myosin II motors localize at both poles

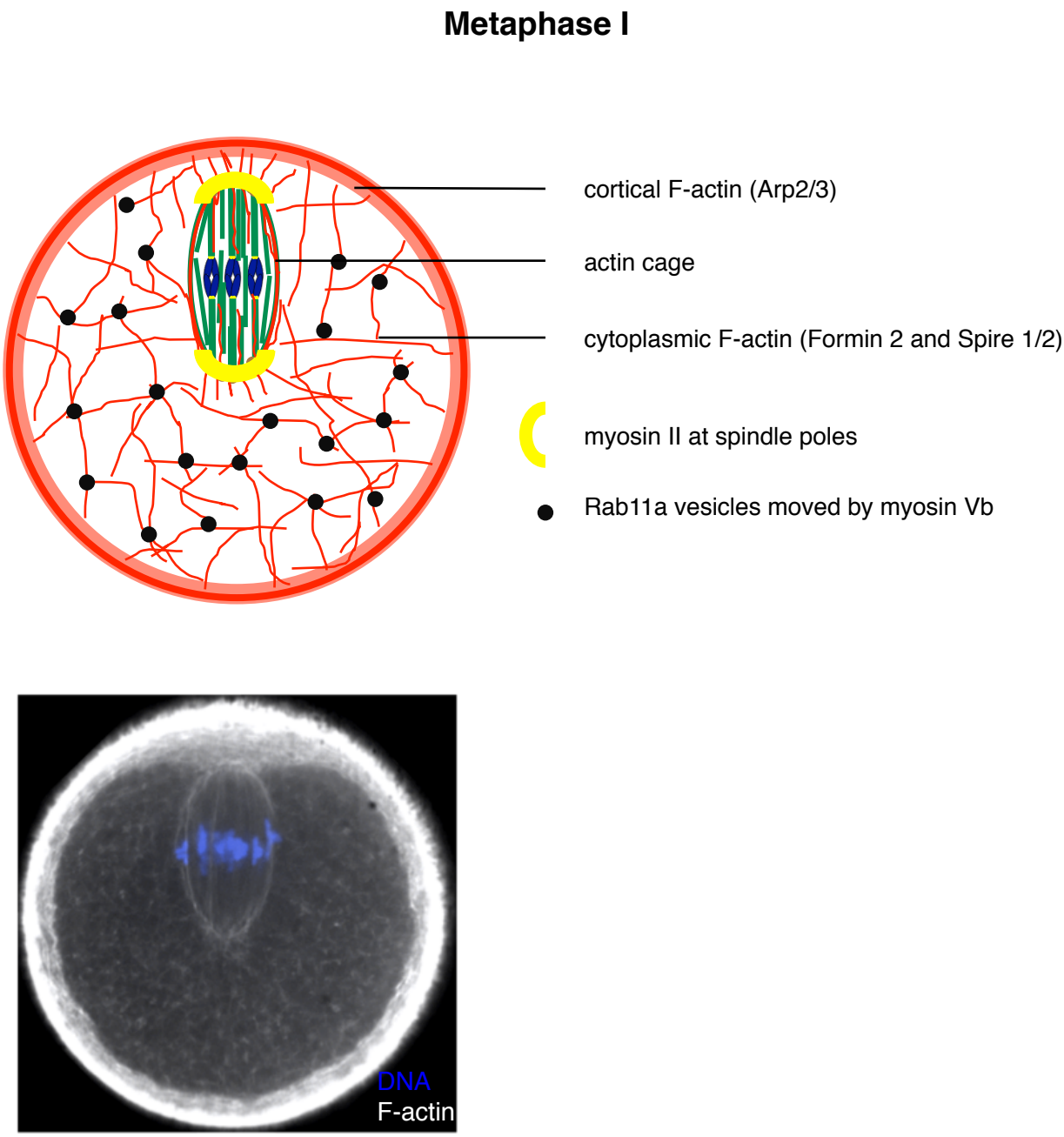

Figure 18: F-actin meshworks in metaphase I mouse oocytes
Spinning disk image from Chaigne et al., 2014. Actin is in red, DNA in blue, microtubules in green and myosin II in yellow.

of the actin cage and exert forces that position the spindle. Inhibition of myosin II activation by MLCK phosphorylation using the ML-7 inhibitor impairs spindle migration (Schuh and Ellenberg, 2008; Chaigne et al., 2013).

c. Myosin Vb

Myosin Vb motors have also been implicated in spindle positioning, by regulating actin meshwork dynamics. The expression of a dominant-negative tail of myosin Vb impairs actin network dynamics and prevents spindle migration in meiosis I mouse oocytes (Holubcova et al., 2013). In contrary to myosin II motors, the effect of myosin Vb is not specific to spindle migration but rather a global effect. Indeed, optical tweezers measurements have shown that the cytoplasm is more viscous in oocytes expressing a dominant-negative myosin Vb (Almonacid et al., 2015). This suggests that the entire meshwork is frozen, preventing the movement of any organelles including the spindle.

4.2.2. Cortical actin

a. Cortical actin thickening

In addition to the cytoplasmic actin network, a subcortical network nucleates progressively during meiosis I (Figure 19). The subcortical network is absent in prophase I and starts to nucleate slowly, becoming visible 3 hours after NEBD in mouse oocytes. At the end of meiosis I, this cortical actin thickening reaches its maximum thickness of 4 μm. At that stage, the actin thickening is uniform along the oocyte cortex except in the region where the spindle meets the cortex (Chaigne et al., 2013; Figure 18).

Interestingly, the subcortical network is nucleated by a different nucleator than the cytoplasmic meshwork. Indeed, inhibition of the branched nucleator Arp2/3 using the CK666 inhibitor (Nolen et al., 2009) does not affect cytoplasmic actin but prevents cortical actin thickening (Chaigne et al., 2013). Conversely, the cortical actin thickening is present in oocytes invalidated for Formin 2 (Chaigne et al., 2013). This

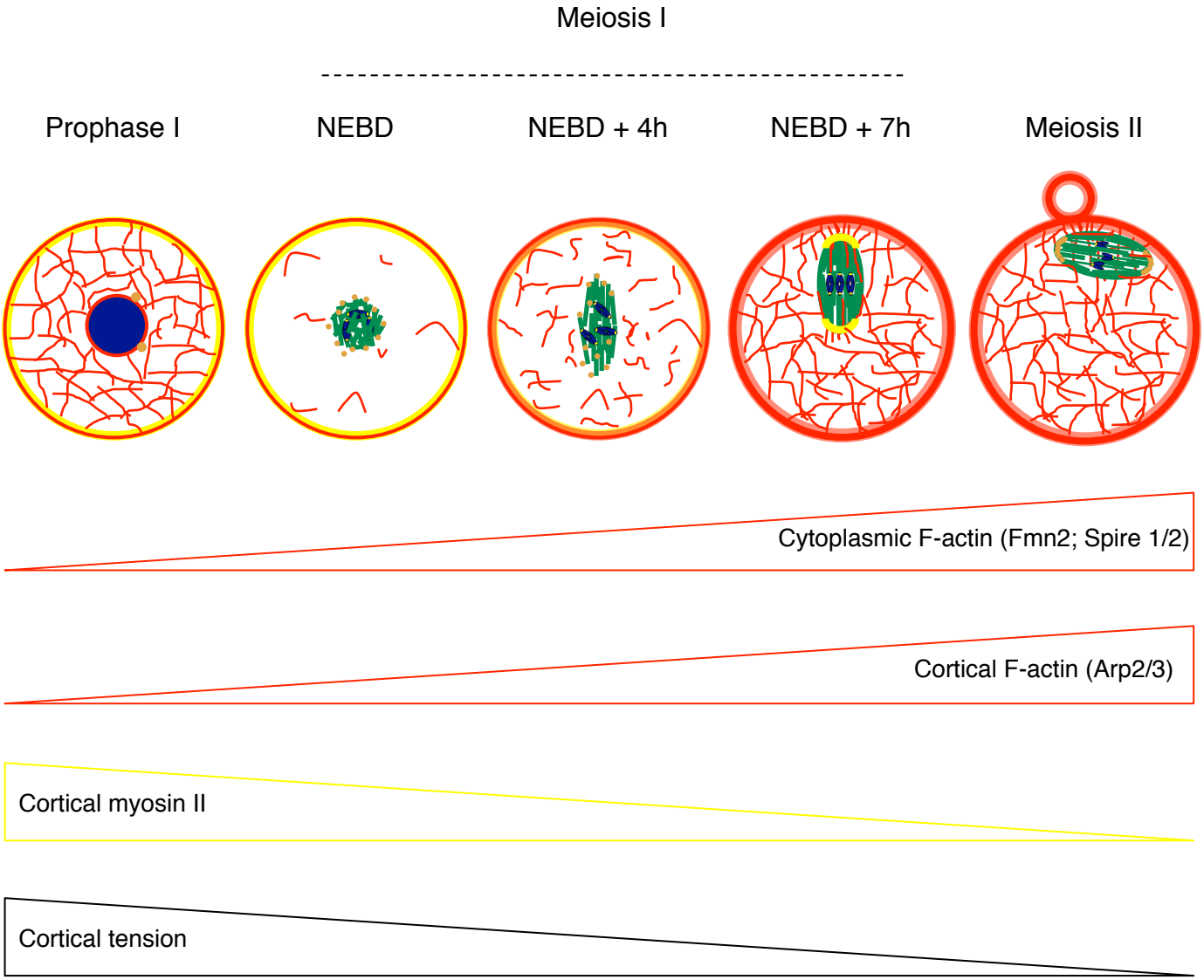

Figure 19: Spindle positioning is actin-dependent in mouse oocytes
Actin is in red, DNA in blue, microtubules in green, aMTOCs in brown and myosin II in yellow. NEBD stands for nuclear envelope breakdown.

suggests that the Arp2/3 complex is the major cortical actin nucleator. The Arp2/3 complex acts downstream of the Mos/MAPK signaling pathway. Indeed, the inhibition or the genetic invalidation of the Mos kinase impairs subcortical actin nucleation and the cortical actin thickening is nucleated concomitantly to MAPK activation, and Wave2 phosphorylation (Chaigne et al., 2013). The subcortical actin is required for spindle migration and its absence in oocytes inhibited for Arp2/3 or invalidated for Mos leads to symmetric divisions (Verlhac et al., 2000; Chaigne et al., 2013).

Since they are formed by distinct nucleators, the subcortical and cytoplasmic networks could be very different in terms of actin architecture. In particular the cytoplasmic actin nucleator Formin 2 nucleates linear filaments whereas the subcortical network nucleator Arp2/3 nucleates branched actin filaments. Furthermore, photoactivation experiments have shown that the cytoplasmic network is also more dynamic than the subcortical one (Chaigne et al., 2013). However, the precise architecture of both networks is still unclear, mostly because of limitations of the F-actin imaging approaches. In live mouse oocytes, the GFP-UtrCH probe is widely used to visualize F-actin (Azoury et al., 2008; Schuh and Ellenberg, 2008; Azoury et al., 2011; Pfender et al., 2011; Schuh, 2011; Holubcova et al., 2013; Chaigne et al., 2013; Chaigne et al., 2015; Almonacid et al., 2015; Mogessie and Schuh, 2017). This fluorescent F-actin probe relies on the calponin homology domain of utrophin (Utr-CH), which is an actin binding protein (Burkel et al., 2007). Although this probe was shown to label F-actin without stabilizing it *in vitro* (Burkel et al., 2007), its overexpression in mouse oocytes can over-stabilize F-actin (Holubcova et al., 2013; Mogessie and Schuh, 2017). Nonetheless, it is important to note that the structures detected using the GFP-UtrCH, such as the actin cage, were also visualized with fluorescent-tagged phalloidin in fixed oocytes (Schuh and Ellenberg, 2008).

At last, the two networks seem very distinct and well separated except where the spindle surrounded by the actin cage is anchored to the cortex. In this region, both networks meet and cytoplasmic actin filaments seem to penetrate the cortex (Chaigne et al., 2013). It would be interesting to know how this region of overlap is built and to gain more insight into the architecture of the actin network where the spindle is anchored to the cortex.

b. Cortical myosin II

In prophase I, myosin II is localized at the oocyte cortex and its repartition seems homogeneous (Larson et al., 2010; Chaigne et al., 2013). Concomitant to the cortical actin thickening, myosin II is progressively chased from the cell cortex (Figure 19). The Mos/MAPK pathway is necessary for myosin II displacement since it does not occur in *mos-/-* oocytes. Surprisingly, precocious nucleation of a cortical actin thickening leads to precocious exclusion of myosin II from the cortex (Chaigne et al., 2015). This result was obtained by expressing a construct called the cVCA (cortical VCA). In this construct, the VCA domain of Wave2, which is a nucleating promoting factor of Arp2/3, was fused to a cortical ERM protein, Ezrin (Figure 20). Expressing the cVCA in mouse oocytes activates the Arp2/3 complex specifically at the cortex independently of the Mos/MAPK pathway and chases myosin II. Hence, Arp2/3-dependent nucleation of cortical actin is sufficient to delocalize myosin II from the cortex in mouse oocytes (Chaigne et al., 2015).

However, the mechanisms of cortical myosin II exclusion are not known. One explanation could be that myosin II preferentially associates with the linear actin network rather than the thick branched actin network. Indeed, actin network architecture can determine myosin II activity (Reymann et al., 2012). In addition, it is not known if the cortical fraction of myosin II is displaced in the cytoplasm and spindle poles after exclusion and how much it represents relative to the total pool of myosin II. At last, the fraction of myosin II that is phosphorylated and active is not known.

Surprisingly, myosin II exclusion from the cortex by the cortical actin thickening leads to a decrease in cortical tension and cortex softening (Larson et al., 2010; Chaigne et al., 2013; Chaigne et al., 2015). This is addressed in details in the next two chapters.

c. Measuring cortical tension in oocytes

In the last decade, the mechanical properties of oocytes started to be explored. Several methods are used to measure cortical tension in cells, most of which consist on measuring the cells response to a mechanical perturbation (see Box1 in Clark et

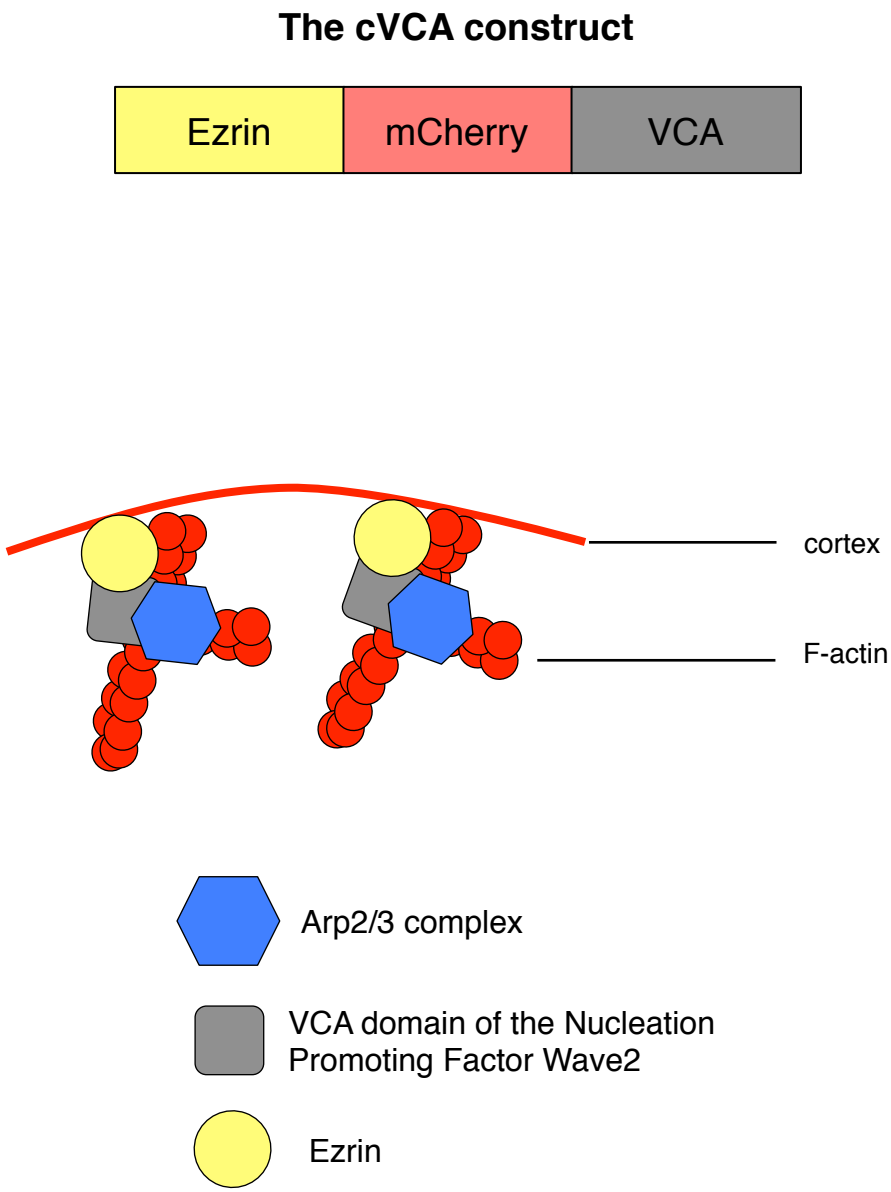

Figure 20: Actin nucleation at the cortex by the cVCA construct

al., 2014). For example, Atomic Force Microscopy (AFM) relies on the mechanical perturbation of a cell by compression. Pressure is applied to the cell by pressing a tip against its surface (Figure 21). By modeling the cell as a liquid drop, the surface tension can be assessed from the force applied and the shape of the compressed cell. During AFM measurements, cells need to resist the forces exerted by the tip. This is not an issue for adherent cells, but it raises a challenge for non-adherent cells such as oocytes because they tend to move laterally under compression forces. Thus non-adherent cells need to be immobilized to resist the compression forces. This was achieved in live mammalian cells by trapping cells in micro-wells or between micro-pillars (Rosenbluth et al., 2006; Li et al., 2013). Another perturbation consists on aspirating cells in a micropipette to extract their cortical tension (Figure 21). The cell is aspirated in a micropipette and the pressure required for cell aspiration is determined. Modeling the cell as a liquid drop and applying the law of Laplace then allows to extract cortical tension (Figure 21 and Michison and Swann, 1954). This last method has been applied in mouse and human oocytes (Larson et al., 2010; Chaigne et al., 2013; Chaigne et al., 2015; Yanez et al., 2016).

d. Cortical tension

The nucleation of the cortical actin thickening in meiosis I chases myosin II from the cortex of mouse oocytes, decreasing cortical tension (Chaigne et al., 2013). Micropipette aspiration showed that cortical tension decreases about sixfold in oocytes between prophase I and metaphase II (Larson et al., 2010). Contrary to cortical stiffening in mitosis, the cortex softens during meiosis I in mouse oocytes. *mos-/-* oocytes, which retain cortical myosin II, have a high cortical tension. cVCA oocytes, which precociously displace cortical myosin II, have a lower cortical tension and thus an extra-soft cortex (Chaigne et al., 2013; Chaigne et al., 2015). All theses results show that cortical actin nucleation and myosin II exclusion from the cortex lead to a decrease in cortical tension in mouse oocytes.

Interestingly, the spindle does not migrate in stiff *mos-/-* oocytes or in extra-soft cVCA oocytes (Verlhac et al., 2000; Chaigne et al., 2013; Chaigne et al., 2015). This suggests that cortical tension has to be gated to allow asymmetric spindle

Atomic Force Microscopy

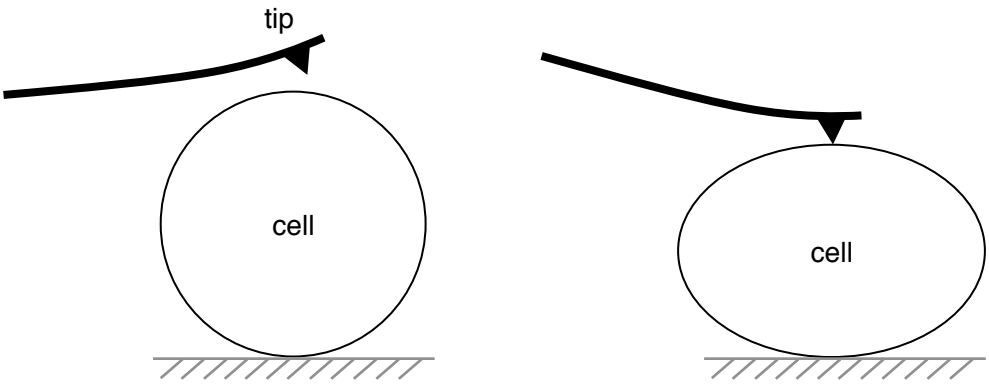

Micropipette aspiration

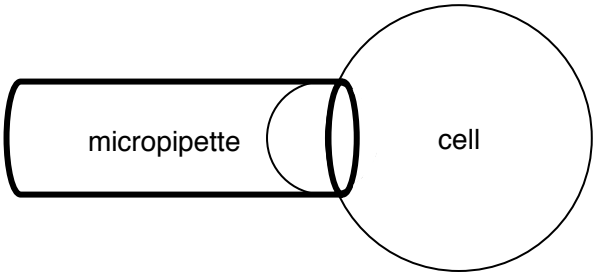

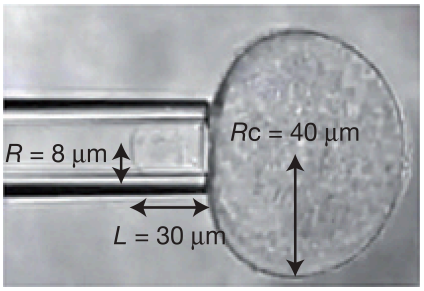

Micropipette aspiration of an oocyte (Chaigne et al., 2014)

Laplace law: $\Delta P_c = 2T_c \left(\frac{1}{R_p} - \frac{1}{R_c} \right)$

T_c: cortical tension
P_c: critical pressure
R_p: pipette radius
R_c: cell radius

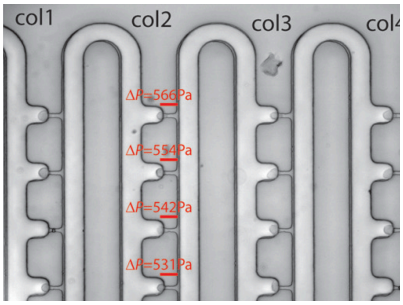

Microfluidic device measuring the cortical tension of Hela cells (Lee and Liu., 2014)

Figure 21: Measuring cortical tension in oocytes

positioning. Theoretical modeling supports these experimental results and predicts a narrow range of cortical tension allowing spindle migration (Figure 22 and Chaigne et al., 2015). In the 2D model, the spindle is modeled as an ellipse with its center of mass moving along its long axis under myosin II pulling forces exerted at both poles. Indeed the spindle always migrates along its long axis (Verlhac et al., 2000), probably due to the high viscosity of the oocyte cytoplasm (Chaigne et al., 2015). After NEBD, the first meiotic spindle forms where the nucleus was, in the central region of the oocyte, and in absence of constraints since the cytoplasmic actin meshwork is dismantled (Azoury et al., 2011). As such, it never forms at the perfect oocyte geometrical center but slightly off-centered (Verlhac et al., 2000) due to biological noise. At this stage, there are no cortical cues and no sign of polarization (Brunet et al., 2011; Fitzharris et al., 2007; Halet et al., 2007). However, because the spindle is slightly off-centered, one side of the spindle is closer to the cell cortex (Verlhac et al., 2000). Myosin II pulling at spindle poles is predicted to be more efficient at the pole closer to the cell cortex, creating a slight imbalance of forces at spindle poles. The decrease in cortical tension further amplifies this imbalance of forces to the benefit of the spindle pole that is closest to the cortex. Indeed, more actin accumulates in this region, offering a bigger overlap for myosin II to pull (Chaigne et al., 2015). This argues that the speed of spindle migration should increase when the spindle approaches the cortex, which is consistent with experimental data (Figure 22). The model also predicts that if cortical tension is too high or too low, such as in *mos-/-* or cVCA oocytes, the forces are balanced at spindle poles because myosin II cannot efficiently pull on the cortex leading to no spindle migration, which is what is observed experimentally (Figure 22).

The forces exerted at spindle poles by the actin network and myosin II were never measured in mouse oocytes. It would be interesting to measure them in oocytes with normal cortical tension as well as in stiff or soft oocytes to further validate this model.

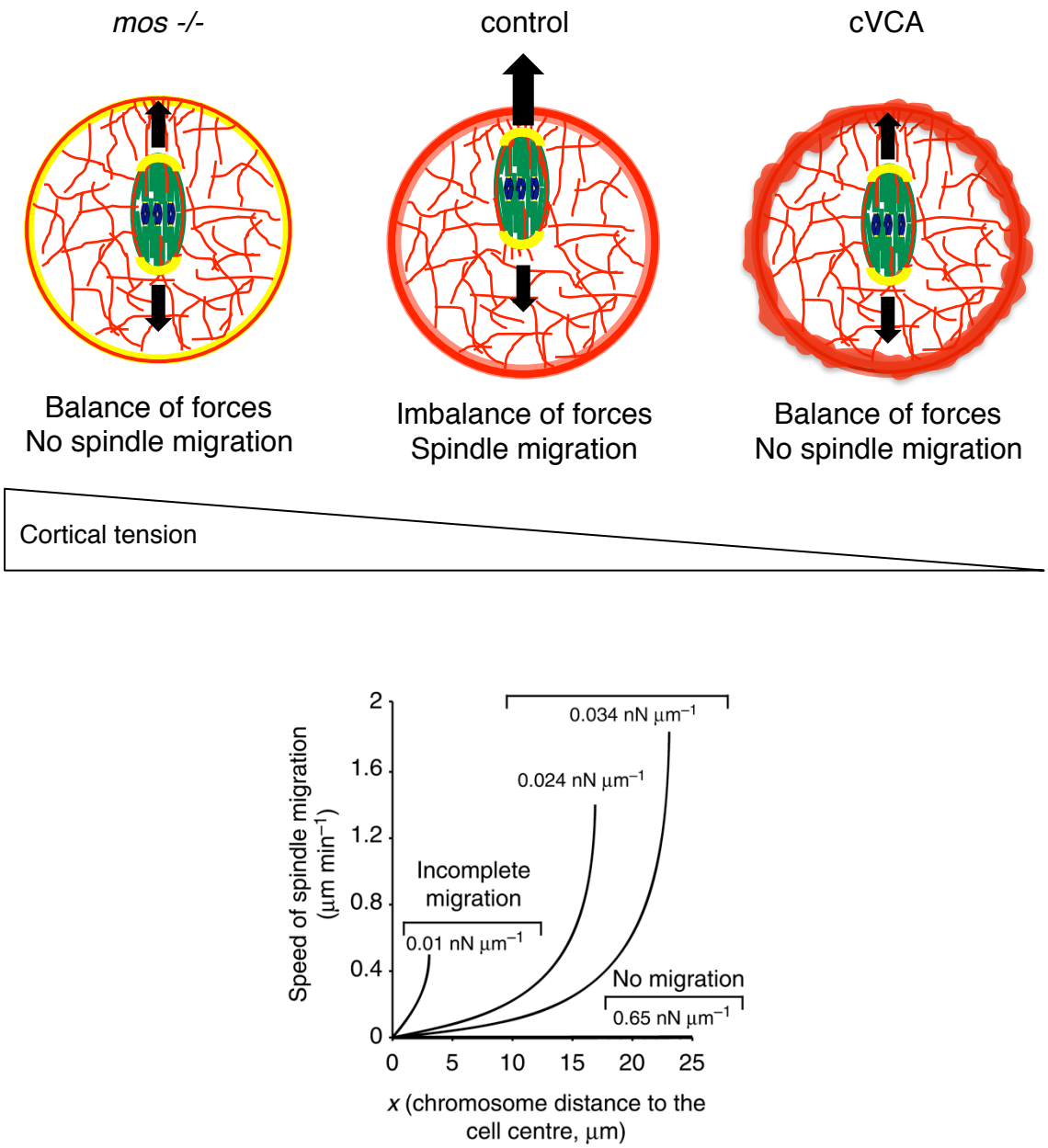

Figure 22: Cortical tension has to be tightly gated to allow asymmetric spindle positioning

Actin is in red, DNA in blue, microtubules in green and myosin II in yellow. The plot represents model prediction of spindle velocity as a function of spindle position for increasing values of cortical tension from Chaigne et al., 2015.

e. Cortical tension as a readout of oocyte quality

A recent study revealed that cortical tension can predict oocyte developmental potential after fertilization in mouse and human (Yanez et al., 2016). In this study, micropipette aspiration was used to measure mechanical properties of human and mouse oocytes and embryos because it is minimally invasive. In particular, mouse embryos implanted in female mice recipients after micropipette aspiration resulted in live birth. The study showed that oocytes or embryos that are too stiff or too soft do not develop past the blastocyst stage. Moreover, cortical mechanics abnormalities correlate with oocyte aging following ovulation in mouse (Mackenzie et al., 2016). Interestingly, aged oocytes have decreased levels of active myosin II and lower cortical tension. Thus supporting the importance of cortical tension to normal oocyte function.

Developmental potential of oocytes and embryos in assisted reproductive technologies is mostly scored based on morphological features such as oocyte and embryo shape and aspect (granular, dark…). However, the predictive value of such criteria is still controversial, mainly because they are very subjective. Measuring cortical mechanics in oocyte by micropipette aspiration is minimally invasive, precise and reproducible. Hence, it could be used as a marker of oocyte and embryo quality to improve assisted reproductive technologies. In the last years, microfluidic analysis of oocyte and embryo biomechanical properties emerged as a tool that could potentially replace traditional single cell approaches (Yanez and Camarillo, 2017). These kind of high throughput and automatized technics were already proposed to measure the mechanical properties of cancer cells. One example includes a microfluidic device trapping single cells in individual micropipette aspiration structures (Lee and Liu., 2015 and Figure 21). Such microfluidic approaches could allow rapid and reproducible measurement of cortical tension of oocytes.

5. Actin in spindle assembly and chromosome alignment

5.1. Mitotic cells

5.1.1. Cortical actin and cortical tension

We have seen before that cortical actin is essential for spindle positioning. In addition to this role, cortical actin is also involved in spindle assembly. In *Drosophila* cells, cortical actin and ERM proteins promotes cell rounding by increasing cortical rigidity during mitosis (Carreno et al., 2008; Kunda et al., 2008). In particular, cells lacking the ERM protein Moesin present spindle and chromosome defects (Lancaster et al., 2013). These cells are flat, thus the spindle cannot form properly in confinement and microtubules cannot reach and capture chromosomes.

Cortical F-actin and myosin II are also required for centrosome separation in *Drosophila* cells (Rosenblatt et al., 2004) and were found to contribute to extra-centrosome clustering in both *Drosophila* cells and cancer cell lines (Kwon et al., 2008).

A recent study found 49 genes involved in mitotic cell rounding, most of which affect cortical myosin II (Toyoda et al., 2017). Among them the endoplasmic reticulum protein FAM134A was identified as important for chromosome alignment and mitotic rounding by localizing cortical myosin II. It must be noted that the effects on chromosome alignment described above are probably indirect since spindle formation is impaired in most of these cases.

5.1.2. Cytoplasmic actin

In addition to the role of cortical actin in spindle assembly and its consequence on chromosome behavior, cytoplasmic actin was observed in spindles of various species. In yeast, actin cables were shown to control spindle morphogenesis (for review see Sandquist et al., 2011). Actin cables have also been reported in *Xenopus* embryos and in plants lacking centrioles (Woolner et al., 2008; for review see

Sandquist et al., 2011; Kunda and Baum, 2009). However, the precise role of actin in spindle function of mitotic cells is still far from clear.

5.2. Actin and chromosomes in oocytes

F-actin driven chromosome movement has been reported in mouse, rat (Ai et al., 2008), horse (Tremoleda et al., 2001), starfish (Lenart et al., 2005; Mori et al., 2011; Bun et al., 2018) and ascidians (Prodon et al., 2006), as well as in human, porcine and ovine oocytes (Mogessie and Schuh, 2017). I will focus on the cases of starfish and mouse oocytes, which have been very well studied.

5.2.1. The case of starfish oocytes

In starfish oocytes, chromosome gathering is achieved by a contractile actin mesh that delivers chromosomes to the spindle (Figure 23, Lénàrt et al., 2005; Mori et al., 2011; Bun et al., 2018). In prophase I, chromosomes are scattered inside a very large nucleus (approximately 70 μm in diameter). Upon NEBD, an F-actin meshwork captures chromosomes and contracts in an isotropic and homogenous manner. This contractile meshwork acts like a fishnet to gather and deliver chromosomes to the cortex where centriole-containing centrosomes are located (Figure 23). Then, centrosomes participate in chromosome capture once chromosomes are close enough to be reached by microtubules. This process of chromosome capture by microtubules needs to be carefully coordinated with chromosome transport by F-actin. Indeed, early capture by microtubules interferes with chromosome migration by F-actin and leads to chromosome loss. Upon NEDB, Arp2/3 nucleates an actin shell around the chromosomes, which sterically blocks microtubule-chromosome attachments (Burdyniuk et al., 2018). Interestingly, this coordination between actin and microtubule assembly could also be conserved in mouse oocytes. The actin meshwork is dismantled at NEBD and reforms progressively during meiosis I with an actin cage around the microtubule spindle. This actin meshwork dismantlement is necessary for chromosome migration (Azoury et al., 2011), probably allowing spindle formation free of any constraints.

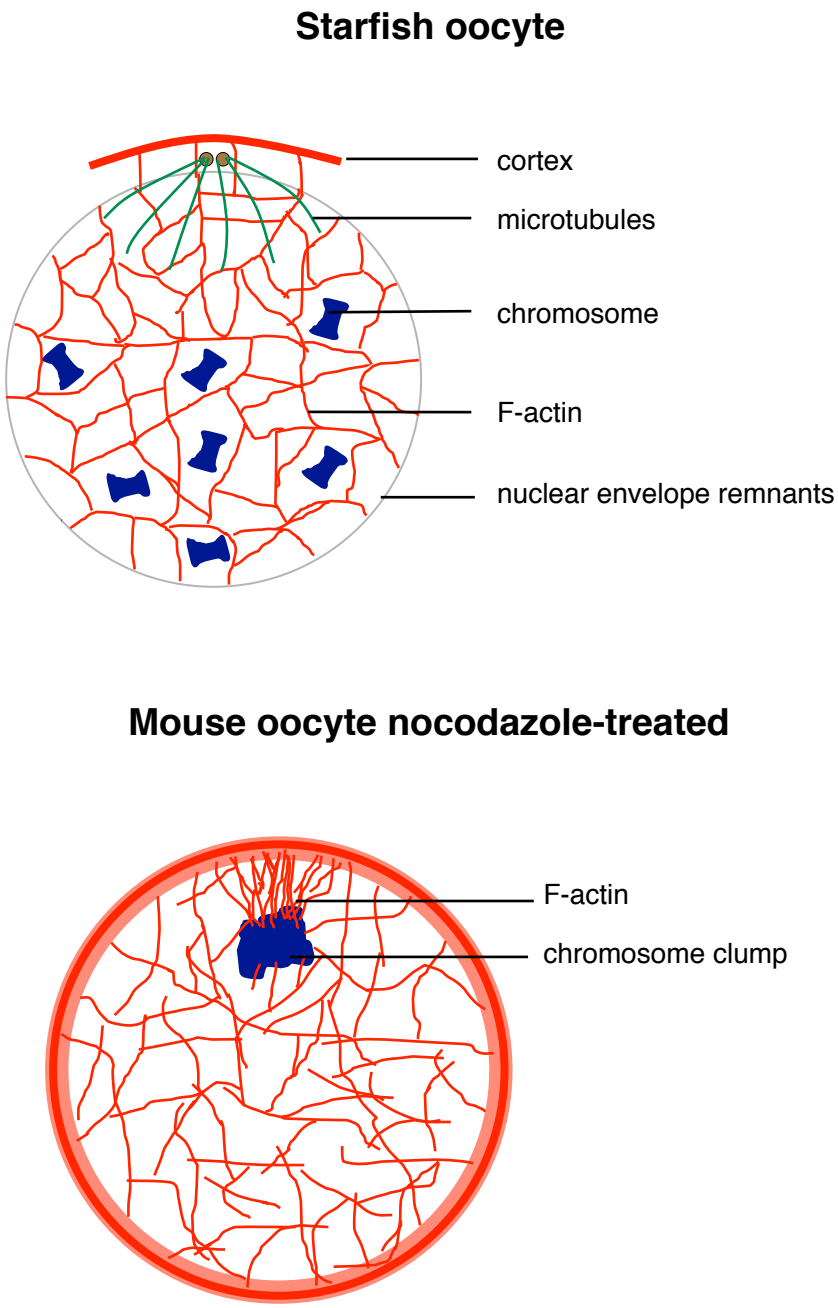

Figure 23: A close interaction between F-actin and chromosomes in oocytes

5.2.2. The case of mouse oocytes

Surprisingly, chromosomes are still able to migrate to the cortex in mouse oocytes treated with nocodazole to depolymerize spindle microtubules (Verlhac et al., 2000; Li et al., 2008; Azoury et al., 2008). Chromosomes are no longer under tension and form a chromatin mass transported to the cortex by the cytoplasmic F-actin meshwork (Figure 23). Contrary to starfish oocytes, the actin network is not contractile in mouse oocytes. This strongly argues that F-actin directly contacts chromosomes. However, it might represent an alternative mechanism, which is not normally required in spindle migration.

Moreover, a recent article suggests that cytoplasmic actin could play a role in chromosome segregation at anaphase I since mild chromosome lagging is observed in *fmn2-/-* oocytes (Mogessie and Schuh, 2017). In these oocytes lacking cytoplasmic actin (including the actin cage), the intensity of k-fibers seems significantly reduced, leading to an anaphase defect. Thus, the authors propose that F-actin could influence chromosome segregation by promoting k-fiber formation.

Overall, the contribution of cytoplasmic actin to chromosome segregation seems conserved in oocytes of many species. In particular, the “actin spindle” is present in mammalian oocytes suggesting that its function in chromosome segregation could be conserved. However, the mechanisms are still unclear. In particular, little is known about the possible direct interaction between actin and chromosomes. Indeed, chromosomes can still migrate to the cortex in mouse oocytes treated with a microtubule-depolymerizing drug (Verlhac et al., 2000; Li et al., 2008; Azoury et al., 2008). Hence, it would be interesting to further characterize the nature of the link between actin and chromosomes.

6. Formation of the actin cap and polarization of the oocyte

Upon meiosis I resumption, oocytes are not polarized (Brunet et al., 2011; Fitzharris et al., 2007; Halet et al., 2007). A thin actin layer and microvilli uniformly cover the cortex. At the end of meiosis I, the spindle reaches the cortex. The Ran-GTP gradient embarked by the chromosomes signals to the cortex, inducing a cortical differentiated

zone called the “actin cap” (Deng et al., 2007). This is the first sign of oocyte polarization. In particular, the cortical region above the chromosomes is devoid of microvilli and enriched in F-actin and myosin II (for review see Chaigne et al., 2012). After polar body extrusion, the meiosis II spindle forms underneath the cortex. Micropipette aspiration demonstrated that cortical tension is 2.5 fold higher in the region above the spindle compared to the opposite cortex (Larson et al., 2010). Thereby, oocytes are mechanically polarized in meiosis II although cortical tension seems homogenous before that stage.

7. Conclusion on meiotic spindle positioning and open questions

In conclusion, spindle positioning in oocytes is mediated by actin only. In particular, it relies on two actin networks: a cytoplasmic actin network and a subcortical actin network. In mammalian oocytes, the cytoplasmic network includes a very thigh connection between the microtubule spindle and the actin cage that could influence chromosome alignment and segregation. The nucleation of a cortical actin thickening leads to a decrease in cortical tension that could also impact spindle morphogenesis and chromosome alignment, as previously described in mitotic cells. Interestingly, it was recently shown that cortical tension influences the developmental potential of oocytes in mouse and human. However, very little is known about the origin of early developmental failure due to cortical tension defects. In particular, the consequences of aberrant cortical tension on chromosome alignment were never investigated in oocytes so far.

RESULTS

I. Shifting meiotic to mitotic spindle assembly in oocytes disrupts chromosome alignment

Context and question: Mitotic spindles assemble from two centrosomes, which are major microtubule organizing centers (MTOCs) that contain centrioles. Meiotic spindles in oocytes, however, lack centrioles. In mouse oocytes, spindle microtubules are nucleated from DNA and multiple acentriolar MTOCs, forming a microtubule ball. Then, microtubules align to form a central array along which acentriolar MTOCs are sorted and clustered prior to completion of spindle assembly in an 'inside-out' mechanism, ending with establishment of the poles. Is this unique "inside - out" spindle assembly required for meiotic spindle function, that is, segregating chromosomes?

Method: I used HSET (kinesin-14) as a tool to shift meiotic spindle assembly towards a mitotic 'outside-in' mode and analyzed the consequences on the fidelity of the division.

Results:

- HSET levels must be tightly gated in meiosis I. HSET inhibition impairs spindle bipolarization whereas slight HSET overexpression (HSET OE) induces extremely fast spindle bipolarization.
- Slight HSET OE forces spindle morphogenesis to become more mitotic-like with rapid spindle bipolarization and pole assembly coupled with focused poles.
- Switching towards mitotic-like spindle assembly in HSET OE oocytes results in severe chromosome alignment abnormalities.

Conclusion: The unique 'inside-out' mechanism of meiotic spindle assembly is essential to prevent chromosome misalignment and production of aneuploidy gametes.

Author contributions:

IB, AK, MHV, and MET designed the experiments, interpreted the results, and wrote the manuscript. IB, IQ, AK, and MET carried out the experiments. TB and PM designed the Fiji plug-in. MET and MHV supervised the project.

Published online: January 12, 2018

Article

TRANSPARENT PROCESS OPEN ACCESS

EMBO reports

Shifting meiotic to mitotic spindle assembly in oocytes disrupts chromosome alignment

Isma Bennabi[1], Isabelle Quéguiner[1], Agnieszka Kolano[2], Thomas Boudier[3], Philippe Mailly[1], Marie-Hélène Verlhac[1,†,*] & Marie-Emilie Terret[1,†,**]

Abstract

Mitotic spindles assemble from two centrosomes, which are major microtubule-organizing centers (MTOCs) that contain centrioles. Meiotic spindles in oocytes, however, lack centrioles. In mouse oocytes, spindle microtubules are nucleated from multiple acentriolar MTOCs that are sorted and clustered prior to completion of spindle assembly in an "inside-out" mechanism, ending with establishment of the poles. We used HSET (kinesin-14) as a tool to shift meiotic spindle assembly toward a mitotic "outside-in" mode and analyzed the consequences on the fidelity of the division. We show that HSET levels must be tightly gated in meiosis I and that even slight overexpression of HSET forces spindle morphogenesis to become more mitotic-like: rapid spindle bipolarization and pole assembly coupled with focused poles. The unusual length of meiosis I is not sufficient to correct these early spindle morphogenesis defects, resulting in severe chromosome alignment abnormalities. Thus, the unique "inside-out" mechanism of meiotic spindle assembly is essential to prevent chromosomal misalignment and production of aneuploidy gametes.

Keywords chromosome misalignment; HSET; meiosis; mitosis; spindle morphogenesis
Subject Category Cell Cycle
DOI 10.15252/embr.201745225 | Received 23 September 2017 | Revised 11 December 2017 | Accepted 13 December 2017 | Published online 12 January 2018
EMBO Reports (2018) 19: 368–381

Introduction

Animal cells generally assemble mitotic spindles using an "outside-in" mechanism that relies on centrosomes acting as dominant microtubule-nucleating centers (MTOCs). The two centrosomes define the spindle poles and thus the spindle axis along which chromosome segregation will take place at anaphase [1,2]. Oocytes however lack canonical centrosomes, the centrioles being lost before the meiotic divisions occur [3,4]. Interestingly, it was shown in *Drosophila* that maintaining functional supernumerary centrioles during female meiotic divisions leads to abnormal meiosis and aborted embryonic development [5], highlighting the fact that centriole loss is essential for successful sexual reproduction. In mouse oocytes, microtubules are nucleated from chromatin and multiple acentriolar microtubule-organizing centers (aMTOCs) composed of pericentriolar material [6–9]. These aMTOCs are perinuclear before meiotic divisions and fragment at NEBD (nuclear envelope breakdown) to become evenly distributed around chromatin [10,11]. Following NEBD, microtubules become nucleated and stabilized first around chromatin, forming a microtubule ball, and then organized into a stable central array via microtubule motors and microtubule-associated proteins, which sort and orient the microtubules [12–17]. aMTOCs are then progressively sorted along this central array [16]. Following spindle bipolarity setup, the aMTOCs become clustered to establish the spindle poles [17]. Meiotic spindles in oocytes are thus assembled "inside-out".

Spindle assembly in oocytes is a very slow process. Spindle bipolarization is achieved by 4 h in mice [12,13] and by around 7 h in humans [18], thus occupying about half the transition time from NEBD to anaphase in these species. It mirrors the long duration of the first meiotic division, as meiosis I requires 8–12 h in mice and more than 20 h in humans [18]. In addition, whereas spindle poles are organized by two centrosomes in mitosis, pole formation is different in meiosis. In mouse oocytes, poles are organized by multiple aMTOCs. Thus, meiotic spindle poles are often less focused than mitotic ones, having this typical barrel-shaped aspect. Are these unique "inside-out" spindle assembly and organization required for meiotic spindle function, that is, segregating chromosomes? To answer this question, we switched meiotic spindle assembly toward a more mitotic-like mode, with rapid bipolarity and focused pole assembly, and looked at chromosome alignment and segregation. To do so, deregulation of HSET levels was used as a tool to alter early stages of spindle morphogenesis. The kinesin-14 HSET is a minus-end-directed microtubule cross-linking motor important for regulating spindle assembly, spindle length, and pole organization [19–25]. During

1 Center for Interdisciplinary Research in Biology (CIRB), College de France, CNRS, INSERM, PSL Research University, Equipe labellisée FRM, Paris, France
2 International Institute of Molecular and Cell Biology, Warsaw, Poland
3 Université Pierre et Marie Curie, Sorbonne Universités, Paris, France
*Corresponding author. Tel: +33144271082; E-mail: marie-helene.verlhac@college-de-france.fr
**Corresponding author. Tel: +33144271692; E-mail: marie-emilie.terret@college-de-france.fr
†These authors contributed equally to this work as senior authors

© 2018 The Authors. Published under the terms of the CC BY 4.0 license

mitosis, HSET can slide anti-parallel microtubules apart and sort them into parallel bundles [26–28]. In contrast, when the orientation of two opposing microtubules is parallel, HSET cross-links them and transports them to the poles [23,26]. We show here that a slight increase in HSET levels accelerates spindle formation, in particular spindle bipolarization and aMTOCs clustering. Importantly, this leads to severe chromosome alignment abnormalities. In an unexpected manner, the unusual length of meiosis I (8 h) is not sufficient to correct early spindle morphogenesis defects, contributing to chromosome misalignment and mis-segregation. Thus, the unique "inside-out" spindle assembly and organization prevent aneuploidy in female gametes.

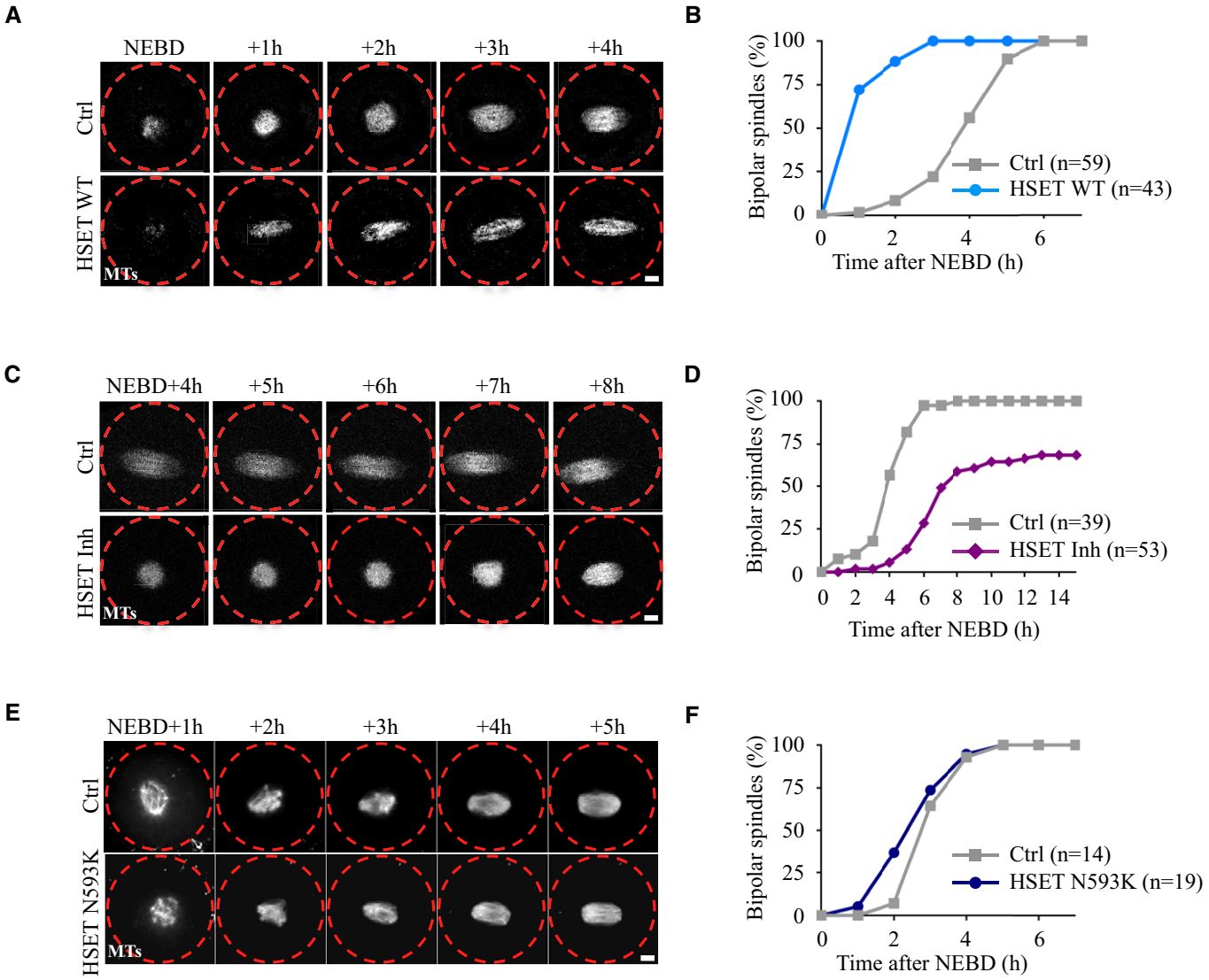

Figure 1. Modification of the timing of spindle bipolarization.

A Time-lapse spinning disk confocal microscopy of oocytes expressing GFP-EB3 (gray) alone (Ctrl, upper panel) or together with HSET WT (lower panel). Spindle bipolarization is advanced in HSET WT expressing oocytes compared to controls. Scale bar 10 μm.

B Graph showing the kinetics of spindle bipolarization in controls (gray squares) vs. HSET WT oocytes (blue dots). The kinetics of bipolarization is accelerated in oocytes overexpressing HSET WT compared to controls.

C Time-lapse spinning disk confocal microscopy of oocytes expressing GFP-EB3 (gray) treated (HSET Inh, lower panel) or not (Ctrl, upper panel) with the HSET inhibitor AZ82. Spindle bipolarization is delayed in oocytes inhibited for HSET. Scale bar 10 μm.

D Graph showing the kinetics of spindle bipolarization in controls (gray squares) vs. oocytes inhibited for HSET (purple diamonds). The kinetics of bipolarization is delayed in oocytes inhibited for HSET compared to controls.

E Time-lapse spinning disk confocal microscopy of control oocytes (Ctrl, upper panel) and oocytes expressing HSET N593K (HSET N593K, lower panel). Spindle bipolarization is slightly advanced in oocytes overexpressing HSET N593K compared to controls. All oocytes were incubated with SiR-Tubulin (gray). Scale bar 10 μm.

F Graph showing the kinetics of spindle bipolarization in controls (gray squares) vs. HSET N593K oocytes (dark blue dots). The kinetics of bipolarization is modestly affected in oocytes overexpressing HSET N593K compared to controls.

© 2018 The Authors

Results

Altering the timing of spindle bipolarization

To modify spindle morphogenesis, we developed an HSET gain-of-function approach. The localization of endogenous HSET was first analyzed in mouse oocytes, by performing immunofluorescence experiments on fixed oocytes. We found that endogenous HSET is localized on the spindle in meiosis I (Fig EV1A, left panel). HSET dynamics and localization were followed in living oocytes, by expressing an exogenous GFP-tagged HSET wild-type (WT) construct. Our exogenous GFP-HSET WT probe displayed the same spindle localization as endogenous HSET (Fig EV1A, middle panel, immunofluorescence) and remained associated with the spindle throughout meiosis I (Fig EV1B, live microscopy). However, HSET WT exogenous expression must be tightly controlled, since too much of it induced spindle collapse and mono-aster formation (see Materials and Methods). We therefore performed experiments with a maximum HSET WT overexpression of 1.6-fold in the whole oocyte (Fig EV1C, immunofluorescence quantification) corresponding to a 4.2-fold accumulation of HSET in the spindle (Fig EV1D, immunofluorescence quantification). Meiotic spindle assembly in the context of an HSET WT overexpression was analyzed by time-lapse spinning disk microscopy. In controls, microtubules formed bipolar spindles within ~4 h after NEBD (Fig 1A, upper panel). In contrast, spindle bipolarization took place much more rapidly in oocytes overexpressing HSET WT (Fig 1A, lower panel and B), skipping the microtubule ball stage described in Ref. [13]. Indeed, the average time of bipolarization setup was achieved in 4 h and 3 min in controls compared to 1 h and 19 min in oocytes overexpressing HSET WT (Figs 1B and EV2A).

The gain-of-function analysis was complemented with an HSET loss-of-function approach. To do so, oocytes were treated with AZ82, a small molecule inhibitor of HSET [29,30], and meiotic spindle assembly was followed using time-lapse spinning disk microscopy. Spindle bipolarization was delayed in HSET-inhibited oocytes (HSET Inh) compared to controls (Ctrl, Fig 1C), requiring 6 h and 55 min in these oocytes (Figs 1D and EV2A). The delay of spindle bipolarization observed with AZ82 could be phenocopied using another allosteric inhibitor of HSET, CW069 (Fig EV2C and D), structurally unrelated to AZ82 [31]. Taken together, and in contrast to previously published observations [20], these results suggest that HSET levels modulate the timing of meiotic spindle bipolarity in meiosis I.

To understand how HSET drastically impacts the timing of spindle bipolarization, we took advantage of a GFP-HSET mutant N593K (HSET N593K) that can cross-link but does not slide microtubules [23]. GFP-HSET N593K localized on the spindle (Fig EV1A, right panel, immunofluorescence) and had similar distribution along the spindle as GFP-HSET WT (compare Fig EV1B and EV1E, live microscopy). It reached even higher expression levels at NEBD+7h (Fig EV1F, quantification of live microscopy). The timing of spindle bipolarization was only slightly advanced in oocytes overexpressing HSET N593K compared to controls (Figs 1E and F, and EV2B). This suggests that, for the most part, changes in the timing of spindle bipolarization require microtubule sliding by HSET.

Accelerating spindle pole assembly

Because spindle bipolarization occurs precociously in oocytes overexpressing HSET WT, we next analyzed the consequences of its overexpression on sorting of the aMTOCs. This process occurs concomitant with spindle bipolarization and is followed by aMTOC clustering, which allows spindle pole focusing. To do this, the behavior of aMTOCs was followed by time-lapse microscopy, using mCherry-Plk4 (Polo-like kinase 4) as a marker [32]. We performed an automated 3D analysis of aMTOCs within the spindle. For that, we developed a Fiji plug-in that converts images obtained using live microcopy to binary images and in 3D finds the spindle poles and calculates the distance of each aMTOC to the closest pole (see Materials and Methods; Fig EV3A). In addition, this plug-in allows extraction of the number and distribution of the aMTOCs together with spindle measurements (length, central width, spindle pole width). The measurements were performed at three time points during meiosis I, spanning the critical steps of spindle morphogenesis in controls (Figs 2A and EV3C, middle panels).

At NEBD+1h30, microtubules form a ball, with aMTOCs dispersed around it [13]. At NEBD+4h30, spindle bipolarization is achieved and a robust central array of microtubules allows the progressive sorting of aMTOCs to the poles [16]. At NEBD+6h30,

Figure 2. Acceleration of aMTOCs sorting and clustering.

A Spinning disk confocal microscopy images showing spindle region magnifications of oocytes overexpressing HSET WT, controls and oocytes inhibited for HSET at NEBD+1h30, +4h30, and +6h30. All oocytes express GFP-EB3 (green) and mCherry-Plk4 (red). Scale bar 10 μm.

B aMTOC sorting in oocytes overexpressing HSET WT (blue dots) and controls (gray dots) at NEBD+1h30, +4h30, and +6h30. The dot plot represents the standard deviation of the repartition of aMTOCs along the axis of the spindle for each oocyte analyzed. Each dot represents an oocyte; the number of oocytes analyzed is written in parentheses. Statistical significance of differences is assessed with a *t*-test with Welch correction where needed: **P*-value = 0.018, ***P*-value = 0.002. As shown on the scheme, when aMTOCs are not sorted, the standard deviation is high; in contrast, when aMTOCs are sorted to the poles, the standard deviation is low.

C aMTOCs clustering in oocytes overexpressing HSET WT (blue dots) and controls (gray dots) at NEBD+1h30, +4h30, and +6h30. The dot plot represents the number of aMTOCs per oocyte. Each dot represents an oocyte; the number of oocytes analyzed for each condition is written in parentheses. Statistical significance of differences is assessed with a *t*-test with Welch correction: **P*-value = 0.011, ***P*-value = 0.003, ****P*-value < 0.0001.

D Super resolution images of aMTOCs using SIM, in fixed controls and HSET WT expressing oocytes (pericentrin antibody: gray). Scale bar 5 and 2 μm.

E Quantification of aMTOCs volume from SIM super-resolution images. Control oocytes gray dots and HSET WT expressing oocytes blue dots. Statistical significance of differences is assessed with a *t*-test with Welch correction: **P*-value = 0.0453.

F FRAP analysis of SiR-Tubulin in controls (gray) and in oocytes overexpressing HSET WT (blue) at NEBD+6h30. SiR-Tubulin was photobleached at spindle poles, and its fluorescence recovery was followed. The SiR-Tubulin fluorescence intensity was normalized so that 1 corresponds to the prebleached value and 0 corresponds to the value at the first time point after bleaching. For a single exponential recovery model, the halftime to fluorescence recovery in controls oocytes is $t_{1/2}$ = 62 s compared to $t_{1/2}$ = 55 s for oocytes overexpressing HSET WT. Data are represented as mean ± SD. Statistical significance of differences for the $t_{1/2}$ is assessed with a Mann–Whitney test: *P*-value = 0.87.

 © 2018 The Authors

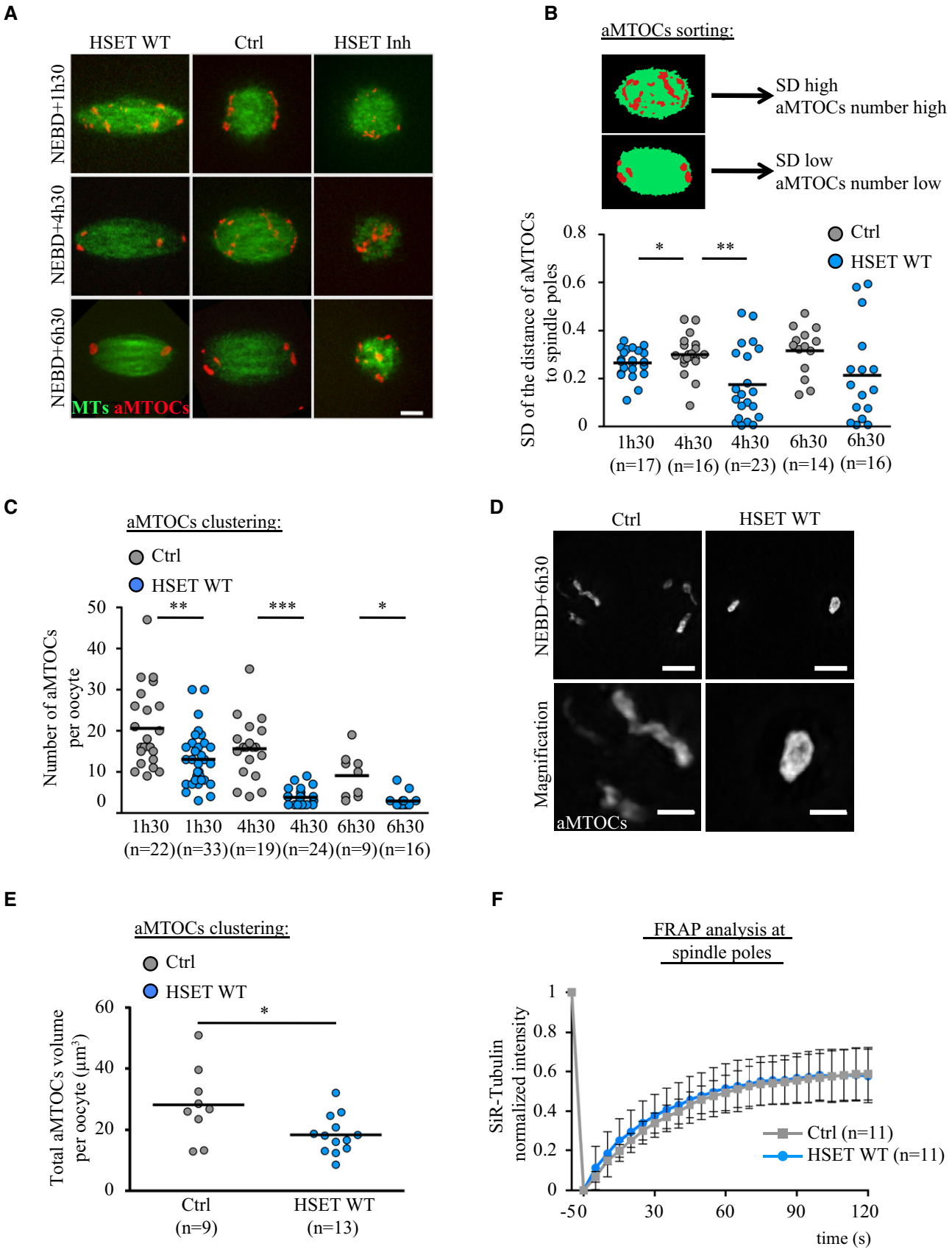
A
HSET WT
Ctrl
HSET Inh
NEBD+1h30
NEBD+4h30
NEBD+6h30
MTs aMTOCs
B
aMTOCs sorting:
SD high
aMTOCs number high
SD low
aMTOCs number low
SD of the distance of aMTOCs to spindle poles
Ctrl
HSET WT
1h30 (n=17)
4h30 (n=16)
4h30 (n=23)
6h30 (n=14)
6h30 (n=16)
C
aMTOCs clustering:
Ctrl
HSET WT
Number of aMTOCs per oocyte
1h30 (n=22)
1h30 (n=33)
4h30 (n=19)
4h30 (n=24)
6h30 (n=9)
6h30 (n=16)
D
Ctrl
HSET WT
NEBD+6h30
Magnification
aMTOCs
E
aMTOCs clustering:
Ctrl
HSET WT
Total aMTOCs volume per oocyte (µm³)
Ctrl (n=9)
HSET WT (n=13)
F
FRAP analysis at spindle poles
SiR-Tubulin normalized intensity
Ctrl (n=11)
HSET WT (n=11)
time (s)

Figure 2.

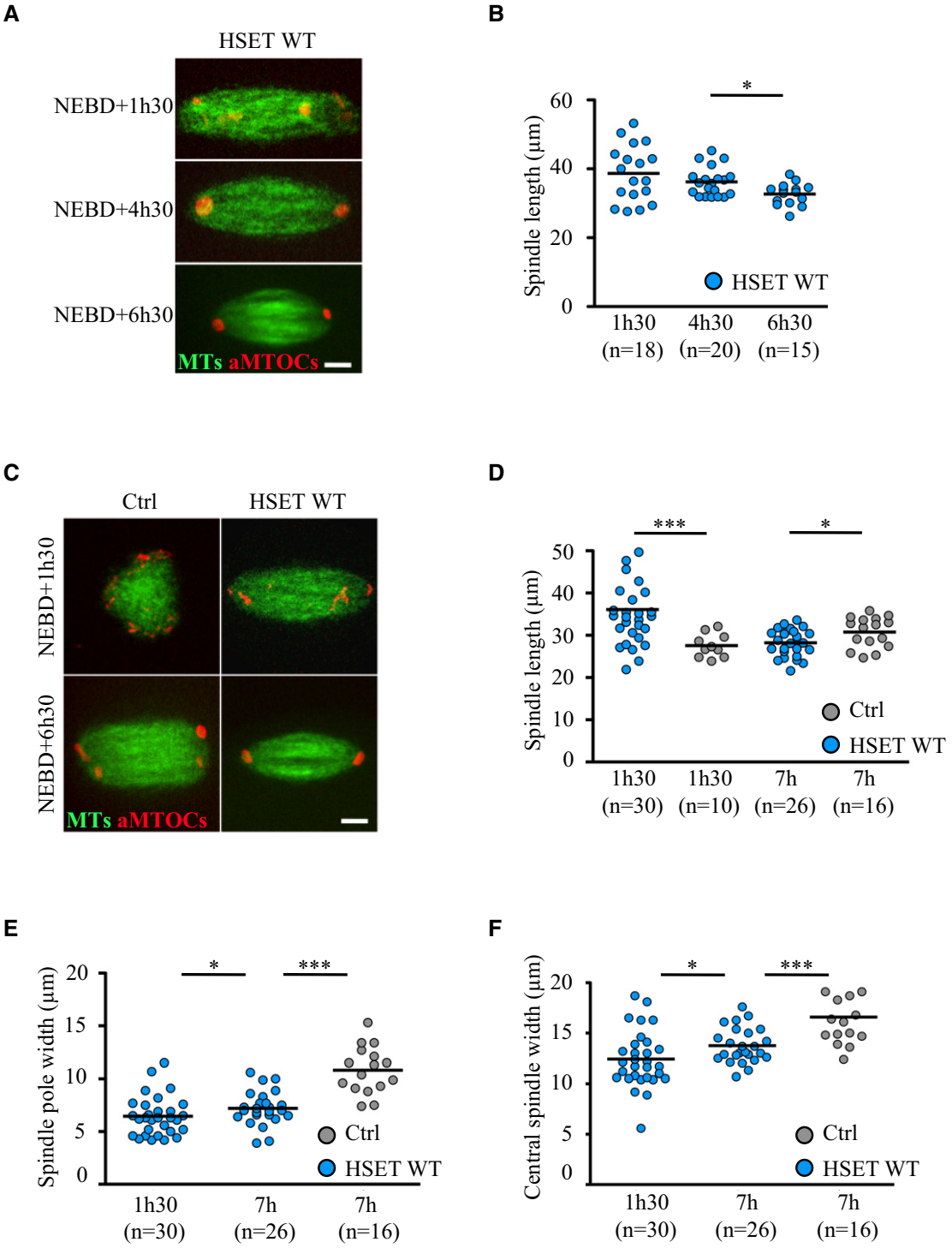

Figure 3. Turning meiosis I spindles into more mitotic ones.

A Spinning disk confocal microscopy images showing spindle region magnifications of oocytes expressing GFP-EB3 (green), mCherry-Plk4 (red), and HSET WT at NEBD+1h30, +4h30, and +6h30. Scale bar 10 µm.

B Quantification in 3D of spindle length in oocytes expressing HSET WT (blue dots) at NEBD+1h30, +4h30, and +6h30. Each dot represents an oocyte; the number of oocytes analyzed is written in parentheses. Statistical significance of differences is assessed with a Mann–Whitney test: *P-value = 0.011.

C Spinning disk confocal microscopy images showing spindle region magnifications of oocytes expressing GFP-EB3 (green) and mCherry-Plk4 (red) together with HSET WT (HSET WT, right panels) or not (Ctrl, left panels) at NEBD+1h30 and NEBD+6h30. Scale bar 10 µm.

D–F Quantification in 3D of spindle length (D) *P-value = 0.022, ***P-value < 0.0001; spindle pole width (E) *P-value = 0.046, ***P-value < 0.0001 and central spindle width (F) *P-value = 0.037, ***P-value < 0.0001 in oocytes overexpressing HSET WT (blue dots) and controls (gray dots) at NEBD+1h30 and NEBD+7h. Each dot represents an oocyte; the number of oocytes analyzed is written in parentheses. Statistical significance of differences is assessed with a Mann–Whitney test.

 © 2018 The Authors

the spindle poles begin to focus following clustering of the aMTOCs. In oocytes inhibited for HSET by treatment with AZ82, the spindle was not yet bipolar at NEBD+6h30 (Figs 2A and EV3C, right panels). Instead, these spindles remained in a ball-shape, as quantified in Fig EV3D. The diameter of the microtubule mass even decreased slightly between the first and last time points in the HSET-inhibited oocytes (Fig EV3D, purple dots, 25 μm at NEBD+1h30 vs. 22 μm at NEBD+6h30), whereas in control oocytes, the spindle elongated (Fig EV3D, gray dots, 26 μm at NEBD+1h30 vs. 33 μm at NEBD+6h30). Therefore, measurements of aMTOCs sorting and clustering were not relevant in oocytes inhibited for HSET and we focused our analysis on oocytes overexpressing HSET WT where spindle bipolarization is advanced.

We first analyzed aMTOC sorting in controls and HSET WT oocytes (Figs 2A and EV3C, middle and left panels). To do so, the distribution of the aMTOCs was measured in 3D along the long axis of the spindle at the time points where the spindle is bipolar (Fig EV3B, each dot corresponds to one aMTOC, the horizontal axis represents an hemi-spindle from the central spindle to the pole, the distance of aMTOCs to the nearest spindle pole is normalized by the spindle length, and no measurements were conducted at NEBD+1h30 in controls since at that stage spindles are not yet bipolar). In controls, the spindle was bipolar at NEBD+4h30 and the aMTOCs were scattered along the spindle's long axis (Fig EV3B, upper panel, all the gray dots are homogeneously distributed along the hemi-spindle). At NEBD+6h30, the aMTOCs were partially sorted and began to accumulate at spindle poles (Fig EV3B, upper panel, gray dots). We also plotted the standard deviation of the distribution of aMTOCs along the axis of the spindle for each oocyte analyzed (Fig 2B, each dot represents one oocyte). Before aMTOCs are sorted, the standard deviation is high; in contrast, once they are sent to the poles, the standard deviation is low (Fig 2B, scheme). In controls, the difference between NEBD+4h30 and +6h30 was small, highlighting the fact that aMTOC sorting is a long and progressive process (Fig 2B, gray dots). In oocytes overexpressing HSET, the spindle was already bipolar at NEBD+1h30 and aMTOCs were scattered along its long axis (Fig EV3B, lower panel, blue dots are homogeneously distributed along the hemi-spindle), resembling the NEBD+4h30 time point in controls. At NEBD+4h30, the aMTOCs were partially sorted as indicated by their substantial accumulation at spindle poles (Fig EV3B, lower panel, blue dots), resembling the NEBD+6h30 time point in controls. By NEBD+6h30, aMTOCs were further sorted (Fig EV3B, lower panel, blue dots). The standard deviation of the distribution of aMTOCs along the axis of the spindle for each oocyte showed the same behavior (Fig 2B, blue dots): The standard deviation at NEBD+1h30 in oocytes overexpressing HSET WT was comparable to the standard deviation at NEBD+4h30 in the controls, and at NEBD+4h30 and 6h30, it was smaller than in the controls. Altogether, these results show that aMTOC sorting takes place precociously in oocytes overexpressing HSET WT.

We then analyzed aMTOC clustering in controls and oocytes overexpressing HSET WT (Figs 2A and EV3C, middle and left panels). To do so, the number of aMTOCs per oocyte was counted in 3D (Fig 2C, each dot represents one oocyte). In controls, the number of aMTOCs diminished in parallel with meiosis I progression (Fig 2C, gray dots). This shows that aMTOCs tend to fuse and cluster during meiosis I. In oocytes overexpressing HSET WT, this process started earlier when the spindle bipolarized around NEBD+1h30, as evidenced by a reduced number of aMTOCs (Fig 2C, compare blue and gray dots). Later during meiosis I, the clustering of aMTOCs continued to be enhanced compared to controls (Fig 2C, compare blue and gray dots). Interestingly, aMTOCs were also more compact in oocytes overexpressing HSET WT compared to controls (Fig 2A and D). First, their organization was different: in controls, aMTOCs formed a typical O-shaped structure circumscribing the poles [9], whereas in oocytes overexpressing HSET WT, they formed a single round entity (Fig 2A and D). Second, they occupied a smaller volume as quantified from the N-SIM super-resolution images (Fig 2E). This suggests that HSET may play a role in the spacing of aMTOCs at spindle poles.

We next assessed whether microtubule dynamics was altered in the hyper-clustered spindle poles of oocytes overexpressing HSET WT. To compare microtubule dynamics, we performed FRAP of SiR-Tubulin at spindle poles at NEBD+6h30 (Fig 2F). Essentially identical recovery curves were observed in oocytes overexpressing HSET WT and controls, indicating that microtubule dynamics at spindle poles was similar in the two groups. This strongly suggests that changes in microtubule nucleation or stability are not the root of the difference in spindle pole focusing.

Figure 4. HSET levels must be tightly gated during early stages of spindle morphogenesis.

A Immunofluorescence on fixed control oocytes showing that endogenous HSET (HSET antibody: gray) is present in mouse oocytes from Prophase I and localized on the spindle at NEBD+1h, NEBD+5h, NEBD+8h, metaphase of meiosis II (MII), and in the nucleus 6 h after parthenogenetic activation. Scale bar 10 μm.

B Endogenous HSET levels progressively increase throughout meiosis I. Endogenous HSET intensity measured for fixed control oocytes in Prophase I, at NEBD+1h, NEBD+5h, NEBD+8h, metaphase of meiosis II (MII), and after activation. Data are represented as mean ± SD. Statistical significance of differences is assessed with a Mann–Whitney test: **P*-value = 0.017, ***P*-value = 0.0017, ****P*-value < 0.0001. The ratio of HSET expression between NEBD+8h and NEBD+1h is 1.7, the ratio of HSET expression between NEBD+1h and Prophase I is 1.6, and the ratio of HSET expression between activated and Prophase I oocytes is 1.28.

C Scheme of the experimental setup for early and late HSET perturbations. DNA is in blue, microtubules in green, aMTOCs in red, NEBD stands for nuclear envelope breakdown.

D Spinning disk confocal microscopy images showing spindle region magnifications of oocytes expressing HSET WT (late HSET OE, cRNA injected at NEBD+4h, left panel), controls (middle panel) and oocytes inhibited for HSET at NEBD+4h (late HSET Inh, right panel), all imaged at NEBD+6h30. All oocytes express mCherry-Plk4 (red), Ctrl and late HSET Inh oocytes express GFP-EB3 (green), and late HSET OE oocytes express GFP-HSET WT (green). Scale bar 10 μm.

E GFP-HSET WT total fluorescence intensity measured in the whole cell was assessed after cRNA injection in early overexpression oocytes (cRNA injected in Prophase I, gray bars) and late overexpression oocytes (cRNA injected at NEBD+4h, blue bar). The number of oocytes analyzed is written in parentheses. The total GFP-HSET WT fluorescence intensity for early HSET overexpression oocytes at NEBD+1h is 2.77 ± 1.47 arbitrary units (a.u.) and 2.40 ± 0.97 a.u. at NEBD+7h compared to 3.95 ± 1.70 a.u. for late HSET overexpression oocytes. Standard deviation is plotted on each bar. Statistical significance of differences is assessed with a Mann–Whitney test: not significant (n.s.) *P*-value = 0.408, **P*-value = 0.048, ****P*-value < 0.0001.

F, G Quantification of the spindle length (F) and spindle pole width (G) in late HSET WT overexpression oocytes (cRNA injected at NEBD+4h) and controls at NEBD+6h30. Statistical significance of differences is assessed with a *t*-test: for (F), not significant (n.s.) *P*-value = 0.06; for (G), not significant (n.s.) *P*-value = 0.96. Each dot represents an oocyte, and the number of oocytes analyzed is written in parentheses.

© 2018 The Authors

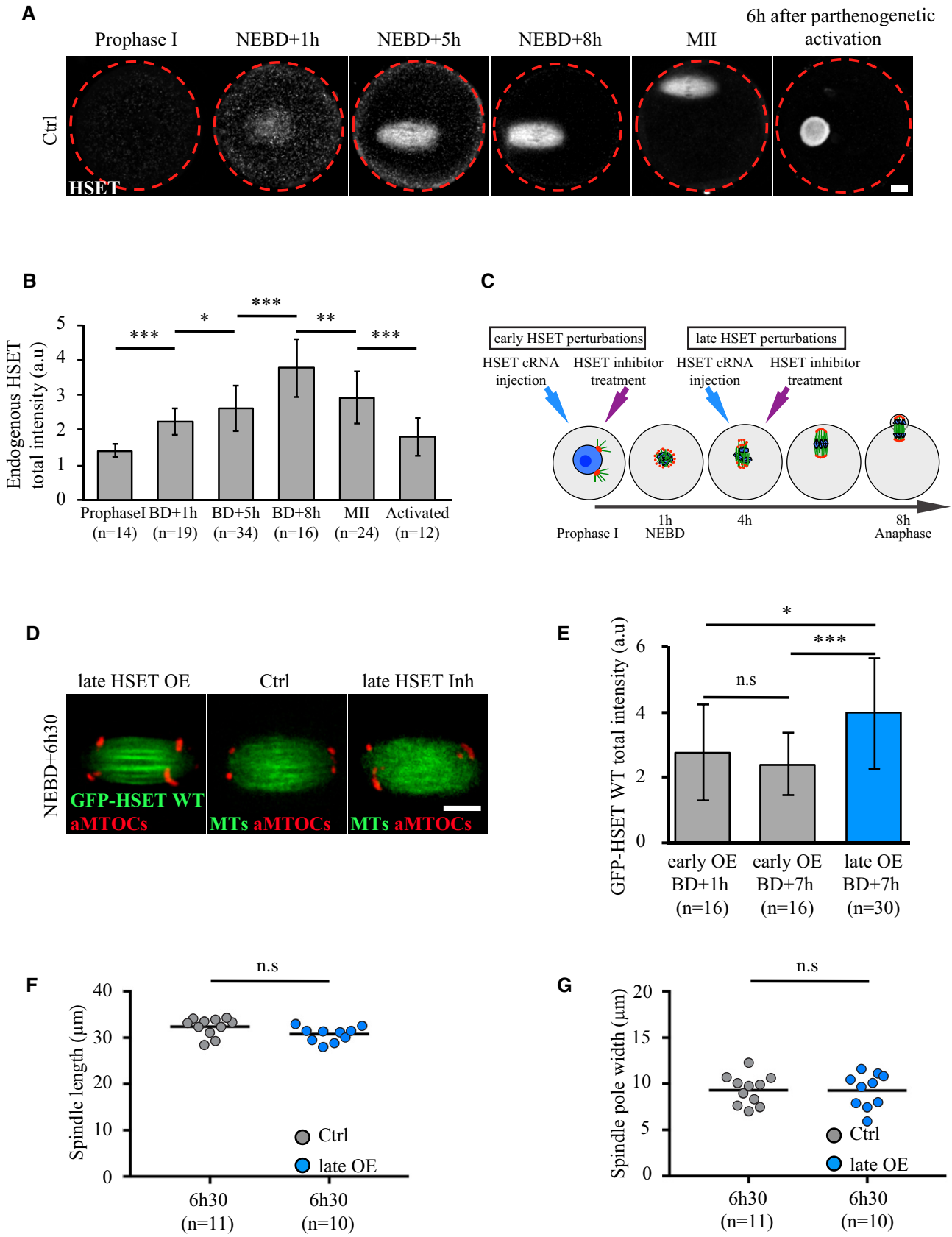

Figure 4.

 © 2018 The Authors

These results thus show that the timing of spindle morphogenesis is accelerated in oocytes overexpressing HSET WT: Spindle bipolarization is established precociously together with more efficient sorting and clustering of aMTOCs, markers of spindle pole assembly. We then analyzed the impact of accelerated kinetics on spindle shape.

Shifting meiotic spindle morphology toward mitotic-like morphology

To determine whether accelerating bipolarization and spindle pole formation affected global spindle shape, spindle length, central spindle width, and spindle pole width were measured at the same time points used to analyze aMTOC behavior. In oocytes overexpressing HSET WT, the spindle was already bipolar at NEBD+1h30. Strikingly, the spindle at this stage was extraordinarily long (Fig 3A, live microscopy), with a mean length of 36 μm and reaching a maximum of 54 μm (Fig 3B). As previously shown, this effect of HSET overexpression on spindle length required microtubule sliding [23], as HSET N593K expressing oocytes displayed spindle lengths similar to controls (Fig EV4A). However, in oocytes overexpressing HSET WT, the spindles progressively shortened (Fig 3B) to reach a size comparable to controls by NEBD+7h (Fig 3D).

Even though spindles in oocytes overexpressing HSET WT did recover in length (Fig 3D), we observed significant alterations in their shapes—both the poles and the central region were thinner, and the poles were pointed in contrast to the typical barrel-shape of meiotic spindle poles (Fig 3A and C). To confirm these observations, we measured spindle pole and central spindle widths at NEBD+1h30 and +7h. Oocytes overexpressing HSET WT displayed significantly reduced pole (Fig 3E) and central spindle widths (Fig 3F) compared to controls. In contrast, the spindle pole width of oocytes expressing HSET N593K was the same as controls (Fig EV4B). Thus, HSET levels, likely due to its microtubule-sliding activity, must be tightly regulated for proper spindle architecture in meiosis I.

HSET level must be tightly gated during early spindle morphogenesis

In an effort to understand how minor deregulation of HSET level impacts the entire process of spindle morphogenesis, endogenous HSET expression levels were measured before, throughout and after meiosis. Levels of HSET were low in Prophase I (1.6 times less than at NEBD+1h, Fig 4A and B). Endogenous HSET levels increased 1.7-fold over the course of 7 h during meiosis I (Fig 4A and B). Interestingly, HSET levels were 1.28 times higher after meiosis (in activated oocytes, mimicking fertilization) compared to Prophase I-arrested oocytes (Fig 4A and B). In addition, HSET was strongly enriched in the female pronucleus after parthenogenetic activation (Fig 4A). Thus, after meiosis, the zygote, comparable in size to the oocyte and similarly devoid of centrioles in rodents, enters the first mitotic division with more HSET than Prophase I-arrested oocytes. Consistently, spindle shape in the zygote is more mitotic-like: elongated, with focused poles [33,34].

Next, we tested whether the alteration of spindle shape observed after HSET WT overexpression was a direct consequence of impairing early spindle morphogenesis via modifying HSET levels prior spindle morphogenesis or was due to the continuous perturbation of HSET levels throughout the first meiotic division. To discriminate between these two hypotheses, HSET levels were modified after early stages of spindle morphogenesis had occurred, namely at NEBD+4h once the spindle was already bipolar (Fig 4C, late HSET perturbations). Spindles were further observed at NEBD+6h30. Spindle shape was comparable to controls—both displaying a typical barrel-shape (Fig 4D, F and G)—following this late HSET increase. This was not due to lower expression levels reached in late versus early perturbations of HSET. Indeed, late injection of GFP-HSET WT allowed the production of levels of HSET that were 1.4 times higher than early injections (Fig 4E, compare gray and blue bars). Thus, the alteration of spindle shape observed after HSET WT overexpression is a direct consequence of impairing early stages of spindle morphogenesis, rather than due to continuous perturbation of HSET levels later during the first meiotic division.

Mitotic-like spindles display defects in chromosome alignment and segregation

We next asked what were the consequences of forcing a mitotic-like mode of spindle morphogenesis on chromosome alignment and segregation. To answer this question, chromosome behavior was followed in living oocytes. Whereas at NEBD+1h30 in controls, the chromosomes were inside the microtubule ball (Fig 5A, upper left panel), in most oocytes overexpressing HSET WT, the chromosomes were scattered from pole to pole along the extended spindles (Fig 5A, upper right panel). This is in striking contrast to the situation in controls where the microtubule ball elongates

Figure 5. Early spindle morphogenesis defects induce errors in chromosome alignment and segregation.

A Spinning disk confocal microscopy images showing spindle region magnifications of controls (left panel) and oocytes overexpressing HSET WT (right panel) at NEBD+1h30 and +6h30. All oocytes express GFP-EB3 (green) and Histone-RFP (blue). The white asterisk marks a chromosome outside of the metaphase plate. Scale bar 10 μm.

B Spinning disk confocal microscopy images showing spindle region magnifications of controls (left panel) and oocytes overexpressing HSET WT (right panel) before and after anaphase. Oocytes express GFP-EB3 (green, left panel) or GFP-HSET WT (green, right panel) and Histone-RFP (blue). The white asterisk marks a lagging chromosome in the oocyte before and after anaphase. Scale bar 10 μm.

C Graph representing the percentage of oocytes with aligned (gray) and not aligned (black) chromosomes before anaphase, quantified for controls (left bar), and oocytes expressing HSET WT (right bar). Statistical significance of differences is assessed with a Fisher test: $^{**}P$-value = 0.006.

D Spinning disk confocal microscopy images showing spindle region magnifications of controls (left panel) and oocytes overexpressing HSET N593K (right panel) before and after anaphase. Oocytes express GFP-EB3 (green, left panel) or GFP-HSET N593K (green, right panel) and Histone-RFP (blue). Scale bar 10 μm.

E Graph representing the percentage of oocytes with aligned (gray) and not aligned (black) chromosomes before anaphase, quantified for controls (left bar) and HSET N593K oocytes (right bar). Statistical significance of differences is assessed with a Fisher test: not significant (n.s.) P-value > 0.99.

© 2018 The Authors

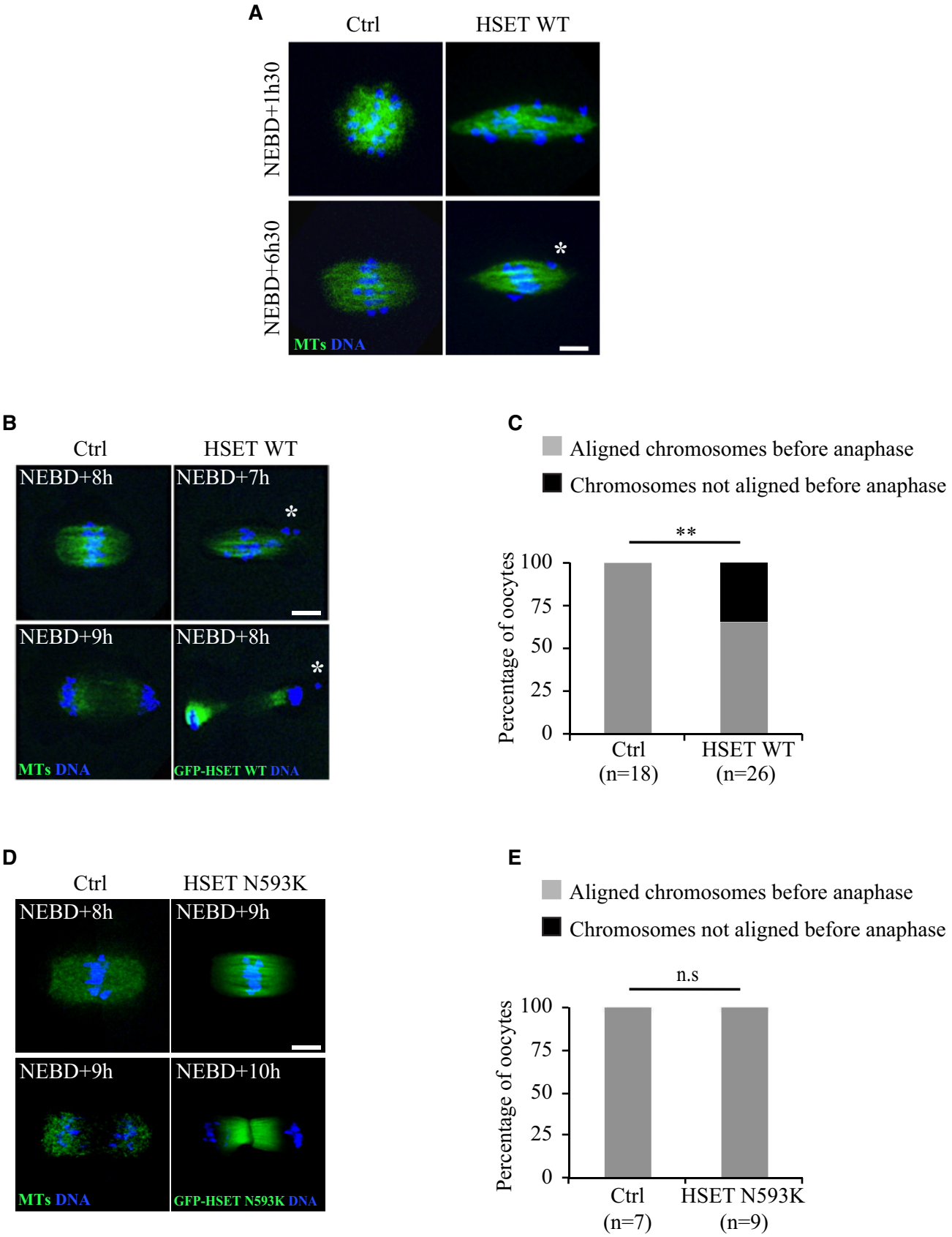

Figure 5.

 © 2018 The Authors

perpendicular to the prometaphase belt, transforming into a barrel-shaped bipolar spindle with the chromosomes gathered in the central region [13,35].

In control oocytes, once the chromosomes have become aligned on the central spindle region to form a metaphase plate, anaphase can occur (Fig 5B, left lower panel). In oocytes overexpressing HSET WT, even when the spindle reached a normal length (Fig 3C and D), the chromosomes remained incompletely aligned on the metaphase plate before anaphase and often presented more than one lagging chromosome outside the metaphase plate (Fig 5A and B, right panels; white asterisks). Indeed, 40% of HSET WT overexpressing oocytes harbored chromosomes that were not aligned before anaphase (Fig 5C, black bar), whereas misalignment was never observed in controls (Fig 5C, gray bar). Despite the presence of misaligned chromosomes, oocytes overexpressing HSET WT nonetheless underwent anaphase, leading to aberrant chromosome segregation (Fig 5B, right lower panel; the white asterisk indicates a chromosome separated from the rest of the main chromosome mass retained in the oocyte after anaphase). Anaphase occurred only with a modest delay (Fig EV5), probably due to the SAC hyposensitivity in meiosis I [36,37].

We then analyzed chromosome alignment in oocytes overexpressing HSET N593K, which in contrast to the HSET WT overexpressing spindles did not bipolarize quickly. In HSET N593K overexpressing oocytes, spindles did not skip the microtubule ball stage (Fig 1E, lower panel) and did not display the mitotic-like spindle shape of oocytes overexpressing HSET WT (Figs 1E and 5D). In addition, the chromosomes were properly aligned on the metaphase plate before anaphase occurred (Fig 5D, right panel and E). These observations further re-enforce the view that chromosome alignment/segregation defects displayed by oocytes overexpressing HSET WT are not a consequence of HSET WT overexpression *per se* but rather a consequence of a shift toward a mitotic mode of spindle morphogenesis.

Discussion

We have shown that HSET levels must be tightly gated during meiosis I and that deregulation of HSET amount can be used as a tool to force spindle morphogenesis to be more mitotic-like in several aspects: accelerated kinetics of spindle bipolarization and spindle pole assembly coupled with focused poles. Interestingly, this mild HSET overexpression may be comparable to the physiological transition from meiosis I to meiosis II and beyond, that is, first zygotic mitosis. This shift toward mitotic-like spindle morphogenesis is sufficient to severely impair chromosome alignment.

Importantly, late HSET perturbations (overexpression or inhibition) have no effect on spindle shape. This strongly argues that the mitotic-like spindle shape observed after perturbing HSET levels early on are not due to a late and cumulative effect of HSET overexpression throughout meiosis I, but are strictly attributable to increasing HSET levels during early stages of meiosis I. In addition, we did not observe similar defects in spindle bipolarization, pole assembly or chromosome alignment in oocytes overexpressing HSET N593K that can cross-link but not slide microtubules [23]. Interestingly, mouse zygotes also lack centrioles, yet assemble spindles with mitotic characteristics: rapid bipolarization and focused pole formation [33,34]. Accordingly, we show that zygotes enter mitosis with more HSET than oocytes when they resume meiosis. This mitotic-like mode of spindle morphogenesis in the absence of centrioles does not create chromosome alignment abnormalities in zygotes, as it does in oocytes. However, chromosome properties are different between meiosis and mitosis. Meiosis I is peculiar since homologous chromosomes linked by chiasmata progressively align and biorient on the metaphase plate, instead of single chromosomes as in mitosis. Thus, the volume, shape, and occupancy of the objects (the chromosomes) moving toward the metaphase plate are strikingly different in meiosis, and chromosomes are active participants in meiotic spindle assembly [38]. We propose that early overexpression of HSET WT accelerates spindle bipolarization through increased microtubule sliding, skipping the microtubule ball stage, and thus scattering the chromosomes along the spindle axis. Although the spindle recovers in length as meiosis I progresses, its shape remains distorted, harboring mitotic-like pointed poles instead of the classical barrel-shaped meiotic spindle. The microtubule ball stage could serve as a chromosome shepherd to avoid precocious chromosome scattering. This strategy is used by starfish oocytes where an actin fishnet that forms at meiosis resumption gathers the chromosomes, which dispersed throughout the volume of the large nucleus [39]. It is likely that for meiotic spindles assembled "inside-out", the initial steps have to be precisely controlled in order to prevent chromosome defects that could persist throughout meiosis I.

We were surprised that these early spindle defects were not fully rescued over the extremely long duration of meiosis I. In particular, more highly focused poles were shown to be associated with fewer chromosome alignment defects in meiosis when the microtubule ball stage was not skipped [40]. One possibility is that, when bypassing the microtubule ball stage, chromosomes are quickly scattered over a long distance and those located near the poles never become aligned on the metaphase plate. Indeed, polar chromosomes can be found occasionally in unmanipulated oocytes and usually are not able to gather on the metaphase plate before anaphase [35,41]. Microtubule dynamics is the same at hyper-focused (HSET WT OE) and normal barrel-shaped spindle poles, and the total amount or the density of microtubules might be reduced at poles (spindle pole width is significantly reduced in HSET WT overexpressing oocytes compared to controls). Taken together, this might impair the efficiency of capturing and aligning chromosomes that have been lost early on at the poles, a phenomenon that occurs more often in HSET WT overexpressing oocytes because of the early chromosome scattering.

In conclusion, forcing meiosis I spindle morphogenesis to be more mitotic-like leads to chromosome alignment abnormalities that cannot be fully reversed. In an unexpected manner, the unusual length of meiosis I (8 h) is not sufficient to correct early spindle morphogenesis defects, contributing to chromosome misalignment and segregation. This could be relevant to other systems as well, spindle formation being even slower in human oocytes, taking ~15 h [18]. Avoiding a mitotic-like mode of spindle morphogenesis could be one reason why most oocytes lose canonical centrosomes. It is thus possible that mouse oocytes, and maybe also human oocytes, eliminated canonical centrosomes to prevent a mitotic-like mode of spindle assembly during meiosis I, thereby to safeguarding against further increases in aneuploidy levels, already high during this specific division in these species [42].

© 2018 The Authors

Materials and Methods

Oocyte collection and culture

Ovaries were collected from 11-week-old OF1 (wt) female mice. Fully-grown oocytes were extracted by shredding the ovaries [43] and then releasing the germ cells in M2 + BSA medium supplemented with 1 μM milrinone to block and synchronize them in Prophase I of meiosis [44]. Meiosis resumption was triggered by transferring oocytes into milrinone-free M2 + BSA medium. All live-culture and imaging were carried out under oil at 37°C.

Oocyte activation

Oocytes in metaphase of meiosis II were incubated 2 h in M2 + BSA medium lacking $CaCl_2$ and supplemented with 10 mM $SrCl_2$. Activated oocytes were then cultured in M2 + BSA medium for 6 h until pronuclear formation.

Constructs

hHSET WT and hHSET N593K were subcloned from plasmids provided by Claire E. Walczak (Indiana University, USA) into a pRN3 plasmid suitable for *in vitro* cRNA transcription. The hHSET WT and N593K expressing plasmids were amplified using One shot Top 10 competent bacteria (Invitrogen), subsequently extracted and purified using mini and midi prep kits (Qiagen).

We used the following constructs: pRN3-GFP-hHSET, pRN3-hHSET, pSpe3-GFP-hHSET-N593K, pRN3-GFP-EB3 [16,17], pRN3-Histone(H2B)-RFP [16,17], pCS2-mCherry-Plk4 [45].

In vitro transcription of cRNAs and microinjection

Plasmids were linearized using appropriate restriction enzymes. cRNAs were synthesized with the mMessage mMachine kit (Ambion) and subsequently purified using the RNAeasy kit (Qiagen). Their concentration was measured using NanoDrop 2000 from ThermoScientific. cRNAs were centrifuged at 4°C during 45 min prior to microinjection into the cytoplasm of oocytes blocked in Prophase I in M2 + BSA medium supplemented with 1 μM milrinone at 37°C. cRNAs were microinjected using an Eppendorf Femtojet microinjector [46]. After microinjection, cRNA translation was allowed for 1 h, and oocytes were then transferred into milrinone-free M2 + BSA medium to allow meiosis resumption and meiotic divisions. For Fig 4C–G, late HSET OE oocytes were microinjected at NEBD+4h.

HSET WT and HSET N593K overexpression experiments

Oocytes were microinjected with 150 ng/μl of hHSET WT cRNAs or 250 ng/μl of GFP-hHSET WT cRNAs. We have observed that this is the optimal concentration to detect interpretable phenotypes whereas lower or higher concentrations gave, respectively, no phenotypes or induced spindle collapse and mono-aster formation. Oocytes were microinjected with 250 ng/μl of GFP-hHSET N593K. After microinjection, cRNA translation was allowed for 1 h and oocytes were transferred into milrinone-free M2 + BSA medium to allow meiosis resumption.

Drug treatment

The AZ82 inhibitor of HSET was a gift from AstraZeneca (USA) [29–30]. AZ82 was stored diluted in DMSO at 100 μM and further diluted in M2 medium to a final concentration of 10 μM. Control experiments were done in M2 + BSA medium supplemented with equivalent concentrations of DMSO.

The CW069 inhibitor of HSET was a gift from Fanni Gergely (Cancer Research UK Cambridge Institute, UK) [31]. CW069 was stored diluted in DMSO at 100 μM and then diluted in M2 medium at a final concentration of 25 μM. Control experiments were done in M2 + BSA medium with equivalent concentrations of DMSO. It had been previously shown that a concentration of 1/100 of DMSO in M2 medium does not perturb oocyte maturation [47].

Live imaging and SIM super-resolution microscopy

Spinning disk movies were acquired using a Plan-APO 40×/1.25NA objective on a Leica DMI6000B microscope enclosed in a thermostatic chamber (Life Imaging Service) equipped with a CoolSnap HQ2/CCD camera coupled to a Sutter filter wheel (Roper Scientific) and a Yokogawa CSU-X1-M1 spinning disk. Metamorph Software (Universal Imaging) was used to collect data.

For SIM super-resolution microscopy of aMTOCs, image acquisition was performed in 3D SIM mode, with a N-SIM Nikon microscope (Nikon Imaging Centre @ Institut Curie-CNRS) before image reconstruction using the NISElements software [48]. The system is equipped with an APO TIRF 100× 1.49NA Oil Immersion, a laser illumination (488 nm at 200 mW and 561 nm at 100 mW), and an EMCCD DU-897 Andor camera.

Immunofluorescence

After *in vitro* culture of oocytes, their zona pellucida was removed by incubation in acid Tyrode's medium (pH = 2.3). Prophase I-arrested oocytes were incubated in M2 + BSA medium supplemented with 0.4% pronase to remove the zona pellucida.

To visualize aMTOCs by SIM, oocytes were fixed 30 min at 30°C in 4% formaldehyde at NEBD+6h30 on coverslips treated with gelatin and polylysine. Permeabilization was achieved by incubating oocytes in 0.5% Triton X-100 in PBS for 10 min at room temperature. Mouse anti-pericentrin antibody (BD Transduction Laboratories) was used at 1:2,000. As secondary antibody, anti-mouse Cy3 (Molecular Probes) was used at 1:600. Slides were mounted in ProLong Gold.

To visualize endogenous HSET and exogenous microinjected hHSET, oocytes were fixed 30 min at 30°C in 3.7% formaldehyde and permeabilized 10 min at room temperature in 0.25% Tween-20–PBS. The HSET antibody was a gift from Renata Basto (Curie Institute, Paris, France). As secondary antibody, anti-rabbit Cy2 (Molecular Probes) was used at 1:200. Chromosomes were stained with Prolong-DAPI (10 μg/ml final DAPI).

FRAP analysis

Images were acquired using a Plan-APO 60×/1.4NA objective on a Ti Nikon microscope enclosed in a thermostatic chamber (Life Imaging Service) equipped with a Flash4.0 V2 CMOS camera

 © 2018 The Authors

(Hamamatsu) coupled to a Yokogawa CSU-X1 spinning disk. Metamorph Software (Universal Imaging) was used to collect data. All oocytes expressed SiR-Tubulin (from Spirochrome reference SC002, used at 0.1 μM). For all oocytes, an identical region of interest (diameter of 5 μm) was bleached at spindle poles. Images were acquired every 5 s for 125 s. One image was taken before bleaching. The SiR-Tubulin fluorescence intensity quantification was performed using the Metamorph software (Universal Imaging). Normalization of the measured fluorescence intensities was performed using the Microsoft Excel software. As the expression levels of SiR-Tubulin vary from one experiment to another, the signal intensity was normalized so that the prebleached value was 1 and the value at the first time point after bleaching was 0.

Quantifications

Metamorph (Universal Imaging), Imaris (Oxford Instruments), and Fiji (NIH) software were used to analyze and process data.

(i) The timing of spindle bipolarization was measured on oocytes expressing GFP-EB3 or SiR-Tubulin (from Spirochrome reference SC002, used at 0.1 μM) using Metamorph software; bipolarity was scored when two poles were distinguishable (see Fig 1A–F).
(ii) For endogenous and exogenous HSET intensity measurements on fixed samples, HSET intensity was measured inside a circle of a fixed size having the mean diameter of all oocytes (see Fig EV1C and D).
(iii) The GFP-HSET WT intensity measurements 3 h after cRNA injection (see Fig 4E) were performed using Metamorph software. After background subtraction, the total fluorescence intensity was measured inside a circle of a fixed size having the mean diameter of all oocytes.
(iv) Chromosome alignment before anaphase was measured on oocytes expressing Histone-RFP using Metamorph software (see Fig 5).
(v) For the aMTOCs 3D analysis (see Fig 2A–C), the input data consist of multichannel *Z*-stack images from spinning disk microscopy, containing bright-field, GFP and RFP channels. A homemade plug-in was developed for ImageJ/Fiji software to analyze aMTOCs position within the spindle. This 3D_Spindle_Analysis plug-in is available at https://github.com/pmailly/3D_Spindle_Analysis. Oocyte boundaries were first extracted with variance filter and triangle method for thresholding from the bright-field channel and used to crop the image in the other two channels. Spindle (GFP channel) was first filtered using 3D Gaussian filter (radius = 2) to reduce noise and then thresholded using MaxEntropy method. aMTOCs (RFP channel) were first filtered using difference of Gaussians (GDSC libraries from Alex Herbert, University of Sussex) to increase spot-like signals, then thresholded using MaxEntropy method. For each channel, 3D objects were segmented using the 3D ImageJ suite [49]. The spindle poles positions were computed as the extremities of the larger diameter of the object (Feret diameter). For each aMTOCs, minimum distances to poles, and border distances to the spindle were computed.
(vi) The spindle length, central spindle width, and spindle pole measurements were performed in 3D using Imaris software (see Figs 3 and EV3D). The spindle poles positions were considered as being the extremities of the larger diameter of the spindle, and spindle length was measured as the distance between poles.
(vii) The aMTOCs volume measurements were performed in 3D using Imaris software (see Fig 2D and E). The input data consist of SIM super-resolution microscopy acquisitions performed in 3D SIM mode, and the total volume of aMTOCs per oocyte was measured.

Statistical analysis

Experiments were repeated at least three times, and a sample of sufficient size was used. The statistical analysis was performed using GraphPad Prism version 7.00 for MacOS, GraphPad Software, La Jolla, California, USA, www.graphpad.com. For comparisons between two groups, the normality of the variables was checked (D'agostino-Pearson normality test) and parametric Student's *t*-tests (with Welch correction when indicated) or non-parametric comparison tests were performed with a confidence interval of 95%. For chromosome alignment experiments, repartitions were analyzed for statistical significance using Fisher's test used with a confidence interval of 95%. All error bars are expressed as standard deviation (SD). Values of $P < 0.05$ were considered significant. In all figures, * corresponds to a P-value < 0.05, ** to a P-value < 0.005, *** to a P-value < 0.0001. n.s.: not statistically significant.

Expanded View for this article is available online.

Acknowledgements
We thank AstraZeneca (USA) for the gift of AZ82, Fanni Gergely (Cancer Research UK Cambridge Institute, UK) for the gift of CW069, and Claire E. Walczak (Indiana University, USA) for the gift of plasmids. We thank Renata Basto (Curie Institute, Paris, France) for sharing the unpublished HSET antibody. We thank Lucie Sengmanivong for her precious help using the N-SIM Nikon microscope from the Nikon Imaging Centre @ Institut Curie-CNRS, member of the France-BioImaging national research infrastructure for confocal microscopy. We thank Christophe Klein (Centre de Recherche des Cordeliers-INSERM, Paris, France) for his help with the FRAP analysis. We also thank Hugh J. Clarke (McGill University, Montreal, Canada) for critical reading of the manuscript, the members of the Verlhac/Terret team for helpful discussions, and Anne Dumas (Collège de France, Paris, France) for her help with MTA writing. We thank the "Fondation Bettencourt Schueller". This work was supported by grants from the Fondation pour la Recherche Médicale (FRM label DEQ20150331758 to MHV), from the Fondation ARC (PJA20131200412 to MET), and from Inca (PLBIO 2016-270-TRAN). This work has received support under the program "Investissements d'Avenir" launched by the French Government and implemented by the ANR, with the references: ANR-14-CE11/DIVACEN/MHV, ANR-10-LABX-54 MEMO LIFE, ANR-11-IDEX-0001-02 PSL* Research University.

Author contributions
IB, AK, M-HV, and M-ET designed the experiments, interpreted the results, and wrote the manuscript. IB, IQ, AK, and M-ET carried out the experiments. TB and PM designed the Fiji plug-in. M-ET and M-HV supervised the project.

Conflict of interest
The authors declare that they have no conflict of interest.

© 2018 The Authors

References

1. Toso A, Winter JR, Garrod AJ, Amaro AC, Meraldi P, McAinsh A (2009) Kinetochore-generated pushing forces separate centrosomes during bipolar spindle assembly. *J Cell Biol* 184: 365 – 372
2. Tanenbaum ME, Medema RH (2010) Mechanisms of centrosome separation and bipolar spindle assembly. *Dev Cell* 19: 797 – 806
3. Sathananthan AH (1997) Mitosis in the human embryo: the vital role of the sperm centrosome (centriole). *Histol Histopathol* 12: 827 – 856
4. Szollosi D, Calarco P, Donahue RP (1972) Absence of centrioles in the first and second meiotic spindles of mouse oocytes. *J Cell Sci* 11: 521 – 541
5. Pimenta-Marques A, Bento I, Lopes CA, Duarte P, Jana SC, Bettencourt-Dias M (2016) A mechanism for the elimination of the female gamete centrosome in *Drosophila melanogaster*. *Science* 353: aaf4866
6. Maro B, Howlett SK, Webb M (1985) Non-spindle microtubule organizing centers in metaphase II-arrested mouse oocytes. *J Cell Biol* 101: 1665 – 1672
7. Gueth-Hallonet C, Antony C, Aghion J, Santa-Maria A, Lajoie-Mazenc I, Wright M, Maro B (1993) gamma-Tubulin is present in acentriolar MTOCs during early mouse development. *J Cell Sci* 105: 157 – 166
8. Palacios MJ, Joshi HC, Simerly C, Schatten G (1993) Gamma-tubulin reorganization during mouse fertilization and early development. *J Cell Sci* 104: 383 – 389
9. Carabatsos MJ, Combelles CM, Messinger SM, Albertini DF (2000) Sorting and reorganization of centrosomes during oocyte maturation in the mouse. *Microsc Res Tech* 49: 435 – 444
10. Luksza M, Queguigner I, Verlhac MH, Brunet S (2013) Rebuilding MTOCs upon centriole loss during mouse oogenesis. *Dev Biol* 382: 48 – 56
11. Clift D, Schuh M (2015) A three-step MTOC fragmentation mechanism facilitates bipolar spindle assembly in mouse oocytes. *Nat Commun* 6: 7217
12. Dumont J, Petri S, Pellegrin F, Terret ME, Bohnsack MT, Rassinier P, Georget V, Kalab P, Gruss OJ, Verlhac MH (2007) A centriole- and RanGTP-independent spindle assembly pathway in meiosis I of vertebrate oocytes. *J Cell Biol* 176: 295 – 305
13. Schuh M, Ellenberg J (2007) Self-organization of MTOCs replaces centrosome function during acentrosomal spindle assembly in live mouse oocytes. *Cell* 130: 484 – 498
14. Brunet S, Dumont J, Lee KW, Kinoshita K, Hikal P, Gruss OJ, Maro B, Verlhac MH (2008) Meiotic regulation of TPX2 protein levels governs cell cycle progression in mouse oocytes. *PLoS One* 3: e3338
15. Fitzharris G (2009) A shift from kinesin 5-dependent metaphase spindle function during preimplantation development in mouse. *Development* 136: 2111 – 2119
16. Breuer M, Kolano A, Kwon M, Li CC, Tsai TF, Pellman D, Brunet S, Verlhac MH (2010) HURP permits MTOC sorting for robust meiotic spindle bipolarity, similar to extra centrosome clustering in cancer cells. *J Cell Biol* 191: 1251 – 1260
17. Kolano A, Brunet S, Silk AD, Cleveland DW, Verlhac MH (2012) Error-prone mammalian female meiosis from silencing the spindle assembly checkpoint without normal interkinetochore tension. *Proc Natl Acad Sci USA* 109: E1858 – E1867
18. Holubcová Z, Blayney M, Elder K, Schuh M (2015) Human oocytes. Error-prone chromosome-mediated spindle assembly favors chromosome segregation defects in human oocytes. *Science* 348: 1143 – 1147
19. Walczak CE, Verma S, Mitchison TJ (1997) XCTK2: a kinesin-related protein that promotes mitotic spindle assembly in *Xenopus laevis* egg extracts. *J Cell Biol* 136: 859 – 870
20. Mountain V, Simerly C, Howard L, Ando A, Schatten G, Compton DA (1999) The kinesin-related protein, HSET, opposes the activity of Eg5 and cross-links microtubules in the mammalian mitotic spindle. *J Cell Biol* 147: 351 – 366
21. Sharp DJ, Yu KR, Sisson JC, Sullivan W, Scholey JM (1999) Antagonistic microtubule-sliding motors position mitotic centrosomes in *Drosophila* early embryos. *Nat Cell Biol* 1: 51 – 54
22. Goshima G, Nedelec F, Vale RD (2005) Mechanisms for focusing mitotic spindle poles by minus end-directed motor proteins. *J Cell Biol* 171: 229 – 240
23. Cai S, Weaver LN, Ems-McClung SC, Walczak CE (2009) Kinesin-14 family proteins HSET/XCTK2 control spindle length by crosslinking and sliding microtubules. *Mol Biol Cell* 20: 1348 – 1359
24. Hepperla AJ, Willey PT, Coombes CE, Schuster BM, Gerami-Nejad M, McClellan M, Mukherjee S, Fox J, Winey M, Odde DJ *et al* (2014) Minus-end-directed Kinesin-14 motors align antiparallel microtubules to control metaphase spindle length. *Dev Cell* 31: 61 – 72
25. Syrovatkina V, Tran PT (2015) Loss of kinesin-14 results in aneuploidy via kinesin-5-dependent microtubule protrusions leading to chromosome cut. *Nat Commun* 6: 7322
26. Fink G, Hajdo L, Skowronek KJ, Reuther C, Kasprzak AA, Diez S (2009) The mitotic kinesin-14 Ncd drives directional microtubule–microtubule sliding. *Nat Cell Biol* 11: 717 – 723
27. Braun M, Drummond DR, Cross RA, McAinsh AD (2009) The kinesin-14 Klp2 organizes microtubules into parallel bundles by an ATP dependent sorting mechanism. *Nat Cell Biol* 11: 724 – 730
28. Hentrich C, Surrey T (2010) Microtubule organization by the antagonistic mitotic motors kinesin-5 and kinesin-14. *J Cell Biol* 189: 465 – 480
29. Wu J, Mikule K, Wang W, Su N, Petteruti P, Gharahdaghi F, Code E, Zhu X, Jacques K, Lai Z *et al* (2013) Discovery and mechanistic study of a small molecule inhibitor for motor protein KIFC1. *ACS Chem Biol* 8: 2201 – 2208
30. Yang B, Lamb ML, Zhang T, Hennessy EJ, Grewal G, Sha L, Zambrowski M, Block MH, Dowling JE, Su N *et al* (2014) Discovery of potent KIFC1 inhibitors using a method of integrated high-throughput synthesis and screening. *J Med Chem* 57: 9958 – 9970
31. Watts CA, Richards FM, Bender A, Bond PJ, Korb O, Kern O, Riddick M, Owen P, Myers RM, Raff J *et al* (2013) Design, synthesis, and biological evaluation of an allosteric inhibitor of HSET that targets cancer cells with supernumerary centrosomes. *Chem Biol* 20: 1399 – 1410
32. Bury L, Coelho PA, Simeone A, Ferries S, Eyers CE, Eyers PA, Zernicka-Goetz M, Glover DM (2017) Plk4 and Aurora A cooperate in the initiation of acentriolar spindle assembly in mammalian oocytes. *J Cell Biol* 216: 3571 – 3590
33. Louvet-Vallée S, Vinot S, Maro B (2005) Mitotic spindles and cleavage planes are oriented randomly in the two-cell mouse embryo. *Curr Biol* 15: 464 – 469
34. Chaigne A, Campillo C, Voituriez R, Gov NS, Sykes C, Verlhac MH, Terret ME (2016) F-actin mechanics control spindle centring in the mouse zygote. *Nat Commun* 7: 10253
35. Kitajima TS, Ohsugi M, Ellenberg J (2011) Complete kinetochore tracking reveals error-prone homologous chromosome biorientation in mammalian oocytes. *Cell* 146: 568 – 581
36. Jones KT, Lane SI (2013) Molecular causes of aneuploidy in mammalian eggs. *Development* 140: 3719 – 3730
37. Touati SA, Wassmann K (2016) How oocytes try to get it right: spindle checkpoint control in meiosis. *Chromosoma* 125: 321 – 335
38. Radford SJ, Nguyen AL, Schindler K, McKim KS (2017) The chromosomal basis of meiotic acentrosomal spindle assembly and function in oocytes. *Chromosoma* 126: 351 – 364

 © 2018 The Authors

39. Lénárt P, Bacher CP, Daigle N, Hand AR, Eils R, Terasaki M, Ellenberg J (2005) A contractile nuclear actin network drives chromosome congression in oocytes. *Nature* 436: 812 – 818
40. Kyogoku H, Kitajima TS (2017) Large cytoplasm is linked to the error-Prone nature of oocytes. *Dev Cell* 41: 287 – 298
41. Gui L, Homer H (2012) Spindle assembly checkpoint signalling is uncoupled from chromosomal position in mouse oocytes. *Development* 139: 1941 – 1946
42. Hassold T, Hall H, Hunt P (2007) The origin of human aneuploidy: where we have been, where we are going. *Hum Mol Genet* 16(Spec No. 2): R203 – R208
43. Verlhac MH, Kubiak JZ, Clarke HJ, Maro B (1994) Microtubule and chromatin behavior follow MAP kinase activity but not MPF activity during meiosis in mouse oocytes. *Development* 120: 1017 – 1025
44. Reis A, Chang HY, Levasseur M, Jones KT (2006) APCcdh1 activity in mouse oocytes prevents entry into the first meiotic division. *Nat Cell Biol* 8: 539 – 540
45. Marthiens V, Rujano MA, Pennetier C, Tessier S, Paul-Gilloteaux P, Basto R (2013) Centrosome amplification causes microcephaly. *Nat Cell Biol* 15: 731 – 740
46. Verlhac MH, Lefebvre C, Guillaud P, Rassinier P, Maro B (2000) Asymmetric division in mouse oocytes: with or without Mos. *Curr Biol* 10: 1303 – 1306
47. Terret ME, Wassmann K, Waizenegger I, Maro B, Peters JM, Verlhac MH (2003) The meiosis I-to-meiosis II transition in mouse oocytes requires separase activity. *Curr Biol* 13: 1797 – 1802
48. Gustafsson MG, Shao L, Carlton PM, Wang CJ, Golubovskaya IN, Cande WZ, Agard DA, Sedat JW (2008) Three-dimensional resolution doubling in wide-field fluorescence microscopy by structured illumination. *Biophys J* 94: 4957 – 4970
49. Ollion J, Cochennec J, Loll F, Escudé C, Boudier T (2013) TANGO: a generic tool for high-throughput 3D image analysis for studying nuclear organization. *Bioinformatics* 29: 1840 – 1841

License: This is an open access article under the terms of the Creative Commons Attribution 4.0 License, which permits use, distribution and reproduction in any medium, provided the original work is properly cited.

Expanded View Figures

Figure EV1. Endogenous HSET and slightly overexpressed exogenous HSET localize to the spindle throughout meiosis I.

A Immunofluorescence showing endogenous HSET (left panel), exogenous HSET WT (middle panel), and exogenous HSET N593K (right panel). Endogenous and exogenous HSET display the same localization: they all localize on the spindle, as observed here on fixed oocytes at NEBD+4h30 (HSET antibody: green; DNA: blue). Note that the spindle is elongated in HSET WT expressing oocytes. Scale bar 10 μm.

B Time-lapse spinning disk confocal microscopy of an oocyte expressing GFP-HSET WT (green) and Histone-RFP (blue). GFP-HSET WT localizes on the spindle throughout meiosis I. The white asterisk marks a chromosome outside of the metaphase plate. Scale bar 5 μm.

C HSET total fluorescence intensity measured in the whole cell for fixed oocytes at NEBD+4h30 expressing HSET WT or not (Ctrl). Data are represented as mean ± SD. The ratio of total HSET WT overexpression is 1.6.

D HSET normalized fluorescence intensity measured on the spindle of fixed oocytes at NEBD+4h30 expressing HSET WT or not (Ctrl). Data are represented as mean ± SD. The ratio of HSET OE on the spindle is 4.2.

E Time-lapse spinning disk confocal microscopy of an oocyte expressing GFP-HSET N593K (green). GFP-HSET N593K displays a localization similar to endogenous or GFP-HSET WT on the spindle throughout meiosis I. Scale bar 10 μm.

F GFP total fluorescence intensity measured in the whole cell for live oocytes at NEBD+7h expressing GFP-HSET WT or GFP-HSET N593K. Data are represented as mean ± SD. Statistical significance of differences is assessed with a *t*-test: ***P*-value = 0.004.

© 2018 The Authors

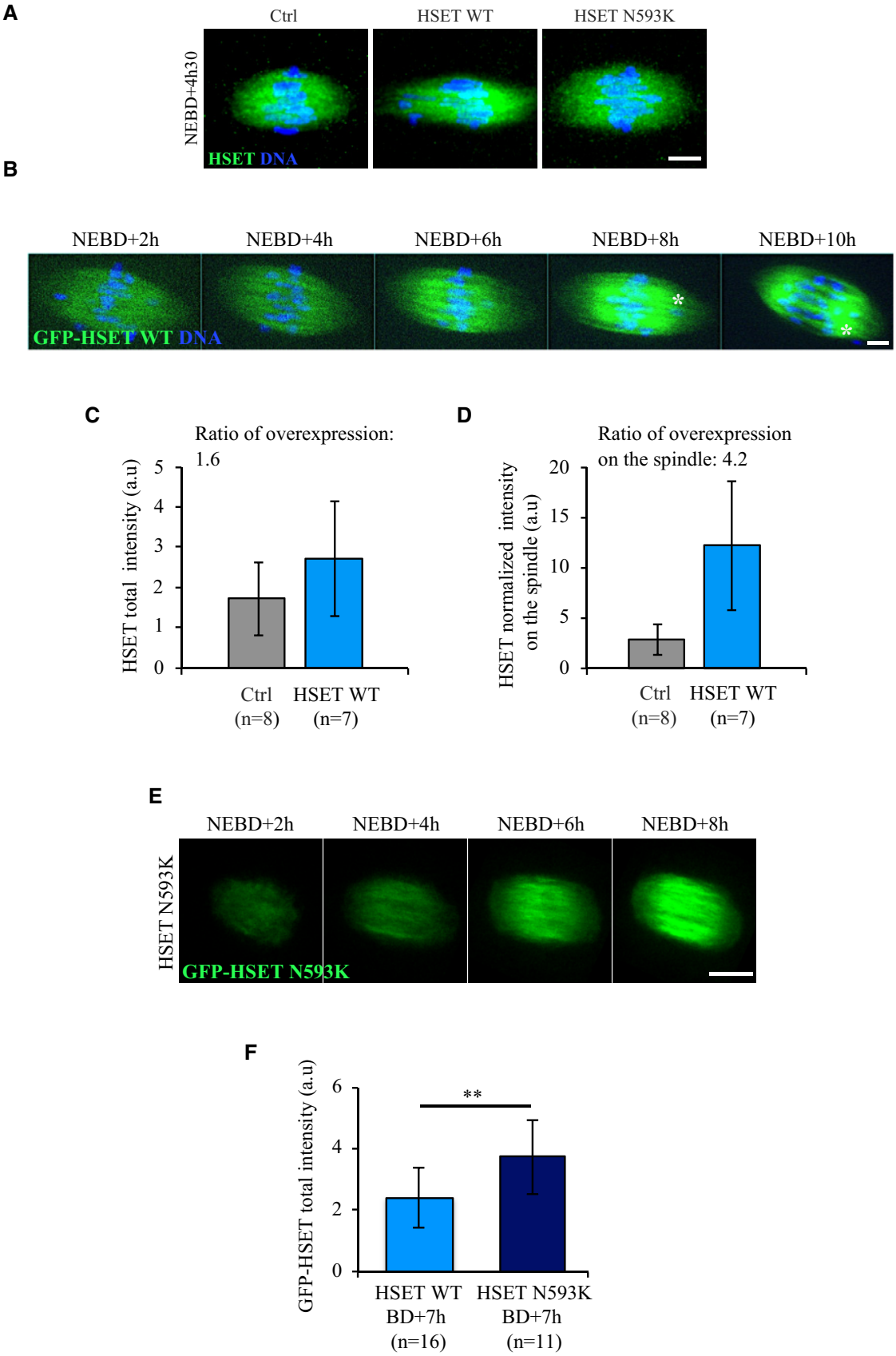

Figure EV1.

© 2018 The Authors

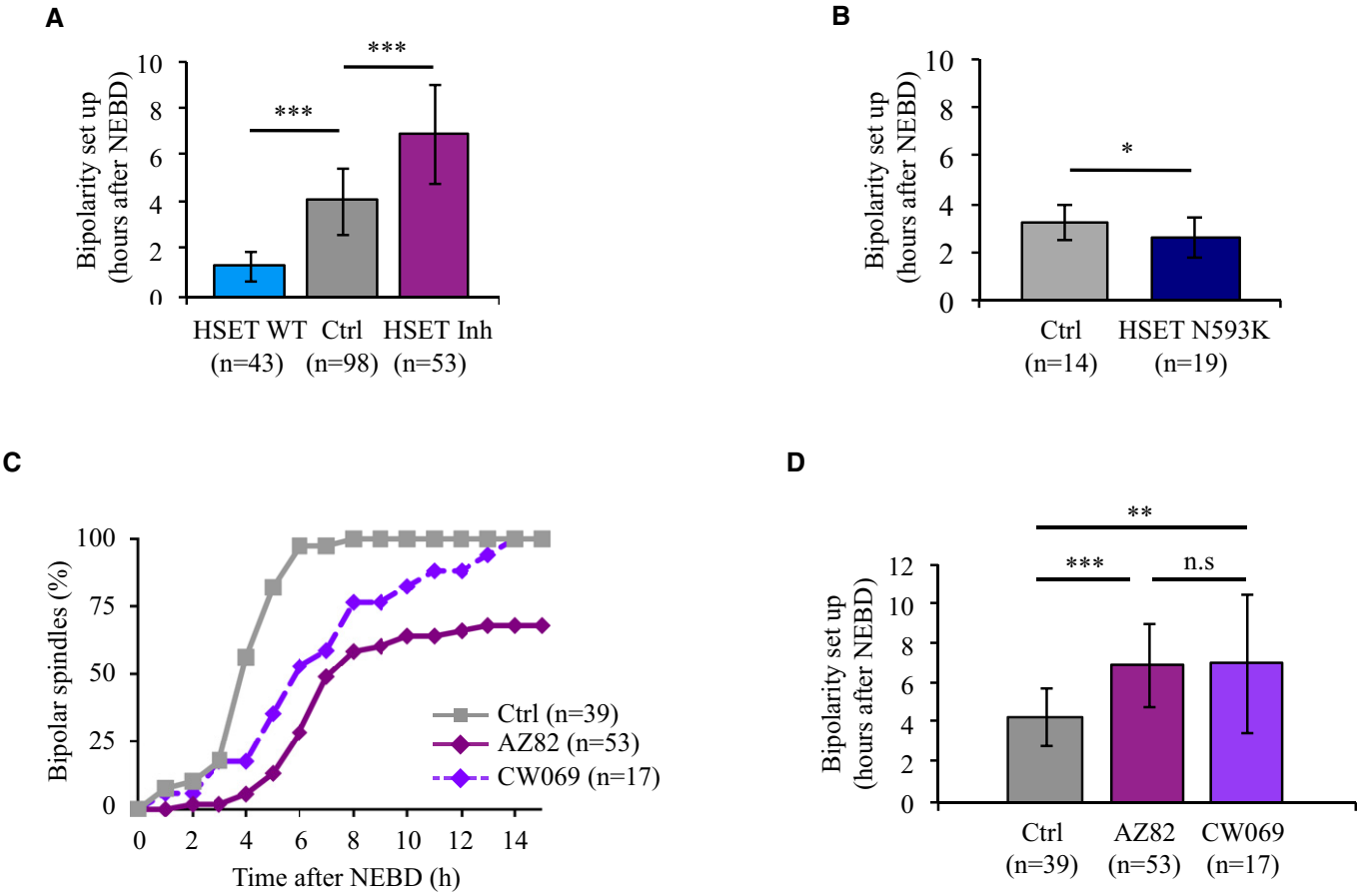

Figure EV2. HSET levels control the timing of spindle bipolarization.

A Histogram showing the mean time of bipolarization setup (data are represented as mean ± SD). Bipolarity was scored when two poles were distinguishable. The mean time of bipolarization setup for oocytes overexpressing HSET WT is 1 h and 19 min (blue bar), compared to 4 h and 3 min for controls (gray bar), ***P-value < 0.0001, compared to 6 h and 55 min for oocytes inhibited for HSET (purple bar), ***P-value < 0.0001. Statistical significance of differences is assessed with a Mann–Whitney test.

B Histogram showing the mean time of bipolarization setup in controls vs. HSET N593K expressing oocytes (data are represented as mean ± SD). Bipolarity was scored when two poles were distinguishable. The mean time of bipolarization setup for oocytes overexpressing HSET N593K is 2 h and 36 min (dark blue bar), compared to 3 h and 10 min for the controls (gray bar). Statistical significance of differences is assessed with a t-test: *P-value = 0.034.

C Graph representing the kinetics of spindle bipolarization in controls (gray) vs. oocytes inhibited for HSET with AZ82 (purple) or CW069 (violet). The number of oocytes analyzed is written in parentheses.

D Histogram showing the mean time of bipolarization setup. Bipolarity was scored when two poles were distinguishable. Data are represented as mean ± SD. The mean time of bipolarization setup for controls (gray bar) is 4 h and 18 min, compared to 6 h and 55 min for oocytes inhibited for HSET with AZ82 (purple bar), compared to 7 h and 0 min for oocytes inhibited for HSET with CW069 (violet bar). Statistical significance of differences is assessed with a Mann–Whitney test: **P-value = 0.007, ***P-value < 0.0001, not significant (n.s.) P-value = 0.929. The number of oocytes analyzed is written in parentheses.

Figure EV3. Spindle morphogenesis after perturbation of HSET levels.

A Principle of the automated 3D analysis of aMTOCs within the spindle. We developed a Fiji plug-in that converts images from spinning disk confocal live microcopy (here a spindle region magnification of an oocyte expressing GFP-EB3 (green) and mCherry-Plk4 (red) at NEBD+6h30, left panel) to binary images (middle panel), and then to 3D images (right panel).

B aMTOCs sorting in controls (gray dots) and oocytes overexpressing HSET WT (blue dots) at NEBD+1h30, +4h30, and +6h30. Each dot is one aMTOC. The vertical axis plots the aMTOCs volume, and the horizontal axis represents an hemi-spindle starting from the central spindle to the pole (as written on the scheme). The distance of aMTOCs to the closest spindle pole is normalized by the spindle length.

C Binary images corresponding to Fig 2A. Scale bar 10 μm.

D Quantification in 3D of the spindle length in controls (gray dots) and oocytes inhibited for HSET (purple dots) at NEBD+1h30, +4h30, and +6h30. Each dot represents an oocyte, the number of oocytes analyzed is written in parentheses. Statistical significance of differences is assessed with a Mann–Whitney test: *P-value = 0.017, **P-value = 0.003, ***P-value < 0.0001.

© 2018 The Authors

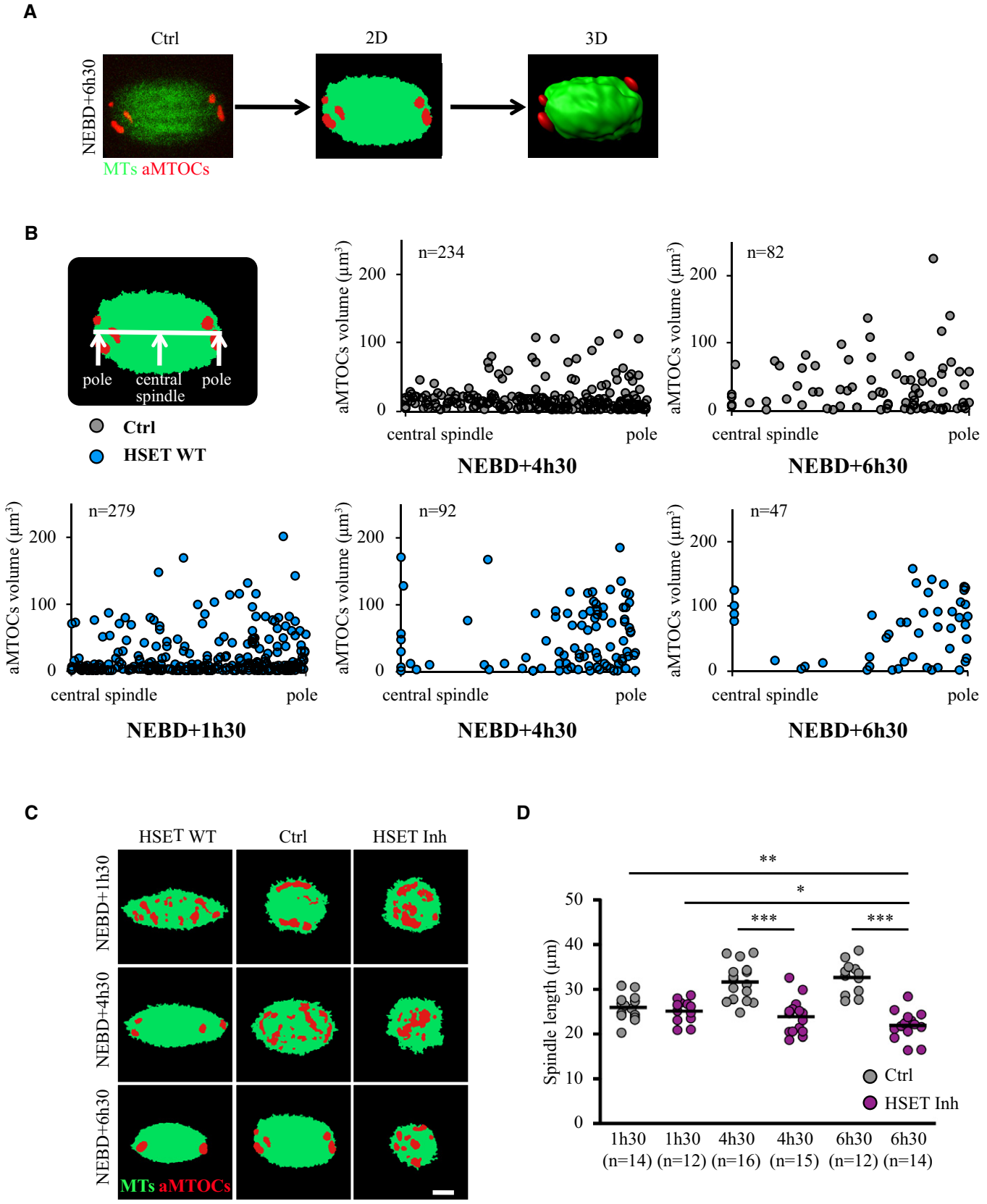

Figure EV3.

© 2018 The Authors

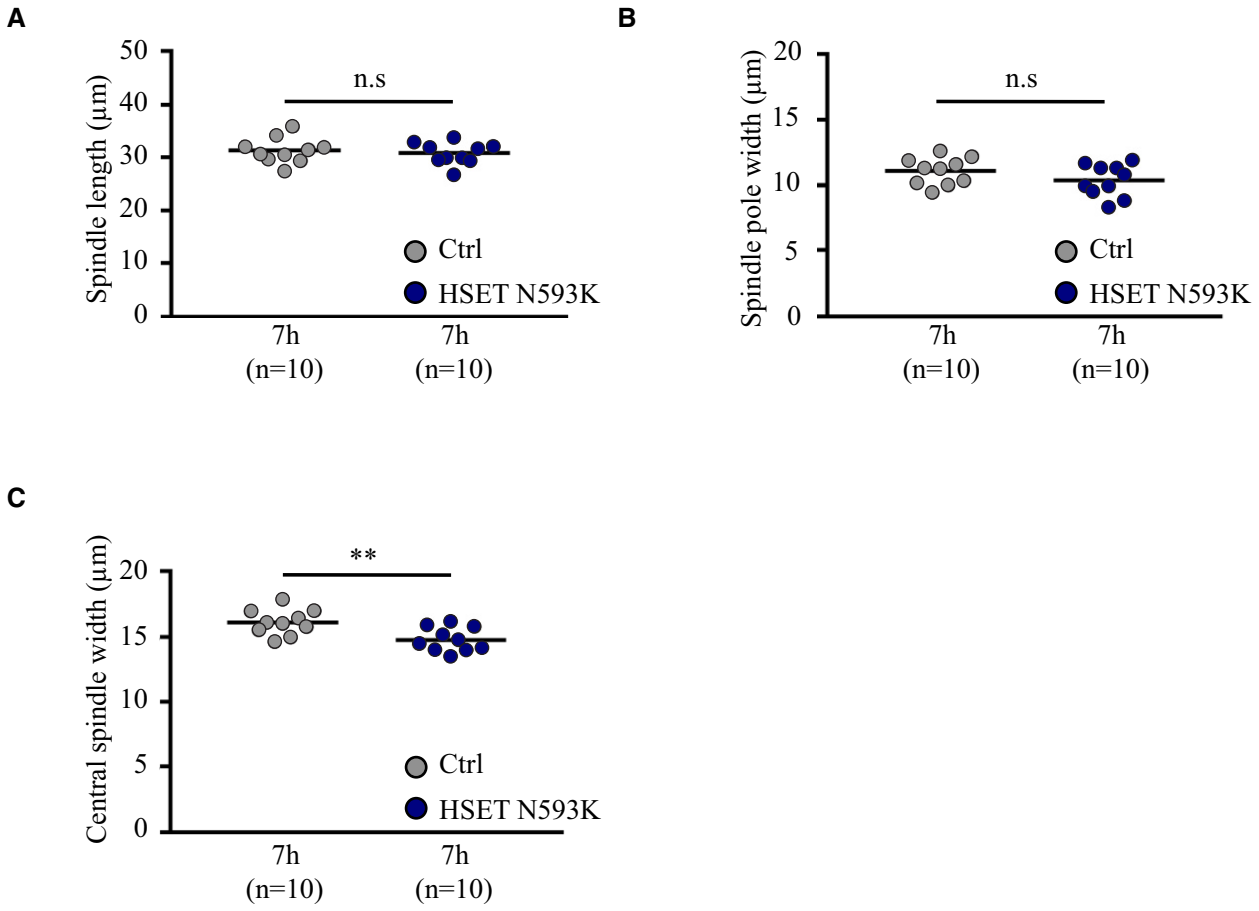

Figure EV4. HSET N593K overexpression does not alter spindle shape.

A–C Quantification in 3D of the spindle length (A) not significant (n.s.) *P*-value = 0.616, spindle pole width (B) not significant (n.s.) *P*-value = 0.175 and central spindle width (C) ***P*-value = 0.006 in oocytes overexpressing HSET N593K (dark blue dots) and controls (gray dots) at NEBD+7h. Each dot represents an oocyte, and the number of oocytes analyzed is written in parentheses. Statistical significance of differences is assessed with a Mann–Whitney test.

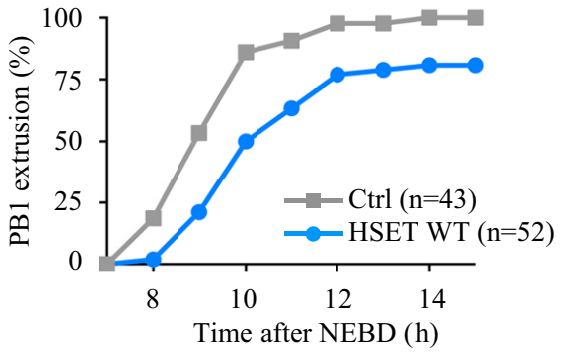

Figure EV5. Anaphase occurs with a modest delay in oocytes overexpressing HSET WT.

Graph representing the kinetics of polar body (PB1) extrusion in controls (gray) vs. HSET WT overexpressing oocytes (blue) obtained from three independent experiments.

© 2018 The Authors

II. Aberrant low cortical tension generates chromosome misalignment in oocyte

Context and question: In mitosis, centrosomes nucleate astral microtubules, which are anchored on a stiff cortex, a consequence of an increase in cortical tension. These astral microtubules transmit forces to the spindle allowing its positioning within the cell. Oocytes are an exception to this rule, lacking canonical centrosomes and astral microtubules, imposing alternative modes of spindle positioning. As a consequence meiotic spindle positioning depends only on F-actin. In particular, it relies on the nucleation of a cortical F-actin thickening that leads to a decrease in cortical tension. Interestingly, cortical tension predicts embryo viability after fertilization in humans: extra-soft oocytes cease development before the blastocyst stage. What are the defects induced by an aberrant low cortical tension potentially leading to a developmental arrest after fertilization?

Method: We used two different tools that nucleate de novo an actin thickening to artificially decrease cortical tension in mouse oocytes, thus creating extra-soft oocytes.

Results:

- Chromosome alignment is severely impaired in extra-soft oocytes despite normal spindle morphogenesis and dynamics.
- The intensity of the forces applied on chromosomes is altered in extra-soft oocytes, potentially impacting chromosome alignment.
- Deregulation of myosin II levels appears to be the main cause of chromosome misalignment, since decreasing myosin II activity in extra-soft oocytes rescues chromosome alignment.

Conclusion: We describe for the first time that aberrant low cortical tension could generate aneuploidy in oocytes, contributing to the very high aneuploidy rate measured in female meiosis.

Author contributions:

IB, MHV and MET conceived and supervised the project. IB performed most experiments. FC characterized the cFH1FH2 construct, MMS did the chromosome tracking experiments, they both analyzed their experiments. IB, MHV and MET analyzed most experiments. CC an MP were involved for the volume measurement experiments. CC and CS were involved for the cortical tension measurement experiments. AO and AG were involved for the computational 3D imaging approach. AC did the original observation that extra-soft oocytes have misaligned chromosomes. IB, MHV and MET wrote the manuscript.

Aberrant low cortical tension generates chromosome misalignment in oocyte.

Isma Bennabi[1], Flora Crozet[1], Marion Manil-Segalen[1], Clotilde Cadart[2], Clément Campillo[3], Agathe Chaigne[5], Alice Othmani[4], Matthieu Piel[2], Cécile Sykes[6], Auguste Genovesio[4], Marie-Hélène Verlhac[1*], Marie-Emilie Terret[1*].

[1] CIRB, Collège de France, UMR7241/U1050, 75005 Paris, France.

[2] Institut Curie/Institut Pierre-Gilles de Gennes, 75005 Paris, France.

[3] LAMBE, Université d'Evry val d'Essonne, UMR 8587, Evry, France.

[4] IBENS, Ecole Normale Supérieure, UMR8197/ U1024, 75005 Paris, France.

[5] MRC Laboratory for Molecular Cell Biology, UCL, London WC1E 6BT, UK.

[6] Institut Curie, Laboratoire Physico-Chimie, UMR168, 75005 Paris, France.

[*] Correspondence should be addressed to M.H.V. (marie-helene.verlhac@college-de-france.fr) or M.E.T. (marie-emilie.terret@college-de-france.fr).

Abstract

Meiosis in human females is error-prone, generating a high basal rate of aneuploid oocytes. Why these cells physiologically produce errors in chromosome segregation remains elusive. Human and mouse oocytes developmental potential is accurately predicted by their mechanical properties. Their stiffness has to be tightly gated to develop into blastocysts. We have previously solved how cortical tension is regulated in oocytes, and showed that modifying their stiffness alters division geometry. In this study, we investigate other defects that could contribute to the early developmental failure due to cortical tension deregulation in the oocyte. We focus on extra-soft oocytes, the most common case in a natural population of human and mouse oocytes. Using two different tools to artificially decrease cortical tension in mouse oocytes, we show that chromosome alignment is severely impaired in extra-soft oocytes, despite normal spindle morphogenesis and dynamics. Defects in the intensity of the forces applied on the chromosomes could contribute to chromosome misalignment, but the main cause of chromosome misalignment is a deregulation of myosin II. We are potentially describing here a new mode of generation of aneuploidies that could be very common in female gametes and contribute to the very high aneuploidy rate measured in female meiosis, a leading cause of infertility and congenital disorders.

Introduction

Sexual reproduction produces new living organisms by combining genetic information from 2 haploid female and male gametes: oocyte and sperm. These cells are created through meiosis, a specialized type of cell division that reduces the chromosome number by half and brings genetic diversity. This process is thus essential for the propagation of species. However, it is poorly controlled, especially in females. Meiosis I in human females is error prone, resulting in aneuploidy and as such is the leading cause of miscarriage and developmental disabilities such as trisomies (Nagaoka et al., 2012). In human oocytes for example, the basal rate of errors is close to 20% in women younger than 35 years of age but increases with maternal age and can be as high as 60% in older women. It is thus a fundamental public health problem in our societies where women tend to post-pone child bearing in order to establish themselves in their career.

It has been shown recently that human and mouse oocytes developmental potential is accurately predicted by mechanical properties within hours after fertilization. Their stiffness has to be tightly controlled in order to develop into blastocysts: too stiff or too soft, embryos will cease development (Yanez et al., 2016). These mechanical properties were measured using a micropipette aspiration technique, as we and other performed on mouse oocytes and embryos (Larson et al., 2010; Chaigne et al., 2013; Chaigne et al., 2015; Chaigne et al., 2016), a minimally invasive technique that could be used very easily in IVF clinics for embryo and oocyte selection. In previous studies, we have deciphered how cortical tension is regulated in mouse oocytes and embryos (Chaigne et al., 2013; Chaigne et al., 2015; Chaigne et al., 2016). Using multidisciplinary approaches, we showed that the nucleation of a cortical F-actin thickening by the Arp2/3 complex in meiosis I excludes myosin-II from the cortex, decreasing cortical tension (Chaigne et al., 2013; Chaigne et al., 2015). This change in cortex mechanics amplifies an initial imbalance of pulling forces exerted by myosin-II at the poles of an actin cage surrounding the microtubule spindle (Azoury et al., 2008; Schuh and Ellenberg, 2008; Chaigne et al., 2015; Mogessie and Schuh, 2017), the forces being stronger at the pole closest to the cortex because of the initial slight asymmetry of nuclear position (Brunet and Maro, 2007). Spindle motion is slow (mean speed of 0.15 μm/min in late meiosis I, Schuh and Ellenberg, 2008) but is amplified by the progressive deformation of the cortex, made possible by lowering of cortical tension. This reduced cortical tension allows the recruitment of filaments between the cortex and the spindle and therefore the amplification of the initial forces. This change in cortex mechanics is required for spindle migration from the oocyte

center to its cortex, generating an asymmetric division in size after anaphase. The asymmetry in size of the meiotic division allows the preservation of maternal stores accumulated during oocyte growth and required for embryo development. Although the drop in cortical tension is required for spindle migration in oocytes, as artificially stiffening the cortex impairs spindle off-centering (Chaigne et al., 2013), spindle migration is also prevented by a too low tension (Chaigne et al., 2015). Thus, the geometry of the division of mouse oocytes depends on a narrow window of cortical tension, regulated by myosin-II cortical localization, itself fine-tuned by actin nucleation. Importantly, cortex softening favors asymmetry of meiotic spindle positioning, whereas we could demonstrate that cortex stiffening in early zygotes, after fertilization, promotes symmetry of the division with spindle centering (Chaigne et al., 2016). The abrupt change in cortex properties between oocyte and early zygote is essential for the meiotic to mitotic transition in terms of geometry of division and appears conserved in humans (Yanez et al., 2016). Thus, we have unraveled that cortical actin mechanics, by regulating cortical tension and thus cell stiffness, impose the geometry of division of oocytes and zygotes (Chaigne et al., 2013; Chaigne et al., 2015; Chaigne et al., 2016). If defects in cortical tension affect the geometry of oocyte and embryo divisions, potentially impacting on their developmental potential (Kyogoku et al., 2017), it may not be the unique cause of arrest in development after fertilization. In this study, we wanted to address the origin of early developmental failure due to cortical tension defects in the oocyte other than perturbation in the asymmetry of the division. We focused on extra-soft oocytes, which represent the most common case in a natural population of human and mouse oocytes. To generate extra-soft oocytes, we used two constructs decreasing cortical tension when expressed in mouse oocytes. First, we used the cVCA construct (Chaigne et al., 2015) that forces Arp2/3-dependent actin nucleation at the cortex of oocytes. This cortical actin thickening chases myosin II from the cortex, which leads to cortical tension decrease and cortex softening (Chaigne et al., 2013; Chaigne et al., 2015). Second, we built a construct that induces ectopic actin nucleation by Formin 2 at the cortex of oocytes. The expression of this construct also induces myosin II cortical displacement and reduction in cortical tension.

Using these two different tools, we show that chromosome alignment is impaired in extra-soft oocytes, despite normal spindle morphogenesis and dynamics as assessed by FRAP analysis. Using a computational bio-imaging approach as well as fluorescence exclusion measurement of oocyte volume, we show that these oocytes are smaller, but that does not impede on their cytoplasmic activity (Almonacid et al., 2015). By performing laser ablation experiments, we

show that the intensity of the forces applied on the chromosomes is reduced in extra-soft oocytes, potentially participating to chromosome misalignment, but not the main contributor. Indeed, myosin II deregulation appears as the main cause of chromosome misalignment, since decreasing myosin II activity in extra-soft oocytes rescues chromosome alignment.

We are potentially describing a new mode of generation of aneuploidies that could be very common in female gametes. Indeed, 36% of oocytes are measured as too soft in a control population (Yanez et al., 2016). A fraction of these naturally soft oocytes might present chromosome alignment defects impeding on their future development after fertilization, contributing to the very high aneuploidy rate measured in female meiosis, a leading cause of infertility.

Results

Extra-soft oocytes due to cVCA expression harbor chromosome alignment defects.

Extra-soft oocytes are the most represented case in a natural population of mouse and human oocytes (Yanez et al., 2016). In order to study this subpopulation of oocytes specifically, we developed tools able to decrease cortical tension. One of them is the cVCA (Figure 1A), a construct that forces branched Arp2/3 dependent nucleation of a cortical F-actin thickening at the cortex, which chases cortical myosin II and leads to a decrease in cortical tension (Chaigne et al., 2015). As a consequence, cVCA expressing oocytes are extra-soft. We followed chromosome alignment and segregation by live spinning-disk microscopy during meiosis I in mouse oocytes expressing the cVCA construct. Whereas chromosomes are aligned on the metaphase I plate in controls, cVCA expressing oocytes display chromosome alignment defects before anaphase I (Figure 1B). We defined oocytes with misaligned chromosomes before anaphase I as having one or several chromosomes lagging away from the metaphase plate. Using this criterion, 48 % of oocytes expressing the cVCA present chromosomes that are not aligned before anaphase I (Figure 1C, right grey bar) compared to 15 % in controls (Figure 1C, left grey bar). cVCA oocytes still undergo anaphase on time despite having misaligned chromosomes (Chaigne et al., 2015), which could potentially lead to aneuploid oocytes. To further analyze chromosome behavior, we performed a linear discriminant analysis (LDA) to find discriminant features describing chromosome alignment 30 minutes before anaphase I in controls and cVCA expressing oocytes. The aspect ratio was

the most significantly different feature between control and cVCA expressing oocytes (Figure 1D). This feature describes the ratio of the width to the height of the ellipsis fitting all the chromosomes. If this ratio is close to 1, it means than the width and height of the ellipsis are similar, describing a circle, and showing that chromosomes are not aligned on the metaphase plate (Figure 1D red circle on the right). On the contrary if the ratio is close to 0, it means that the width is much smaller than the height and that chromosomes are aligned (Figure 1D red ellipsis on the left). For the controls, the aspect ratio is close to 0 (Figure 1D), showing that the chromosomes are aligned on the metaphase plate, fitting in a flat ellipsis. In cVCA expressing oocytes, the aspect ratio is scattered over the horizontal axis between 0 and 1, showing that chromosomes are less aligned than in controls (Figure 1D). Thus, the computational approach allowed to quantify and validate the chromosome alignment defects of cVCA expressing oocytes harboring a low cortical tension. We then analyzed chromosome movement by tracking individual chromosomes on the metaphase I plate during 20 minutes at the end of meiosis I (6 hours and thirty minutes after nuclear envelope breakdown, BD + 6h30). Individual chromosomes tracks suggest that chromosomes explore more space in metaphase I cVCA expressing oocytes than in controls (Figure 1E for representative examples, tracks are longer in cVCA expressing oocytes compared to controls), which is confirmed by their mean square displacement (MSD) analysis (Figure 1F). The mean square displacement (MSD) represents the space explored by single chromosomes and is obtained by averaging the square of the distance travelled per unit of time. Fitting of the MSD slopes to a simple linear model and statistical comparison of the slopes reveal different chromosome motion in cVCA expressing oocytes (Figure 1F blue curve) compared to controls (Figure 1F black curve). Interestingly, the movement of chromosomes in cVCA expressing oocytes is less confined, suggesting that chromosomes explore more space. However, their velocity is comparable to controls (compare black bar and blue bar in Figure S1A). Altogether, these data indicate that chromosome behavior is impaired in extra-soft cVCA expressing oocytes, which leads to chromosome misalignment on the metaphase I plate.

In addition, cVCA expressing oocytes also display strong cortical deformations due to their decrease in cortical tension (Figure S1B, compare red contours in control and cVCA expressing oocytes). These deformations are stable at long time scales (Figure S1C spanning 1h30) and at short time scales observed by high-frequency video microscopy (Supplementary movie S1, acquisitions every 500 milliseconds during 5 minutes at the end of meiosis I). Using a linear discriminant (LDA) analysis, we found that the contour area is the most

discriminant feature describing the shape of cVCA expressing oocytes. Most of the cVCA expressing population of oocytes is shifted towards small values of contour area (Figure S1D, blue bars). Differently, control oocytes are more spread, ranging from values of contour area comparable to cVCA expressing oocytes, to bigger values (Figure S1D, black bars). This suggests that cVCA expressing oocytes are smaller than controls. To test this in 3D, we took advantage of the fluorescence exclusion measurement (FXm) method initially described in Zlotek-Zlotkiewicz et al., 2015 (Figure S1E) in order to measure the volume of control and cVCA expressing oocytes. The mean volume of cVCA expressing oocytes (blue dots) is reduced by 9.45 % compared to controls (black dots, Figure S1F), as quantified at BD + 6h30. We then wondered what could be the consequences of this volume decrease, and in particular if it could impact cytoplasmic activity. Cytoplasmic activity represents the movement of the fluid substance (cytoplasm) within a cell. The cytoplasmic motion translates in the movement of intracellular components. We assessed oocyte cytoplasmic activity by tracking the movement of vesicles using high-frequency spinning-disk microscopy (Supplementary movie S2), as previously described by Almonacid et al., 2015. The MSD plots describing vesicle movement in the cytoplasm are similar, suggesting that the cytoplasmic activity is not impaired in oocytes expressing the cVCA (Figure S1G). Cytoplasmic activity contributes to nucleus positioning at the oocyte center in prophase I (Almonacid et al., 2015). Coherent with our results, the nucleus is accurately positioned in extra-soft cVCA expressing oocytes (Almonacid et al., 2015), suggesting again that the cytoplasmic activity is identical in control and cVCA expressing oocytes.

Extra-soft oocytes due to cFH1FH2 expression have chromosome alignment defects in metaphase I.

We then wondered whether impaired chromosome alignment was specific to cVCA expressing oocytes or if it would be observed in other oocytes with reduced cortical tension. To answer this question, we built a construct that forces linear actin nucleation by Formin 2 at the cortex of mouse oocytes. This construct was obtained by fusing the FH1FH2 actin nucleating domain of Formin 2 to Ezrin (Figure 2A). Similar to the cVCA, the cFH1FH2 construct localizes specifically to the oocyte cortex (Figure S2A, bottom left panel). Unlike the cVCA construct and probably due to the difference in the nature of the network nucleated (branched for the cVCA versus linear for the cFH1FH2), oocytes expressing the cFH1FH2 do not nucleate a cortical actin thickening (Figure S2A right panels and S2B). Cortical actin was labeled with GFP-UtrCH and visualized by confocal spinning disk microscopy in prophase I

oocytes (in grey levels in the magnified insets, Figure S2A). The mean cortical actin thickness in prophase I oocytes expressing the cFH1FH2 construct is of 0.67 ± 0.14 µm (Figure S2B, magenta bar) comparable to 0.63 ± 0.15 µm in controls (Figure S2B, black bar). Surprisingly, expression of the cFH1FH2 construct is sufficient to chase myosin II from the cortex (Figure 2B and 2C). We quantified the fluorescence signal intensity of myosin II labeled with a GFP-coupled intrabody (Nizak et al., 2003) in the cytoplasm and the cortex. Myosin II is enriched at the cortex of prophase I control oocytes (Figure 2B left panels, Figure 2C black bar, Chaigne et al., 2013; Chaigne et al., 2015) but displaced from the cortex and enriched in the cytoplasm of oocytes expressing the cFH1FH2 in prophase I (Figure 2B right panel, Figure 2C magenta bar). These data show that unregulated nucleation of linear actin by Formin 2 at the cortex of oocytes is sufficient to chase myosin II, suggesting that myosin II could be chased by steric hindrance and not by preferential binding to linear actin nucleated by Formin 2 or branched actin nucleated by Arp2/3 at the cortex of mouse oocytes. At last, cFH1FH2 expression induces a significant decrease in cortical tension. Indeed, the value of cortical tension measured by micropipette aspiration is 0.41 ± 0.24 nN/µm in oocytes expressing the cFH1FH2 in prophase I and 3.58 ± 1.10 nN/µm in control oocytes (Figure 2D). Thus, cortical myosin II removal in cFH1FH2 expressing oocytes leads to cortex softening as in cVCA expressing oocytes. Comparable to what was observed with the cVCA construct, meiosis I spindle migration is impaired in cFH1FH2 expressing oocytes (Figure S2C, D). The spindle did not migrate in 58.3 % of cFH1FH2 oocytes versus 16.6 % of controls. This reinforces the fact that cortical tension impacts meiosis I spindle migration in mouse oocytes (Chaigne et al., 2013; Chaigne et al., 2015).

Very interestingly, cFH1FH2 expressing oocytes also display chromosome alignment defects, similarly to cVCA expressing ones (Figure 2E-F). In controls, chromosomes are aligned on the metaphase I plate at the end of meiosis I (Figure 2E, upper panel), whereas chromosomes in oocytes expressing the cFH1FH2 do not form a proper metaphase plate (Figure 2E, bottom panel). In particular, 58 % of cFH1FH2 oocytes have misaligned chromosome before anaphase (Figure 2F, right bar) against 19 % of controls (Figure 2F, left bar). To further quantify chromosome alignment, we measured the width of the bounding box corresponding to the minimal area that encompasses the metaphase I plate as a readout for chromosome alignment (Figure 2G, yellow square and yellow dash line). If chromosomes are misaligned, the bounding box width should be larger than when chromosomes are tightly aligned. Indeed, the bounding box width is increased before anaphase in cFH1FH2 expressing oocytes (14.07

± 4.55 µm, Figure 2G magenta bar) compared to controls (10.67 ± 1.90 µm, Figure 2G black bar). The bounding box width is used in the following figures to assess chromosome alignment since it gives results that are consistent with the chromosomes aspect ratio coming from the computational imaging approach (Figure 1D).

In conclusion, myosin II is displaced from the cortex in cFH1FH2 expressing oocytes, leading to a cortical tension decrease. Interestingly, extra-soft cFH1FH2 expressing oocytes harbor a high rate of misaligned chromosomes in meiosis I, a feature shared with cVCA expressing ones. Altogether, these results suggest that chromosome alignment errors could be a hallmark of oocytes with too low cortical tension, the most common defect in a natural population of mouse and human oocytes (Yanez et al., 2016).

Forces transmitted to chromosomes are altered in extra-soft oocytes.

We then asked what could induce the chromosome defects observed in extra-soft oocytes. First, we analyzed spindle morphogenesis. Indeed, it was shown in mitotic cells that aberrant cortical tension impairs spindle formation, leading to chromosome segregation errors (Lancaster et al., 2013). In particular, cells lacking the ERM protein Moesin present spindle and chromosome defects (Lancaster et al., 2013). These cells are flat; thus, the spindle cannot form properly in confinement and microtubules cannot reach and capture chromosomes. We monitored spindle morphogenesis by live spinning disk microscopy during meiosis I in mouse oocytes incubated with SiR-Tubulin to label microtubules (Figure 3A). Although they have misaligned chromosomes (Figure 3 bottom panel), the spindle appears to form properly in cVCA expressing oocytes (Figure 3A, second panel) as in controls (Figure 3A, upper panel). Consistent with this observation, the spindle length of extra-soft cVCA expressing oocytes is comparable to controls at BD + 6h30. The average spindle length is 29.93 ± 1.64 µm in cVCA expressing oocytes (Figure 3B, blue bar) and 29.27 ± 1.80 µm in controls (Figure 3B, black bar). In addition, we performed FRAP analysis of SiR-Tubulin-labeled microtubules within the spindle at BD + 6h30 (illustration in Figure 3C yellow dot) when kinetochore fibers are already present (for review see Bennabi et al., 2016). The recovery curves are essentially the same in cVCA expressing oocytes (Figure 3C, blue curve) than in controls (Figure 3C, black curve), suggesting that the dynamics of spindle microtubules is similar. Coherent with this observation, chromosome velocity in cVCA expressing oocytes is comparable to controls (compare black bar and blue bar in Figure S1A). All these data indicate that spindle morphogenesis and dynamics are comparable to controls in extra-soft

cVCA expressing oocytes. This is not surprising considering that contrary to mitotic cells, mouse oocytes are very large cells (diameter ≈ 80 µm). Hence, the spindle is not constrained despite the strong cortical deformations present in cVCA expressing oocytes. Moreover, it was shown previously that the expression of the cVCA does not alter the architecture or the dynamics of the cytoplasmic actin network (Chaigne et al., 2015), two features that if modified could have potentially affected spindle formation (Azoury et al., 2011).

Next, we assessed the forces applied on chromosomes. Previous work showed that spindle migration is impaired in too soft oocytes, suggesting that the forces applied on the spindle are altered (Chaigne et al., 2015). This was also predicted by a theoretical model and confirmed experimentally (Chaigne et al., 2015). In addition, chromosome migration from the center of the oocyte to the cortex depends only on F-actin (Verlhac et al., 2000; Schuh and Ellenberg, 2008; Li et al., 2008; Azoury et al., 2008) and not on the presence of astral microtubules as in mitotic cells (Théry et al., 2007; Fink et al., 2011; Kwon et al., 2015) since oocytes are devoid of centrioles and astral microtubules (Sathananthan et al., 1997; Szollosi et al., 1972). Actin is organized in a cytoplasmic meshwork including an actin cage around the microtubule spindle, which is connected to the subcortical actin network (Figure 4A, Azoury et al., 2008; Schuh and Ellenberg, 2008; Chaigne et al., 2015; Mogessie and Schuh, 2017). We assessed the forces transmitted to chromosomes in controls and cVCA expressing oocytes by performing laser ablation. In control oocytes, the F-actin cytoplasmic meshwork was cut between the spindle pole and the closest cortex at BD + 6h30 on several Z stacks spanning the entire thickness of the metaphase plate (Figure 4A yellow dotted line and Figure S3A). Laser ablation did not damage oocytes since they all extruded a polar body and arrested in metaphase II normally following ablation (data not shown). After laser ablation, the response of Histone(H2B)-GFP labeled chromosomes was monitored by live microscopy during 1 minute. Microtubules were visualized using very low doses of EB3-GFP to follow the spindle and make sure that the ablation was not performed within the spindle and away from spindle poles (Figure 4B, S3B and S3D). Before laser ablation, the chromosomes are clustered and aligned on the metaphase plate in control oocytes at BD + 6h30 (Figure 4B, upper left panel t=0 min). Around 1 minute after laser cutting of the spindle attachment to the cortex, the metaphase plate shrinks (Figure 4B, upper middle panel). As a readout, we measured the width of the bounding box, which is the minimal area that encompasses the metaphase plate, before and after laser ablation (Figure 4B in plain and dotted yellow lines respectively). The width of the bounding box decreases progressively after ablation (Figure 4B upper panels, Figure 4C black curve) suggesting that the cytoplasmic and cortical actin networks transmit

forces to the chromosomes, maybe participating in putting them under tension in the spindle. We validated this observation by following the metaphase plate behavior in BD + 3h control oocytes because at that stage the spindle-cortex attachment is not formed yet, the cytoplasmic actin meshwork starting to assemble around BD + 3h (Azoury et al., 2008; Azoury et al., 2011). As expected laser ablation did not impact chromosome behavior when the spindle was not anchored to the cortex (Figure S3B and S3C compare green and black curves). In addition, we never observed progressive decrease of width of the bounding box englobing the metaphase I plate width without laser ablation in oocytes at BD + 6h30 (Figure S3D and S3E compare red and black curves).

In oocytes expressing the cVCA, chromosomes are scattered on the metaphase plate before ablation at BD + 6h30 (Figure 4B, bottom left panel t=0 min). After cutting of the spindle-cortex connection, the chromosomes remain scattered on the metaphase plate, which remains stable in width (Figure 4B bottom panels and Figure 4C blue curve). This suggests that, at that stage, the intensity of the forces applied on the chromosomes is reduced in cVCA expressing oocytes compared to controls. This result validates the mathematical modeling of spindle migration predicting that the balance and intensity of forces transmitted to the spindle are diminished in extra-soft oocytes harboring a lower cortical tension (Chaigne et al., 2015). Interestingly, another type of oocytes, the *Fmn2 -/-* oocytes, have reduced forces applied on their spindle. Indeed, *Fmn2 -/-* oocytes are invalidated for the cytoplasmic actin nucleator Formin 2 and lack the cytoplasmic meshwork and the actin cage (Azoury et al., 2008; Schuh and Ellenberg, 2008). As a consequence, the spindle is not attached to the cortex and does not migrate (Leader et al., 2002; Dumont et al., 2007). Thus, in *Fmn2-/-* oocytes, the actin networks do not apply forces on the spindle or chromosomes. However, *Fmn2 -/-* oocytes do not have chromosome alignment defects in metaphase I (Figure 4D chromosomes are aligned on the metaphase plate in Ctrl and *Fmn2 -/-* oocytes; Mogessie and Schuh, 2017). Thus, a reduction in intensity of forces applied on chromosomes in cVCA expressing oocytes is unlikely to be the mechanism involved in the generation of misaligned chromosomes.

Decreasing myosin II activity in extra-soft oocytes rescues chromosome alignment.

Oocytes expressing the cVCA or the cFH1FH2 share chromosome alignment defects (Figure 1B and Figure 2E) and too soft cortex (Figure 2D and Chaigne et al., 2015). In addition, they both displace precociously myosin II from the cortex as observed by myosin II labeling using a GFP-coupled intrabody (Figure 2B and Chaigne et al., 2015). It is known that myosin II localizes at the cortex in prophase I and at spindle poles during meiosis I in mouse oocytes

(Schuh and Ellenberg, 2008; Chaigne et al., 2013). In particular, the active phosphorylated form of myosin II localizes at both poles of the actin cage (figure 5A left panel) and exerts forces to position it. Indeed, inhibition of myosin II activation by MLCK phosphorylation using the ML-7 inhibitor (Figure 5A right panel, the active form of myosin II has disappeared from spindle poles after ML-7 treatment) impairs spindle migration (Schuh and Ellenberg, 2008; Chaigne et al., 2013 and Figure S4A lower panel the chromosomes are at the center of the oocyte in the ML-7 treated oocyte compared to the control oocyte in the upper panel harboring off-centered chromosomes). Myosin II is chased from the cortex in extra-soft cVCA and cFH1FH2 oocytes and enriched in the cytoplasm (Chaigne et al., 2015; Figure 2B and 2C). Hence, we wondered if higher levels of myosin II on the spindle could affect chromosome alignment in these two conditions. To test this hypothesis, we first visualized active myosin II by staining against its phosphorylated light chain pMLC2. Myosin II localizes on the spindle and its poles at BD + 6h30 in control oocytes (Figure 5A left panel). This staining is specific since it disappears in oocytes treated with the ML-7 inhibitor (Figure 5A right panel). Active myosin II is also enriched on the spindle and spindle poles in oocytes expressing the cVCA (Figure 5A, middle panel). Even if active myosin II seems more enriched on the spindle in cVCA expressing oocyte compare to controls (Figure 5A left and middle panels), we could not quantify it, due to the high background generated by this antibody rendering quantifications problematic. Next, we inhibited the activation of myosin II by using ML-7. As described above, cVCA expressing oocytes present chromosome misalignment in metaphase I (Figure 1B lower panel, Figure 5B upper panel). However, these chromosome defects are no longer observed in extra-soft oocytes treated with ML-7. Instead of being scattered along an extended metaphase plate, chromosomes are aligned on the metaphase I plate until anaphase in cVCA expressing oocytes treated with ML-7-treated (Figure 5B bottom panel). In particular, inhibition of myosin II activity rescues the width of the bounding box englobing the metaphase I plate. As observed in cFH1FH2 oocytes, the bounding box width is larger in cVCA expressing oocytes (Figure 5C, compare middle blue bar 14.61 ± 3.25 µm with black bar 10.67 ± 1.90 µm). Interestingly, the bounding box width is significantly rescued in ML-7 treated cVCA expressing oocytes and is comparable to controls (Figure 5C, right light blue bar 11.81 ± 2.04 µm). If ML-7 treatment rescues metaphase plate alignment in extra-soft oocytes it does not impact chromosome velocity or alignment in control oocytes (Figure S4A, S4B and S1A). Finally, all these data argue that altered myosin II activity impacts chromosome alignment on the metaphase I plate in extra-soft oocytes.

Discussion

We show that chromosome alignment is impacted by artificial reduction of cortex tension in mouse oocytes. Surprisingly, decreasing myosin II activity in these oocytes rescues chromosome alignment. A recent study identified genes involved in mitotic cell rounding, most of which affect cortical myosin II (Toyoda et al., 2017). Among them the endoplasmic reticulum protein FAM134A was identified as important for chromosome alignment and mitotic rounding by localizing cortical myosin II. Lower levels of active myosin II and lower cortical tension were also observed in aged oocytes (Mackenzie et al., 2016). We show that myosin II is displaced from the cortex and enriched in the cytoplasm in extra-soft oocytes (Chaigne et al., 2015; figure 2B-C). In addition, myosin II localizes on the spindle and its poles in mouse oocytes (Schuch and Ellenberg, 2008; figure 5A). Thus, higher myosin II levels on the spindle could potentially impact chromosome behavior in these extra-soft oocytes. Recently it was shown in mouse oocytes that actin promotes the formation of kinetochore fibers. Decreasing or increasing actin in the spindle respectively reduced or increased k-fibers, impeding on chromosome segregation at anaphase I but not on chromosome alignment in meiosis I (Mogessie and Schuh, 2017). The chromosome misalignment phenotype we describe here is not dependent on microtubule dynamics. In extra-soft oocytes, spindle morphogenesis and dynamics as assessed by FRAP analysis are normal, and chromosomes move as the same speed as in the controls (Figure 3A, 3B, 3C and S1A). The fact that myosin II deregulation can impact chromosome alignment is unexpected because the alignment of chromosomes in meiosis I is usually thought to be mainly microtubule and kinesin dependent. However, there are evidences showing that myosin II is involved in microtubule functions. Myosin II localizes to the spindle and is implicated in kinetochore microtubule flux in metaphase I carne fly spermatocytes (Silverman-Gravira and Forer, 2003; Forer et al., 2007). It is also localized to chromosome arms and to the spindle in PtK1 cells (Robinson and Snyder, 2005). In addition, myosin II is required for proper spindle assembly and positioning in mitotic cells (Rosenblatt et al., 2004) and mouse cardiac myocytes (Ma et al., 2010). Another interesting example is the mechanosentive role of cortical myosin II on microtubule growth in endothelial cells, where inhibition of myosin II activity prevents MCAK mediated MT growth (D'angelo et al., 2017). At last, myosin II was shown to interact directly with kinesins in astrocytes, essential for their migration (Feng et al., 2016). Since we lack proper tools to investigate how myosin II impacts chromosome

alignment in our model, it would be interesting to address it by computational modeling or using *in vitro* models as described in Reymann et al., 2012 and Ennomani et al., 2016.

Our results describe that aberrant low cortical tension generates chromosome misalignment in oocytes, potentially leading to aneuploidy. This new mode of generation of aneuploidies could be very common in female gametes. Indeed, 36% of mouse and human oocytes are measured as too soft in a control population (Yanez et al., 2016) and cortical mechanics abnormalities are associated with post-ovulatory aging (Mackenzie et al., 2016). Thus, some of these naturally soft oocytes could have chromosome alignment defects impeding on their future development after fertilization, contributing to the very high aneuploidy rate measured in female meiosis, a leading cause of infertility (Hassold and Hunt, 2001; Hassold et al., 2007; Nagaoka et al., 2012). Cortical tension is extremely variable in a control population of oocytes (Larson et al., 2010; Chaigne et al., 2013; Chaigne et al., 2015; Yanez et al., 2016; Figure 2D). It is possible that depending on the extent of cortical tension deregulation, different phenotypes could be triggered, ranging from aberrant division geometry (Chaigne et al., 2013; Chaigne et al., 2015), chromosome mis-alignment (our present study), and maybe yet undiscovered phenotypes. Our study focused on extra-soft oocytes, the most frequent cortical tension defect. However, 19% of mouse and human oocytes are measured as too stiff in a natural population (Yanez et al., 2016). These extra-stiff oocytes also cease their development rapidly after fertilization. In these oocytes, myosin II is retained at the cortex, leading to aberrant division geometry (Chaigne et al., 2013, Chaigne et al., 2015). Chromosome alignment defects were never observed in these oocytes (Verlhac et al., 1996; Verlhac et al., 2000; Chaigne et al., 2013), so the reason why they cease development remains still elusive. Thus, it would be interesting to investigate if aberrant cortical tension correlates with aneuploidy in normal populations of mouse and human oocytes, and what range of cortical tension is associated with a specific phenotype. Measures of cortical mechanical properties could serve as a minimally invasive technique to assess oocyte developmental potential for assisted reproductive technology, as explored already for tumors (for reviews see Lekka, 2016; Sant et al., 2017). Our study could therefore help to develop new criteria of oocyte and embryo quality to improve assisted reproductive technologies.

At last, aberrant cortical tension, and especially cortex softening, is found in a variety of cancer cells (Guck et al., 2005; Suresh et al., 2005; Hou et al., 2009; Xu et al., 2012). Myosin II deregulation has been described in several human diseases such as neuronal disorders, cancers and vascular disease (Newell-Litwa et al., 2015). Interestingly, overexpression of

myosin II is implicated in cancer progression and metastasis, and myosin II regulatory pathway genes are increasingly found in disease-associated copy-number variants, particularly in neuronal disorders such as autism and schizophrenia (Newell-Litwa et al., 2015), stressing the importance of its regulation. The mechanisms described in this study could therefore be relevant in a broader context.

Material and methods

Oocyte collection, culture and microinjection.

Ovaries were collected from 11-week-old OF1 (wt) or *Fmn2-/-* (Leader et al., 2002) female mice. Fully-grown oocytes were extracted by shredding the ovaries (Verlhac et al., 1994) in M2+BSA medium supplemented with 1 μM milrinone to block and synchronize them in Prophase I (Reis et al., 2006). Transferring oocytes into milrinone-free M2+BSA medium triggers meiosis resumption. All live-culture and imaging were carried out under oil at 37°C.

Constructs.

We used the following constructs: pRN3-Histone(H2B)-GFP (Manil-Segalen et al., 2018), pRN3-EB3-GFP (Breuer et al., 2010), pspe3-GFP-UtrCH (Azoury et al., 2008), pRN3-SF9-GFP (Nizak et al., 2003; Chaigne et al., 2013), pRN3-EzTD-mCherry-VCA (Chaigne et al., 2015), pRN3-EzTD-mCherry (Dard et al., 2004; Chaigne et al., 2015).

The pRN3-EzTD-mCherry-FH1-FH2 was constructed by cloning a linker GGSGGGSG connected to the FH1-FH2 domain of Formin 2 (amino acids 734 to 1578) amplified from a pCS2-FH1-FH2-eGFP (Almonacid et al., 2018) into pRN3-EzTD-mCherry (Dard et al., 2004; Chaigne et al., 2015).

In vitro transcription of cRNAs and microinjection.

Plasmids were linearized using appropriate restriction enzymes. cRNAs were synthesized with the mMessage mMachine kit (Ambion) and subsequently purified using the RNAeasy kit (Qiagen). Their concentration was measured using NanoDrop 2000 from ThermoScientific. cRNAs were centrifuged at 4°C during 45 minutes prior to microinjection into the cytoplasm of oocytes blocked in Prophase I in M2+BSA medium supplemented with 1 μM milrinone at 37°C. cRNAs were microinjected using an Eppendorf Femtojet microinjector (Verlhac et al., 2000). After microinjection, cRNA translation was allowed for 1 or 2 hours, oocytes were then transferred into milrinone-free M2+BSA medium to allow meiosis resumption and meiotic divisions.

Drug treatments.

ML-7 (Calbiochem, Ref 475880) was diluted at 30 mM in DMSO and stored at 4°C. After dilution in M2 medium, it was used on oocytes at 60 μM. ML-7 was added on OF1 oocytes 5 hours after nuclear envelope breakdown because at that stage the spindle is bipolar but did not

yet migrate to the closest cortex (Verlhac et al., 2000). Control experiments were conducted in M2+BSA medium with equivalent concentrations of DMSO.

Nile red stain (Sigma, Ref N3013) was used to label the total pool of vesicles. It was diluted at 5 mg/ml 1 in DMSO and stored at room temperature. It was used on oocytes at 10 μg/ml.

Immunofluorescence.

After *in vitro* culture of oocytes, their zona pellucida was removed by incubation in acid Tyrode's medium (pH = 2.3). Oocytes were fixed for 30 min at 37°C in 100 mM HEPES (pH 7) (titrated with KOH), 50m MEGTA (pH 7) (titrated with KOH), 10mM MgSO4, 2% Formaldehyde (MeOH free), 0.3% Triton X-100 on coverslips treated with gelatin and polylysine. Oocytes were left in PBS, 0.1% Triton X-100 overnight at 4°C. After 20 min of blocking in 0.1% Triton X-100, 3% BSA, antibody staining was performed in PBS, 0.1% Triton X-100, 3% BSA. As primary antibody, we used rabbit anti-Phospho-MLC2 (Ser19) (Cell Signaling; 1:100). As secondary antibody, we used Alexa-488-labeled anti-rabbit (Molecular Probes; 1:500). DNA was stained with Prolong-DAPI (10 μg/mL final DAPI).

Live imaging

Spinning Disk movies were acquired using 1) a Plan-APO 40x/1.25NA objective on a Leica DMI6000B microscope enclosed in a thermostatic chamber (Life Imaging Service) equipped with a CoolSnap HQ2/CCD-camera coupled to a Sutter filter wheel (Roper Scientific) and a Yokogawa CSU-X1-M1 spinning disk or 2) a Plan-APO 60x/1.4NA objective on a Ti Nikon microscope enclosed in a thermostatic chamber (Life Imaging Service) equipped with a cMOS camera coupled to a Yokogawa CSU-X1 spinning disk. Metamorph Software (Universal Imaging) was used to collect data.

Chromosome movement analysis.

Oocytes were microinjected in prophase I with cRNAs encoding Histone(H2B)-GFP with or without cRNAs encoding EzTD-mCherry-VCA to label the chromosomes and decrease or not cortical tension. After microinjection, cRNA translation was allowed for 1h. Oocytes were then treated or not with ML-7 at BD + 5h, and imaged under a spinning disk at BD + 6h30. Oocytes were positioned so that their spindle was parallel to the plane of observation and illuminated with an excitation wavelength of 561 nm during 300 ms (first timepoint only) and 491 nm during 300 ms (all timepoints). Acquisitions were done every 20 seconds for 20

minutes, on three planes (z-steps of 2 μm) focused on the chromosomes. The manual tracking plugin on Fiji (NIH) was used to track chromosome movement and velocity. Only the chromosomes individualized and visible on the 3 planes for the whole duration of the movie were tracked.

Oocyte volume measurement using FXm.

The FXm (Fluorescence eXclusion measurement) method was initially described in Zlotek-Zlotkiewicz et al., 2015 and a detailed protocol is available in Cadart et al., 2017. Measurements were made in PDMS chambers that consisted in a simple straight 113 μm high channel. A 2 mm diameter inlet and a 0.5 mm diameter outlet were punched on either side of the channel. The chambers were irreversibly bound to glass-bottomed Petri dishes (Fluorodishes) by plasma treatment. To prevent cell adhesion of the cell and allow reusing the chamber for successive measurements on different cells, chambers were coated with PLL-g-PEG (1%). Before starting the experiment, the chamber was rinsed with M2+BSA medium containing 0,5 mg/mL of 70kDa FITC-Dextran (Sigma, Ref FD70S). Oocytes were measured one by one. Each time, the cell was deposited with a mouth-pipette in the inlet. In order to aspirate the oocyte into the middle of the chamber in a controlled manner, a 250 μL glass syringe was plugged to the outlet via an approximately 30 cm long PTFE tube previously filled with 100 μL of the M2+BSA dextran solution. The oocyte was then positioned in the center of the chamber and far from the borders of the channel. The chamber was then transferred to a Leica DMIRBE inverted microscope. Bright field and fluorescence images (excitation wavelength of 491 nm) were acquired using a 10X NA0.3 objective. For the image analysis, a home-made Matlab software described in Cadart et al., 2017 was used. Briefly, fluorescent signal was calibrated for every image using the fluorescence intensity (I_{min}) under the borders of the chamber ($h_{min} = 0$) and the intensity (I_{max}) of the background around the cell ($h_{max} = chamber\ height = 113\ \mu m$). The calibration factor α was then calculated as follows : $\alpha = (I_{max} - I_{min})\ /\ h_{max}$. The volume of the cell (V_{cell}) was obtained by integrating the fluorescence intensity collected under the cell : $V_{cell} = \iint_{x,y} \frac{I_{max} - I_{x,y}}{\alpha}\ dxdy$

Cytoplamic activity measurements.

The total vesicles stained with Nile red contained in oocytes at BD + 6h30 were imaged every 500ms with the stream acquisition mode of Metamorph on excitation at 491 nm.

Nile Red-labeled-vesicle tracking and MSD quantification was performed as described in

Almonacid et al., 2015 as follows. After subtracting the background, time-lapse videos were realigned using the rigidbody algorithm of the stackreg plugin in Fiji and then denoised on Metamorph using the Safir denoising program (Roper Scientific). Stacks were then corrected for bleaching using the Histogram Matching algorithm in Fiji and thresholded on Metamorph to generate a binary stack of vesicles. Tracking was then performed on these binary vesicles videos with the TrackMate plugin in Fiji (http://fiji.sc/TrackMate) using DoG detector with a detected object diameter adjusted according to the pattern of vesicles, a thresholding of 1 and sub-pixel localization, and the following settings for gap closing in the simple LAP tracker: linking maximum distance of 1 µm, gap closing maximum distance of 1 µm and a maximum gap of 2 frames allowed. Tracks were filtered according to their duration, considering only tracks lasting for more than 25 s. The results of the tracking, including the diameter and the velocities of the vesicles, were provided as Excel and xml files. The velocities values correspond to the mean velocity of a vesicle within a track.

For mean square displacement (MSD) analysis of vesicles trajectories, we used the @msdanalyzer MATLAB class described in: http://bradleymonk.com/matlab/msd/MSDTuto.html. Trajectories were provided in the xml files from Fiji TrackMate analysis.

Cortical tension measurements.

Cortical tension was measured by micropipette aspiration as described in Chaigne et al., 2013. Briefly, the zona pellucida of prophase I arrested oocytes was removed by incubating oocytes into M2 + BSA medium supplemented with 0.4% pronase. Oocytes were loaded onto a chamber equilibrated with M2 + BSA medium. A glass micropipette of a diameter 5 times smaller than the oocyte diameter was connected to a water reservoir of adjustable height to apply a defined aspiration pressure. Zero aspiration pressure was set before each experiment by checking the absence of visible flow inside the pipette. Observations were made through an inverted microscope (Axiovert 200, Zeiss) equipped with a x40 immersion oil objective (Neofluar 1.3 NA) and connected to a CCD camera (XC-ST70CE, Sony). For every applied pressure, we monitored the length L of the oocyte portion aspirated in the pipette as a function of time and derived the speed dL/dt at which the oocyte cortex enters the pipette. Then, we extrapolated the critical aspiration pressure ΔP_c at which dL/dt=0 from the plot dL/dt versus the aspiration pressure. To obtain the cortical tension T_c, we used the viscous drop model previously used for cells (Evans et al., 1989),

$$T_c = \frac{R\Delta P_c}{2\left(1-\frac{R}{R_c}\right)}$$

where R is the pipette radius and Rc is the cell radius.

In prophase I, the absolute values of cortical tension for *wt*, and cVCA expressing oocytes are 3.58 +/- 1.1 and 0.41 +/- 0.2 nN/μm respectively.

FRAP analysis.

Images were acquired using a Plan-APO 60x/1.4NA objective on a Ti Nikon microscope enclosed in a thermostatic chamber (Life Imaging Service) equipped with a Evolve EMCCD camera coupled to a Yokogawa CSU-X1 spinning disk. Metamorph Software (Universal Imaging) was used to collect data. All oocytes expressed SiR-Tubulin (from Spirochrome reference SC002, used at 0.1 μM). For all oocytes an identical region of interest was bleached in the spindle. Images were acquired every 2 seconds for 180 seconds. One image was taken before bleaching. The SiR-Tubulin fluorescence intensity quantification was performed using the Metamorph software (Universal Imaging). Normalization was performed using the Microsoft Excel software. As the expression levels of SiR-Tubulin varies from one experiment to another, the signal intensity was normalized so that the prebleached value was 1 and the value at the first time-point after bleaching was 0.

Laser ablation.

Laser ablation was performed as described in Bennabi and Segalen., 2018. We used a 355 laser and i-LAS^2 module (Roper Scientific) coupled to a Leica DMI6000B microscope enclosed in a thermostatic chamber (Life Imaging Service) equipped with a Retiga 3 CCD camera (QImaging) coupled to a Sutter filter wheel (Roper Scientific) and a Yokogawa CSU-X1-M1 spinning disc using a Plan-APO 40x/1.25 NA objective. Metamorph (Universal Imaging) was used to process the data. After calibrating the system, the ablation zone (ROI) was determined. It consisted of a line positioned after the spindle pole in the cytoplasm of the oocyte. To perform the laser ablation, the spindle must be oriented with its long axis parallel to the observation plane. The laser ablation parameters used were as follows: 350 nm laser Z thickness 10 μm, dZ 1 μm. Oocytes were then images after ablation with the following parameters: 491 nm laser power during 500 ms, acquisitions every 20 seconds for 2 minutes, on one plane.

Metaphase plate width was measured by performing bounding boxes containing all the chromosomes with the Fiji (NIH) software. The Microsoft Excel software was used to normalize the data.

Quantifications.

- Metamorph (Universal Imaging), Imaris (Oxford Instruments) and Fiji (NIH) software were used to analyze and process data.

- Chromosome alignment before anaphase was assessed on oocytes expressing Histone(H2B)-GFP using Metamorph software.

- Metaphase plate width was measured by performing bounding boxes with the Fiji (NIH) software. Measurements were done 30 minutes before anaphase only on spindles parallel to the imaging plane.

- Myosin-II cortical enrichment was quantified by measuring the ratio of the cortical and cytoplasmic SF9-GFP (Nizak et al., 2003) fluorescence intensities. Oocytes expressed SF9-GFP alone (controls) and together with the cFH1FH2 construct for five hours in Prophase I. The background was removed from all images analyzed using Metamorph software. Cytoplasmic and cortical integrated fluorescence intensities were measured randomly six times in each compartment (cortex and cytoplasm) per oocyte using the same square ROI of 0,91 μm^2 (region smaller than the cortex width). Measurements were taken on one focal plane (corresponding to the oocyte longest diameter). The cortical fluorescence intensity per square pixels was then divided by the cytoplasmic one.

- Cortical thickness measurements were performed as described in Chaigne et al., 2013. Briefly, cortical thickness, consisting of the cortical outer layer (stable throughout meiosis I) and the cortical inner layer (absent in Prophase I and progressively nucleated after nuclear envelope breackdown in controls) was measured manually using Fiji software. Oocytes expressed GFP-UtrCH alone (controls) and together with the cFH1FH2 construct for five hours in Prophase I. Six measures per oocyte were randomly taken along the cortex on one focal plane (corresponding to the oocyte longest diameter). The difference between the cytoplasmic and cortical GFP-UtrCH signals was strong enough to discriminate between the two actin networks and to detect the cortical actin network boundary.

- Spindle migration was quantified by measuring distances between the centroid of the oocyte and the centroid of the spindle (oocytes were incubated in SiR-Tubulin at 0.1 μM) using the Fiji (NIH) software. Measuring the distance traveled between the centroid of the spindle relative to the centroid of the oocyte allows discriminating between oocyte movement and spindle movement. Measurements were performed at two timepoints: 4 hours before anaphase I when the spindle has not yet started to migrate to the cortex and 30 minutes before anaphase I when the spindle has almost reached the cortex in the controls. Analyses were done on a Z-projection of 8 stacks of 4μm, allowing to get the entire spindle. Only spindle parallels to the plane of observation were quantified.

- The spindle length measurements were performed using Metamorph software. Spindle length was measured as the distance between poles in spindles parallel to the imaging plane only.

- Computation of MSD for chromosome movement. For each tracked cluster representing either a chromosome either a group of chromosomes in a given spindle, the squared distances for all possible time steps (dt) were computed and averaged per time step producing an individual MSD value per dt, thus an MSD curve per cluster. All curves corresponding to all clusters of a given nucleus were averaged to obtained one MSD curve per nucleus. Following this, all curves corresponding to a nucleus were averaged per condition to produce one MSD curve per condition.

Quantitative image analysis.

- Computation of chromosomes shape. Detections were obtained from manually cropped region of interest around the chromosomes using the Phansalkar thresholding method with radius 130 available in Fiji. All pixels of the detection were subsequently used to compute a covariance matrix. Eigenvalues Lmin and Lmax were obtained after diagonalization of this matrix and the aspect ratio (Lmin/Lmax) was reported for each cell.
- Computation of oocytes area at the last image before division. Using a dedicated python script, anisotropic diffusion was first applied to the oocyte contour channel in order to reduce noise. An automated Otsu threshold was then performed and the largest connected component was kept as the oocyte segmentation. The total number of pixels of the oocyte segmentation was then converted to an area using pixel size.

Statistical analysis.

Experiments were repeated at least three times and a sample of sufficient size was used. The statistical analysis was performed using GraphPad Prism version 7.00 for MacOS, GraphPad Software, La Jolla, California, USA, www.graphpad.com. For comparisons between two groups, the normality of the variables was checked (D'agostino-Pearson normality test) and parametric Student's t-tests (with Welch correction when indicated) or non-parametric comparison tests were performed with a confidence interval of 95%. For chromosome alignment experiments, repartitions were analyzed for statistical significance using Fisher's test used with a confidence interval of 95%. For volume measurements, a wilcoxon rank sum test was performed to compare the mean of the two conditions.

To compare the regression slope values for MSDs, we did a Welch's test of the regression models, as presented in Andrade et al., 2014 (as the residual variances of the models were not equal).

All error bars are expressed as standard deviation (SD). Values of $P<0.05$ were considered significant. In all figures, * corresponds to a P-value <0.05, ** to a P-value <0.005, *** to a P-value <0.0001. n.s: not statistically significant.

References

Almonacid, M., W.W. Ahmed, M. Bussonnier, P. Mailly, T. Betz, R. Voituriez, N.S. Gov, and M.-H. Verlhac. 2015. Active diffusion positions the nucleus in mouse oocytes. *Nat. Cell Biol.* 17:470–479. doi:10.1038/ncb3131.

Almonacid M, El-Hayek S, Othmani A, Queguiner I, Coulpier F, Lemoine S, Bastianelli L, Klein C, Piolot T, Mailly P, et al.: Active fluctuations modulate gene expression in mouse oocytes. bioRxiv 2018, doi:10.1101/347310.

Andrade, J.M., and M.G. Estévez-Pérez. 2014. Statistical comparison of the slopes of two regression lines: A tutorial. *Anal. Chim. Acta*. 838:1–12. doi:10.1016/j.aca.2014.04.057.

Azoury, J., K.W. Lee, V. Georget, P. Hikal, and M.-H. Verlhac. 2011. Symmetry breaking in mouse oocytes requires transient F-actin meshwork destabilization. *Development*. 138:2903–2908. doi:10.1242/dev.060269.

Azoury, J., K.W. Lee, V. Georget, P. Rassinier, B. Leader, and M.-H. Verlhac. 2008. Spindle Positioning in Mouse Oocytes Relies on a Dynamic Meshwork of Actin Filaments. *Curr. Biol.* 18:1514–1519. doi:10.1016/j.cub.2008.08.044.

Bennabi, I., and M. Manil-Ségalen. 2018. Laser Ablation of Microtubule–Chromosome Attachment in Mouse Oocytes. *In* Mouse Oocyte Development. M.-H. Verlhac and M.-E. Terret, editors. Springer New York, New York, NY. 153–161.

Bennabi, I., M.-E. Terret, and M.-H. Verlhac. 2016. Meiotic spindle assembly and chromosome segregation in oocytes. *J. Cell Biol.* 215:611–619. doi:10.1083/jcb.201607062.

Breuer, M., A. Kolano, M. Kwon, C.-C. Li, T.-F. Tsai, D. Pellman, S. Brunet, and M.-H. Verlhac. 2010. HURP permits MTOC sorting for robust meiotic spindle bipolarity, similar to extra centrosome clustering in cancer cells. *J. Cell Biol.* 191:1251–1260. doi:10.1083/jcb.201005065.

Brunet, S., and B. Maro. 2007. Germinal vesicle position and meiotic maturation in mouse oocyte. *Reproduction*. 133:1069–1072. doi:10.1530/REP-07-0036.

Cadart, C., S. Monnier, J. Grilli, R. Attia, E. Terriac, B. Baum, M. Cosentino-Lagomarsino, and M. Piel. 2017. Size control in mammalian cells involves modulation of both growth rate and cell cycle duration. doi:10.1101/152728.

Chaigne, A., C. Campillo, N.S. Gov, R. Voituriez, J. Azoury, C. Umaña-Diaz, M. Almonacid, I. Queguiner, P. Nassoy, C. Sykes, M.-H. Verlhac, and M.-E. Terret. 2013. A soft cortex is essential for asymmetric spindle positioning in mouse oocytes. *Nat. Cell Biol.* 15:958–966. doi:10.1038/ncb2799.

Chaigne, A., C. Campillo, N.S. Gov, R. Voituriez, C. Sykes, M.H. Verlhac, and M.E. Terret. 2015. A narrow window of cortical tension guides asymmetric spindle positioning in the mouse oocyte. *Nat. Commun.* 6:6027. doi:10.1038/ncomms7027.

Chaigne, A., C. Campillo, R. Voituriez, N.S. Gov, C. Sykes, M.-H. Verlhac, and M.-E. Terret. 2016. F-actin mechanics control spindle centring in the mouse zygote. *Nat. Commun.* 7:10253. doi:10.1038/ncomms10253.

D'Angelo, L., N.M. Myer, and K.A. Myers. 2017. MCAK-mediated regulation of endothelial cell microtubule dynamics is mechanosensitive to myosin-II contractility. *Mol. Biol. Cell*. 28:1223–1237. doi:10.1091/mbc.e16-05-0306.

Dard, N., S. Louvet-Vallée, A. Santa-Maria, and B. Maro. 2004. Phosphorylation of ezrin on threonine

T567 plays a crucial role during compaction in the mouse early embryo. *Dev. Biol.* 271:87–97. doi:10.1016/j.ydbio.2004.03.024.

Dumont, J., K. Million, K. Sunderland, P. Rassinier, H. Lim, B. Leader, and M.-H. Verlhac. 2007. Formin-2 is required for spindle migration and for the late steps of cytokinesis in mouse oocytes. *Dev. Biol.* 301:254–265. doi:10.1016/j.ydbio.2006.08.044.

Ennomani, H., G. Letort, C. Guérin, J.-L. Martiel, W. Cao, F. Nédélec, E.M. De La Cruz, M. Théry, and L. Blanchoin. 2016. Architecture and Connectivity Govern Actin Network Contractility. *Curr. Biol.* 26:616–626. doi:10.1016/j.cub.2015.12.069.

Evans, E., and A. Yeung. 1989. Apparent viscosity and cortical tension of blood granulocytes determined by micropipet aspiration. *Biophys. J.* 56:151–160. doi:10.1016/S0006-3495(89)82660-8.

Feng, J., Z. Hu, H. Chen, J. Hua, R. Wu, Z. Dong, L. Qiang, Y. Liu, P.W. Baas, and M. Liu. 2016. Depletion of kinesin-12, a myosin-IIB-interacting protein, promotes migration of cortical astrocytes. *J. Cell Sci.* 129:2438–2447. doi:10.1242/jcs.181867.

Fink, J., N. Carpi, T. Betz, A. Bétard, M. Chebah, A. Azioune, M. Bornens, C. Sykes, L. Fetler, D. Cuvelier, and M. Piel. 2011. External forces control mitotic spindle positioning. *Nat. Cell Biol.* 13:771–778. doi:10.1038/ncb2269.

Forer, A., T. Spurck, and J.D. Pickett-Heaps. 2007. Actin and myosin inhibitors block elongation of kinetochore fibre stubs in metaphase crane-fly spermatocytes. *Protoplasma*. 232:79–85. doi:10.1007/s00709-007-0265-8.

Guck, J., S. Schinkinger, B. Lincoln, F. Wottawah, S. Ebert, M. Romeyke, D. Lenz, H.M. Erickson, R. Ananthakrishnan, D. Mitchell, J. Käs, S. Ulvick, and C. Bilby. 2005. Optical Deformability as an Inherent Cell Marker for Testing Malignant Transformation and Metastatic Competence. *Biophys. J.* 88:3689–3698. doi:10.1529/biophysj.104.045476.

Hassold, T., H. Hall, and P. Hunt. 2007. The origin of human aneuploidy: where we have been, where we are going. *Hum. Mol. Genet.* 16:R203–R208. doi:10.1093/hmg/ddm243.

Hassold, T., and P. Hunt. 2001. To err (meiotically) is human: the genesis of human aneuploidy. *Nat. Rev. Genet.* 2:280–291.

Hou, H.W., Q.S. Li, G.Y.H. Lee, A.P. Kumar, C.N. Ong, and C.T. Lim. 2009. Deformability study of breast cancer cells using microfluidics. *Biomed. Microdevices*. 11:557–564. doi:10.1007/s10544-008-9262-8.

Kwon, M., M. Bagonis, G. Danuser, and D. Pellman. 2015. Direct Microtubule-Binding by Myosin-10 Orients Centrosomes toward Retraction Fibers and Subcortical Actin Clouds. *Dev. Cell*. 34:323–337. doi:10.1016/j.devcel.2015.06.013.

Kyogoku, H., and T.S. Kitajima. 2017. Large Cytoplasm Is Linked to the Error-Prone Nature of Oocytes. *Dev. Cell*. 41:287–298.e4. doi:10.1016/j.devcel.2017.04.009.

Lancaster, O.M., M. Le Berre, A. Dimitracopoulos, D. Bonazzi, E. Zlotek-Zlotkiewicz, R. Picone, T. Duke, M. Piel, and B. Baum. 2013. Mitotic Rounding Alters Cell Geometry to Ensure Efficient Bipolar Spindle Formation. *Dev. Cell*. 25:270–283. doi:10.1016/j.devcel.2013.03.014.

Larson, S.M., H.J. Lee, P. Hung, L.M. Matthews, D.N. Robinson, and J.P. Evans. 2010. Cortical mechanics and meiosis II completion in mammalian oocytes are mediated by myosin-II and Ezrin-Radixin-Moesin (ERM) proteins. *Mol. Biol. Cell*. 21:3182–3192.

Leader, B., H. Lim, M.J. Carabatsos, A. Harrington, J. Ecsedy, D. Pellman, R. Maas, and P. Leder. 2002. Formin-2, polyploidy, hypofertility and positioning of the meiotic spindle in mouse oocytes.

Nat. Cell Biol. 4:921–928. doi:10.1038/ncb880.

Lekka, M. 2016. Discrimination Between Normal and Cancerous Cells Using AFM. *BioNanoScience*. 6:65–80. doi:10.1007/s12668-016-0191-3.

Li, H., F. Guo, B. Rubinstein, and R. Li. 2008. Actin-driven chromosomal motility leads to symmetry breaking in mammalian meiotic oocytes. *Nat. Cell Biol.* 10:1301–1308. doi:10.1038/ncb1788.

Mackenzie, A.C.L., D.D. Kyle, L.A. McGinnis, H.J. Lee, N. Aldana, D.N. Robinson, and J.P. Evans. 2016. Cortical mechanics and myosin-II abnormalities associated with post-ovulatory aging: implications for functional defects in aged eggs. *Mol. Hum. Reprod.* 22:397–409. doi:10.1093/molehr/gaw019.

Manil-Ségalen, M., M. Łuksza, J. Kannaan, V. Marthiens, S.I.R. Lane, K.T. Jones, M.-É. Terret, R. Basto, and M.-H. Verlhac. 2018. Gene editing can generate fragile bivalents in mouse oocytes. doi:10.1101/350272.

Mogessie, B., and M. Schuh. 2017. Actin protects mammalian eggs against chromosome segregation errors. *Science*. 357:eaal1647. doi:10.1126/science.aal1647.

Nagaoka, S.I., T.J. Hassold, and P.A. Hunt. 2012. Human aneuploidy: mechanisms and new insights into an age-old problem. *Nat. Rev. Genet.* 13:493–504. doi:10.1038/nrg3245.

Newell-Litwa, K.A., R. Horwitz, and M.L. Lamers. 2015. Non-muscle myosin II in disease: mechanisms and therapeutic opportunities. *Dis. Model. Mech.* 8:1495–1515. doi:10.1242/dmm.022103.

Nizak, C., S. Martin-Lluesma, S. Moutel, A. Roux, T.E. Kreis, B. Goud, and F. Perez. 2003a. Recombinant antibodies against subcellular fractions used to track endogenous Golgi protein dynamics in vivo. *Traffic Cph. Den.* 4:739–753.

Reis, A., H.-Y. Chang, M. Levasseur, and K.T. Jones. 2006. APCcdh1 activity in mouse oocytes prevents entry into the first meiotic division. *Nat. Cell Biol.* 8:539–540.

Reymann, A.-C., R. Boujemaa-Paterski, J.-L. Martiel, C. Guérin, W. Cao, H.F. Chin, E.M. De La Cruz, M. Théry, and L. Blanchoin. 2012. Actin network architecture can determine myosin motor activity. *Science*. 336:1310–1314. doi:10.1126/science.1221708.

Robinson, R.W., and J.A. Snyder. 2005. Localization of myosin II to chromosome arms and spindle fibers in PtK1 cells: a possible role for an actomyosin system in mitosis. *Protoplasma*. 225:113–122. doi:10.1007/s00709-005-0085-7.

Rosenblatt, J., L.P. Cramer, B. Baum, and K.M. McGee. 2004. Myosin II-dependent cortical movement is required for centrosome separation and positioning during mitotic spindle assembly. *Cell*. 117:361–372.

Sant, G.R., K.B. Knopf, and D.M. Albala. 2017. Live-single-cell phenotypic cancer biomarkers-future role in precision oncology? *NPJ Precis. Oncol.* 1:21. doi:10.1038/s41698-017-0025-y.

Sathananthan, A.H. 1997. Mitosis in the human embryo: the vital role of the sperm centrosome (centriole). *Histol. Histopathol.* 12:827–856.

Schuh, M., and J. Ellenberg. 2008. A New Model for Asymmetric Spindle Positioning in Mouse Oocytes. *Curr. Biol.* 18:1986–1992. doi:10.1016/j.cub.2008.11.022.

Silverman-Gavrila, R.V., and A. Forer. 2003. Myosin localization during meiosis I of crane-fly spermatocytes gives indications about its role in division. *Cell Motil. Cytoskeleton*. 55:97–113.

Suresh, S., J. Spatz, J.P. Mills, A. Micoulet, M. Dao, C.T. Lim, M. Beil, and T. Seufferlein. 2005. Connections between single-cell biomechanics and human disease states: gastrointestinal cancer and malaria. *Acta Biomater.* 1:15–30. doi:10.1016/j.actbio.2004.09.001.

Szollosi, D., P. CALARCO, and R.P. Donahue. 1972. Absence of centrioles in the first and second meiotic spindles of mouse oocytes. *J. Cell Sci.* 11:521–541.

Théry, M., A. Jiménez-Dalmaroni, V. Racine, M. Bornens, and F. Jülicher. 2007. Experimental and theoretical study of mitotic spindle orientation. *Nature*. 447:493–496. doi:10.1038/nature05786.

Toyoda, Y., C.J. Cattin, M.P. Stewart, I. Poser, M. Theis, T.V. Kurzchalia, F. Buchholz, A.A. Hyman, and D.J. Müller. 2017. Genome-scale single-cell mechanical phenotyping reveals disease-related genes involved in mitotic rounding. *Nat. Commun.* 8. doi:10.1038/s41467-017-01147-6.

Verlhac, M.H., J.Z. Kubiak, H.J. Clarke, and B. Maro. 1994. Microtubule and chromatin behavior follow MAP kinase activity but not MPF activity during meiosis in mouse oocytes. *Dev. Camb. Engl.* 120:1017–1025.

Verlhac, M.H., J.Z. Kubiak, M. Weber, G. Géraud, W.H. Colledge, M.J. Evans, and B. Maro. 1996. Mos is required for MAP kinase activation and is involved in microtubule organization during meiotic maturation in the mouse. *Dev. Camb. Engl.* 122:815–822.

Verlhac, M.-H., C. Lefebvre, P. Guillaud, P. Rassinier, and B. Maro. 2000. Asymmetric division in mouse oocytes: with or without Mos. *Curr. Biol.* 10:1303–1306.

Xu, W., R. Mezencev, B. Kim, L. Wang, J. McDonald, and T. Sulchek. 2012. Cell Stiffness Is a Biomarker of the Metastatic Potential of Ovarian Cancer Cells. *PLoS ONE*. 7:e46609. doi:10.1371/journal.pone.0046609.

Yanez, L.Z., J. Han, B.B. Behr, R.A. Reijo Pera, and D.B. Camarillo. 2016. Human oocyte developmental potential is predicted by mechanical properties within hours after fertilization. *Nat. Commun.* 7:10809. doi:10.1038/ncomms10809.

Zlotek-Zlotkiewicz, E., S. Monnier, G. Cappello, M. Le Berre, and M. Piel. 2015. Optical volume and mass measurements show that mammalian cells swell during mitosis. *J. Cell Biol.* 211:765–774. doi:10.1083/jcb.201505056.

Acknowledgments

Authors wish to thank Gaëlle Letort a post-doctoral fellow in the lab for her help with plotting the MSDs curves and fitting them. We also thank Rafaele Attia for making the PDMS chambers needed for oocyte volume measurements. We thank Clément Nizak (ESPCI), Maria Almonacid from the lab and the imaging facility of the CIRB for their input on imaging quantification. At last, we thank Marie Anfosso, a master student, for her help characterizing the cFH1FH2 construct, and the members of the Verlhac/Terret team for helpful discussions and critical reading of the manuscript. This work was supported by grants from the Fondation pour la Recherche Médicale (FRM Label to MHV-DEQ20150331758), from the ANR (ANR-14-CE11 to MHV, ANR-16-CE13 to MET) and from the Labex Memolife (to MHV). This work has received support from the Fondation Bettencourt Schueller, support under the program « Investissements d'Avenir » launched by the French Government and implemented by the ANR, with the references: ANR-10-LABX-54 MEMO LIFE, ANR-11-IDEX-0001-02 PSL* Research University.

Author contributions

IB, MHV and MET conceived and supervised the project. IB performed most experiments. FC characterized the cFH1FH2 construct, MMS did the chromosome tracking experiments, they both analyzed their experiments. IB, MHV and MET analyzed most experiments. CC an MP were involved for the volume measurement experiments. CC and CS were involved for the cortical tension measurement experiments. AO and AG were involved for the computational 3D imaging approach. AC did the original observation that extra-soft oocytes have misaligned chromosomes. IB, MHV and MET wrote the manuscript, which was seen and corrected by all authors.

A

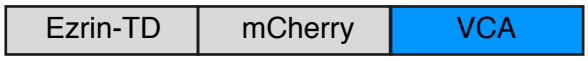

B

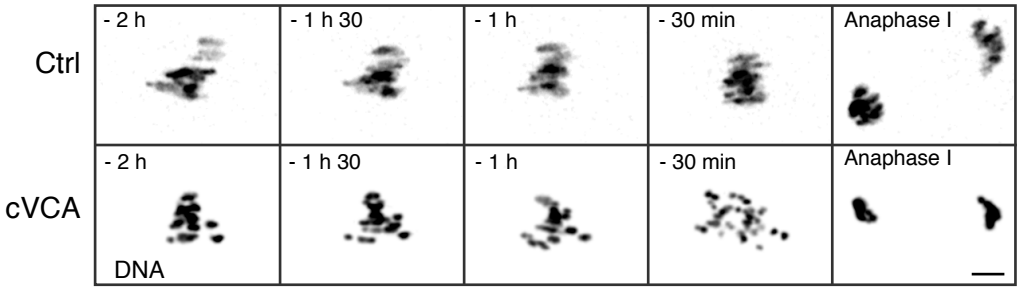

C

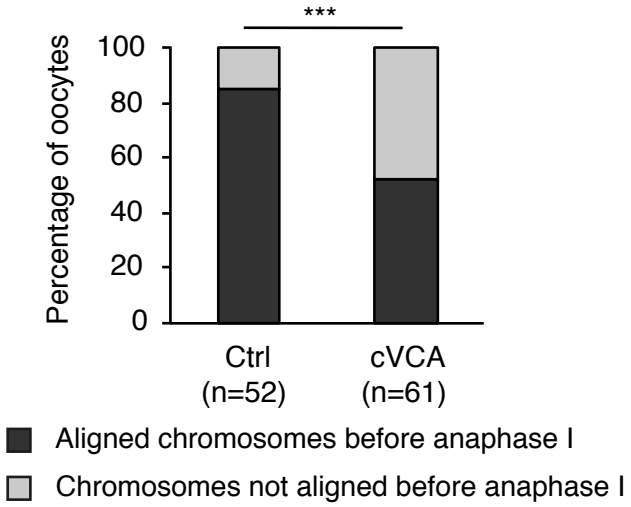

D

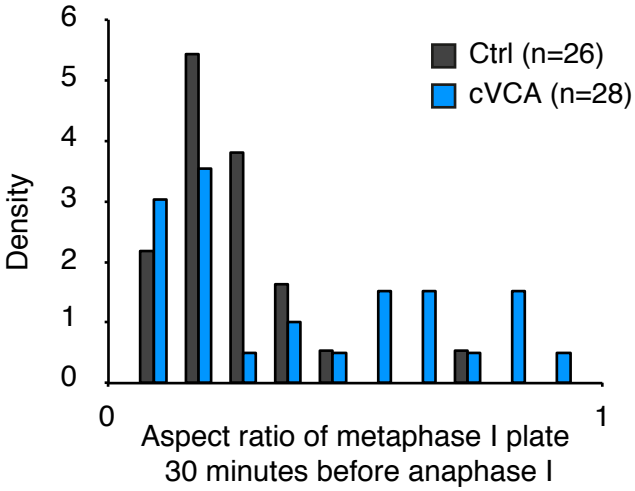

E

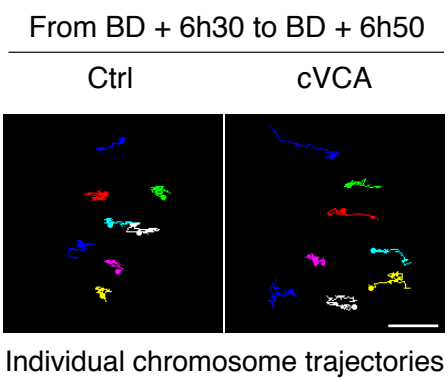

F

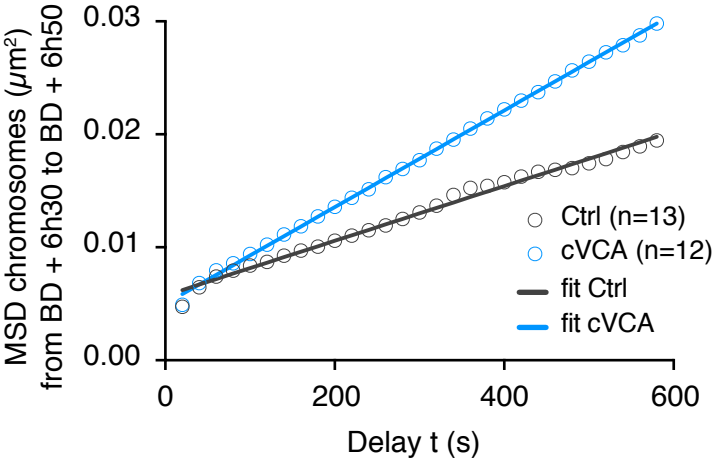

Figure 1

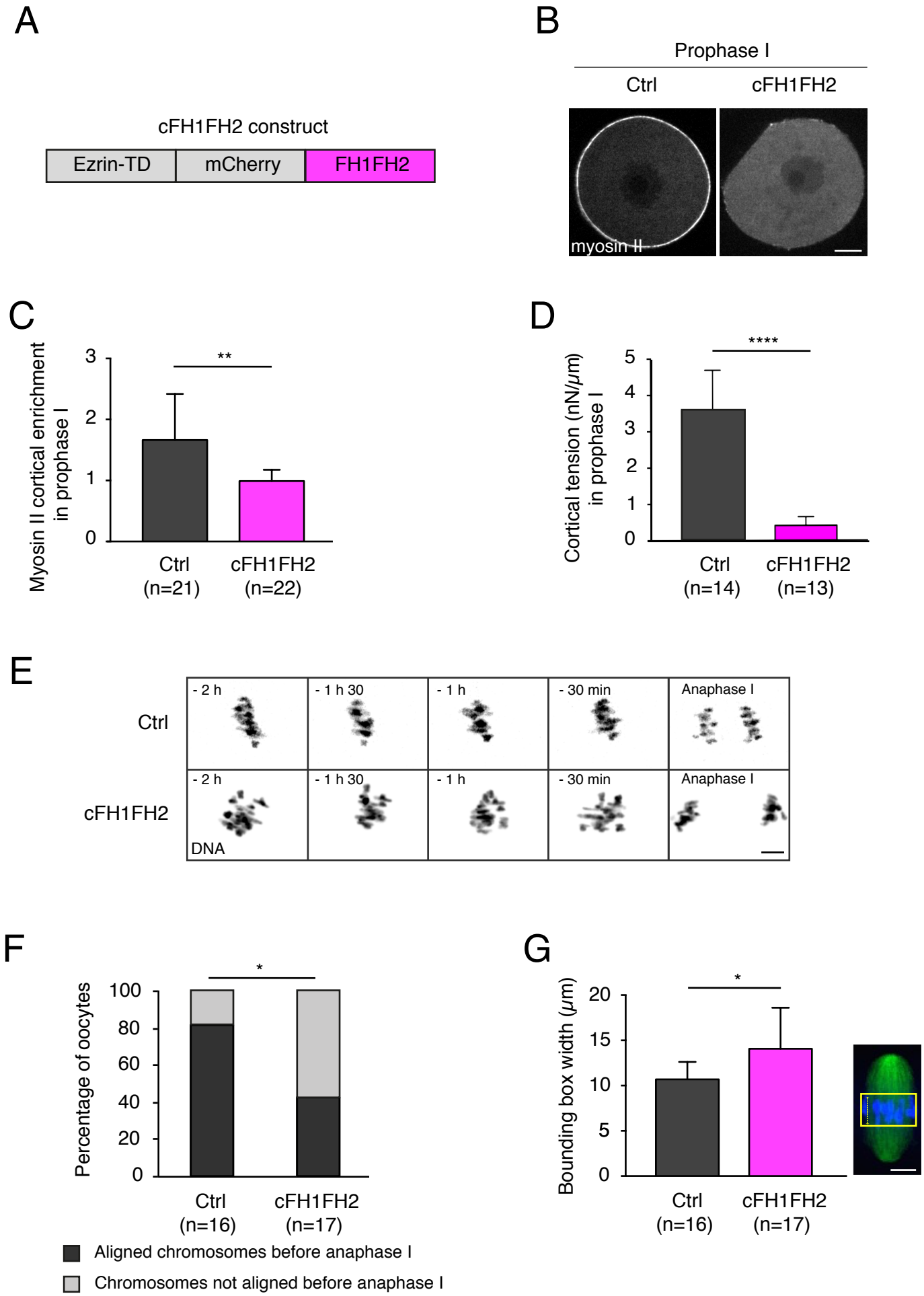
A
cFH1FH2 construct
Ezrin-TD
mCherry
FH1FH2
B
Prophase I
Ctrl
cFH1FH2
myosin II
C
Myosin II cortical enrichment in prophase I
3
2
1
0
**
Ctrl (n=21)
cFH1FH2 (n=22)
D
Cortical tension (nN/μm) in prophase I
5
4
3
2
1
0
****
Ctrl (n=14)
cFH1FH2 (n=13)
E
Ctrl
cFH1FH2
- 2 h
- 1 h 30
- 1 h
- 30 min
Anaphase I
DNA
F
Percentage of oocytes
100
80
60
40
20
0
*
Ctrl (n=16)
cFH1FH2 (n=17)
Aligned chromosomes before anaphase I
Chromosomes not aligned before anaphase I
G
Bounding box width (μm)
20
15
10
5
0
*
Ctrl (n=16)
cFH1FH2 (n=17)

Figure 2

A

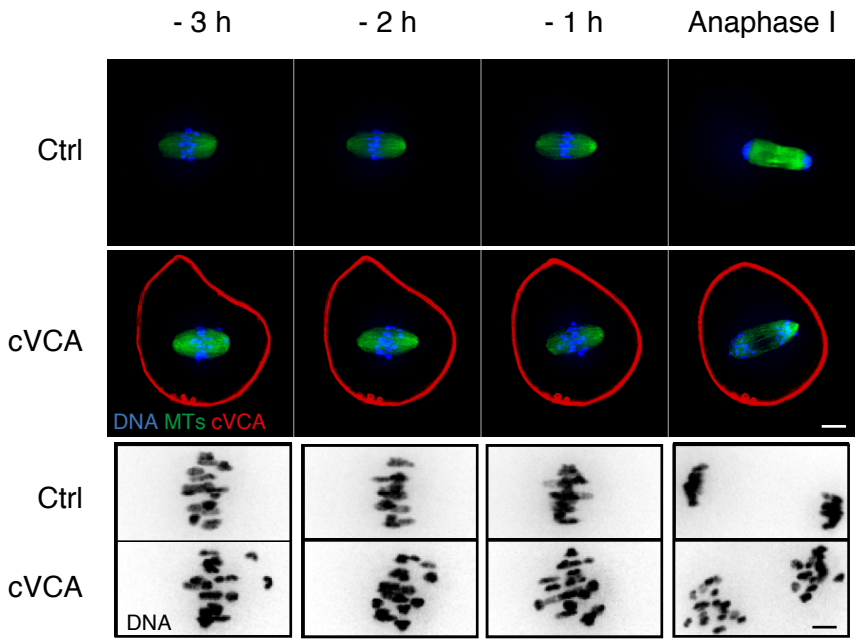
- 3 h
- 2 h
- 1 h
Anaphase I
Ctrl
cVCA
DNA MTs cVCA
Ctrl
cVCA
DNA

B

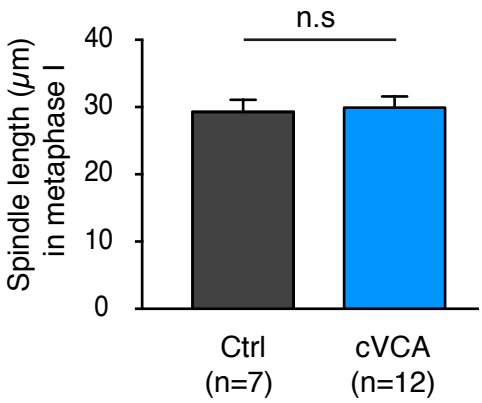
n.s
Spindle length (μm) in metaphase I
40
30
20
10
0
Ctrl (n=7)
cVCA (n=12)

C

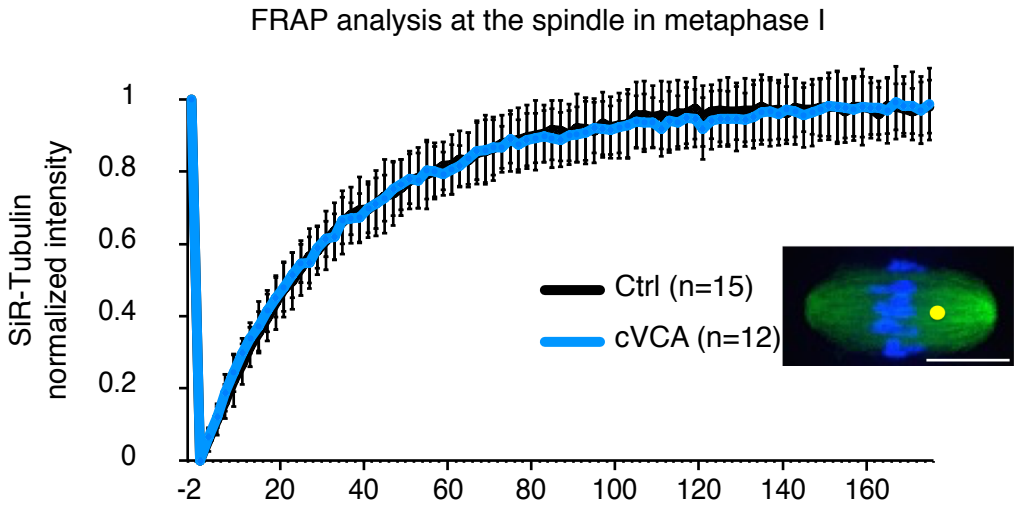
FRAP analysis at the spindle in metaphase I
SiR-Tubulin normalized intensity
1
0.8
0.6
0.4
0.2
0
-2
20
40
60
80
100
120
140
160
Ctrl (n=15)
cVCA (n=12)

Figure 3

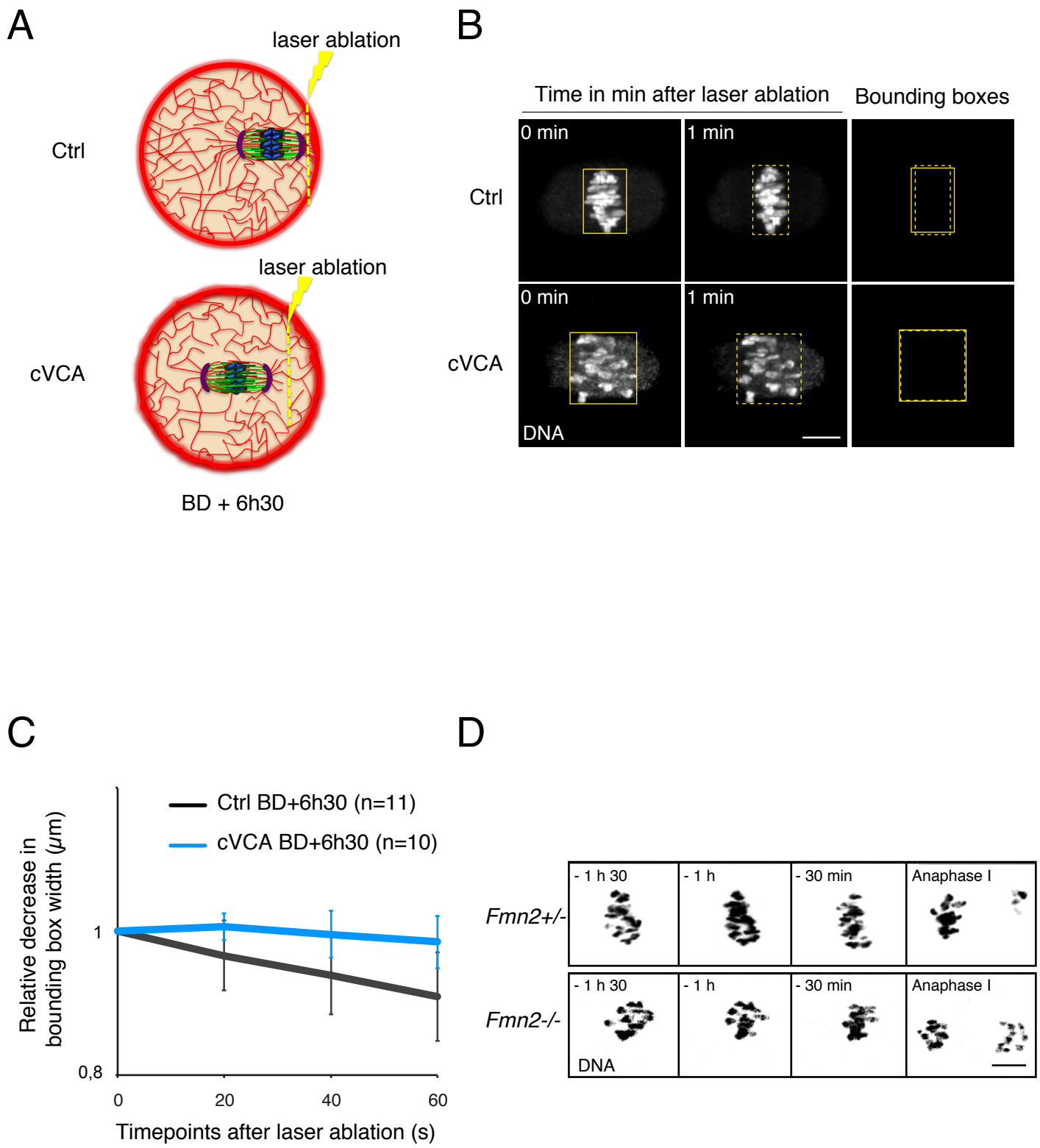
A
laser ablation
Ctrl
laser ablation
cVCA
BD + 6h30
B
Time in min after laser ablation
Bounding boxes
0 min
1 min
Ctrl
0 min
1 min
cVCA
DNA
C
Ctrl BD+6h30 (n=11)
cVCA BD+6h30 (n=10)
Relative decrease in bounding box width (µm)
1
0,8
0
20
40
60
Timepoints after laser ablation (s)
D
Fmn2+/-
- 1 h 30
- 1 h
- 30 min
Anaphase I
Fmn2-/-
- 1 h 30
- 1 h
- 30 min
Anaphase I
DNA

Figure 4

A

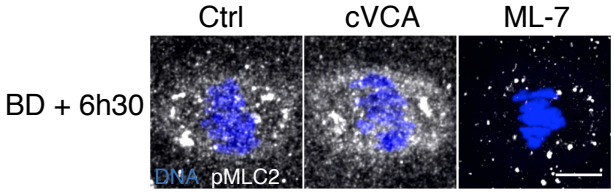
Ctrl
cVCA
ML-7
BD + 6h30
DNA pMLC2

B

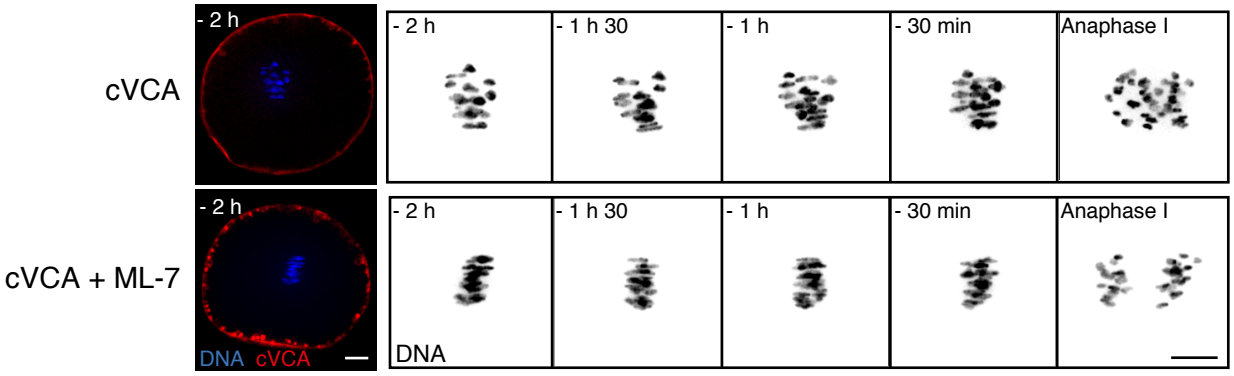
cVCA
cVCA + ML-7
- 2 h
- 1 h 30
- 1 h
- 30 min
Anaphase I
DNA cVCA
DNA

C

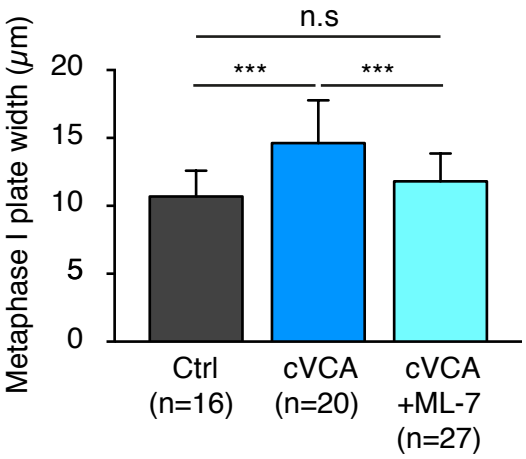
n.s
***
***
Metaphase I plate width (μm)
20
15
10
5
0
Ctrl (n=16)
cVCA (n=20)
cVCA +ML-7 (n=27)

Figure 5

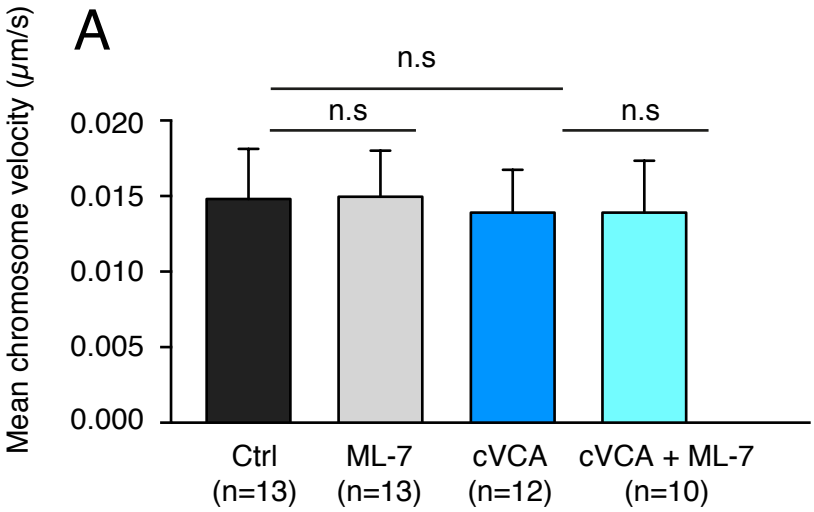
A
Mean chromosome velocity (μm/s)
0.020
0.015
0.010
0.005
0.000
n.s
n.s
n.s
Ctrl (n=13)
ML-7 (n=13)
cVCA (n=12)
cVCA + ML-7 (n=10)

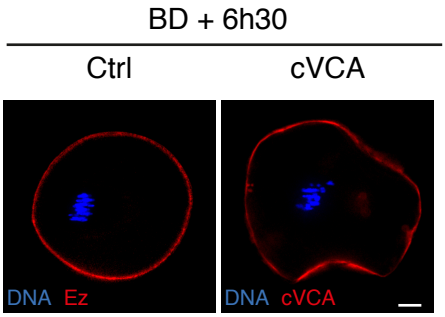
B
BD + 6h30
Ctrl
cVCA
DNA Ez
DNA cVCA

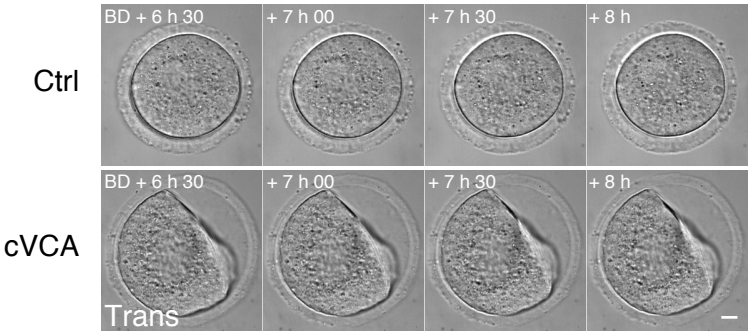
C
Ctrl
cVCA
BD + 6 h 30
+ 7 h 00
+ 7 h 30
+ 8 h
Trans

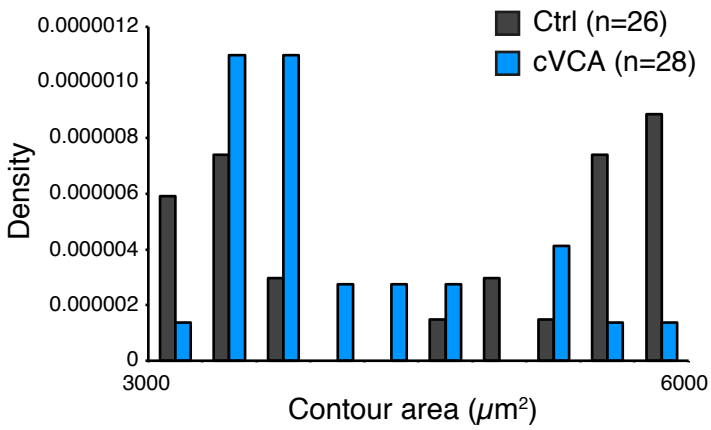
D
Ctrl (n=26)
cVCA (n=28)
Density
0.0000012
0.0000010
0.000008
0.000006
0.000004
0.000002
0
3000
6000
Contour area (μm²)

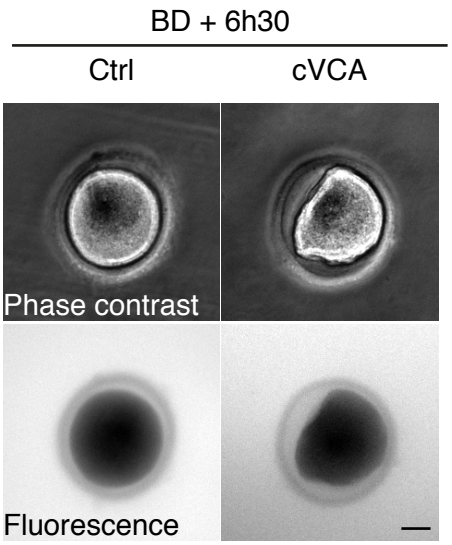
E
BD + 6h30
Ctrl
cVCA
Phase contrast
Fluorescence

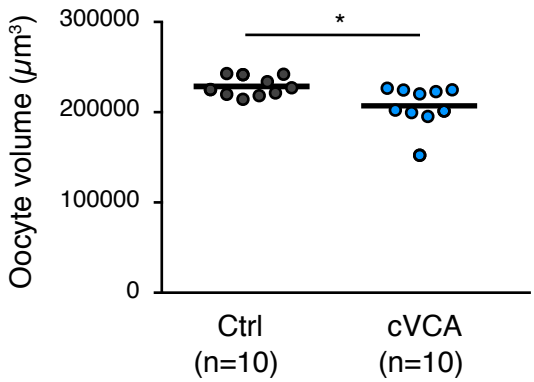
F
Oocyte volume (μm³)
300000
200000
100000
0
*
Ctrl (n=10)
cVCA (n=10)

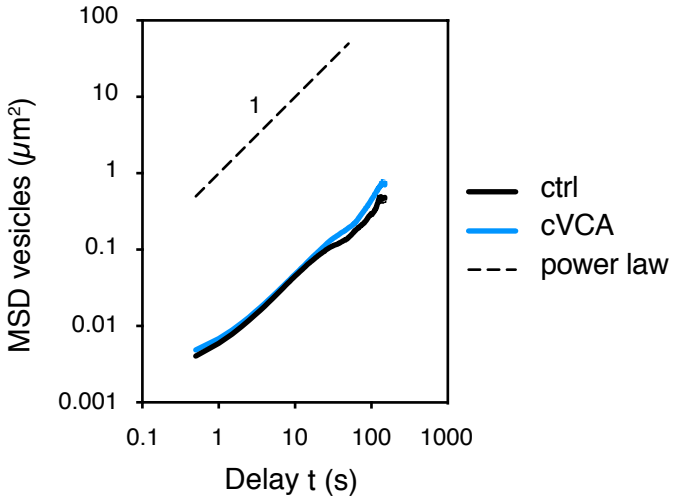
G
MSD vesicles (μm²)
100
10
1
0.1
0.01
0.001
1
0.1
1
10
100
1000
Delay t (s)
ctrl
cVCA
power law

Figure S1

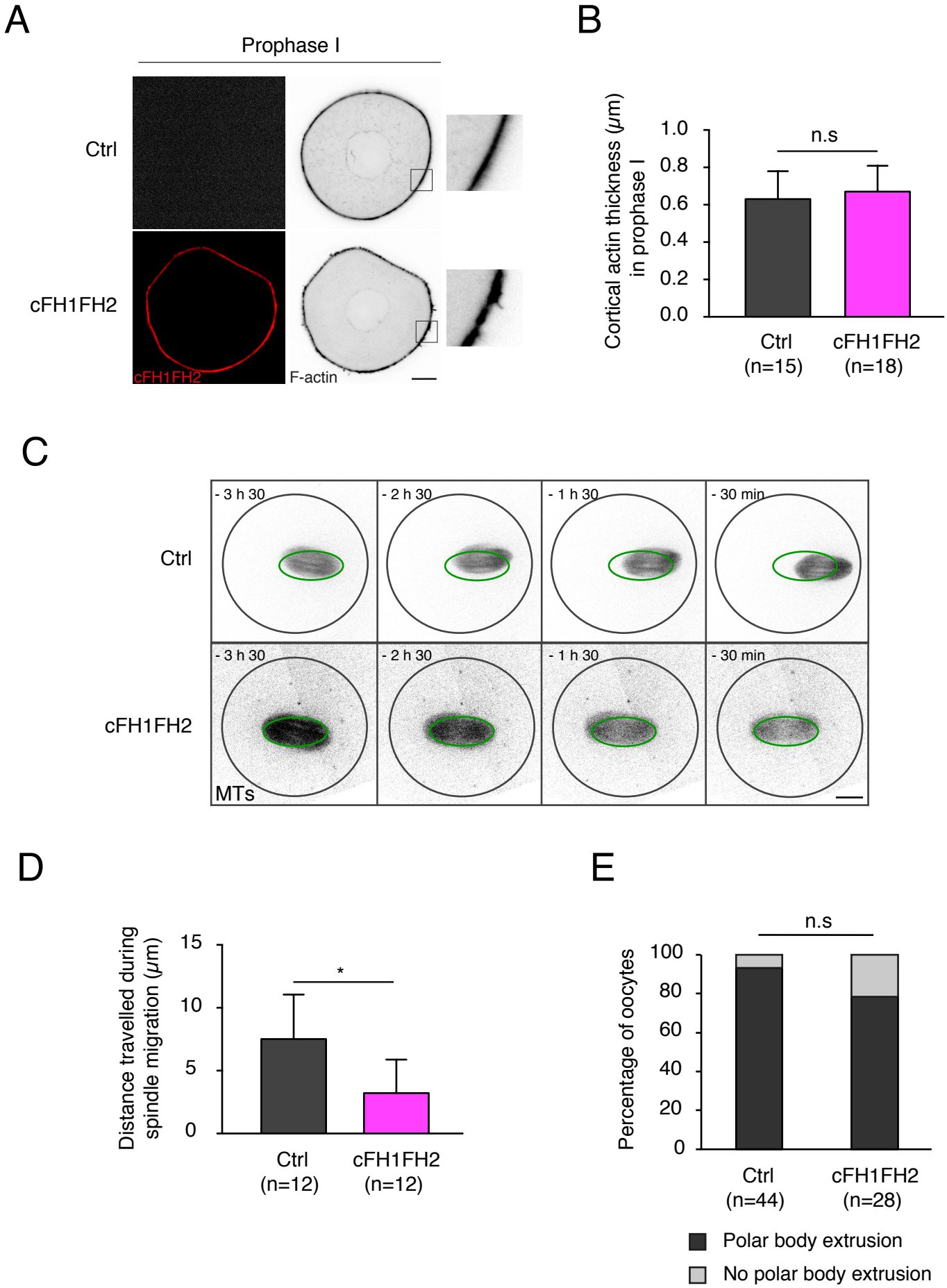
A
Prophase I
Ctrl
cFH1FH2
cFH1FH2
F-actin
B
Cortical actin thickness (µm) in prophase I
1.0
0.8
0.6
0.4
0.2
0.0
n.s
Ctrl (n=15)
cFH1FH2 (n=18)
C
Ctrl
cFH1FH2
- 3 h 30
- 2 h 30
- 1 h 30
- 30 min
MTs
D
Distance travelled during spindle migration (µm)
15
10
5
0
*
Ctrl (n=12)
cFH1FH2 (n=12)
E
Percentage of oocytes
100
80
60
40
20
0
n.s
Ctrl (n=44)
cFH1FH2 (n=28)
Polar body extrusion
No polar body extrusion

Figure S2

A

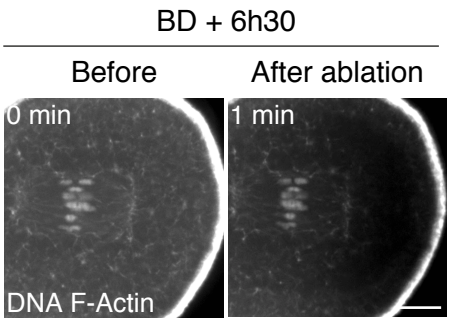

B

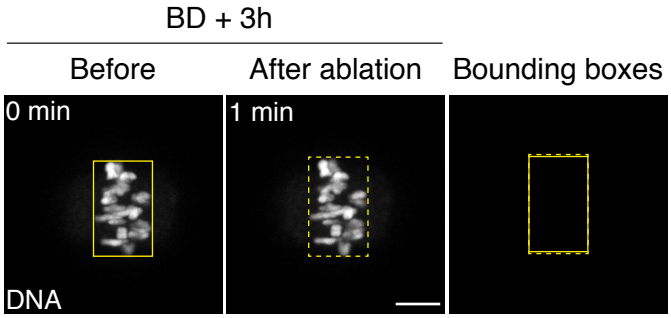

C

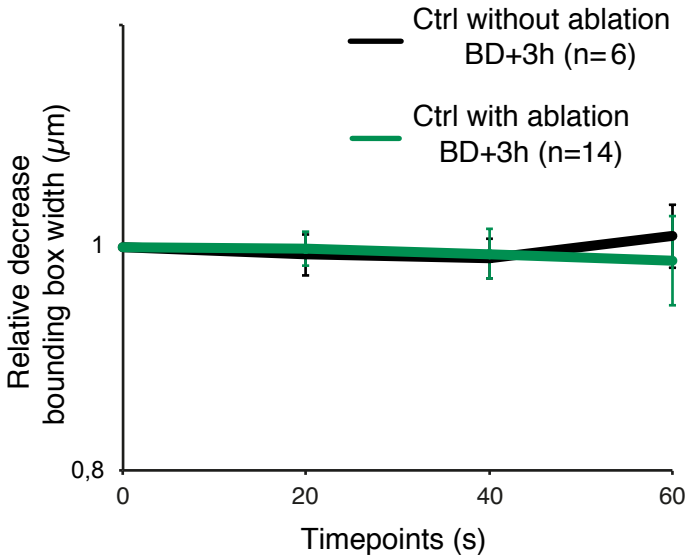

D

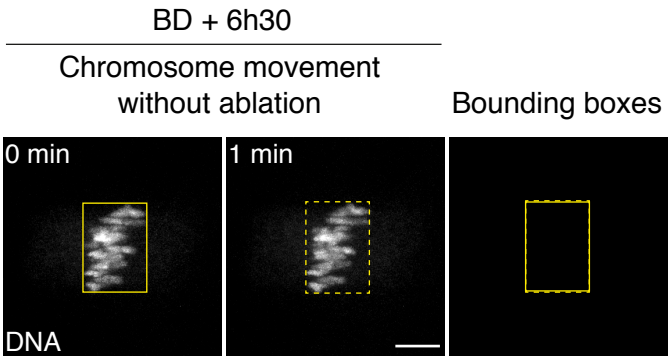

E

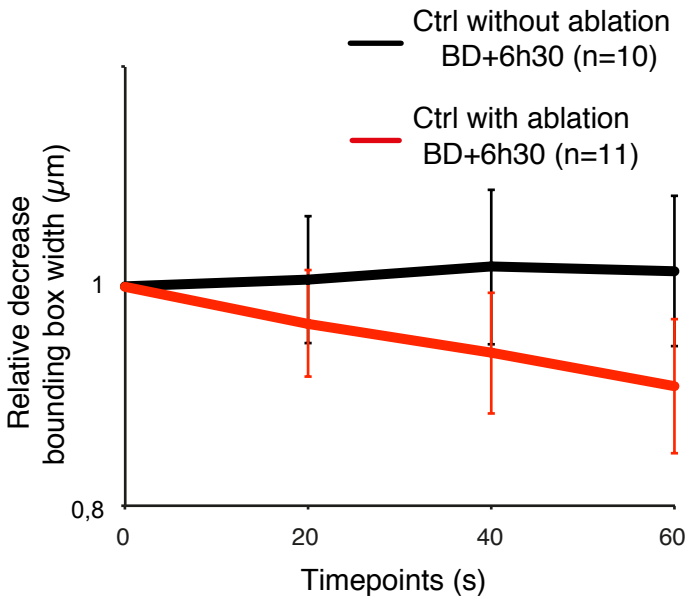

Figure S3

A

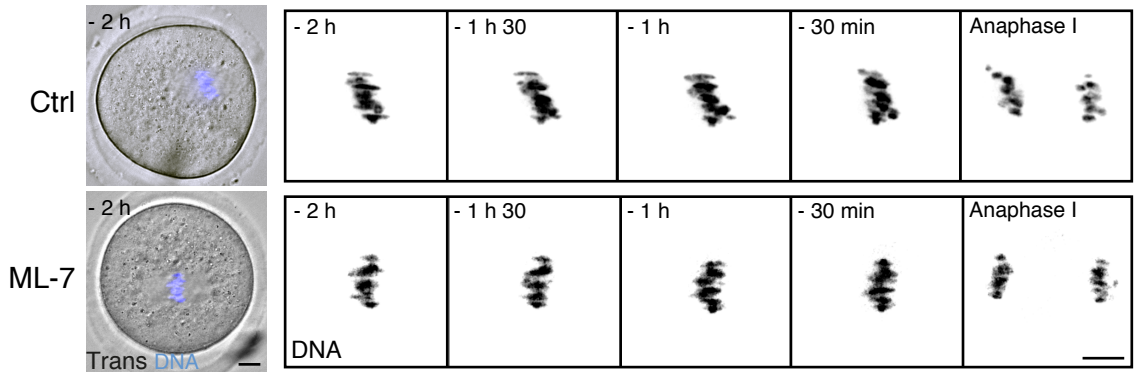
Ctrl
ML-7
- 2 h
Trans DNA
- 2 h
- 1 h 30
- 1 h
- 30 min
Anaphase I
DNA

B

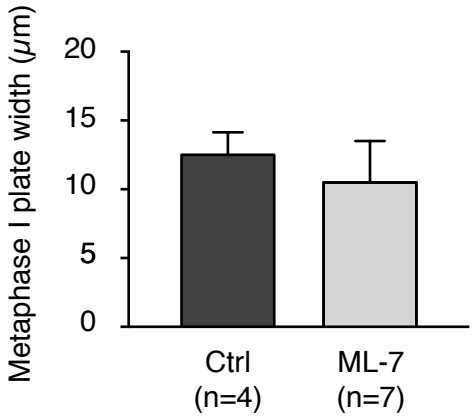
Metaphase I plate width (μm)
20
15
10
5
0
Ctrl
(n=4)
ML-7
(n=7)

Figure S4

Figures legends

Figure 1: Extra-soft oocytes due to cVCA expression have chromosome alignment defects during metaphase I.

(A) The cVCA construct allows actin nucleation by Arp2/3 at the cortex of mouse oocytes, generating extra-soft oocytes (Chaigne et al., 2015). The VCA domain of Wave2, a nucleation promoting factor of Arp2/3, is fused to the cortical ERM protein Ezrin.

(B) Time-lapse confocal spinning disk images of oocytes expressing Histone(H2B)-GFP (black) alone (Ctrl, upper panel) or together with cVCA (bottom panel). Acquisitions were taken every 30 minutes starting 2 hours before anaphase I. Scale bar: 10 µm.

(C) Extra-soft oocytes display a high rate of misaligned chromosomes. Bar graph representing the percentage of oocytes with aligned (dark grey) and not aligned (light grey) chromosomes 30 minutes before anaphase I as quantified for controls (left bar), and cVCA expressing oocytes (right bar). The numbers of oocytes analyzed (n) are displayed in the figure. Data are from 10 independent experiments. Statistical significance of differences is assessed with a Chi-square test: ***P-value=0.0003.

(D) Graph representing the aspect ratio for controls (black) and cVCA expressing oocytes (blue). Quantifications were performed 30 minutes before anaphase I. The numbers of oocytes analyzed (n) are displayed in the figure. Data are from 7 independent experiments. Statistical significance of differences is assessed with a Kolmogorov-Smirnov test: *P-value=0.013.

(E) Examples of individual chromosome tracking in control (Ctrl, left panel) and cVCA expressing oocytes (cVCA, right panel) between 6 hours and 30 minutes after nuclear envelope breakdown (BD + 6h30) and 20 minutes later (BD + 6h50). Each color represents one chromosome track. Scale bar: 5 µm.

(F) Chromosome movement is less confined in extra-soft oocytes (cVCA, blue). The graph represents the mean square displacement (MSD) of individual chromosomes in metaphase I. Chromosome movement was analyzed between BD + 6h30 and BD+ 6h50. A total of 59 chromosomes were analyzed among 13 control oocytes and 60 chromosomes were analyzed among 12 cVCA expressing oocytes. Data are from 4 independent experiments. MSD data are

fitted to a simple linear regression model (R^2>0.97). Statistical significance of differences of slopes between ctrl and cVCA is assessed with a Welch's test: ***P-value <0.0001.

Figure 2: Extra-soft oocytes due to cFH1FH2 expression have chromosome alignment defects in metaphase I.

(A) The cFH1FH2 construct allows actin nucleation by Formin 2 at the cortex of mouse oocytes. The FH1 and FH2 domains of Formin 2, which possess actin nucleation activity, are fused to the cortical ERM protein Ezrin.

(B) Myosin II is excluded from the cortex in cFH1FH2 oocytes. Confocal spinning disk images of oocytes expressing SF9-GFP (myosin II intrabody, white) alone (Ctrl, left panel) or together with cFH1FH2 (right panel). Prophase I oocytes are observed 5h after cRNA injection. Scale bar: 10 µm.

(C) Graph representing the ratio between the average intensities of cortical and cytoplasmic myosin II in prophase I arrested oocytes 5 hours after expression of SF9-GFP alone (black, left bar) or SF9-GFP and cFH1FH2 (magenta, right bar). Six measurements were taken in the cortex and the cytoplasm for each oocyte. The numbers of oocytes analyzed (n) are displayed in the figure. Data are from 2 independent experiments. The mean and standard deviation (SD) are shown. Statistical significance of differences is assessed with a Mann-Whitney test: **P-value=0.0013.

(D) Cortical tension in decreased in cFH1FH2 oocytes. The graph shows cortical tension values in Ctrl (black, left bar) and cFH1FH2 expressing oocytes (magenta, right bar). Measurements were performed by micropipette aspiration in prophase I arrested oocytes 5 hours after cRNA injection. The numbers of oocytes analyzed are displayed in the figure. Data are from 3 independent experiments. The mean and standard deviation (SD) are shown. Statistical significance of differences is assessed with a Mann-Whitney test: *** P-value <0.0001.

(E) Time-lapse images of oocytes expressing Histone(H2B)-GFP (black) alone (Ctrl, upper panel) or with cFH1FH2 (bottom panel). Acquisitions were taken every 30 minutes starting 2 hours before anaphase I. Scale bar: 10 µm.

(F) cFH1FH2 oocytes display a high rate of misaligned chromosomes. Bar graph representing the percentage of oocytes with aligned (dark grey) and not aligned (light grey) chromosomes

30 minutes before anaphase I, quantified for controls (left bar), and cFH1FH2 expressing oocytes (right bar). The numbers of oocytes analyzed (n) are displayed in the figure. Data are from 3 independent experiments. Statistical significance of differences is assessed with a Fisher's test: *P-value=0.0324.

(G) Graph showing the width of the bounding box containing the metaphase plate 30 minutes before anaphase I in Ctrl (black) and cFH1FH2 expressing oocytes (magenta). The numbers of oocytes analyzed (n) are displayed in the figure. Data obtained from 3 independent experiments. The mean and standard deviation (SD) are represented. Statistical significance of differences is tested with a Mann-Whitney test: *P-value=0.01. The bounding box corresponds to the yellow square in the image of spindle with chromosomes aligned on the metaphase plate, and its width the yellow dashed line. Scale bar: 5 µm.

Figure 3: Aberrant low cortical tension does not impair spindle formation during meiosis I.

(A) Time-lapse confocal spinning disk images of oocytes expressing Histone(H2B)-GFP (blue) alone (Ctrl, upper panel) or together with cVCA (red, second panel). Microtubules (MTs, green) are visualized with SiR-Tubulin. Movies start 3 hours before anaphase I, which corresponds here to 6 hours after nuclear envelope breakdown (BD + 6h). Acquisitions were taken every hour. The two bottom panels are magnification of the chromosomes (black) from the upper panels. Scale bars: 10 µm.

(B) Spindle length quantifications for control (black, left bar) and cVCA expressing oocytes (blue, right bar) in metaphase I. Quantifications were performed at BD + 7h. Data are from 4 independent experiments. The mean and standard deviation (SD) are shown. Statistical significance is determined with a Mann-Whitney test: n.s P-value=0.432.

(C) FRAP analysis of microtubule dynamics in the spindle in metaphase I for control (black) and cVCA expressing oocytes (blue). Quantification was performed at BD + 6h30. SiR-Tubulin was photobleached in the spindle, between the spindle poles and the metaphase plate (yellow dot in the image of spindle with chromosomes aligned on the metaphase plate, scale bar: 10 µm). Then SiR-Tubulin fluorescence recovery was followed. The fluorescence intensity was normalized so that 1 corresponds to the prebleached value. For a single exponential recovery model, the halftime to fluorescence recovery in controls oocytes is t1/2=22.54 s compared to t1/2=22.18 s for cVCA expressing oocytes. Data are represented as

mean _ SD. Statistical significance of differences for the t1/2 is assessed with a t test: P-value=0.63.

Figure 4: The intensity of forces transmitted to the chromosomes is altered in extra-soft oocytes.

(A) Laser ablation of the attachment between the spindle and the cortex in Ctrl and cVCA expressing oocytes. The yellow dotted line represents the region of interest used for ablation. Actin is in red, microtubules in green, chromosomes in blue and myosin II in purple.

(B) Confocal spinning disk images at BD + 6h30 (metaphase I) of oocytes expressing Histone(H2B)-GFP (grey) in control oocytes (upper panel) or in cVCA expressing oocytes (bottom panel). Bounding boxes of the metaphase I plate are represented in solid lines before ablation (left) and dotted lines 1 min after ablation (right). Scale bar: 10 µm.

(C) The graph represents the relative decrease of the metaphase I plate bounding boxes every 20 seconds (s) during 1 minute in control (black) and cVCA expressing oocytes (blue). The numbers of oocytes analyzed (n) are displayed in the figure. Data are compiled from 5 independent experiments. The mean and standard deviation (SD) are shown for each timepoints. The bounding boxes width were normalized so that 1 corresponds to the width before ablation at t=0 seconds.

(D) Time-lapse confocal spinning disk images of control (upper panel) and *Fmn2-/-* (lower panel) oocytes expressing Histone(H2B)-GFP (black). Acquisitions were taken every 30 minutes starting 1 hour 30 minutes before anaphase I. Scale bar: 10 µm.

Figure 5: Decreasing myosin II activity in extra-soft oocytes rescues chromosome alignment.

(A) Immunofluorescence of oocytes stained for pMLC2 (white, showing endogenous active phosphorylated myosin-II) and DNA (blue) at BD + 6h30. The left panel corresponds to a control oocyte (Ctrl), the middle one to a cVCA expressing oocyte (cVCA) and the right one to an oocyte treated with ML-7. Scale bar: 5 µm.

(B) Confocal spinning disk images of metaphase I oocytes expressing Histone(H2B)-GFP (blue in the left panel, black in the right panels) and cVCA (red, left panel). Oocytes were treated with DMSO (cVCA, upper panel) or ML-7 to reduce myosin II activity (cVCA ML-7,

lower panel). Acquisitions were taken every 30 minutes starting 2 hours before anaphase I. Scale bar: 10 µm.

(C) Bar graph representing the metaphase I plate width 30 minutes before anaphase I in control (black, left), cVCA (blue, middle) and cVCA expressing oocytes treated with ML-7 (light blue, right). The numbers of oocytes analyzed (n) are displayed in the figure. Data are from 6 independent experiments. The mean and standard deviation (SD) are shown. Statistical significance of differences is assessed with a Mann-Whitney test: n.s P-value=0.1708 and ***P-value<0.0001.

Figure S1: Cell volume but not cytoplasmic activity is reduced in cVCA expressing oocytes with lower cortical tension.

(A) Graph representing the mean chromosome velocity in Ctrl (black bar), ML-7 treated (grey bar), cVCA expressing (blue) and cVCA expressing ML-7 treated oocytes (light blue). Statistical significance of differences is assessed with a Mann-Whitney test: P-value=0.902 for Ctrl (black) versus ML-7 treated (grey), P-value=0.144 for cVCA expressing (blue) versus cVCA expressing ML-7 treated (light blue) and P-value=0.923 for Ctrl (black) versus cVCA expressing (blue) oocytes.

(B) The cortex is deformed in cVCA oocytes. Confocal spinning disk images of control (left) and cVCA (right) expressing oocytes in metaphase I (BD + 6h30). Chromosomes are labeled with Histone(H2B)-GFP (blue). The cortex is labeled with Ezrin-mCherry in controls (left, red) and cVCA-mCherry in cVCA expressing oocytes (right, red). Scale bar: 10 µm.

(C) Transmitted light video of control (upper panel) and cVCA expressing oocytes (bottom panel). Oocytes are stable in shape between BD + 6h30 and BD + 8h. Acquisitions were taken every 30 minutes. Scale bar: 10 µm.

(D) Contour area values for control (black) and cVCA expressing oocytes (blue). Quantifications were performed 30 minutes before anaphase I. The numbers of oocytes analyzed (n) are displayed in the figure. Data are from 7 independent experiments. Statistical significance of differences is assessed with a t-test: *P-value=0.015.

(E) For volume measurements, oocytes are in chambers filled with fluorescent dextran (fluorescence in the bottom panel). Left: control. Right: cVCA expressing oocyte. Scale bar: 20 µm.

(F) Oocyte volume is reduced in cVCA expressing oocytes (blue) compared to controls (black). Each dot represents the volume (μm^3) of one oocyte from 3 independent experiments. A Wilcoxon rank sum test was performed to compare the mean (black line) of the two conditions: *P-value=0.0232.

(G) The motion of Nile red-labeled vesicles is similar in cVCA expressing oocytes (blue) compared to controls (black), suggesting comparable cytoplasmic activity. The dashed line represents a power law of 1. MSD data are fitted to a simple linear regression model (R^2>0.97). Data are from 3 independent experiments.

Figure S2: Characterization of cFH1FH2 expressing oocytes.

(A) Confocal spinning disk images of control oocytes expressing GFP-UtrCH alone (black, upper panel) or with cFH1FH2 (red, bottom left panel) in prophase I. Prophase I oocytes are observed 5h after cRNA injection. Only one Z plane is shown. Squares show magnifications of the cortical actin network. Scale bar: 10 µm.

(B) The thickness of the cortical actin network in prophase I oocytes 5h after cRNA injection is similar in controls (black) and cFH1FH2 expressing oocytes (magenta). Data are from 2 independent experiments. The numbers of oocytes analyzed (n) are displayed in the figure. Statistical significance was tested with a t-test: n.s P-value=0.426.

(C) Confocal spinning-disk images showing spindle movement in control (upper panel) and cFH1FH2 expressing oocytes (bottom panel). The spindle is visualized with SiR-Tubulin labeling the microtubules (MTs, black). The black circles highlight the oocyte contour; the green ovals mark initial spindle positions. Acquisitions were taken every hour starting 30 minutes before anaphase I. Scale bar: 10 µm.

(D) Bar graph showing the distance traveled by the spindle between 4 hours before anaphase and 30 minutes before anaphase. Left bar: control (black). Right bar: cFH1FH2 (magenta). Data are from 6 independent experiments. The numbers of oocytes analyzed (n) are displayed in the figure. Statistical significance of the differences was assessed with a t-test: * P-value=0.0091.

(E) Rate of polar body extrusion in control (left bar) and cFH1FH2 expressing oocytes (right bar). Data are from 4 independent experiments. The numbers of oocytes analyzed (n) are displayed in the figure. Statistical significance tested with a Fisher's test: n.s P-value=0.14.

Figure S3: Laser ablation of the spindle-cortex attachment.

(A) Laser ablation of F-actin between the spindle and the closest oocyte cortex at BD + 6h30. Left: confocal spinning image before ablation of a control oocyte. Right: image 1 minute after ablation. Oocytes are expressing Histone(H2B)-GFP to label chromosomes (grey) and GFP-UtrCH to label F-actin (also in grey). Scale bar: 10 µm.

(B) Laser ablation in early meiosis I (BD + 3h). At that stage, oocytes lack the cytoplasmic actin meshwork and thus the spindle-cortex connection. Left: image before ablation, chromosomes bounding box is represented in solid line. Right: image 1 minute after ablation, chromosomes bounding box is represented in dotted line. Oocytes are expressing Histone(H2B)-GFP (grey) to label chromosomes. Scale bar: 10 µm.

(C) The relative decrease of the chromosome plate bounding boxes at BD + 3h without laser ablation (back) or following ablation (green). The mean and standard deviation (SD) are displayed. The bounding boxes width were normalized so that 1 corresponds to the width before ablation at t=0 seconds (s). The numbers of oocytes analyzed (n) are displayed in the figure.

(D) Chromosome movement without ablation in metaphase I (BD + 6h30). Left: the bounding box of the metaphase I plate is represented in solid line. Right: image 1 minute after, the bounding box is represented in dotted line. Oocytes are expressing Histone(H2B)-GFP (grey). Scale bar: 10 µm.

(E) The relative decrease of the chromosome plate bounding boxes at BD + 6h30 without laser ablation (back) or following ablation (red). The mean and standard deviation (SD) are displayed. The bounding boxes width were normalized so that 1 corresponds to the width before ablation at t=0 seconds (s). The numbers of oocytes analyzed (n) are displayed in the figure.

Figure S4: Lower myosin II activity does not impact chromosome behavior in oocytes with normal cortical tension.

(A) Left panels: Confocal spinning images of metaphase I control oocytes treated with DMSO (up) or ML-7 (bottom). Chromosomes are labeled with Histone(H2B)-GFP (blue). Note that the spindle does not migrate to the cell cortex in ML-7 treated oocytes. Right panels: Time-

lapse images of the same oocytes before anaphase I, acquisitions every 30 minutes. Chromosomes are in black. Scale bar: 10 µm.

(B) Graph representing the width of the metaphase I plate 30 minutes before anaphase I in Ctrl (black, left bar) and ML-7 treated oocytes (grey, right bar). The numbers of oocytes analyzed (n) are displayed in the figure. Data are from 2 independent experiments. The mean and standard deviation (SD) are shown.

DISCUSSION

Discussion

It has been known for over a decade that female meiosis is highly prone to chromosome segregation errors (Hassold and Hunt, 2001; Hassold et al., 2007; Nagaoka et al., 2012). During my PhD, I studied chromosome alignment and segregation in mouse oocytes from two different angles. First, we showed that the unique 'inside-out' mechanism of meiotic spindle assembly is essential to prevent chromosome misalignment. Second, we showed that oocytes with aberrant low cortical tension present severe chromosome alignment defects. Although very different, these two aspects of oocyte biology could both contribute to the high rate of aneuploidy observed in female meiosis, which is a leading cause of infertility.
Below, I will first discuss my results on the unique "inside-out" mode of oocyte spindle assembly and whether it is required for proper chromosome segregation. Next, I will discuss the influence of F-actin on chromosome segregation in oocytes. In particular, the nucleation of a cortical F-actin thickening leading to a decrease in cortical tension and the mechanisms of F-actin driven chromosome movement.

I. Particularities of the "inside-out" spindle assembly in oocytes

1. Are the effects of kinesin-14 on spindle assembly kinesin-5-dependent?

Our results show that inhibition of the minus-end directed kinesin-14 in mouse oocytes impairs spindle bipolarization, whereas slight kinesin-14 overexpression induces rapid bipolarization and pole assembly leading to chromosome alignment defects. Interestingly, the plus-end directed kinesin-5 was shown to be essential for spindle bipolarization in meiosis and mitosis. Indeed, kinesin-5 inhibition in *Xenopus* extracts and mouse oocytes results in monopolar spindles (Walczak et al., 1998; Kapoor et al., 2000; Mailhes et al., 2004; Schuh and Ellenberg, 2007; Fitzharris, 2009). It has been proposed that kinesin-14 and kinesin-5 motors generate antagonistic forces. In particular, the activities of both motors must be coordinated to promote spindle bipolarity and regulate spindle length (for review see Goshima and Scholey, 2010). *In vitro* studies and computational modeling suggest that kinesin-14

rapidly aligns antiparallel microtubules, thus allowing recruitment of kinesin-5 to the spindle midzone and further spindle elongation (Hepperla et al., 2014). In fission yeast, depletion of kinesin-5 abolishes spindle bipolarization. However, spindle bipolarity can be rescued by depletion of kinesin-14, highlighting their antagonistic activities (Rincon et al., 2017). In these spindles lacking both kinesin-5 and kinesin-14, spindle bipolarization relies on microtubule bundling by PRC1 (Ase1) and microtubule stabilization by CLASP (Cls1) (Rincon et al., 2017). Still in fission yeast, loss of kinesin-14 results in loss of microtubule focusing at spindle poles. Microtubules are then push apart by the microtubule sliding activity of kinesin-5, forming long protrusions (Syrovatkina and Tran, 2015). These kinesin-5-dependent spindle defects in the context of kinesin-14 depletion lead to aneuploidy. In *Drosophila* oocytes, depletion of kinesin-5 results in spindle asymmetry with centromere repartition biased towards one pole (Radford et al., 2017). Centromere asymmetry in these oocytes depends on kinesin-14 as well, since invalidation of both kinesin-14 and kinesin-5 restores symmetry (Radford et al., 2017). It is thus possible that the effects of kinesin-14 perturbations on mouse oocyte spindle assembly depend on kinesin-5, such as spindle length increase or changes in the timing of bipolarization. It would be interesting to quantify the levels of kinesin-5 relative to kinesin-14 levels during meiosis I spindle assembly and observe the effects of kinesin-14 deregulation in the absence of kinesin-5 activity, by treating mouse oocytes with monastrol for example (Mailhes et al., 2004). We could also test if simultaneous depletion of kinesin-14 and kinesin-5 restores spindle bipolarity. In that case, spindle bipolarization could be mainly achieved by microtubule crosslinkers such as HURP and NuMA (Breuer et al., 2010; Kolano et al., 2012). If so, we would expect spindle bipolarization to be even slower in the absence of microtubule motors.

2. Is the microtubule ball stage important to prevent chromosome defects in oocytes?

As mentioned above, spindle bipolarization is extremely fast in mouse oocytes slightly overexpressing the kinesin-14 HSET. These oocytes skip the microtubule ball stage and harbor scattered chromosomes along the extended spindle (Figure 24). It is likely that when skipping the microtubule ball stage, chromosomes are quickly

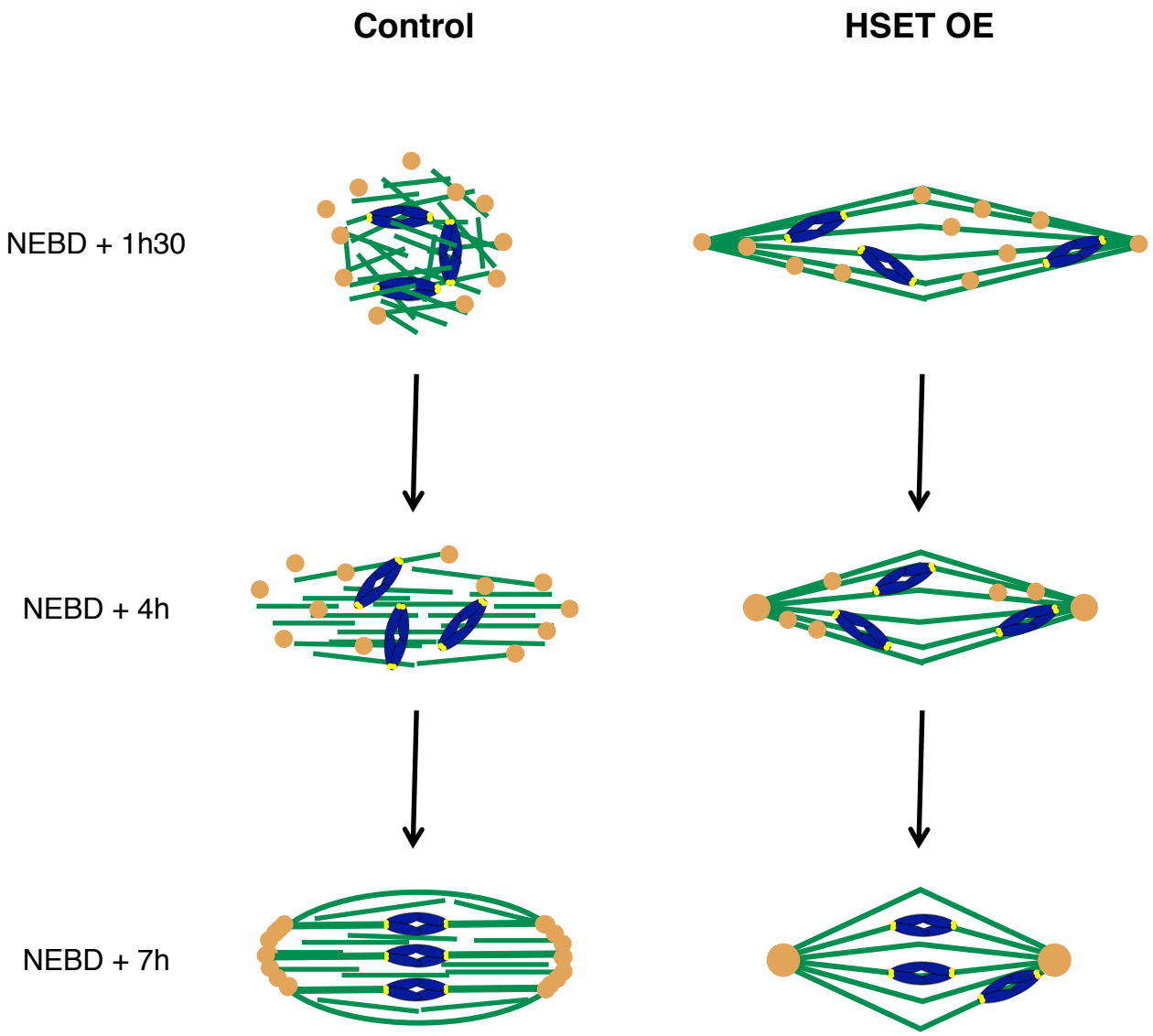

Figure 24: Mouse oocytes overexpressing the kinesin-14 (HSET OE) skip the microtubule ball stage.
DNA is in blue, microtubules in green, kinetochores in yellow and aMTOCs in brown.

scattered over a long distance and those located near the poles never become aligned on the metaphase plate (Figure 24).

Thus, the microtubule ball stage could serve as a safeguard mechanism to avoid precocious chromosome dispersion. This strategy resembles chromosome gathering throughout the volume of the large nucleus in starfish oocytes (Lénàrt et al., 2005; Mori et al., 2011). One possibility is that for meiotic spindles assembled in a large oocyte volume, the initial steps have to be precisely controlled in order to prevent chromosome defects that could persist throughout meiosis I. This hypothesis could be tested using computational models of spindle assembly. As mentioned in the introduction, models of meiotic spindle bipolarization have been proposed before (Burbank et al., 2007; Loughlin et al., 2010). However, such models begin with microtubules already aligned for modeling of a steady-state bipolar structure. The same models could be used to model early spindle assembly, focusing on the transition between a microtubule ball and a steady-state bipolar spindle. In addition, these models considered a fixed chromosome plate. Instead, we could model individual chromosomes and monitor how they move during spindle assembly. This would allow to determine if chromosomes are misaligned when skipping the microtubule ball stage. In addition, such model would allow to test which components (microtubule motors, crosslinkers, aMTOCs etc…) are required to transition from a ball of microtubules to a steady-state metaphase spindle. Interestingly, spindle bipolarization is also slow in oocytes of other species. In particular this process is even slower and less stable in human oocytes that do not contain aMTOCs, the spindle undergoing multiple rounds of multipolarity and collapsing before its final bipolarization (approximately 6 hours, Holubcova et al., 2015). This type of model could test the role of aMTOCs on spindle early morphogenesis, allowing modelization of human versus mouse spindles. It could help understand why most oocytes are devoid of aMTOCs and what is the cost of lacking aMTOCs, human oocytes being more aneuploid than mouse ones for example.

In conclusion, skipping the microtubule ball stage forces spindle morphogenesis to be more mitotic-like and leads to chromosome alignment abnormalities. Avoiding rapid bipolarization and a mitotic-like mode of spindle morphogenesis could be one reason why most oocytes lose canonical centrosomes.

It is thus possible that oocytes eliminated canonical centrosomes to prevent a mitotic-like mode of spindle assembly during meiosis I and higher levels of aneuploidy. Why some oocytes kept aMTOCs while others did not remains a mystery. Ultimately, the entire process of meiosis I spindle assembly is extremely slow. It could be explained by the lack of centrioles and canonical centrosomes. Indeed, in animal mitotic cells the two centrosomes define the spindle axis and promote rapid spindle bipolarization. The generation of *Drosophila* mutants lacking centrioles showed that mitosis without centrioles is slower in these mutant cells (Basto et al., 2006). Hence, slow spindle assembly in oocytes might be due to the lack of canonical centrosomes. Ultimately, reintroducing centrioles in oocytes could answer these questions, but up to now all the attempts failed, reinforcing the fact that centriole loss is an active process essential for oocyte biology (Zoran et al., 1993; Manil-Ségalen et al., *In press*).

II. Spindle positioning by F-actin and consequences on chromosome behavior

1. Forces generated by the actin networks in meiosis I oocytes

a. Forces within the cytoplasmic meshwork?

In mouse oocytes, spindle migration requires two actin networks: the cytoplasmic meshwork and the subcortical network. Within the cytoplasmic network, active myosin II localizes on the spindle, enriched at spindle poles, and produces pulling forces necessary for spindle positioning (Simerly et al., 1998; Schuh and Ellenberg, 2008; Chaigne et al., 2013). It is still unclear how the F-actin cytoplasmic meshwork drives spindle migration. For instance, this meshwork is not contractile as in starfish oocytes (Lénàrt et al., 2005; Mori et al., 2011; Bun et al., 2018). The cytoplasmic meshwork includes an actin cage in mouse oocytes and other species including human and pig (Mogessie and Schuh, 2017), which connects the spindle to the cortex and transmits myosin II dependent forces allowing its migration. However, the forces within the network were never measured. Measuring forces in the meshwork and especially at spindle poles could allow verifying these observations. Laser ablation could be considered to solve this problem as it was previously used to

study spindle positioning by astral microtubules (Grill et al., 2001; Grill et al., 2003; Labbé et al., 2004; Pecreaux et al., 2006 and Riche et al., 2013). However, this method could not be suited for mouse oocytes because the spindle is embedded in a dense actin meshwork filling the entire cytoplasm. Although laser ablation could potentially allow to assess the balance and the relative intensity of forces at each pole, it will not provide an absolute measure of the forces. Similarly to studies of spindle positioning in mitotic cells and aster centration in sea urchin embryos, this could be achieved using *in vivo* optical or magnetic tweezers (Garzon-Coral et al., 2016; Tanimoto et al., 2018). It should be feasible in mouse oocytes since optical tweezers were already used to measure the mechanical properties of the cytoplasm (Almonacid et al., 2015).

In addition, theoretical modeling predicted an unbalance of forces necessary for spindle migration (Chaigne et al., 2015 and Figure 25A). The meiosis I spindle forms slightly off-centered (Verlhac et al., 2000). Thereby, the model predicts that myosin II pulling is more efficient at the spindle pole closer to the cell cortex, creating a slight imbalance of forces. This imbalance of forces at spindle poles is amplified by a certain range of cortical tension decrease. In oocytes that are too stiff or too soft, the forces are balanced at the poles because myosin II pulling is inefficient (Chaigne et al., 2015). Measuring forces at spindle poles in control oocytes as well as in oocytes with aberrant cortical tension would allow to confirm this theoretical model.

b. Influence of the cytoplasmic network architecture for force generation?

The importance of the architecture of the cytoplasmic meshwork is not known. The F-actin cytoplasmic meshwork is nucleated by the cooperation of the linear actin nucleator Formin 2 and Spire 1/2 (Azoury et al., 2008; Schuh and Ellenberg, 2008; Pfender et al., 2011; Almonacid et al., 2015). It would be interesting to known if the architecture of the network is specific or if a different architecture, such as branched filaments nucleated by Arp2/3, could also generate forces and promote spindle migration. Preliminary data from the lab show that a “VCA construct” can nucleate a cytoplasmic F-actin network dependent on Arp2/3 (Figure 25B). The “VCA construct” uses the same VCA domain as the “cortical VCA (cVCA) construct” but without fusion

A

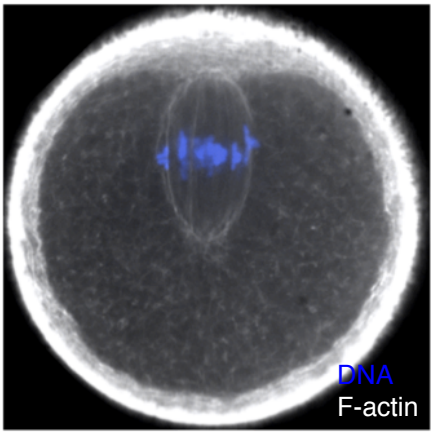

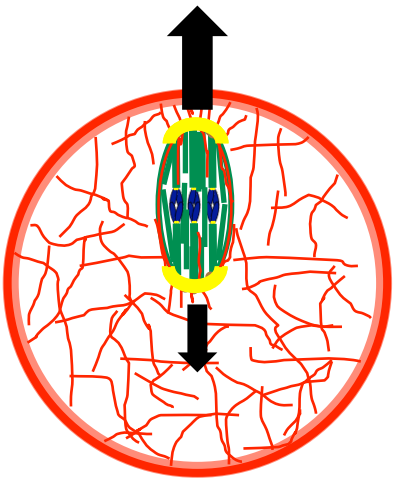

Imbalance of forces
Spindle migration

B

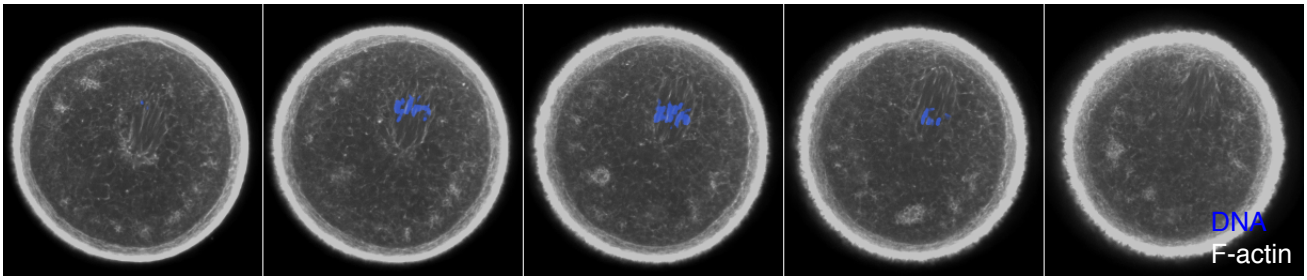

Figure 25: Forces within the cytoplasmic meshwork

(A) Spinning disk image from Chaigne et al., 2014 of a control oocytes in metaphase. Illustration: actin is in red, DNA in blue, microtubules in green and myosin II in yellow.
(B) Z-stacks of a *Fmn2-/-* oocyte expressing the VCA leading to Arp2/3 dependent nucleation of a cytoplasmic actin meshwork.

to the cortically localized Ezrin. Thus, the VCA is expressed in the cytoplasm where it induces Arp2/3-dependent F-actin nucleation. To discriminate between cytoplasmic F-actin nucleated by Formin 2 and F-actin nucleation by Arp2/3, the VCA was expressed in *Fmn2-/-* oocytes that lack the cytoplasmic actin meshwork. Surprisingly, expression of the VCA in these oocytes induces the formation of a cytoplasmic meshwork including an actin cage around the spindle (Figure 25B). The presence of a cytoplasmic actin meshwork and an actin cage in the absence of Formin 2 nucleation potentially highlights the contribution of Spire1/2 nucleation and suggests that Formin 2 acts as an elongator during meiosis I, as previously proposed (Pfender et al., 2011; Montaville et al., 2014). Although this VCA nucleated meshwork seems roughly similar to the Formin 2-dependent meshwork, further insights into its architecture and dynamics are required. More specifically, it would be interesting to know if the cytoplasmic VCA meshwork is functional, allowing nucleus centering and spindle positioning. In addition, since actin architecture was shown to influence myosin II activity, the localization of myosin II at spindle poles could also be tested (Reymann et al., 2012, Ennomani et al., 2016).

2. A link between F-actin and chromosomes/microtubules in chromosome segregation?

Interestingly, chromosomes migrate to the cortex in the absence of microtubules in mouse oocytes (Verlhac et al., 2000; Li et al., 2008; Azoury et al., 2008). Indeed, in oocytes treated with nocodazole to depolymerize spindle microtubules, chromosomes are still able to migrate to the cortex. In particular, F-actin appears more dense in the chromosome region facing the closest cortex (Azoury et al., 2008). As mentioned before, the F-actin cytoplasmic meshwork is not contractile in mouse oocytes, contrary to starfish oocytes (Lénàrt et al., 2005; Mori et al., 2011; Bun et al., 2018). Thus, it is possible that F-actin directly contacts chromosomes to drive their motion. For instance, actin nucleation by Arp2/3 was described around chromosomes in starfish oocytes (Burdyniuk et al., 2018). It would be interesting to look more closely at the contacts between F-actin and chromosomes in the absence of microtubules, for example to see if F-actin contacts directly kinetochores. We could also assess if chromatin is able to migrate in oocytes treated

with nocodazole in which the attachments with F-actin are cut by laser ablation. However, direct actin-chromosome contacts in the absence of polymerized microtubules might represent an alternative mechanism, not normally required in spindle migration.

In a control situation, the spindle and chromosomes are surrounded by an actin cage, within the cytoplasmic meshwork, necessary for spindle migration. This suggests an interaction between polymerized actin and microtubules. In addition, it was recently shown that F-actin could promote k-fiber formation in mouse oocytes, which has consequences on chromosome segregation (Mogessie and Schuh, 2017). So what could be the link between actin and spindle microtubules? The unconventional myosin X binds both actin and microtubule filaments (Divito and Cheney, 2008). This activity is required for spindle morphogenesis and positioning in *Xenopus* embryos (Woolner et al., 2008). However, preliminary data from the lab suggests that microtubule-actin binding by myosin X is not required for spindle positioning in mouse oocytes. Indeed, oocytes invalidated for myosin X do not seem to have spindle migration defects. Thus, other candidates could be involved. For example, the mammalian diaphanous-related (mDia) formins are able to bind microtubules. Interestingly, some evidence suggests that the mDia3 formin promotes k-fiber stabilization (Yasuda et al., 2004; Cheng et al., 2011 and for review see Mao, 2011). The +TIP CLIP-170 can also bind to an mDia formin, which increases F-actin polymerization (Henty-Ridilla et al., 2016). In addition, F-actin-microtubule interaction mediated by the crosslinking protein ACF7 and the minus-ends-tracking protein CAMSAP3 was described in epithelial cells (Ning et al., 2016).

Finally, chromosome movement via F-actin has been described in oocytes of various species. Interestingly, the actin cage is conserved in mammalian oocytes (Mogessie and Schuh, 2017). Moreover, studies have shown that cytoplasmic actin plays a role in mitotic spindle morphogenesis (for review see Sandquist et al., 2011; Kunda and Baum, 2009). This suggests that the role of actin in chromosome movement and its tight connection with the spindle could be widely conserved.

3. Myosin II activity and impact on chromosome behavior in meiosis I

a. Regulation of cortical myosin II activity in mouse oocytes?

In addition to the cytoplasmic F-actin network, a subcortical F-actin network is progressively nucleated during meiosis I. F-actin nucleation at the cortex leads to cortical myosin II displacement and decreases cortical tension. Forcing actin nucleation at the cortex of mouse oocytes using the cVCA and cFH1FH2 constructs is sufficient to chase myosin II from the cortex, leading to cortical tension decrease (see results part). These tools activate actin nucleation by two distinct nucleators. The cVCA induces nucleation of branched actin by the Arp2/3 complex (Chaigne et al., 2015), whereas actin nucleation using cFH1FH2 depends on the linear actin nucleator Formin 2. Myosin II activity was shown to be influenced by actin network architecture (Reymann et al., 2012; Ennomani et al., 2016). However in mouse oocyte, actin nucleation by both nucleators induces cortical myosin II displacement, suggesting that myosin II does not preferably associate with either networks at the cortex. Yet, it would require better imaging resolution to determine the precise architecture of both cortical networks in order to confirm this result. Nonetheless, this raises the question of how cortical F-actin nucleation delocalizes myosin II. One explanation could be that myosin II is chased by steric hindrance following actin nucleation. An additional mechanism could also rely on the preferential association of myosin II with mechanically stretched F-actin (Uyeda et al., 2011). Nucleation of a dense and stable subcortical actin layer could reduce F-actin stretching, thus creating a feedback loop that delocalizes cortical myosin II and decreases tension.

b. Influence of myosin II on chromosome alignment?

We show that chromosome alignment is severely impaired in oocytes harboring an aberrant low cortical tension. Myosin II is chased from the cortex precociously and enriched in the cytoplasm in these extra-soft oocytes (Chaigne et al., 2015 and results) where it localizes on the spindle (Schuch and Ellenberg, 2008 and results). Surprisingly, decreasing myosin II activity in extra-soft oocytes rescues chromosome alignment. However, the mechanism remains unclear.

There are evidences showing that myosin II is involved in spindle and chromosome functions. Myosin II localizes to the spindle and is implicated in kinetochore microtubule flux in metaphase I carne fly spermatocytes (Silverman-Gravira and Forer, 2003). It is also localized to chromosome arms and to the spindle in PtK1 cells (Robinson and Snyder, 2005). In addition, myosin II is required for proper spindle assembly and positioning in PtK2 cells (Rosenblatt et al., 2004) and mouse cardiac myocytes (Ma et al., 2010). Another interesting example is the mechanosentive role of cortical myosin II on microtubule growth in endothelial cells, where inhibition of myosin II activity prevents MCAK mediated MT growth (D'angelo et al., 2017). At last, myosin II was shown to interact directly with kinesins in astrocytes, essential for their migration (Feng et al., 2016). Thus, myosin II could potentially exert forces on the actin cage and the spindle that are transmitted to chromosomes, impacting chromosome alignment in these extra-soft oocytes. Since inhibition of myosin II activity using ML-7 rescues metaphase plate alignment in cVCA extra-soft oocytes, it would be interesting to know if these results could be reproduced using ML-7 in extra-soft cFH1FH2 expressing oocytes. In addition, to confirm that chromosome misalignment in soft oocytes is myosin II-dependent, we could express the cVCA in oocytes knockout for isoforms of myosin heavy chain *Myh9* and *Myh10* (Maître et al., 2016) and in *Fmn2*-/- oocytes. We expect chromosomes to be properly aligned in *Myh9*/*Myh10* knockout oocytes and in *Fmn2*-/- oocytes expressing the cVCA. However, these experiments might be difficult to do since *Fmn2*-/- oocytes expressing the cVCA die, certainly because of their lack of internal scaffold (unpublished results) and *Myh9*/*Myh10* knockout oocytes are flat and thus difficult to inject and image (unpublished results). At last, we would like to analyze the consequences of an artificial increase of myosin II activity on chromosome behavior and alignment. We could answer this question by using the myosin light chain phosphatase inhibitor Calyculin A, which leads to myosin II over-activation in various models (Ishihara et al., 1989; Firmino et al., 2016; Herbomel et al., 2017). We would use this drug on control oocytes and expect chromosomes to be misaligned as in cVCA expressing oocytes. In parallel, and with more quantitative data, it would be interesting to turn to computational modeling or *in vitro* models as

described in Reymann et al., 2012 and Ennomani et al., 2016 to investigate how myosin II could impact chromosome alignment.

4. Cortical tension: a new criterion of oocyte and embryo quality

We show that chromosome alignment defect is a hallmark of oocytes with lower than normal cortical tension. Aberrant cortical tension could thus generate aneuploidy in oocytes. Human and mouse oocytes developmental potential is accurately predicted by mechanical properties within hours after fertilization. In particular, embryos that are too stiff or too soft will cease their development rapidly after fertilization (Yanez et al., 2016). Some of these naturally soft oocytes could have chromosome alignment defects impeding on their future development after fertilization, contributing to the very high aneuploidy rate measured in female meiosis, a leading cause of infertility (Hassold and Hunt, 2001; Hassold et al., 2007; Nagaoka et al., 2012).

Cortical tension is extremely variable in a control population of oocytes (Larson et al., 2010; Chaigne et al., 2013, Chaigne et al., 2015; Yanez 2016). It is therefore possible that depending on the extent of cortical tension deregulation, different phenotypes could be triggered, ranging from aberrant division geometry (Chaigne et al., 2013; Chaigne et al., 2015), chromosome alignment defects, and maybe yet undiscovered phenotypes. We performed our study using extra-soft oocytes because they are the most represented in a natural population of oocytes. Indeed, 36% of mouse and human oocytes are measured as too soft in a normal population (Yanez et al., 2016). However, 19% of mouse and human oocytes were also measured as too stiff in this study. In these extra-stiff oocytes myosin II is retained at the cortex, leading to aberrant division geometry (Chaigne et al., 2013; Chaigne et al., 2015). It seems that chromosome alignment defects were never observed in stiff oocytes (Verlhac et al., 1996; Verlhac et al., 2000; Chaigne et al., 2013). Hence, the cause leading to developmental failure in stiff oocytes remains elusive.

At last, it would be important to investigate if an aberrant cortical tension correlates with aneuploidy in a normal population of mouse and human oocytes. Cortical tension could be assessed by micropipette aspiration. Indeed, this method was shown to be non invasive as mouse embryos implanted in female mice

recipients after micropipette aspiration resulted in live birth. However, this single-cell method is rather slow compared to atomic force microscopy (AFM) for example. High-throughput analysis of oocyte cortical tension could also be performed by using microfluidic approaches, already used in cancer cells (Lee and Liu., 2015). If they also prove to be non invasive, these tools would allow systematic measurement of oocyte cortical tension that could have practical applications. This could help to develop new criteria of oocyte and embryo quality to improve assisted reproductive technologies.

REFERENCES

Ai, J.-S., Wang, Q., Li, M., Shi, L.-H., Ola, S.I., Xiong, B., Yin, S., Chen, D.-Y., and Sun, Q.-Y. (2008). Roles of microtubules and microfilaments in spindle movements during rat oocyte meiosis. J. Reprod. Dev. 54, 391–396.

Almonacid, M., Ahmed, W.W., Bussonnier, M., Mailly, P., Betz, T., Voituriez, R., Gov, N.S., and Verlhac, M.-H. (2015). Active diffusion positions the nucleus in mouse oocytes. Nat. Cell Biol. 17, 470–479.

Almonacid, M., Terret, M.-E., and Verlhac, M.-H. (2017). Control of nucleus positioning in mouse oocytes. Seminars in Cell & Developmental Biology.

Alvarez Sedó, C., Schatten, H., Combelles, C.M., and Rawe, V.Y. (2011). The nuclear mitotic apparatus (NuMA) protein: localization and dynamics in human oocytes, fertilization and early embryos. Mol. Hum. Reprod. 17, 392–398.

Azimzadeh, J., Wong, M.L., Downhour, D.M., Sánchez Alvarado, A., and Marshall, W.F. (2012). Centrosome loss in the evolution of planarians. Science 335, 461–463.

Azoury, J., Lee, K.W., Georget, V., Rassinier, P., Leader, B., and Verlhac, M.-H. (2008). Spindle Positioning in Mouse Oocytes Relies on a Dynamic Meshwork of Actin Filaments. Curr. Biol. 18, 1514–1519.

Azoury, J., Lee, K.W., Georget, V., Hikal, P., and Verlhac, M.-H. (2011). Symmetry breaking in mouse oocytes requires transient F-actin meshwork destabilization. Development 138, 2903–2908.

Balboula, A.Z., and Schindler, K. (2014). Selective disruption of aurora C kinase reveals distinct functions from aurora B kinase during meiosis in mouse oocytes. PLoS Genet. 10, e1004194.

Basto, R., Lau, J., Vinogradova, T., Gardiol, A., Woods, C.G., Khodjakov, A., and Raff, J.W. (2006). Flies without centrioles. Cell 125, 1375–1386.

Bayliss, R., Sardon, T., Vernos, I., and Conti, E. (2003). Structural basis of Aurora-A activation by TPX2 at the mitotic spindle. Mol. Cell 12, 851–862.

Bazzi, H., and Anderson, K.V. (2014). Acentriolar mitosis activates a p53-dependent apoptosis pathway in the mouse embryo. Proc. Natl. Acad. Sci. U. S. A. 111, E1491–E1500.

Beaven, R., Bastos, R.N., Spanos, C., Romé, P., Cullen, C.F., Rappsilber, J., Giet, R., Goshima, G., and Ohkura, H. (2017). 14-3-3 regulation of Ncd reveals a new mechanism for targeting proteins to the spindle in oocytes. J. Cell Biol. 216, 3029–3039.

Bloemink, M.J., and Geeves, M.A. (2011). Shaking the myosin family tree: biochemical kinetics defines four types of myosin motor. Semin. Cell Dev. Biol. 22, 961–967.

Borrego-Pinto, J., Somogyi, K., Karreman, M.A., König, J., Müller-Reichert, T., Bettencourt-Dias, M., Gönczy, P., Schwab, Y., and Lénárt, P. (2016). Distinct mechanisms eliminate mother and daughter centrioles in meiosis of starfish oocytes. J. Cell Biol. 212, 815–827.

Braun, M., Drummond, D.R., Cross, R.A., and McAinsh, A.D. (2009). The kinesin-14 Klp2 organizes microtubules into parallel bundles by an ATP-dependent sorting mechanism. Nat. Cell Biol. 11, 724–730.

Braun, M., Lansky, Z., Szuba, A., Schwarz, F.W., Mitra, A., Gao, M., Lüdecke, A., ten Wolde, P.R., and Diez, S. (2017). Changes in microtubule overlap length regulate kinesin-14-driven microtubule sliding. Nat. Chem. Biol. 13, 1245–1252.

Breuer, M., Kolano, A., Kwon, M., Li, C.-C., Tsai, T.-F., Pellman, D., Brunet, S., and Verlhac, M.-H. (2010). HURP permits MTOC sorting for robust meiotic spindle bipolarity, similar to extra centrosome clustering in cancer cells. J. Cell Biol. 191, 1251–1260.

Brunet, S., and Maro, B. (2005). Cytoskeleton and cell cycle control during meiotic maturation of the mouse oocyte: integrating time and space. Reproduction 130, 801–811.

Brunet, S., and Maro, B. (2007). Germinal vesicle position and meiotic maturation in mouse oocyte. Reproduction 133, 1069–1072.

Brunet, S., and Verlhac, M.H. (2011). Positioning to get out of meiosis: the asymmetry of division. Hum. Reprod. Update 17, 68–75.

Brunet, S., Santa Maria, A., Guillaud, P., Dujardin, D., Kubiak, J.Z., and Maro, B. (1999). Kinetochore fibers are not involved in the formation of the first meiotic spindle in mouse oocytes, but control the exit from the first meiotic M phase. J. Cell Biol. 146, 1–12.

Brunet, S., Dumont, J., Lee, K.W., Kinoshita, K., Hikal, P., Gruss, O.J., Maro, B., and Verlhac, M.-H. (2008). Meiotic Regulation of TPX2 Protein Levels Governs Cell Cycle Progression in Mouse Oocytes. PLoS ONE 3, e3338.

Bun, P., Dmitrieff, S., Belmonte, J.M., Nédélec, F.J., and Lénárt, P. (2018). A disassembly-driven mechanism explains F-actin-mediated chromosome transport in starfish oocytes. eLife 7.

Burbank, K.S., Mitchison, T.J., and Fisher, D.S. (2007). Slide-and-cluster models for spindle assembly. Curr. Biol. CB 17, 1373–1383.

Burdyniuk, M., Callegari, A., Mori, M., Nedelec, F., and Lenart, P. (2018). F-actin patches nucleated on chromosomes coordinate capture by microtubules in oocyte meiosis.

Burkel, B.M., von Dassow, G., and Bement, W.M. (2007). Versatile fluorescent probes for actin filaments based on the actin-binding domain of utrophin. Cell Motil. Cytoskeleton 64, 822–832.

Bury, L., Coelho, P.A., Simeone, A., Ferries, S., Eyers, C.E., Eyers, P.A., Zernicka-Goetz, M., and Glover, D.M. (2017). Plk4 and Aurora A cooperate in the initiation of acentriolar spindle assembly in mammalian oocytes. J. Cell Biol. 216, 3571–3590.

Cai, S., Weaver, L.N., Ems-McClung, S.C., and Walczak, C.E. (2009). Kinesin-14 family proteins HSET/XCTK2 control spindle length by cross-linking and sliding microtubules. Mol. Biol. Cell 20, 1348–1359.

Campellone, K.G., and Welch, M.D. (2010). A nucleator arms race: cellular control of actin assembly. Nat. Rev. Mol. Cell Biol. 11, 237–251.

Carabatsos, M.J., Combelles, C.M., Messinger, S.M., and Albertini, D.F. (2000). Sorting and reorganization of centrosomes during oocyte maturation in the mouse. Microsc. Res. Tech. 49, 435–444.

Carreno, S., Kouranti, I., Glusman, E.S., Fuller, M.T., Echard, A., and Payre, F. (2008). Moesin and its activating kinase Slik are required for cortical stability and microtubule organization in mitotic cells. J. Cell Biol. 180, 739–746.

Cesario, J., and McKim, K.S. (2011). RanGTP is required for meiotic spindle organization and the initiation of embryonic development in Drosophila. J. Cell Sci. 124, 3797–3810.

Chaigne, A., Verlhac, M.-H., and Terret, M.-E. (2012). Spindle positioning in mammalian oocytes. Exp. Cell Res. 318, 1442–1447.

Chaigne, A., Campillo, C., Gov, N.S., Voituriez, R., Azoury, J., Umaña-Diaz, C., Almonacid, M., Queguiner, I., Nassoy, P., Sykes, C., et al. (2013). A soft cortex is essential for asymmetric spindle positioning in mouse oocytes. Nat. Cell Biol. 15, 958–966.

Chaigne, A., Verlhac, M.-H., and Terret, M.-E. (2014). [Cortex softening: a prerequisite for the asymmetry of oocyte first division]. Med Sci (Paris) 30, 18–21.

Chaigne, A., Campillo, C., Gov, N.S., Voituriez, R., Sykes, C., Verlhac, M.H., and Terret, M.E. (2015). A narrow window of cortical tension guides asymmetric spindle positioning in the mouse oocyte. Nat. Commun. 6, 6027.

Cheeseman, I.M., and Desai, A. (2008). Molecular architecture of the kinetochore–microtubule interface. Nat. Rev. Mol. Cell Biol. 9, 33–46.

Cheng, L., Zhang, J., Ahmad, S., Rozier, L., Yu, H., Deng, H., and Mao, Y. (2011). Aurora B Regulates Formin mDia3 in Achieving Metaphase Chromosome Alignment. Dev. Cell 20, 342–352.

Chesarone, M.A., DuPage, A.G., and Goode, B.L. (2010). Unleashing formins to remodel the actin and microtubule cytoskeletons. Nat. Rev. Mol. Cell Biol. 11, 62–74.

Chmátal, L., Yang, K., Schultz, R.M., and Lampson, M.A. (2015). Spatial Regulation of Kinetochore Microtubule Attachments by Destabilization at Spindle Poles in Meiosis I. Curr. Biol. CB 25, 1835–1841.

Chugh, P., Clark, A.G., Smith, M.B., Cassani, D.A.D., Dierkes, K., Ragab, A., Roux, P.P., Charras, G., Salbreux, G., and Paluch, E.K. (2017). Actin cortex architecture regulates cell surface tension. Nat. Cell Biol. 19, 689–697.

Clark, A.G., Dierkes, K., and Paluch, E.K. (2013). Monitoring Actin Cortex Thickness in Live Cells. Biophys. J. 105, 570–580.

Clark, A.G., Wartlick, O., Salbreux, G., and Paluch, E.K. (2014). Stresses at the cell surface during animal cell morphogenesis. Curr. Biol. CB 24, R484–R494.

Clift, D., and Schuh, M. (2015). A three-step MTOC fragmentation mechanism facilitates bipolar spindle assembly in mouse oocytes. Nat. Commun. 6, 7217.

Colin Alexandra, Almonacid Maria, Ahmed Wylie, Betz Timo, Terret Marie-Emilie, Voituriez Raphaël, Gueroui Zoher, Verlhac Marie-Hélène. Centering based on active diffusion in mouse ovocytes is non-specific. *In preparation*

Colombié, N., Głuszek, A.A., Meireles, A.M., and Ohkura, H. (2013). Meiosis-specific stable binding of augmin to acentrosomal spindle poles promotes biased microtubule assembly in oocytes. PLoS Genet. 9, e1003562.

Conduit, P.T., and Raff, J.W. (2010). Cnn dynamics drive centrosome size asymmetry to ensure daughter centriole retention in Drosophila neuroblasts. Curr. Biol. CB 20, 2187–2192.

Cullen, C.F., and Ohkura, H. (2001). Msps protein is localized to acentrosomal poles to ensure bipolarity of Drosophila meiotic spindles. Nat. Cell Biol. 3, 637–642.

Cytrynbaum, E.N., Sommi, P., Brust-Mascher, I., Scholey, J.M., and Mogilner, A. (2005). Early spindle assembly in Drosophila embryos: role of a force balance involving cytoskeletal dynamics and nuclear mechanics. Mol. Biol. Cell 16, 4967–4981.

D'Angelo, L., Myer, N.M., and Myers, K.A. (2017). MCAK-mediated regulation of endothelial cell microtubule dynamics is mechanosensitive to myosin-II contractility. Mol. Biol. Cell 28, 1223–1237.

Das, A., Shah, S.J., Fan, B., Paik, D., DiSanto, D.J., Hinman, A.M., Cesario, J.M., Battaglia, R.A., Demos, N., and McKim, K.S. (2016). Spindle Assembly and Chromosome Segregation Requires Central Spindle Proteins in Drosophila Oocytes. Genetics 202, 61–75.

Davydenko, O., Schultz, R.M., and Lampson, M.A. (2013). Increased CDK1 activity determines the timing of kinetochore-microtubule attachments in meiosis I. J. Cell Biol. 202, 221–229.

Deng, M., Suraneni, P., Schultz, R.M., and Li, R. (2007). The Ran GTPase mediates chromatin signaling to control cortical polarity during polar body extrusion in mouse oocytes. Dev. Cell 12, 301–308.

Deng, M., Gao, J., Suraneni, P., and Li, R. (2009). Kinetochore-independent chromosome poleward movement during anaphase of meiosis II in mouse eggs. PloS One 4, e5249.

Desai, A., and Mitchison, T.J. (1997). Microtubule polymerization dynamics. Annu. Rev. Cell Dev. Biol. 13, 83–117.

Divito, M. M., & Cheney, R. E. (2008). Myosin X. Myosins, 403-419.

Dumont, J., and Desai, A. (2012). Acentrosomal spindle assembly and chromosome segregation during oocyte meiosis. Trends Cell Biol. 22, 241–249.

Dumont, S., and Mitchison, T.J. (2009). Force and length in the mitotic spindle. Curr. Biol. CB 19, R749–R761.

Dumont, J., Petri, S., Pellegrin, F., Terret, M.-E., Bohnsack, M.T., Rassinier, P., Georget, V., Kalab, P., Gruss, O.J., and Verlhac, M.-H. (2007a). A centriole- and RanGTP-independent spindle assembly pathway in meiosis I of vertebrate oocytes. J. Cell Biol. 176, 295–305.

Dumont, J., Million, K., Sunderland, K., Rassinier, P., Lim, H., Leader, B., and Verlhac, M.-H. (2007b). Formin-2 is required for spindle migration and for the late steps of cytokinesis in mouse oocytes. Dev. Biol. 301, 254–265.

Dumont, J., Oegema, K., and Desai, A. (2010). A kinetochore-independent mechanism drives anaphase chromosome separation during acentrosomal meiosis. Nat. Cell Biol. 12, 894–901.

Endow, S.A., and Komma, D.J. (1997). Spindle dynamics during meiosis in Drosophila oocytes. J. Cell Biol. 137, 1321–1336.

Ennomani, H., Letort, G., Guérin, C., Martiel, J.-L., Cao, W., Nédélec, F., De La Cruz, E.M., Théry, M., and Blanchoin, L. (2016). Architecture and Connectivity Govern Actin Network Contractility. Curr. Biol. 26, 616–626.

Eppig, J.J., and O'Brien, M.J. (1996). Development in vitro of mouse oocytes from primordial follicles. Biol. Reprod. 54, 197–207.

Etemad, B., and Kops, G.J.P.L. (2016). Attachment issues: kinetochore transformations and spindle checkpoint silencing. Curr. Opin. Cell Biol. 39, 101–108.

Eyers, P.A., Erikson, E., Chen, L.G., and Maller, J.L. (2003). A novel mechanism for activation of the protein kinase Aurora A. Curr. Biol. CB 13, 691–697.

Fehon, R.G., McClatchey, A.I., and Bretscher, A. (2010). Organizing the cell cortex: the role of ERM proteins. Nat. Rev. Mol. Cell Biol. 11, 276–287.

Feng, J., Hu, Z., Chen, H., Hua, J., Wu, R., Dong, Z., Qiang, L., Liu, Y., Baas, P.W., and Liu, M. (2016). Depletion of kinesin-12, a myosin-IIB-interacting protein, promotes migration of cortical astrocytes. J. Cell Sci. 129, 2438–2447.

Fink, G., Hajdo, L., Skowronek, K.J., Reuther, C., Kasprzak, A.A., and Diez, S. (2009). The mitotic kinesin-14 Ncd drives directional microtubule-microtubule sliding. Nat. Cell Biol. 11, 717–723.

Fink, J., Carpi, N., Betz, T., Bétard, A., Chebah, M., Azioune, A., Bornens, M., Sykes, C., Fetler, L., Cuvelier, D., et al. (2011). External forces control mitotic spindle positioning. Nat. Cell Biol. 13, 771–778.

Firmino, J., Rocancourt, D., Saadaoui, M., Moreau, C., and Gros, J. (2016). Cell Division Drives Epithelial Cell Rearrangements during Gastrulation in Chick. Dev. Cell 36, 249–261.

FitzHarris, G. (2009). A shift from kinesin 5-dependent metaphase spindle function during preimplantation development in mouse. Development 136, 2111–2119.

FitzHarris, G. (2012). Anaphase B Precedes Anaphase A in the Mouse Egg. Curr. Biol. 22, 437–444.

FitzHarris, G., Marangos, P., and Carroll, J. (2007). Changes in endoplasmic reticulum structure during mouse oocyte maturation are controlled by the cytoskeleton and cytoplasmic dynein. Dev. Biol. 305, 133–144.

Gard, D.L. (1991). Organization, nucleation, and acetylation of microtubules in Xenopus laevis oocytes: a study by confocal immunofluorescence microscopy. Dev. Biol. 143, 346–362.

Garzon-Coral, C., Fantana, H.A., and Howard, J. (2016). A force-generating machinery maintains the spindle at the cell center during mitosis. Science 352, 1124–1127.

Głuszek, A.A., Cullen, C.F., Li, W., Battaglia, R.A., Radford, S.J., Costa, M.F., McKim, K.S., Goshima, G., and Ohkura, H. (2015). The microtubule catastrophe promoter Sentin delays stable kinetochore–microtubule attachment in oocytes. J. Cell Biol. 211, 1113–1120.

Gopalakrishnan, J., Chim, Y.-C.F., Ha, A., Basiri, M.L., Lerit, D.A., Rusan, N.M., and Avidor-Reiss, T. (2012). Tubulin nucleotide status controls Sas-4-dependent pericentriolar material recruitment. Nat. Cell Biol. 14, 865–873.

Goshima, G., and Scholey, J.M. (2010). Control of mitotic spindle length. Annu. Rev. Cell Dev. Biol. 26, 21–57.

Goshima, G., and Vale, R.D. (2003). The roles of microtubule-based motor proteins in mitosis: comprehensive RNAi analysis in the Drosophila S2 cell line. J. Cell Biol. 162, 1003–1016.

Goshima, G., Wollman, R., Stuurman, N., Scholey, J.M., and Vale, R.D. (2005). Length Control of the Metaphase Spindle. Curr. Biol. 15, 1979–1988.

Goshima, G., Mayer, M., Zhang, N., Stuurman, N., and Vale, R.D. (2008). Augmin: a protein complex required for centrosome-independent microtubule generation within the spindle. J. Cell Biol. 181, 421–429.

Grill, S.W., Gönczy, P., Stelzer, E.H., and Hyman, A.A. (2001). Polarity controls forces governing asymmetric spindle positioning in the Caenorhabditis elegans embryo. Nature 409, 630–633.

Grill, S.W., Howard, J., Schäffer, E., Stelzer, E.H.K., and Hyman, A.A. (2003). The distribution of active force generators controls mitotic spindle position. Science 301, 518–521.

Gruss, O.J., Carazo-Salas, R.E., Schatz, C.A., Guarguaglini, G., Kast, J., Wilm, M., Le Bot, N., Vernos, I., Karsenti, E., and Mattaj, I.W. (2001). Ran induces spindle assembly by reversing the inhibitory effect of importin alpha on TPX2 activity. Cell 104, 83–93.

Gueth-Hallonet, C., Antony, C., Aghion, J., Santa-Maria, A., Lajoie-Mazenc, I., Wright, M., and Maro, B. (1993). gamma-Tubulin is present in acentriolar MTOCs during early mouse development. J. Cell Sci. 105 (Pt 1), 157–166.

Gundersen, G.G., and Worman, H.J. (2013). Nuclear Positioning. Cell 152, 1376–1389.

Halet, G., and Carroll, J. (2007). Rac Activity Is Polarized and Regulates Meiotic Spindle Stability and Anchoring in Mammalian Oocytes. Dev. Cell 12, 309–317.

Hammer, J.A., and Sellers, J.R. (2011). Walking to work: roles for class V myosins as cargo transporters. Nat. Rev. Mol. Cell Biol. 13, 13–26.

Hassold, T., and Hunt, P. (2001). To err (meiotically) is human: the genesis of human aneuploidy. Nat. Rev. Genet. 2, 280–291.

Hassold, T., Hall, H., and Hunt, P. (2007). The origin of human aneuploidy: where we have been, where we are going. Hum. Mol. Genet. 16, R203–R208.

Heald, R., Tournebize, R., Blank, T., Sandaltzopoulos, R., Becker, P., Hyman, A., and Karsenti, E. (1996). Self-organization of microtubules into bipolar spindles around artificial chromosomes in Xenopus egg extracts. Nature 382, 420–425.

Hentrich, C., and Surrey, T. (2010). Microtubule organization by the antagonistic mitotic motors kinesin-5 and kinesin-14. J. Cell Biol. 189, 465–480.

Henty-Ridilla, J.L., Rankova, A., Eskin, J.A., Kenny, K., and Goode, B.L. (2016). Accelerated actin filament polymerization from microtubule plus ends. Science 352, 1004–1009.

Hepperla, A.J., Willey, P.T., Coombes, C.E., Schuster, B.M., Gerami-Nejad, M., McClellan, M., Mukherjee, S., Fox, J., Winey, M., Odde, D.J., et al. (2014). Minus-end-directed Kinesin-14 motors align antiparallel microtubules to control metaphase spindle length. Dev. Cell 31, 61–72.

Herbomel, G., Hatte, G., Roul, J., Padilla-Parra, S., Tassan, J.-P., and Tramier, M. (2017). Actomyosin-generated tension on cadherin is similar between dividing and non-dividing epithelial cells in early Xenopus laevis embryos. Sci. Rep. 7.

Holubcová, Z., Howard, G., and Schuh, M. (2013). Vesicles modulate an actin network for asymmetric spindle positioning. Nat. Cell Biol. 15, 937–947.

Holubcová, Z., Blayney, M., Elder, K., and Schuh, M. (2015). Human oocytes. Error-prone chromosome-mediated spindle assembly favors chromosome segregation defects in human oocytes. Science 348, 1143–1147.

Ishihara, H., Martin, B.L., Brautigan, D.L., Karaki, H., Ozaki, H., Kato, Y., Fusetani, N., Watabe, S., Hashimoto, K., and Uemura, D. (1989). Calyculin A and okadaic acid: inhibitors of protein phosphatase activity. Biochem. Biophys. Res. Commun. 159, 871–877.

Jang, J.K., Rahman, T., and McKim, K.S. (2005). The kinesinl ike protein Subito contributes to central spindle assembly and organization of the meiotic spindle in Drosophila oocytes. Mol. Biol. Cell 16, 4684–4694.

Jang, J.K., Rahman, T., Kober, V.S., Cesario, J., and McKim, K.S. (2007). Misregulation of the Kinesin-like Protein Subito Induces Meiotic Spindle Formation in the Absence of Chromosomes and Centrosomes. Genetics 177, 267–280.

Kalab, P., Pu, R.T., and Dasso, M. (1999). The ran GTPase regulates mitotic spindle assembly. Curr. Biol. CB 9, 481–484.

Kapitein, L.C., Peterman, E.J.G., Kwok, B.H., Kim, J.H., Kapoor, T.M., and Schmidt, C.F. (2005). The bipolar mitotic kinesin Eg5 moves on both microtubules that it crosslinks. Nature 435, 114–118.

Kapoor, T.M., Mayer, T.U., Coughlin, M.L., and Mitchison, T.J. (2000). Probing spindle assembly mechanisms with monastrol, a small molecule inhibitor of the mitotic kinesin, Eg5. J. Cell Biol. 150, 975–988.

Kardon, J.R., and Vale, R.D. (2009). Regulators of the cytoplasmic dynein motor. Nat. Rev. Mol. Cell Biol. 10, 854–865.

Kashina, A.S., Baskin, R.J., Cole, D.G., Wedaman, K.P., Saxton, W.M., and Scholey, J.M. (1996). A bipolar kinesin. Nature 379, 270–272.

Kelly, A.E., Sampath, S.C., Maniar, T.A., Woo, E.M., Chait, B.T., and Funabiki, H. (2007). Chromosomal Enrichment and Activation of the Aurora B Pathway Are Coupled to Spatially Regulate Spindle Assembly. Dev. Cell 12, 31–43.

Khodjakov, A., Cole, R.W., Oakley, B.R., and Rieder, C.L. (2000). Centrosome-independent mitotic spindle formation in vertebrates. Curr. Biol. CB 10, 59–67.

Kinoshita, K., Noetzel, T.L., Pelletier, L., Mechtler, K., Drechsel, D.N., Schwager, A., Lee, M., Raff, J.W., and Hyman, A.A. (2005). Aurora A phosphorylation of TACC3/maskin is required for centrosome-dependent microtubule assembly in mitosis. J. Cell Biol. 170, 1047–1055.

Kirkham, M., Müller-Reichert, T., Oegema, K., Grill, S., and Hyman, A.A. (2003). SAS-4 is a C. elegans centriolar protein that controls centrosome size. Cell 112, 575–587.

Kirschner, M., and Mitchison, T. (1986). Beyond self-assembly: from microtubules to morphogenesis. Cell 45, 329–342.

Kitajima, T.S., Ohsugi, M., and Ellenberg, J. (2011). Complete Kinetochore Tracking Reveals Error-Prone Homologous Chromosome Biorientation in Mammalian Oocytes. Cell 146, 568–581.

Koffa, M.D., Casanova, C.M., Santarella, R., Köcher, T., Wilm, M., and Mattaj, I.W. (2006). HURP is part of a Ran-dependent complex involved in spindle formation. Curr. Biol. CB 16, 743–754.

Kolano, A., Brunet, S., Silk, A.D., Cleveland, D.W., and Verlhac, M.-H. (2012). Error-prone mammalian female meiosis from silencing the spindle assembly checkpoint without normal interkinetochore tension. Proc. Natl. Acad. Sci. 109, E1858–E1867.

Kovar, D.R., Harris, E.S., Mahaffy, R., Higgs, H.N., and Pollard, T.D. (2006). Control of the Assembly of ATP- and ADP-Actin by Formins and Profilin. Cell 124, 423–435.

Kunda, P., and Baum, B. (2009). The actin cytoskeleton in spindle assembly and positioning. Trends Cell Biol. 19, 174–179.

Kunda, P., Pelling, A.E., Liu, T., and Baum, B. (2008). Moesin Controls Cortical Rigidity, Cell Rounding, and Spindle Morphogenesis during Mitosis. Curr. Biol. 18, 91–101.

Kwon, M., Godinho, S.A., Chandhok, N.S., Ganem, N.J., Azioune, A., Thery, M., and Pellman, D. (2008). Mechanisms to suppress multipolar divisions in cancer cells with extra centrosomes. Genes Dev. 22, 2189–2203.

Kwon, M., Bagonis, M., Danuser, G., and Pellman, D. (2015). Direct Microtubule-Binding by Myosin-10 Orients Centrosomes toward Retraction Fibers and Subcortical Actin Clouds. Dev. Cell 34, 323–337.

Laband, K., Le Borgne, R., Edwards, F., Stefanutti, M., Canman, J.C., Verbavatz, J.-M., and Dumont, J. (2017). Chromosome segregation occurs by microtubule pushing in oocytes. Nat. Commun. 8.

Labbé, J.-C., McCarthy, E.K., and Goldstein, B. (2004). The forces that position a mitotic spindle asymmetrically are tethered until after the time of spindle assembly. J. Cell Biol. 167, 245–256.

Lancaster, O.M., Le Berre, M., Dimitracopoulos, A., Bonazzi, D., Zlotek-Zlotkiewicz, E., Picone, R., Duke, T., Piel, M., and Baum, B. (2013). Mitotic Rounding Alters Cell Geometry to Ensure Efficient Bipolar Spindle Formation. Dev. Cell 25, 270–283.

Lane, S.I.R., Yun, Y., and Jones, K.T. (2012). Timing of anaphase-promoting complex activation in mouse oocytes is predicted by microtubule-kinetochore attachment but not by bivalent alignment or tension. Development 139, 1947–1955.

Lansbergen, G., and Akhmanova, A. (2006). Microtubule Plus End: A Hub of Cellular Activities: Microtubule Plus-End-Tracking Proteins. Traffic 7, 499–507.

Larson, S.M., Lee, H.J., Hung, P., Matthews, L.M., Robinson, D.N., and Evans, J.P. (2010). Cortical mechanics and meiosis II completion in mammalian oocytes are mediated by myosin-II and Ezrin-Radixin-Moesin (ERM) proteins. Mol. Biol. Cell 21, 3182–3192.

Lawo, S., Bashkurov, M., Mullin, M., Ferreria, M.G., Kittler, R., Habermann, B., Tagliaferro, A., Poser, I., Hutchins, J.R.A., Hegemann, B., et al. (2009). HAUS, the 8-subunit human Augmin complex, regulates centrosome and spindle integrity. Curr. Biol. CB 19, 816–826.

Lawrence, C.J., Dawe, R.K., Christie, K.R., Cleveland, D.W., Dawson, S.C., Endow, S.A., Goldstein, L.S.B., Goodson, H.V., Hirokawa, N., Howard, J., et al. (2004). A standardized kinesin nomenclature: Table I. J. Cell Biol. 167, 19–22.

Lee, L.M., and Liu, A.P. (2015). A microfluidic pipette array for mechanophenotyping of cancer cells and mechanical gating of mechanosensitive channels. Lab. Chip 15, 264–273.

Lénárt, P., Bacher, C.P., Daigle, N., Hand, A.R., Eils, R., Terasaki, M., and Ellenberg, J. (2005). A contractile nuclear actin network drives chromosome congression in oocytes. Nature 436, 812–818.

Levi, M., Ghetler, Y., Shulman, A., and Shalgi, R. (2013). Morphological and molecular markers are correlated with maturation-competence of human oocytes. Hum. Reprod. 28, 2482–2489.

Li, M. (2018). Immobilization Methods for Observing Living Mammalian Suspended Cells by AFM. In Investigations of Cellular and Molecular Biophysical Properties by Atomic Force Microscopy Nanorobotics, (Singapore: Springer Singapore), pp. 21–31.

Li, H., Guo, F., Rubinstein, B., and Li, R. (2008). Actin-driven chromosomal motility leads to symmetry breaking in mammalian meiotic oocytes. Nat. Cell Biol. 10, 1301–1308.

Liu, J., Wang, Q.-C., Wang, F., Duan, X., Dai, X.-X., Wang, T., Liu, H.-L., Cui, X.-S., Kim, N.-H., and Sun, S.-C. (2012). Nucleation Promoting Factors Regulate the Expression and Localization of Arp2/3 Complex during Meiosis of Mouse Oocytes. PLoS ONE 7, e52277.

Loughlin, R., Heald, R., and Nédélec, F. (2010). A computational model predicts Xenopus meiotic spindle organization. J. Cell Biol. 191, 1239–1249.

Loughlin, R., Wilbur, J.D., McNally, F.J., Nédélec, F.J., and Heald, R. (2011). Katanin contributes to interspecies spindle length scaling in Xenopus. Cell 147, 1397–1407.

Łuksza, M., Queguigner, I., Verlhac, M.-H., and Brunet, S. (2013). Rebuilding MTOCs upon centriole loss during mouse oogenesis. Dev. Biol. 382, 48–56.

Ma, X., Jana, S.S., Anne Conti, M., Kawamoto, S., Claycomb, W.C., and Adelstein, R.S. (2010). Ablation of Nonmuscle Myosin II-B and II-C Reveals a Role for Nonmuscle Myosin II in Cardiac Myocyte Karyokinesis. Mol. Biol. Cell 21, 3952–3962.

Machesky, L.M. (1994). Purification of a cortical complex containing two unconventional actins from Acanthamoeba by affinity chromatography on profilin-agarose. J. Cell Biol. 127, 107–115.

Mackenzie, A.C.L., Kyle, D.D., McGinnis, L.A., Lee, H.J., Aldana, N., Robinson, D.N., and Evans, J.P. (2016). Cortical mechanics and myosin-II abnormalities associated with post-ovulatory aging: implications for functional defects in aged eggs. Mol. Hum. Reprod. 22, 397–409.

Mailhes, J.B., Mastromatteo, C., and Fuseler, J.W. (2004). Transient exposure to the Eg5 kinesin inhibitor monastrol leads to syntelic orientation of chromosomes and aneuploidy in mouse oocytes. Mutat. Res. Toxicol. Environ. Mutagen. 559, 153–167.

Maître, J.-L., Turlier, H., Illukkumbura, R., Eismann, B., Niwayama, R., Nédélec, F., and Hiiragi, T. (2016). Asymmetric division of contractile domains couples cell positioning and fate specification. Nature 536, 344–348.

Manandhar, G. (2005). Centrosome Reduction During Gametogenesis and Its Significance. Biol. Reprod. 72, 2–13.

Manandhar, G., Sutovsky, P., Joshi, H.C., Stearns, T., and Schatten, G. (1998). Centrosome Reduction during Mouse Spermiogenesis. Dev. Biol. 203, 424–434.

Manil-Ségalen Marion, Łuksza Małgorzata, Kannaan Joanne, Marthiens Véronique, Lane Simon I.R., Jones Keith T., Terret Marie-Emilie, Basto Renata, Verlhac Marie-Hélène. Chromosome structural anomalies due to aberrant spindle forces exerted at gene editing sites in meiosis. J. Cell Biol. *In press*

Mao, Y. (2011). FORMIN a link between kinetochores and microtubule ends. Trends Cell Biol. 21, 625–629.

Maro, B., Howlett, S.K., and Webb, M. (1985). Non-spindle microtubule organizing centers in metaphase II-arrested mouse oocytes. J. Cell Biol. 101, 1665–1672.

Matthews, L.R., Carter, P., Thierry-Mieg, D., and Kemphues, K. (1998). ZYG-9, a Caenorhabditis elegans protein required for microtubule organization and function, is a component of meiotic and mitotic spindle poles. J. Cell Biol. 141, 1159–1168.

Matthies, H.J., McDonald, H.B., Goldstein, L.S., and Theurkauf, W.E. (1996). Anastral meiotic spindle morphogenesis: role of the non-claret disjunctional kinesin-like protein. J. Cell Biol. 134, 455–464.

Mazumdar, M., and Misteli, T. (2005). Chromokinesins: multitalented players in mitosis. Trends Cell Biol. 15, 349–355.

McNally, F.J. (2013). Mechanisms of spindle positioning. J. Cell Biol. 200, 131–140.

McNally, K.L., Martin, J.L., Ellefson, M., and McNally, F.J. (2010). Kinesin-dependent transport results in polarized migration of the nucleus in oocytes and inward movement of yolk granules in meiotic embryos. Dev. Biol. 339, 126–140.

Mendoza, M.C., Er, E.E., Zhang, W., Ballif, B.A., Elliott, H.L., Danuser, G., and Blenis, J. (2011). ERK-MAPK drives lamellipodia protrusion by activating the WAVE2 regulatory complex. Mol. Cell 41, 661–671.

Merdes, A., Ramyar, K., Vechio, J.D., and Cleveland, D.W. (1996). A complex of NuMA and cytoplasmic dynein is essential for mitotic spindle assembly. Cell 87, 447–458.

Meunier, S., and Vernos, I. (2016). Acentrosomal Microtubule Assembly in Mitosis: The Where, When, and How. Trends Cell Biol. 26, 80–87.

Mitchison, T., and Kirschner, M. (1984). Dynamic instability of microtubule growth. Nature 312, 237–242.

Mitsushima, M., Aoki, K., Ebisuya, M., Matsumura, S., Yamamoto, T., Matsuda, M., Toyoshima, F., and Nishida, E. (2010). Revolving movement of a dynamic cluster of actin filaments during mitosis. J. Cell Biol. 191, 453–462.

Miyazaki, A., Kamitsubo, E., and Nemoto, S.-I. (2000). Premeiotic Aster as a Device to Anchor the Germinal Vesicle to the Cell Surface of the Presumptive Animal Pole in Starfish Oocytes. Dev. Biol. 218, 161–171.

Miyazaki, A., Kato, K.H., and Nemoto, S. (2005). Role of microtubules and centrosomes in the eccentric relocation of the germinal vesicle upon meiosis reinitiation in sea-cucumber oocytes. Dev. Biol. 280, 237–247.

Mogessie, B., and Schuh, M. (2017). Actin protects mammalian eggs against chromosome segregation errors. Science 357, eaal1647.

Molodtsov, M.I., Mieck, C., Dobbelaere, J., Dammermann, A., Westermann, S., and Vaziri, A. (2016). A Force-Induced Directional Switch of a Molecular Motor Enables Parallel Microtubule Bundle Formation. Cell 167, 539–552.e14.

Montaville, P., Jégou, A., Pernier, J., Compper, C., Guichard, B., Mogessie, B., Schuh, M., Romet-Lemonne, G., and Carlier, M.-F. (2014). Spire and Formin 2 Synergize and Antagonize in Regulating Actin Assembly in Meiosis by a Ping-Pong Mechanism. PLoS Biol. 12, e1001795.

Mori, M., Monnier, N., Daigle, N., Bathe, M., Ellenberg, J., and Lénárt, P. (2011). Intracellular Transport by an Anchored Homogeneously Contracting F-Actin Meshwork. Curr. Biol. 21, 606–611.

Mountain, V., Simerly, C., Howard, L., Ando, A., Schatten, G., and Compton, D.A. (1999). The kinesin-related protein, HSET, opposes the activity of Eg5 and cross-links microtubules in the mammalian mitotic spindle. J. Cell Biol. 147, 351–366.

Nachury, M.V., Maresca, T.J., Salmon, W.C., Waterman-Storer, C.M., Heald, R., and Weis, K. (2001). Importin beta is a mitotic target of the small GTPase Ran in spindle assembly. Cell 104, 95–106.

Nagaoka, S.I., Hassold, T.J., and Hunt, P.A. (2012). Human aneuploidy: mechanisms and new insights into an age-old problem. Nat. Rev. Genet. 13, 493–504.

Nédélec, F. (2002). Computer simulations reveal motor properties generating stable antiparallel microtubule interactions. J. Cell Biol. 158, 1005–1015.

Nédélec, F., Surrey, T., and Karsenti, E. (2003). Self-organisation and forces in the microtubule cytoskeleton. Curr. Opin. Cell Biol. 15, 118–124.

Ning, W., Yu, Y., Xu, H., Liu, X., Wang, D., Wang, J., Wang, Y., and Meng, W. (2016). The CAMSAP3-ACF7 Complex Couples Noncentrosomal Microtubules with Actin Filaments to Coordinate Their Dynamics. Dev. Cell 39, 61–74.

Nolen, B.J., Tomasevic, N., Russell, A., Pierce, D.W., Jia, Z., McCormick, C.D., Hartman, J., Sakowicz, R., and Pollard, T.D. (2009). Characterization of two classes of small molecule inhibitors of Arp2/3 complex. Nature 460, 1031–1034.

Oegema, K., Desai, A., Rybina, S., Kirkham, M., and Hyman, A.A. (2001). Functional analysis of kinetochore assembly in Caenorhabditis elegans. J. Cell Biol. 153, 1209–1226.

Paul, A., and Pollard, T. (2008). The Role of the FH1 Domain and Profilin in Formin-Mediated Actin-Filament Elongation and Nucleation. Curr. Biol. 18, 9–19.

Pecreaux, J., Röper, J.-C., Kruse, K., Jülicher, F., Hyman, A.A., Grill, S.W., and Howard, J. (2006). Spindle oscillations during asymmetric cell division require a threshold number of active cortical force generators. Curr. Biol. CB 16, 2111–2122.

Petry, S., Pugieux, C., Nédélec, F.J., and Vale, R.D. (2011). Augmin promotes meiotic spindle formation and bipolarity in Xenopus egg extracts. Proc. Natl. Acad. Sci. U. S. A. 108, 14473–14478.

Pfender, S., Kuznetsov, V., Pleiser, S., Kerkhoff, E., and Schuh, M. (2011). Spire-Type Actin Nucleators Cooperate with Formin-2 to Drive Asymmetric Oocyte Division. Curr. Biol. 21, 955–960.

Pimenta-Marques, A., Bento, I., Lopes, C. a. M., Duarte, P., Jana, S.C., and Bettencourt-Dias, M. (2016). A mechanism for the elimination of the female gamete centrosome in Drosophila melanogaster. Science 353, aaf4866.

Pollard, T.D. (2016). Actin and Actin-Binding Proteins. Cold Spring Harb. Perspect. Biol. 8, a018226.

Pring, M., Evangelista, M., Boone, C., Yang, C., and Zigmond, S.H. (2003). Mechanism of Formin-Induced Nucleation of Actin Filaments. Biochemistry (Mosc.) 42, 486–496.

Prodon, F., Chenevert, J., and Sardet, C. (2006). Establishment of animal–vegetal polarity during maturation in ascidian oocytes. Dev. Biol. 290, 297–311.

Radford, S.J., Jang, J.K., and McKim, K.S. (2012). The Chromosomal Passenger Complex Is Required for Meiotic Acentrosomal Spindle Assembly and Chromosome Biorientation. Genetics 192, 417–429.

Radford, S.J., Go, A.M.M., and McKim, K.S. (2017). Cooperation Between Kinesin Motors Promotes Spindle Symmetry and Chromosome Organization in Oocytes. Genetics 205, 517–527.

Reymann, A.-C., Boujemaa-Paterski, R., Martiel, J.-L., Guérin, C., Cao, W., Chin, H.F., De La Cruz, E.M., Théry, M., and Blanchoin, L. (2012). Actin network architecture can determine myosin motor activity. Science 336, 1310–1314.

Riche, S., Zouak, M., Argoul, F., Arneodo, A., Pecreaux, J., and Delattre, M. (2013). Evolutionary comparisons reveal a positional switch for spindle pole oscillations in Caenorhabditis embryos. J. Cell Biol. 201, 653–662.

Rincon, S.A., Lamson, A., Blackwell, R., Syrovatkina, V., Fraisier, V., Paoletti, A., Betterton, M.D., and Tran, P.T. (2017). Kinesin-5-independent mitotic spindle assembly requires the antiparallel microtubule crosslinker Ase1 in fission yeast. Nat. Commun. 8, 15286.

Robinson, R.W., and Snyder, J.A. (2005). Localization of myosin II to chromosome arms and spindle fibers in PtK1 cells: a possible role for an actomyosin system in mitosis. Protoplasma 225, 113–122.

Romero, S., Le Clainche, C., Didry, D., Egile, C., Pantaloni, D., and Carlier, M.-F. (2004). Formin is a processive motor that requires profilin to accelerate actin assembly and associated ATP hydrolysis. Cell 119, 419–429.

Rosenblatt, J., Cramer, L.P., Baum, B., and McGee, K.M. (2004). Myosin II-dependent cortical movement is required for centrosome separation and positioning during mitotic spindle assembly. Cell 117, 361–372.

Rosenbluth, M.J., Lam, W.A., and Fletcher, D.A. (2006). Force Microscopy of Nonadherent Cells: A Comparison of Leukemia Cell Deformability. Biophys. J. 90, 2994–3003.

Rotty, J.D., Wu, C., and Bear, J.E. (2013). New insights into the regulation and cellular functions of the ARP2/3 complex. Nat. Rev. Mol. Cell Biol. 14, 7.

Sagot, I., Rodal, A.A., Moseley, J., Goode, B.L., and Pellman, D. (2002). An actin nucleation mechanism mediated by Bni1 and Profilin. Nat. Cell Biol. 4, 626–631.

Salbreux, G., Charras, G., and Paluch, E. (2012). Actin cortex mechanics and cellular morphogenesis. Trends Cell Biol. 22, 536–545.

Sampath, S.C., Ohi, R., Leismann, O., Salic, A., Pozniakovski, A., and Funabiki, H. (2004). The Chromosomal Passenger Complex Is Required for Chromatin-Induced Microtubule Stabilization and Spindle Assembly. Cell 118, 187–202.

Sánchez-Huertas, C., and Lüders, J. (2015). The augmin connection in the geometry of microtubule networks. Curr. Biol. CB 25, R294–R299.

Sandquist, J.C., Kita, A.M., and Bement, W.M. (2011). And the Dead Shall Rise: Actin and Myosin Return to the Spindle. Dev. Cell 21, 410–419.

Schaffner, S.C., and José, J.V. (2006). Biophysical model of self-organized spindle formation patterns without centrosomes and kinetochores. Proc. Natl. Acad. Sci. 103, 11166–11171.

Schuh, M. (2011). An actin-dependent mechanism for long-range vesicle transport. Nat. Cell Biol. 13, 1431–1436.

Schuh, M., and Ellenberg, J. (2007). Self-Organization of MTOCs Replaces Centrosome Function during Acentrosomal Spindle Assembly in Live Mouse Oocytes. Cell 130, 484–498.

Schuh, M., and Ellenberg, J. (2008). A New Model for Asymmetric Spindle Positioning in Mouse Oocytes. Curr. Biol. 18, 1986–1992.

Sharp, D.J., Yu, K.R., Sisson, J.C., Sullivan, W., and Scholey, J.M. (1999). Antagonistic microtubule-sliding motors position mitotic centrosomes in Drosophila early embryos. Nat. Cell Biol. 1, 51–54.

Silljé, H.H.W., Nagel, S., Körner, R., and Nigg, E.A. (2006). HURP is a Ran-importin beta-regulated protein that stabilizes kinetochore microtubules in the vicinity of chromosomes. Curr. Biol. CB 16, 731–742.

Silverman-Gavrila, R.V., and Forer, A. (2003). Myosin localization during meiosis I of crane-fly spermatocytes gives indications about its role in division. Cell Motil. Cytoskeleton 55, 97–113.

Simerly, C., Nowak, G., De Lanerolle, P., and Schatten, G. (1998). Differential expression and functions of cortical myosin IIA and IIB isotypes during meiotic maturation, fertilization, and mitosis in mouse oocytes and embryos. Mol. Biol. Cell 9, 2509–2525.

Skold, H.N., Komma, D.J., and Endow, S.A. (2005). Assembly pathway of the anastral Drosophila oocyte meiosis I spindle. J. Cell Sci. 118, 1745–1755.

Srayko, M., O'toole, E.T., Hyman, A.A., and Müller-Reichert, T. (2006). Katanin disrupts the microtubule lattice and increases polymer number in C. elegans meiosis. Curr. Biol. CB 16, 1944–1949.

Stewart, M.P., Helenius, J., Toyoda, Y., Ramanathan, S.P., Muller, D.J., and Hyman, A.A. (2011). Hydrostatic pressure and the actomyosin cortex drive mitotic cell rounding. Nature 469, 226–230.

Still, I.H., Vince, P., and Cowell, J.K. (1999). The third member of the transforming acidic coiled coil-containing gene family, TACC3, maps in 4p16, close to translocation breakpoints in multiple myeloma, and is upregulated in various cancer cell lines. Genomics 58, 165–170.

Sumiyoshi, E., Fukata, Y., Namai, S., and Sugimoto, A. (2015). Caenorhabditis elegans Aurora A kinase is required for the formation of spindle microtubules in female meiosis. Mol. Biol. Cell 26, 4187–4196.

Sun, S.-C., Xu, Y.-N., Li, Y.-H., Lee, S.-E., Jin, Y.-X., Cui, X.-S., and Kim, N.-H. (2011). WAVE2 regulates meiotic spindle stability, peripheral positioning and polar body emission in mouse oocytes. Cell Cycle 10, 1853–1860.

Surrey, T., Nedelec, F., Leibler, S., and Karsenti, E. (2001). Physical properties determining self-organization of motors and microtubules. Science 292, 1167–1171.

Syrovatkina, V., and Tran, P.T. (2015). Loss of kinesin-14 results in aneuploidy via kinesin-5-dependent microtubule protrusions leading to chromosome cut. Nat. Commun. 6.

Szollosi, D., CALARCO, P., and Donahue, R.P. (1972). Absence of centrioles in the first and second meiotic spindles of mouse oocytes. J. Cell Sci. 11, 521–541.

Tanenbaum, M.E., and Medema, R.H. (2010). Mechanisms of Centrosome Separation and Bipolar Spindle Assembly. Dev. Cell 19, 797–806.

Tanimoto, H., Sallé, J., Dodin, L., and Minc, N. (2018). Physical forces determining the persistency and centring precision of microtubule asters. Nat. Phys.

Théry, M., Racine, V., Pépin, A., Piel, M., Chen, Y., Sibarita, J.-B., and Bornens, M. (2005). The extracellular matrix guides the orientation of the cell division axis. Nat. Cell Biol. 7, 947–953.

Tissot, N., Lepesant, J.-A., Bernard, F., Legent, K., Bosveld, F., Martin, C., Faklaris, O., Bellaïche, Y., Coppey, M., and Guichet, A. (2017). Distinct molecular cues ensure a robust microtubule-dependent nuclear positioning in the Drosophila oocyte. Nat. Commun. 8, 15168.

Toso, A., Winter, J.R., Garrod, A.J., Amaro, A.C., Meraldi, P., and McAinsh, A.D. (2009). Kinetochore-generated pushing forces separate centrosomes during bipolar spindle assembly. J. Cell Biol. 184, 365–372.

Touati, S.A., and Wassmann, K. (2016). How oocytes try to get it right: spindle checkpoint control in meiosis. Chromosoma 125, 321–335.

Tournier, F., Karsenti, E., and Bornens, M. (1989). Parthenogenesis in Xenopus eggs injected with centrosomes from synchronized human lymphoid cells. Dev. Biol. 136, 321–329.

Toyoda, Y., Cattin, C.J., Stewart, M.P., Poser, I., Theis, M., Kurzchalia, T.V., Buchholz, F., Hyman, A.A., and Müller, D.J. (2017). Genome-scale single-cell mechanical phenotyping reveals disease-related genes involved in mitotic rounding. Nat. Commun. 8.

Toyoshima, F., and Nishida, E. (2007). Integrin-mediated adhesion orients the spindle parallel to the substratum in an EB1- and myosin X-dependent manner. EMBO J. 26, 1487–1498.

Tremoleda, J.L., Schoevers, E.J., Stout, T.A.E., Colenbrander, B., and Bevers, M.M. (2001). Organisation of the cytoskeleton during in vitro maturation of horse oocytes. Mol. Reprod. Dev. 60, 260–269.

Tsai, M.-Y., Wiese, C., Cao, K., Martin, O., Donovan, P., Ruderman, J., Prigent, C., and Zheng, Y. (2003). A Ran signalling pathway mediated by the mitotic kinase Aurora A in spindle assembly. Nat. Cell Biol. 5, 242–248.

Tseng, B.S., Tan, L., Kapoor, T.M., and Funabiki, H. (2010). Dual detection of chromosomes and microtubules by the chromosomal passenger complex drives spindle assembly. Dev. Cell 18, 903–912.

Tsou, A.-P., Yang, C.-W., Huang, C.-Y.F., Yu, R.C.-T., Lee, Y.-C.G., Chang, C.-W., Chen, B.-R., Chung, Y.-F., Fann, M.-J., Chi, C.-W., et al. (2003). Identification of a novel cell cycle regulated gene, HURP, overexpressed in human hepatocellular carcinoma. Oncogene 22, 298–307.

Uehara, R., Nozawa, R., Tomioka, A., Petry, S., Vale, R.D., Obuse, C., and Goshima, G. (2009). The augmin complex plays a critical role in spindle microtubule generation for mitotic progression and cytokinesis in human cells. Proc. Natl. Acad. Sci. U. S. A. 106, 6998–7003.

Uyeda, T.Q.P., Iwadate, Y., Umeki, N., Nagasaki, A., and Yumura, S. (2011). Stretching Actin Filaments within Cells Enhances their Affinity for the Myosin II Motor Domain. PLoS ONE 6, e26200.

Vavylonis, D., Kovar, D.R., O'Shaughnessy, B., and Pollard, T.D. (2006). Model of Formin-Associated Actin Filament Elongation. Mol. Cell 21, 455–466.

Verlhac, M.-H., Lefebvre, C., Guillaud, P., Rassinier, P., and Maro, B. (2000). Asymmetric division in mouse oocytes: with or without Mos. Curr. Biol. 10, 1303–1306.

Vicente-Manzanares, M., Ma, X., Adelstein, R.S., and Horwitz, A.R. (2009). Non-muscle myosin II takes centre stage in cell adhesion and migration. Nat. Rev. Mol. Cell Biol. 10, 778–790.

Walczak, C.E., Mitchison, T.J., and Desai, A. (1996). XKCM1: a Xenopus kinesin-related protein that regulates microtubule dynamics during mitotic spindle assembly. Cell 84, 37–47.

Walczak, C.E., Verma, S., and Mitchison, T.J. (1997). XCTK2: a kinesin-related protein that promotes mitotic spindle assembly in Xenopus laevis egg extracts. J. Cell Biol. 136, 859–870.

Walczak, C.E., Vernos, I., Mitchison, T.J., Karsenti, E., and Heald, R. (1998). A model for the proposed roles of different microtubule-based motor proteins in establishing spindle bipolarity. Curr. Biol. CB 8, 903–913.

Wandke, C., Barisic, M., Sigl, R., Rauch, V., Wolf, F., Amaro, A.C., Tan, C.H., Pereira, A.J., Kutay, U., Maiato, H., et al. (2012). Human chromokinesins promote chromosome congression and spindle microtubule dynamics during mitosis. J. Cell Biol. 198, 847–863.

Wassmann, K. (2013). Sister chromatid segregation in meiosis II: Deprotection through phosphorylation. Cell Cycle 12, 1352–1359.

Watanabe, Y. (2012). Geometry and force behind kinetochore orientation: lessons from meiosis. Nat. Rev. Mol. Cell Biol. 13, 370–382.

Welch, M.D., DePace, A.H., Verma, S., Iwamatsu, A., and Mitchison, T.J. (1997). The Human Arp2/3 Complex Is Composed of Evolutionarily Conserved Subunits and Is Localized to Cellular Regions of Dynamic Actin Filament Assembly. J. Cell Biol. 138, 375–384.

Wignall, S.M., and Villeneuve, A.M. (2009). Lateral microtubule bundles promote chromosome alignment during acentrosomal oocyte meiosis. Nat. Cell Biol. 11, 839–844.

Wittmann, T., Wilm, M., Karsenti, E., and Vernos, I. (2000). TPX2, A novel xenopus MAP involved in spindle pole organization. J. Cell Biol. 149, 1405–1418.

Wollman, R., Cytrynbaum, E.N., Jones, J.T., Meyer, T., Scholey, J.M., and Mogilner, A. (2005). Efficient Chromosome Capture Requires a Bias in the "Search-and-Capture" Process during Mitotic-Spindle Assembly. Curr. Biol. 15, 828–832.

Woodruff, J.B., Wueseke, O., Viscardi, V., Mahamid, J., Ochoa, S.D., Bunkenborg, J., Widlund, P.O., Pozniakovsky, A., Zanin, E., Bahmanyar, S., et al. (2015). Centrosomes. Regulated assembly of a supramolecular centrosome scaffold in vitro. Science 348, 808–812.

Woolley, D.M., and Fawcett, D.W. (1973). The degeneration and disappearance of the centrioles during the development of the rat spermatozoon. Anat. Rec. 177, 289–301.

Woolner, S., O'Brien, L.L., Wiese, C., and Bement, W.M. (2008). Myosin-10 and actin filaments are essential for mitotic spindle function. J. Cell Biol. 182, 77–88.

Yan, L.-Y., Huang, J.-C., Zhu, Z.-Y., Lei, Z.-L., Shi, L.-H., Nan, C.-L., Zhao, Z.-J., Ouyang, Y.-C., Song, X.-F., Sun, Q.-Y., et al. (2006). NuMA distribution and microtubule configuration in rabbit oocytes and cloned embryos. Reprod. Camb. Engl. 132, 869–876.

Yanez, L.Z., and Camarillo, D.B. (2017). Microfluidic analysis of oocyte and embryo biomechanical properties to improve outcomes in assisted reproductive technologies. MHR Basic Sci. Reprod. Med. 23, 235–247.

Yanez, L.Z., Han, J., Behr, B.B., Reijo Pera, R.A., and Camarillo, D.B. (2016). Human oocyte developmental potential is predicted by mechanical properties within hours after fertilization. Nat. Commun. 7, 10809.

Yasuda, S., Oceguera-Yanez, F., Kato, T., Okamoto, M., Yonemura, S., Terada, Y., Ishizaki, T., and Narumiya, S. (2004). Cdc42 and mDia3 regulate microtubule attachment to kinetochores. Nature 428, 767–771.

Yoshida, S., Kaido, M., and Kitajima, T.S. (2015). Inherent Instability of Correct Kinetochore-Microtubule Attachments during Meiosis I in Oocytes. Dev. Cell 33, 589–602.

Zoran, S.S., Simerly, C.R., and Schatten, G. (1993). Microtubule organization in mouse oocytes after micro-injection of sea urchin sperm heads, midpieces and centrosomal complexes. Biol. Res. 26, 453–453.

ANNEXES

Published Online: 22 November, 2016 | Supp Info: http://doi.org/10.1083/jcb.201607062
Downloaded from jcb.rupress.org on July 22, 2018

Meiotic spindle assembly and chromosome segregation in oocytes

Isma Bennabi, Marie-Emilie Terret, and Marie-Hélène Verlhac

Centre for Interdisciplinary Research in Biology, Collège de France, Centre National de la Recherche Scientifique, Institut National de la Santé et de la Recherche Médicale, PSL Research University, Paris 75006, France

Oocytes accumulate maternal stores (proteins, mRNAs, metabolites, etc.) during their growth in the ovary to support development after fertilization. To preserve this cytoplasmic maternal inheritance, they accomplish the difficult task of partitioning their cytoplasm unequally while dividing their chromosomes equally. Added to this complexity, most oocytes, for reasons still speculative, lack the major microtubule organizing centers that most cells use to assemble and position their spindles, namely canonical centrosomes. In this review, we will address recent work on the mechanisms of meiotic spindle assembly and chromosome alignment/segregation in female gametes to try to understand the origin of errors of oocyte meiotic divisions. The challenge of oocyte divisions appears indeed not trivial because in both mice and humans oocyte meiotic divisions are prone to chromosome segregation errors, a leading cause of frequent miscarriages and congenital defects.

Introduction

Sexual reproduction relies on the fusion of paternal and maternal haploid gametes—the sperm and the extremely large oocyte, respectively—forming a new diploid organism. Meiotic divisions contribute solely to the formation of haploid gametes. They consist of two successive divisions, without intervening DNA replication, meiosis I and II, which reduce the genetic content by half. It has been known for over a decade that female meiosis is highly prone to chromosome segregation errors, especially in humans (Hassold and Hunt, 2001; Hassold et al., 2007; Nagaoka et al., 2012). At least 10% of human pregnancies produce aneuploid embryos (presenting a gain or loss of entire chromosomes), inducing spontaneous abortions and congenital defects such as trisomies, for which incidence increases with maternal age (Nagaoka et al., 2012). In eukaryotes, the structure orchestrating chromosome alignment and segregation during cell division is the microtubule spindle. In mitotic cells, the microtubules that compose the spindle are mostly nucleated from centrosomes acting as major microtubule organizing centers (MTOCs). Canonical centrosomes are composed of a pair of centrioles surrounded by pericentriolar material (PCM) that possesses microtubule nucleation activity. The microtubule slow-growing end (minus end) is tethered to the PCM of the centrosome, whereas the fast growing (plus end) is directed toward chromosomes. At mitosis entry, centrosomes separate on opposite sides of the nuclear envelope, defining the future spindle poles and allowing bipolar spindle formation. Whereas the majority of male gametes retain centrosomes containing centrioles, in oocytes of most metazoan species, centrioles are eliminated before meiotic divisions (Szollosi et al., 1972; Manandhar et al., 2005). Thus, spindle morphogenesis and positioning are atypical in these cells. The lack of centrosomes could favor the asymmetric partitioning of the cytoplasm by reducing the distance between the pole of the spindle that is anchored to the cortex and the cell cortex. Indeed, astral microtubules, a subpopulation of microtubules connecting the spindle pole to the cortex in most mitotic cells, are absent in most oocytes because of the lack of centrioles. However, as a result of the large size of oocytes, even when centrosomes are retained, oocytes can still divide extremely asymmetrically, as in starfish. In these oocytes, centriole-containing centrosomes participate in chromosome capture once chromosomes are close enough to be reached by microtubules. Chromosome gathering is, however, achieved by a contractile actin mesh that delivers chromosomes to the spindle (Lénárt et al., 2005). Interestingly, the lack of centrioles imposes atypical modes of spindle assembly in oocytes that we are going to review in this study.

Centrosome-independent microtubule nucleation

In mitosis, the spindle is formed by microtubules that are nucleated from canonical centrosomes. Although centrosome-mediated spindle formation is dominant in most mitotic cells, mitosis can still take place in the absence of centrosomes, showing that other centrosome-independent pathways can participate in spindle formation (Khodjakov et al., 2000; Basto et al., 2006; Azimzadeh et al., 2012; Bazzi and Anderson, 2014). These centrosome-independent pathways become dominant in cells lacking centrosomes such as oocytes. Indeed, because most oocytes lack canonical centrosomes, they use alternative

Correspondence to Isma Bennabi: isma.bennabi@college-de-france.fr; or Marie-Hélène Verlhac: marie-helene.verlhac@college-de-france.fr

Abbreviations used: aMTOC, acentriolar microtubule organizing center; CDK1, cyclin-dependent kinase 1; CPC, chromosomal passenger complex; MTOC, microtubule organizing center; NEBD, nuclear envelope breakdown; NuMa, nuclear mitotic apparatus; PCM, pericentriolar material; SAF, spindle assembly factor; TACC, transforming acidic coiled coil.

© 2016 Bennabi et al. This article is distributed under the terms of an Attribution–Noncommercial–Share Alike–No Mirror Sites license for the first six months after the publication date (see http://www.rupress.org/terms). After six months it is available under a Creative Commons License (Attribution–Noncommercial–Share Alike 3.0 Unported license, as described at http://creativecommons.org/licenses/by-nc-sa/3.0/).

The Rockefeller University Press $30.00
J. Cell Biol. Vol. 215 No. 5 611–619
https://doi.org/10.1083/jcb.201607062

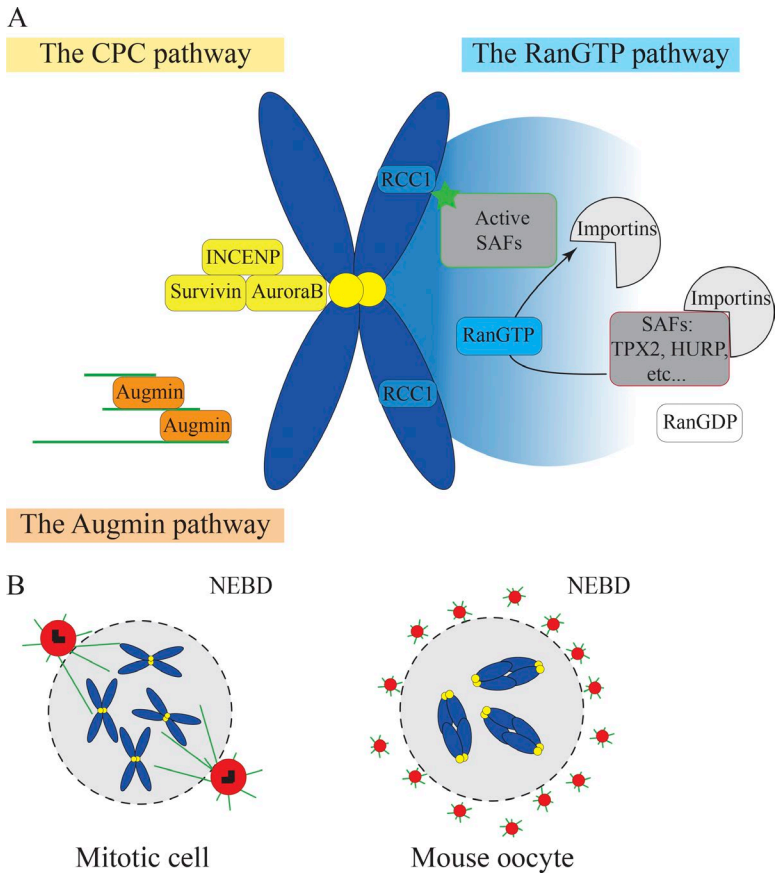

Figure 1. **Pathways replacing centrosomes for microtubule nucleation in oocytes.** (A) The three microtubule nucleation pathways: the RanGTP pathway, CPC pathway, and Augmin pathway. (B) Microtubule nucleation by centrosomes in mitotic cells (left) and by multiple aMTOCs in mouse oocytes (right). For A and B, DNA is in blue, microtubules in green, kinetochores in yellow, pericentriolar material in red, and centrioles in black.

pathways to nucleate microtubules (Fig. 1 A). Among them, the RanGTP pathway has been very well described (Fig. 1 A). The small Ran GTPase (Ras-like nuclear protein) is present in a gradient around chromosomes both in mitotic and meiotic cells. The RanGTP active form is produced by the Ran guanosine exchange factor regulator of chromosome condensation 1 (RCC1) that is localized on chromosomes (Kalab et al., 1999). This gradient locally activates spindle assembly factors (SAFs), such as, for example, targeting protein for Xklp2 (Tpx2), that participate in microtubule nucleation, interaction, and stabilization as well as motor activities (Meunier and Vernos, 2016). These SAFs interact with importins via their NLS and are kept inhibited. The RanGTP gradient is proposed to promote the dissociation of SAFs from their inhibitory binding to importins, causing their local activation and release (Gruss et al., 2001; Nachury et al., 2001). In human oocytes, RanGTP inhibition seems to delay microtubule nucleation and impair spindle formation (Holubcová et al., 2015). However, human oocytes used in this study were atretic (oocytes from patients receiving in vitro fertilization that did not spontaneously resume meiosis in response to hormonal treatment), and thus, they might not behave similarly to healthy human oocytes. Differently, inhibition of RanGTP delays but does not impair spindle assembly in mouse and *Drosophila melanogaster* oocytes (Dumont et al., 2007; Cesario and McKim, 2011). This suggests that although the RanGTP pathway is involved in microtubule nucleation for spindle assembly in the absence of centrosomes, other pathways seem important. Among these, the Augmin pathway (Fig. 1 A) generates new microtubules along preexisting microtubules (Sánchez-Huertas and Lüders, 2015). The Augmin complex is composed of eight proteins (named HAUS 1–8) able to recruit γ-tubulin to the sides of microtubules within the spindle (Goshima et al., 2008; Lawo et al., 2009; Uehara et al., 2009). In *Xenopus laevis* egg extracts, Augmin depletion results in reduced microtubule nucleation and multipolar spindle formation, suggesting a role of the Augmin complex in spindle bipolarization (Petry et al., 2011). In fruit flies, Augmin compensates for the lack of centrosomes by promoting microtubules nucleation at meiotic spindle poles (Colombié et al., 2013). Similarly, the chromosomal passenger complex (CPC) pathway (Fig. 1 A) is also involved in microtubule stabilization and spindle assembly in *Xenopus* egg extracts and *Drosophila* oocytes (Sampath et al., 2004; Kelly et al., 2007; Tseng et al., 2010; Radford et al., 2012; Das et al., 2016). The CPC is associated with kinetochores and is composed of the Aurora B/C kinase, the inner centromeric protein (INCENP), Survivin, and Borealin (Dumont and Desai, 2012). In *Caenorhabditis elegans* oocytes, Katanin increases the density of small microtubules by severing preexisting ones and could thus contribute to microtubule formation by amplifying microtubule nucleation via other pathways (Srayko et al., 2006).

In addition to these microtubule nucleation pathways, mouse oocytes contain acentriolar MTOCs (aMTOCs) capable of nucleating microtubules (Fig. 1 B). At nuclear envelope breakdown (NEBD), the nucleation capacity of these aMTOCs is low, but it increases throughout meiosis I. Indeed, levels of the RanGTPase effector TPX2 (Wittmann et al., 2000) rise progressively during meiosis I (Brunet et al., 2008), which intensifies the extent of phosphorylation of the aMTOC protein transforming acidic coiled coil 3 (TACC) and increases microtubule nucleation activity at aMTOCs (Still et al., 1999; Bayliss et al., 2003; Eyers et al., 2003; Tsai et al., 2003; Kinoshita et al., 2005; Brunet et al., 2008). These aMTOCs are perinuclear

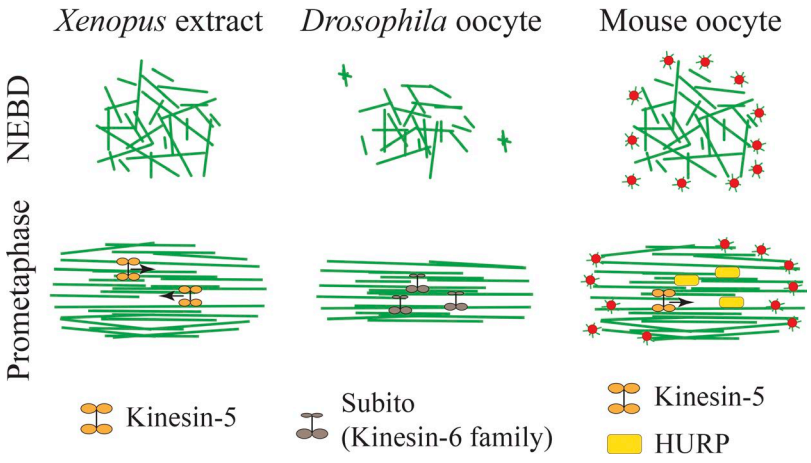

Figure 2. **Spindle bipolarization.** Organization of microtubules into a bipolar array via microtubule motors and microtubule-associated proteins in *Xenopus* egg extracts, *Drosophila*, and mouse oocytes between NEBD and prometaphase. Microtubules are in green and aMTOCs in red.

before meiotic divisions (Fig. 1 B) so that they can be readily distributed around the chromatin when NEBD occurs (Łuksza et al., 2013). Although the exact composition of these structures is not exhaustively known, they contain classical PCMs such as γ-tubulin and pericentrin and are likely bona fide PCMs (Gueth-Hallonet et al., 1993; Carabatsos et al., 2000). In mitotic cells, the PCM size is regulated by centrioles such that microtubule nucleation is carefully regulated (Kirkham et al., 2003; Conduit and Raff, 2010; Gopalakrishnan et al., 2012; Woodruff et al., 2015). In mouse oocytes, the size of the PCM seems to scale with the cell volume, but the regulatory mechanisms at play are unknown (Łuksza et al., 2013). Surprisingly, such acentriolar MTOCs are not detected on the nuclear envelope in prophase I or at later stages in spindle poles from *Xenopus*, *C. elegans*, *Drosophila*, and human atretic oocytes (Gard, 1991; Matthies et al., 1996; Srayko et al., 2006; Holubcová et al., 2015). Although all of these microtubule nucleation pathways are essential for spindle assembly in the absence of nucleation by centrosomes, little is known about their relative contribution in oocytes and how they interact.

Spindle bipolarization

Once microtubules are formed, the spindle must assemble in a bipolar fashion to accurately segregate chromosomes in two distinct groups. In mitotic cells, centrosomes are duplicated during interphase of the cell cycle, and cells enter mitosis with two centrosomes. At the onset of mitosis, the two centrosomes separate and nucleate microtubules (Fig. 1 B). Duplicated centrosomes thus form the spindle axis and promote rapid spindle bipolarization (Toso et al., 2009; Tanenbaum and Medema, 2010). In oocytes, spindle bipolarization does not rely on a bipolar axis predefined by the two separated centrosomes. Instead, spindle bipolarization is a sequential and slow process. It can take up to 12 min in *C. elegans*, 4 h in mouse, and 6.5 h in human atretic oocytes, which corresponds to around half of the transition time from NEBD to anaphase in these species (Dumont et al., 2007; Schuh and Ellenberg, 2007; Holubcová et al., 2015; Sumiyoshi et al., 2015) and 40 min in *Drosophila* oocytes (Sköld et al., 2005). In the absence of centrosomes, the establishment of a bipolar spindle depends on the sorting and stabilization of microtubules into a central array via microtubule motors and microtubule-associated proteins (Heald et al., 1996; Walczak et al., 1998). A crucial step in this process is the transformation of an unorganized ball of microtubules into a bipolar array presenting antiparallel microtubules in opposite orientations. This is achieved via the sorting and bundling of microtubules by plus end–directed microtubule motors (Fig. 2). Among them, Kinesin-5 (Eg5) was shown to be essential for the establishment and maintenance of spindle bipolarity in *Xenopus* extracts and mouse oocytes (Fig. 2) because its inhibition results in monopolar spindles (Walczak et al., 1998; Kapoor et al., 2000; Mailhes et al., 2004; Schuh and Ellenberg, 2007; Fitzharris, 2009). In *Drosophila,* the Kinesin-6 family member Subito facilitates spindle bipolarization (Fig. 2) by promoting the formation of a central microtubule array (Jang et al., 2005, 2007). In particular, CPC central spindle proteins such as INC ENP and Aurora B fail to localize to this central region in subito mutants. In mice, where oocytes assemble a meiotic spindle in the presence of multiple aMTOCs, these aMTOCs have to be properly organized to ensure correct spindle bipolarization. Before NEBD, aMTOCs are decondensed by Polo-like kinase 1 (PLK1); upon NEBD, they are spread along the nuclear envelope by a microtubule- and dynein-dependent mechanism; and after NEBD, aMTOCs are fragmented in smaller structures by Kinesin-5 (Łuksza et al., 2013; Clift and Schuh, 2015). This fragmentation process is essential for bipolar spindle formation, as a failure to fragment aMTOCs induces defects in bipolar spindle assembly and chromosome alignment. Next, concomitant to the formation of a central microtubule array, aMTOCs are progressively sorted along the central spindle into distinct poles between NEBD and 4 h after (Schuh and Ellenberg, 2007; Breuer et al., 2010). A key player in this process is the microtubule-associated protein and RanGTPase factor hepatoma up-regulated protein (HURP), which has a role very comparable to the one of Subito in *Drosophila* (Tsou et al., 2003). HURP is recruited by Kinesin-5 to the central spindle (Fig. 2) and permits aMTOCs sorting by facilitating microtubule stability in this region (Breuer et al., 2010). The stabilization of microtubules in the region of overlap of antiparallel microtubules provides tracks on which motors can bind aMTOCs as their cargo and transport them to spindle poles.

Interestingly, in human atretic oocytes in which spindle bipolarization is extremely slow, most spindles fail to maintain a bipolar shape but instead go through phases of multipolarity (Holubcová et al., 2015). Such unstable spindles are rarely observed in mitotic spindles or meiotic spindles from other species, except in oocytes from the *hurp*$^{-/-}$ strain (Breuer et al., 2010), thus raising the question of the nature of the regulatory mechanisms at play in this type of human oocyte favoring this instability.

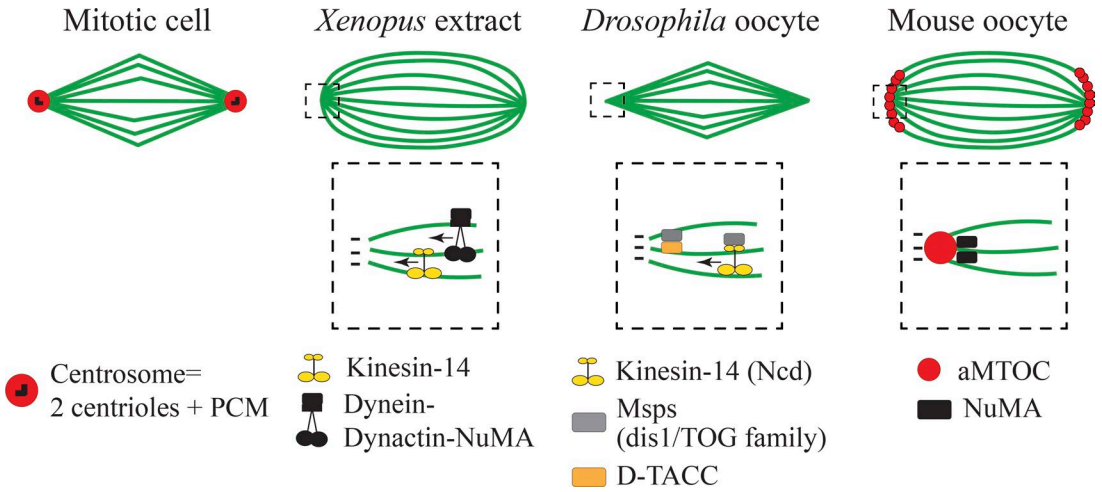

Figure 3. **Spindle pole formation and final spindle shape.** Top rows show spindle shape in metaphase in mitotic cells, *Xenopus* egg extracts, *Drosophila*, and mouse oocytes. The dashed square shows magnification of the spindle pole where microtubule motors and microtubule-associated proteins organize microtubule minus ends. Microtubules are in green.

Spindle pole formation

Spindle poles in mitosis are organized by a single centrosome (Fig. 3). Pole formation in oocytes is differentbecause it is not organized by a single entity. The formation of spindle poles, which is the region where microtubule minus ends are converging, relies on the activity of microtubule motors and microtubule-associated proteins (Fig. 3). *Drosophila* excepted, most oocytes present spindle poles that are less focused than in mitosis, having this typical barrel-shape aspect. Studies in *Xenopus* egg extracts have shown that Dynein and Kinesin-14 minus-end motors (Fig. 3) shape the poles by focusing microtubule minus ends in these regions (Heald et al., 1996; Walczak et al., 1998). In *Drosophila* oocytes, nonclaret disjunctional (Ncd; Kinesin-14) prevents pole splitting and multipolar spindle formation (Fig. 3; Endow and Komma, 1997; Sköld et al., 2005). Furthermore, Dynein in a complex with Dynactin and nuclear mitotic apparatus (NuMa) are essential to cross-link parallel microtubules (in the same orientation) and thus tether together microtubule minus ends at meiotic spindle poles in *Xenopus* egg extracts (Fig. 3; Merdes et al., 1996). Acentrosomal poles in *Drosophila* oocytes contain the microtubule-associated protein mini-spindles (Msps), which is a member of the defect in sister chromatid disjoining 1/tumor overexpression gene (dis1/TOG) family conserved in *C. elegans*, *Xenopus*, and humans. Msps is recruited to spindle poles by Kinesin-14 (Ncd) and D-TACC (Fig. 3), where it prevents loss of bipolarity possibly by stabilization of microtubules ends (Cullen and Ohkura, 2001). The *C. elegans* homologue ZYG-9 is enriched at spindle poles and required for spindle assembly (Matthews et al., 1998). Remarkably, the function of NuMa in tethering microtubule minus ends is conserved in acentriolar spindles. Indeed, the microtubule-associated protein NuMa accumulates at the poles in rabbit, human, and mouse oocytes (Yan et al., 2006; Alvarez Sedó et al., 2011; Kolano et al., 2012). In mouse oocytes, NuMa is required for the formation of barrel-shaped spindle poles as well as microtubule minus-end cohesion (Fig. 3) because its impairment causes hyperfocused poles that often lose microtubule connection (Kolano et al., 2012).

In mouse oocytes, the discrete aMTOCs organize spindle poles (Fig. 3). After their bipolar sorting, aMTOCs progressively cluster together between 4 and 7 h after NEBD and will contribute to the cohesion and integrity of spindle poles (Kolano et al., 2012). Even though not addressed so far, if the sorting of aMTOCs fails to be optimal, the number of aMTOCs at each pole might not be identical and could thus favor force imbalance within the spindle compared with mitotic spindles where the poles are formed by equivalent centrosomes. This would resemble the process of clustering of extra-centrosomes in cancer cells in which unbalanced poles favor chromosome missegregation (Kwon et al., 2008; Breuer et al., 2010). In *C. elegans*, *Drosophila*, *Xenopus*, and humans, microtubule minus ends do not seem to be anchored to discrete aMTOC entities (Fig. 3). Although they are not anchored to detectable structures, their poles are shaped by a combination of factors as described above (in this section). In addition, most meiotic spindle poles, with the exception of *Drosophila*, have a broad shape compared with the more focused mitotic spindle poles, which could be related to the lack of tight organizers, the centrosomes (Fig. 3). Thus, meiotic spindle poles could possibly be less robust than the mitotic ones that are anchored to distinct centrosomes.

Chromosome alignment

After a bipolar spindle is formed, chromosomes align in the spindle equator. In mitosis, the "search and capture" model states that microtubules growing toward the chromosomes are rapidly captured and stabilized by the kinetochores, establishing stable kinetochore–microtubule attachments (Kirschner and Mitchison, 1986; Wollman et al., 2005). In oocytes, chromosome alignment is a much slower and progressive process that depends on the interaction of microtubules with chromosome arms and kinetochores. The interaction of chromosome arms with microtubules and microtubule motors, which also exist in the short prometaphase of mitotic cells, are thought to generate forces pushing chromosomes toward the spindle equator (Mazumdar and Misteli, 2005; Cheeseman and Desai, 2008; Cai et al., 2009; Wandke et al., 2012). In *C. elegans*, the kinesin-like protein KPL-19 localizes to a nonkinetochore chromatin region where microtubules contact chromosomes and could promote the motion of chromosomes toward the equator (Wignall and Villeneuve, 2009).

An EM study has suggested that mouse oocytes establish extremely delayed kinetochore–microtubule attachments

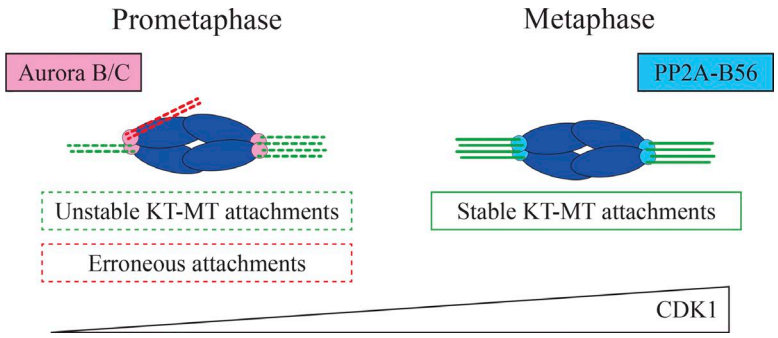

Figure 4. **Establishment of stable kinetochore–microtubule attachments in mouse oocytes.** Mouse oocytes form stable kinetochore–microtubule (KT-MT) attachments only at late metaphase I. Aurora B/C phosphorylation destabilizes kinetochore–microtubule attachments, whereas PP2A-B56 dephosphorylation activity stabilizes the attachments. This process is regulated by a progressive increase in CDK1 activity. DNA is in blue.

(K-fibers), 1 to 2 h before anaphase (Brunet et al., 1999). However, even though stable K-fibers appear to be formed late in mouse oocytes, this does not exclude the possibility that microtubules could establish earlier contacts with kinetochores. Indeed, kinetochore–microtubule attachments are observed after calcium or cold treatment 3 to 4 h before anaphase (Lane et al., 2012). Yet K-fiber stability varies until late metaphase I (Fig. 4). A study with high-resolution live microscopy revealed that almost all kinetochores undergo multiple steps of error correction before engaging into stable bipolar attachments (Kitajima et al., 2011). Thus, K-fibers may not have been well preserved during EM fixation procedures and failed to be detected at earlier stages (Brunet et al., 1999). It may be interesting to reanalyze in more detail the timing of apparition of K-fibers by EM. The delay in K-fiber formation depends on cyclin-dependent kinase 1 (CDK1) activity (Fig. 4), which increases very gradually throughout meiosis I (Davydenko et al., 2013). A precocious increase in CDK1 activity leads to premature stable kinetochore–microtubule attachments and lagging chromosomes at anaphase. Aurora B/C phosphorylation activity destabilizes the attachments, whereas protein phosphatase 2A-B56 (PP2A-B56), recruited at kinetochores by an increase in CDK1 activity, stabilizes kinetochore–microtubule attachments (Fig. 4; Yoshida et al., 2015). Using a genetic approach, it has been shown in mouse oocytes that Aurora C corrects erroneous kinetochore attachments (Balboula and Schindler, 2014). In addition, kinetochore microtubule stability is regulated by their position within the spindle, as they can undergo Aurora A–dependent destabilization near spindle poles (Chmátal et al., 2015). It is thought that a delay in K-fiber formation would prevent the stabilization of erroneous attachments before bipolar spindle formation, a very slow and unsteady process in meiosis I.

A recent study has shown that stable K-fibers formation is also slow in *Drosophila* oocytes (Głuszek et al., 2015) but depends on an alternative mechanism. The catastrophe-promoting complex Sentin–EB1 (end-binding protein 1) is responsible for delaying stable K-fiber attachments by regulating microtubule end dynamics. Mutant oocytes for *sentin* present more stable K-fibers early on in meiosis I, which is deleterious for bivalent segregation. Thus, one could speculate that slow K-fiber formation might be beneficial in the context of spindles organized from multiple aMTOCs or from chromosomes that might produce more merotelic attachments than spindles organized from centrosomes (when one kinetochore is attached to the two spindle poles).

Chromosome segregation

Once chromosomes are aligned on the spindle equator, pulling by K-fibers drives chromosome separation. In mitotic cells, chromosome separation is driven first by shortening of the kinetochore–microtubule attachments (anaphase A) and then by spindle elongation (anaphase B). In mouse oocytes, the opposite happens: first, the spindle elongates by a Kinesin-5–dependent mechanism, and then kinetochore–microtubule attachments shorten (FitzHarris, 2012). Interestingly, in nematodes, K-fibers align chromosomes but are not required for chromosome separation at anaphase (Dumont et al., 2010). Instead, it is proposed that microtubule assembly between chromosomes promotes their separation. This is consistent with the fact that spindle poles almost completely disappear at anaphase in this species. In addition, *C. elegans* chromosomes are holocentric presenting kinetochores ensheathing the entire chromosome length (Oegema et al., 2001). Although the presence of holocentric chromosomes could favor microtubule nucleation between chromosomes at anaphase, it could also promote the formation of merotelic attachments. Whether this kinetochore-independent separation mechanism is conserved in mammalian oocytes is still unknown, even though spindles lacking K-fibers are still able to undergo anaphase in mouse oocytes (Deng et al., 2009).

In mitosis, sister kinetochores are attached to opposite poles before segregation (bi-oriented), and cohesins (protein complexes holding the sister chromatid together) are cleaved at anaphase, leading to separation. In meiosis, sister kinetochores are attached to the same pole (mono-orientation), whereas homologous chromosomes are attached to opposite poles (Watanabe, 2012). At anaphase I, the meiotic-specific cohesin Rec8 is protected from cleavage at centromeres, permitting the separation of homologous chromosomes but not the separation of sister chromatids. Loss of cohesion is a leading cause of age-associated chromosome segregation errors (Chiang et al., 2010; Lister et al., 2010). The recently discovered kinetochore factor meiotic kinetochore factor (MEIKIN) is conserved from yeast to humans and required for both mono-orientation and cohesion protection (Kim et al., 2015). This suggests that MEIKIN could be a novel candidate implicated in age-associated chromosome segregation errors.

Why lose centrioles?

Lack of centrioles in oocytes imposes atypical modes of spindle formation that might contribute to the inherent high rate of chromosome segregation errors observed in meiosis. A puzzling observation is that whereas centrioles and PCMs are lost in oocytes of most metazoan species, mouse oocytes still retain multiple discrete PCMs or aMTOCs that can participate in bipolar spindle formation. In contrast to most species, sperm centrioles degenerate in rodents during spermatogenesis and thus are not contributed by the sperm at fertilization (Woolley and Fawcett, 1973; Manandhar et al., 1998). Instead, centrioles progressively

assemble de novo in early embryos (Gueth-Hallonet et al., 1993). How centrioles are generated in rodent early embryos is not known. Nevertheless, these discrete PCMs could serve as templates for a later generation of centriole-containing centrosomes in the embryo.

Whether they possess discrete PCM foci at their poles or not, oocyte meiotic spindles appear to be fragile with steps of assembly that are slow and even unstable, as in humans. In addition, their shapes are often peculiar. Female meiotic spindles of many species are small and do not closely scale to cell size unlike mitotic spindles (Crowder et al., 2015). In mouse after fertilization and until centrioles assemble de novo at the 64-cell stage (Gueth-Hallonet et al., 1993), the spindle transitions from a meiotic shape to a mitotic one: the aMTOCs number sequentially decreases, poles become more focused, and the length of the spindle scales with the size of the cell (Courtois et al., 2012). This raises the question of the contribution of the centrosome in spindle size scaling. Furthermore, the large size of oocytes could dilute some components required for spindle morphogenesis and thus contribute to the fact that spindle size does not strictly correlate with cell size.

Still, very little is known about why and how centrioles are eliminated in oocytes of most species. One hypothesis is that centriole elimination prevents multipolar spindle formation in the first embryonic division after introduction of the sperm centrioles upon fertilization. However, in rodents, the sperm does not contribute with a centriole. Another hypothesis would be that it prevents parthenogenesis (egg activation in the absence of fertilization) because injection of centrosomes in *Xenopus* eggs induces activation without fertilization (Tournier et al., 1989). Recent studies have started to unravel how centrioles are removed in oocytes. In starfish, meiotic divisions take place in the presence of centriole-containing centrosomes. Mother centrioles are eliminated by extrusion into polar bodies, and the remaining daughter centriole is degraded in the cytoplasm (Borrego-Pinto et al., 2016). In the fruit fly, centriole elimination is a progressive process that ends up just before meiotic spindle assembly. It is dependent on PLK1 because its loss triggers PCM down-regulation, which leads to centriole removal. Centriole maintenance by perturbing this process results in spindle assembly defects in oocytes and early embryos and thus to female sterility (Pimenta-Marques et al., 2016). The absence of canonical centrosomes constitutes one of the many factors that could contribute to the innate susceptibility of oocyte to produce errors in chromosome segregation. However, despite its contribution to oocyte aneuploidy, centriole elimination must likely be crucial for gamete fitness of most metazoan species.

Conclusion

Recent advances have shed light on the mechanisms of spindle assembly in both mitosis and meiosis. It appears that oocytes use the same nucleation pathways as mitotic cells, namely the RanGTP, Augmin, and CPC pathways, with the exception that they are dominant in this study, in the absence of a centrosome pathway. Although they share common pathways, meiotic spindles are not just mitotic spindles without centrosomes, and these pathways are likely regulated in a meiosis-specific manner. Yet one can speculate that in the absence of centrosomes, the initial conditions might be key parameters influencing the entire process of spindle assembly with consequences on chromosome segregation. Oocytes have to face circumstances in which the critical mass of microtubules to capture and gather chromosomes could be limiting early on when they are polymerized only locally around chromosomes. This effect could be amplified by the fact that oocytes present huge nuclei (30 µm wide in the mouse and up to 450 µm in *Xenopus*), such that the volume at which the spindle starts assembling is gigantic compared with one of mitotic cells. It might be so that the critical concentration for tubulin to polymerize might be much more difficult to reach than in somatic cells when the nucleus breaks down, reinforcing the importance of pathways acting as catalyzers/amplifiers of tubulin polymerization locally around chromosomes. How these pathways, and yet-to-be-discovered ones, interact to promote early stages of spindle assembly has not been thoroughly addressed and remains an important question for future studies.

Acknowledgments

This work was supported by grants from the Agence Nationale de la Recherche (ANR-14-CE11-0002 to M.-H. Verlhac) and from the Fondation pour la Recherche Médicale (Team FRM 2015 to M.-H. Verlhac). This work has received support under the program Investissements d'Avenir launched by the French government and implemented by the Agence Nationale de la Recherche, with references ANR-10-LABX-54 MEMO LIFE and ANR-11-IDEX-0001-02 PSL* Research University.

The authors declare no competing financial interests.

Submitted: 18 July 2016
Revised: 10 October 2016
Accepted: 2 November 2016

References

Alvarez Sedó, C., H. Schatten, C.M. Combelles, and V.Y. Rawe. 2011. The nuclear mitotic apparatus (NuMA) protein: Localization and dynamics in human oocytes, fertilization and early embryos. *Mol. Hum. Reprod.* 17:392–398. http://dx.doi.org/10.1093/molehr/gar009

Azimzadeh, J., M.L. Wong, D.M. Downhour, A. Sánchez Alvarado, and W.F. Marshall. 2012. Centrosome loss in the evolution of planarians. *Science.* 335:461–463. http://dx.doi.org/10.1126/science.1214457

Balboula, A.Z., and K. Schindler. 2014. Selective disruption of aurora C kinase reveals distinct functions from aurora B kinase during meiosis in mouse oocytes. *PLoS Genet.* 10:e1004194. http://dx.doi.org/10.1371/journal.pgen.1004194

Basto, R., J. Lau, T. Vinogradova, A. Gardiol, C.G. Woods, A. Khodjakov, and J.W. Raff. 2006. Flies without centrioles. *Cell.* 125:1375–1386. http://dx.doi.org/10.1016/j.cell.2006.05.025

Bayliss, R., T. Sardon, I. Vernos, and E. Conti. 2003. Structural basis of Aurora-A activation by TPX2 at the mitotic spindle. *Mol. Cell.* 12:851–862. http://dx.doi.org/10.1016/S1097-2765(03)00392-7

Bazzi, H., and K.V. Anderson. 2014. Acentriolar mitosis activates a p53-dependent apoptosis pathway in the mouse embryo. *Proc. Natl. Acad. Sci. USA.* 111:E1491–E1500. http://dx.doi.org/10.1073/pnas.1400568111

Borrego-Pinto, J., K. Somogyi, M.A. Karreman, J. König, T. Müller-Reichert, M. Bettencourt-Dias, P. Gönczy, Y. Schwab, and P. Lénárt. 2016. Distinct mechanisms eliminate mother and daughter centrioles in meiosis of starfish oocytes. *J. Cell Biol.* 212:815–827. http://dx.doi.org/10.1083/jcb.201510083

Breuer, M., A. Kolano, M. Kwon, C.-C. Li, T.-F. Tsai, D. Pellman, S. Brunet, and M.-H. Verlhac. 2010. HURP permits MTOC sorting for robust meiotic spindle bipolarity, similar to extra centrosome clustering in cancer cells. *J. Cell Biol.* 191:1251–1260. http://dx.doi.org/10.1083/jcb.201005065

Brunet, S., A.S. Maria, P. Guillaud, D. Dujardin, J.Z. Kubiak, and B. Maro. 1999. Kinetochore fibers are not involved in the formation of the first meiotic spindle in mouse oocytes, but control the exit from the first meiotic M phase. *J. Cell Biol.* 146:1–12. http://dx.doi.org/10.1083/jcb.146.1.1

Brunet, S., J. Dumont, K.W. Lee, K. Kinoshita, P. Hikal, O.J. Gruss, B. Maro, and M.-H. Verlhac. 2008. Meiotic regulation of TPX2 protein levels

governs cell cycle progression in mouse oocytes. *PLoS One.* 3:e3338. http://dx.doi.org/10.1371/journal.pone.0003338

Cai, S., C.B. O'Connell, A. Khodjakov, and C.E. Walczak. 2009. Chromosome congression in the absence of kinetochore fibres. *Nat. Cell Biol.* 11:832–838. http://dx.doi.org/10.1038/ncb1890

Carabatsos, M.J., C.M. Combelles, S.M. Messinger, and D.F. Albertini. 2000. Sorting and reorganization of centrosomes during oocyte maturation in the mouse. *Microsc. Res. Tech.* 49:435–444. http://dx.doi.org/10.1002/(SICI)1097-0029(20000601)49:5<435::AID-JEMT5>3.0.CO;2-H

Cesario, J., and K.S. McKim. 2011. RanGTP is required for meiotic spindle organization and the initiation of embryonic development in *Drosophila*. *J. Cell Sci.* 124:3797–3810. http://dx.doi.org/10.1242/jcs.084855

Cheeseman, I.M., and A. Desai. 2008. Molecular architecture of the kinetochore-microtubule interface. *Nat. Rev. Mol. Cell Biol.* 9:33–46. http://dx.doi.org/10.1038/nrm2310

Chiang, T., F.E. Duncan, K. Schindler, R.M. Schultz, and M.A. Lampson. 2010. Evidence that weakened centromere cohesion is a leading cause of age-related aneuploidy in oocytes. *Curr. Biol.* 20:1522–1528. http://dx.doi.org/10.1016/j.cub.2010.06.069

Chmátal, L., K. Yang, R.M. Schultz, and M.A. Lampson. 2015. Spatial regulation of kinetochore microtubule attachments by destabilization at spindle poles in meiosis I. *Curr. Biol.* 25:1835–1841. http://dx.doi.org/10.1016/j.cub.2015.05.013

Clift, D., and M. Schuh. 2015. A three-step MTOC fragmentation mechanism facilitates bipolar spindle assembly in mouse oocytes. *Nat. Commun.* 6:7217. http://dx.doi.org/10.1038/ncomms8217

Colombié, N., A.A. Głuszek, A.M. Meireles, and H. Ohkura. 2013. Meiosis-specific stable binding of augmin to acentrosomal spindle poles promotes biased microtubule assembly in oocytes. *PLoS Genet.* 9:e1003562. http://dx.doi.org/10.1371/journal.pgen.1003562

Conduit, P.T., and J.W. Raff. 2010. Cnn dynamics drive centrosome size asymmetry to ensure daughter centriole retention in *Drosophila* neuroblasts. *Curr. Biol.* 20:2187–2192. http://dx.doi.org/10.1016/j.cub.2010.11.055

Courtois, A., M. Schuh, J. Ellenberg, and T. Hiiragi. 2012. The transition from meiotic to mitotic spindle assembly is gradual during early mammalian development. *J. Cell Biol.* 198:357–370. http://dx.doi.org/10.1083/jcb.201202135

Crowder, M.E., M. Strzelecka, J.D. Wilbur, M.C. Good, G. von Dassow, and R. Heald. 2015. A comparative analysis of spindle morphometrics across metazoans. *Curr. Biol.* 25:1542–1550. http://dx.doi.org/10.1016/j.cub.2015.04.036

Cullen, C.F., and H. Ohkura. 2001. Msps protein is localized to acentrosomal poles to ensure bipolarity of *Drosophila* meiotic spindles. *Nat. Cell Biol.* 3:637–642. http://dx.doi.org/10.1038/35083025

Das, A., S.J. Shah, B. Fan, D. Paik, D.J. DiSanto, A.M. Hinman, J.M. Cesario, R.A. Battaglia, N. Demos, and K.S. McKim. 2016. Spindle assembly and chromosome segregation requires central spindle proteins in *Drosophila* oocytes. *Genetics.* 202:61–75. http://dx.doi.org/10.1534/genetics.115.181081

Davydenko, O., R.M. Schultz, and M.A. Lampson. 2013. Increased CDK1 activity determines the timing of kinetochore-microtubule attachments in meiosis I. *J. Cell Biol.* 202:221–229. http://dx.doi.org/10.1083/jcb.201303019

Deng, M., J. Gao, P. Suraneni, and R. Li. 2009. Kinetochore-independent chromosome poleward movement during anaphase of meiosis II in mouse eggs. *PLoS One.* 4:e5249. http://dx.doi.org/10.1371/journal.pone.0005249

Dumont, J., and A. Desai. 2012. Acentrosomal spindle assembly and chromosome segregation during oocyte meiosis. *Trends Cell Biol.* 22:241–249. http://dx.doi.org/10.1016/j.tcb.2012.02.007

Dumont, J., S. Petri, F. Pellegrin, M.-E. Terret, M.T. Bohnsack, P. Rassinier, V. Georget, P. Kalab, O.J. Gruss, and M.-H. Verlhac. 2007. A centriole- and RanGTP-independent spindle assembly pathway in meiosis I of vertebrate oocytes. *J. Cell Biol.* 176:295–305. http://dx.doi.org/10.1083/jcb.200605199

Dumont, J., K. Oegema, and A. Desai. 2010. A kinetochore-independent mechanism drives anaphase chromosome separation during acentrosomal meiosis. *Nat. Cell Biol.* 12:894–901. http://dx.doi.org/10.1038/ncb2093

Endow, S.A., and D.J. Komma. 1997. Spindle dynamics during meiosis in *Drosophila* oocytes. *J. Cell Biol.* 137:1321–1336. http://dx.doi.org/10.1083/jcb.137.6.1321

Eyers, P.A., E. Erikson, L.G. Chen, and J.L. Maller. 2003. A novel mechanism for activation of the protein kinase Aurora A. *Curr. Biol.* 13:691–697. http://dx.doi.org/10.1016/S0960-9822(03)00166-0

Fitzharris, G. 2009. A shift from kinesin 5-dependent metaphase spindle function during preimplantation development in mouse. *Development.* 136:2111–2119. http://dx.doi.org/10.1242/dev.035089

FitzHarris, G. 2012. Anaphase B precedes anaphase A in the mouse egg. *Curr. Biol.* 22:437–444. http://dx.doi.org/10.1016/j.cub.2012.01.041

Gard, D.L. 1991. Organization, nucleation, and acetylation of microtubules in *Xenopus laevis* oocytes: A study by confocal immunofluorescence microscopy. *Dev. Biol.* 143:346–362. http://dx.doi.org/10.1016/0012-1606(91)90085-H

Głuszek, A.A., C.F. Cullen, W. Li, R.A. Battaglia, S.J. Radford, M.F. Costa, K.S. McKim, G. Goshima, and H. Ohkura. 2015. The microtubule catastrophe promoter Sentin delays stable kinetochore-microtubule attachment in oocytes. *J. Cell Biol.* 211:1113–1120. http://dx.doi.org/10.1083/jcb.201507006

Gopalakrishnan, J., Y.-C.F. Chim, A. Ha, M.L. Basiri, D.A. Lerit, N.M. Rusan, and T. Avidor-Reiss. 2012. Tubulin nucleotide status controls Sas-4-dependent pericentriolar material recruitment. *Nat. Cell Biol.* 14:865–873. http://dx.doi.org/10.1038/ncb2527

Goshima, G., M. Mayer, N. Zhang, N. Stuurman, and R.D. Vale. 2008. Augmin: A protein complex required for centrosome-independent microtubule generation within the spindle. *J. Cell Biol.* 181:421–429. http://dx.doi.org/10.1083/jcb.200711053

Gruss, O.J., R.E. Carazo-Salas, C.A. Schatz, G. Guarguaglini, J. Kast, M. Wilm, N. Le Bot, I. Vernos, E. Karsenti, and I.W. Mattaj. 2001. Ran induces spindle assembly by reversing the inhibitory effect of importin alpha on TPX2 activity. *Cell.* 104:83–93. http://dx.doi.org/10.1016/S0092-8674(01)00193-3

Gueth-Hallonet, C., C. Antony, J. Aghion, A. Santa-Maria, I. Lajoie-Mazenc, M. Wright, and B. Maro. 1993. gamma-Tubulin is present in acentriolar MTOCs during early mouse development. *J. Cell Sci.* 105:157–166.

Hassold, T., and P. Hunt. 2001. To err (meiotically) is human: The genesis of human aneuploidy. *Nat. Rev. Genet.* 2:280–291. http://dx.doi.org/10.1038/35066065

Hassold, T., H. Hall, and P. Hunt. 2007. The origin of human aneuploidy: Where we have been, where we are going. *Hum. Mol. Genet.* 16 Spec No. 2:R203–R208. http://dx.doi.org/10.1093/hmg/ddm243

Heald, R., R. Tournebize, T. Blank, R. Sandaltzopoulos, P. Becker, A. Hyman, and E. Karsenti. 1996. Self-organization of microtubules into bipolar spindles around artificial chromosomes in *Xenopus* egg extracts. *Nature.* 382:420–425. http://dx.doi.org/10.1038/382420a0

Holubcová, Z., M. Blayney, K. Elder, and M. Schuh. 2015. Human oocytes. Error-prone chromosome-mediated spindle assembly favors chromosome segregation defects in human oocytes. *Science.* 348:1143–1147. http://dx.doi.org/10.1126/science.aaa9529

Jang, J.K., T. Rahman, and K.S. McKim. 2005. The kinesinlike protein Subito contributes to central spindle assembly and organization of the meiotic spindle in *Drosophila* oocytes. *Mol. Biol. Cell.* 16:4684–4694. http://dx.doi.org/10.1091/mbc.E04-11-0964

Jang, J.K., T. Rahman, V.S. Kober, J. Cesario, and K.S. McKim. 2007. Misregulation of the kinesin-like protein Subito induces meiotic spindle formation in the absence of chromosomes and centrosomes. *Genetics.* 177:267–280. http://dx.doi.org/10.1534/genetics.107.076091

Kalab, P., R.T. Pu, and M. Dasso. 1999. The ran GTPase regulates mitotic spindle assembly. *Curr. Biol.* 9:481–484. http://dx.doi.org/10.1016/S0960-9822(99)80213-9

Kapoor, T.M., T.U. Mayer, M.L. Coughlin, and T.J. Mitchison. 2000. Probing spindle assembly mechanisms with monastrol, a small molecule inhibitor of the mitotic kinesin, Eg5. *J. Cell Biol.* 150:975–988. http://dx.doi.org/10.1083/jcb.150.5.975

Kelly, A.E., S.C. Sampath, T.A. Maniar, E.M. Woo, B.T. Chait, and H. Funabiki. 2007. Chromosomal enrichment and activation of the aurora B pathway are coupled to spatially regulate spindle assembly. *Dev. Cell.* 12:31–43. http://dx.doi.org/10.1016/j.devcel.2006.11.001

Khodjakov, A., R.W. Cole, B.R. Oakley, and C.L. Rieder. 2000. Centrosome-independent mitotic spindle formation in vertebrates. *Curr. Biol.* 10:59–67. http://dx.doi.org/10.1016/S0960-9822(99)00276-6

Kim, J., K. Ishiguro, A. Nambu, B. Akiyoshi, S. Yokobayashi, A. Kagami, T. Ishiguro, A.M. Pendas, N. Takeda, Y. Sakakibara, et al. 2015. Meikin is a conserved regulator of meiosis-I-specific kinetochore function. *Nature.* 517:466–471. http://dx.doi.org/10.1038/nature14097

Kinoshita, K., T.L. Noetzel, L. Pelletier, K. Mechtler, D.N. Drechsel, A. Schwager, M. Lee, J.W. Raff, and A.A. Hyman. 2005. Aurora A phosphorylation of TACC3/maskin is required for centrosome-dependent microtubule assembly in mitosis. *J. Cell Biol.* 170:1047–1055. http://dx.doi.org/10.1083/jcb.200503023

Kirkham, M., T. Müller-Reichert, K. Oegema, S. Grill, and A.A. Hyman. 2003. SAS-4 is a *C. elegans* centriolar protein that controls centrosome size. *Cell.* 112:575–587. http://dx.doi.org/10.1016/S0092-8674(03)00117-X

Kirschner, M., and T. Mitchison. 1986. Beyond self-assembly: From microtubules to morphogenesis. *Cell.* 45:329–342. http://dx.doi.org/10.1016/0092-8674(86)90318-1

Kitajima, T.S., M. Ohsugi, and J. Ellenberg. 2011. Complete kinetochore tracking reveals error-prone homologous chromosome biorientation in mammalian oocytes. *Cell.* 146:568–581. http://dx.doi.org/10.1016/j.cell.2011.07.031

Kolano, A., S. Brunet, A.D. Silk, D.W. Cleveland, and M.-H. Verlhac. 2012. Error-prone mammalian female meiosis from silencing the spindle assembly checkpoint without normal interkinetochore tension. *Proc. Natl. Acad. Sci. USA.* 109:E1858–E1867. http://dx.doi.org/10.1073/pnas.1204686109

Kwon, M., S.A. Godinho, N.S. Chandhok, N.J. Ganem, A. Azioune, M. Thery, and D. Pellman. 2008. Mechanisms to suppress multipolar divisions in cancer cells with extra centrosomes. *Genes Dev.* 22:2189–2203. http://dx.doi.org/10.1101/gad.1700908

Lane, S.I.R., Y. Yun, and K.T. Jones. 2012. Timing of anaphase-promoting complex activation in mouse oocytes is predicted by microtubule-kinetochore attachment but not by bivalent alignment or tension. *Development.* 139:1947–1955. http://dx.doi.org/10.1242/dev.077040

Lawo, S., M. Bashkurov, M. Mullin, M.G. Ferreria, R. Kittler, B. Habermann, A. Tagliaferro, I. Poser, J.R.A. Hutchins, B. Hegemann, et al. 2009. HAUS, the 8-subunit human Augmin complex, regulates centrosome and spindle integrity. *Curr. Biol.* 19:816–826. http://dx.doi.org/10.1016/j.cub.2009.04.033

Lénárt, P., C.P. Bacher, N. Daigle, A.R. Hand, R. Eils, M. Terasaki, and J. Ellenberg. 2005. A contractile nuclear actin network drives chromosome congression in oocytes. *Nature.* 436:812–818. http://dx.doi.org/10.1038/nature03810

Lister, L.M., A. Kouznetsova, L.A. Hyslop, D. Kalleas, S.L. Pace, J.C. Barel, A. Nathan, V. Floros, C. Adelfalk, Y. Watanabe, et al. 2010. Age-related meiotic segregation errors in mammalian oocytes are preceded by depletion of cohesin and Sgo2. *Curr. Biol.* 20:1511–1521. http://dx.doi.org/10.1016/j.cub.2010.08.023

Łuksza, M., I. Queguigner, M.-H. Verlhac, and S. Brunet. 2013. Rebuilding MTOCs upon centriole loss during mouse oogenesis. *Dev. Biol.* 382:48–56. http://dx.doi.org/10.1016/j.ydbio.2013.07.029

Mailhes, J.B., C. Mastromatteo, and J.W. Fuseler. 2004. Transient exposure to the Eg5 kinesin inhibitor monastrol leads to syntelic orientation of chromosomes and aneuploidy in mouse oocytes. *Mutat. Res.* 559:153–167. http://dx.doi.org/10.1016/j.mrgentox.2004.01.001

Manandhar, G., P. Sutovsky, H.C. Joshi, T. Stearns, and G. Schatten. 1998. Centrosome reduction during mouse spermiogenesis. *Dev. Biol.* 203:424–434. http://dx.doi.org/10.1006/dbio.1998.8947

Manandhar, G., H. Schatten, and P. Sutovsky. 2005. Centrosome reduction during gametogenesis and its significance. *Biol. Reprod.* 72:2–13. http://dx.doi.org/10.1095/biolreprod.104.031245

Matthews, L.R., P. Carter, D. Thierry-Mieg, and K. Kemphues. 1998. ZYG-9, a *Caenorhabditis elegans* protein required for microtubule organization and function, is a component of meiotic and mitotic spindle poles. *J. Cell Biol.* 141:1159–1168. http://dx.doi.org/10.1083/jcb.141.5.1159

Matthies, H.J., H.B. McDonald, L.S. Goldstein, and W.E. Theurkauf. 1996. Anastral meiotic spindle morphogenesis: Role of the non-claret disjunctional kinesin-like protein. *J. Cell Biol.* 134:455–464. http://dx.doi.org/10.1083/jcb.134.2.455

Mazumdar, M., and T. Misteli. 2005. Chromokinesins: Multitalented players in mitosis. *Trends Cell Biol.* 15:349–355. http://dx.doi.org/10.1016/j.tcb.2005.05.006

Merdes, A., K. Ramyar, J.D. Vechio, and D.W. Cleveland. 1996. A complex of NuMA and cytoplasmic dynein is essential for mitotic spindle assembly. *Cell.* 87:447–458. http://dx.doi.org/10.1016/S0092-8674(00)81365-3

Meunier, S., and I. Vernos. 2016. Acentrosomal microtubule assembly in mitosis: the where, when, and how. *Trends Cell Biol.* 26:80–87. http://dx.doi.org/10.1016/j.tcb.2015.09.001

Nachury, M.V., T.J. Maresca, W.C. Salmon, C.M. Waterman-Storer, R. Heald, and K. Weis. 2001. Importin beta is a mitotic target of the small GTPase Ran in spindle assembly. *Cell.* 104:95–106. http://dx.doi.org/10.1016/S0092-8674(01)00194-5

Nagaoka, S.I., T.J. Hassold, and P.A. Hunt. 2012. Human aneuploidy: Mechanisms and new insights into an age-old problem. *Nat. Rev. Genet.* 13:493–504. http://dx.doi.org/10.1038/nrg3245

Oegema, K., A. Desai, S. Rybina, M. Kirkham, and A.A. Hyman. 2001. Functional analysis of kinetochore assembly in *Caenorhabditis elegans*. *J. Cell Biol.* 153:1209–1226. http://dx.doi.org/10.1083/jcb.153.6.1209

Petry, S., C. Pugieux, F.J. Nédélec, and R.D. Vale. 2011. Augmin promotes meiotic spindle formation and bipolarity in *Xenopus* egg extracts. *Proc. Natl. Acad. Sci. USA.* 108:14473–14478. http://dx.doi.org/10.1073/pnas.1110412108

Pimenta-Marques, A., I. Bento, C.A. Lopes, P. Duarte, S.C. Jana, and M. Bettencourt-Dias. 2016. A mechanism for the elimination of the female gamete centrosome in *Drosophila melanogaster*. *Science.* 353:aaf4866. http://dx.doi.org/10.1126/science.aaf4866

Radford, S.J., J.K. Jang, and K.S. McKim. 2012. The chromosomal passenger complex is required for meiotic acentrosomal spindle assembly and chromosome biorientation. *Genetics.* 192:417–429. http://dx.doi.org/10.1534/genetics.112.143495

Sampath, S.C., R. Ohi, O. Leismann, A. Salic, A. Pozniakovski, and H. Funabiki. 2004. The chromosomal passenger complex is required for chromatin-induced microtubule stabilization and spindle assembly. *Cell.* 118:187–202. http://dx.doi.org/10.1016/j.cell.2004.06.026

Sánchez-Huertas, C., and J. Lüders. 2015. The augmin connection in the geometry of microtubule networks. *Curr. Biol.* 25:R294–R299. http://dx.doi.org/10.1016/j.cub.2015.02.006

Schuh, M., and J. Ellenberg. 2007. Self-organization of MTOCs replaces centrosome function during acentrosomal spindle assembly in live mouse oocytes. *Cell.* 130:484–498. http://dx.doi.org/10.1016/j.cell.2007.06.025

Sköld, H.N., D.J. Komma, and S.A. Endow. 2005. Assembly pathway of the anastral *Drosophila* oocyte meiosis I spindle. *J. Cell Sci.* 118:1745–1755. http://dx.doi.org/10.1242/jcs.02304

Srayko, M., E.T. O'toole, A.A. Hyman, and T. Müller-Reichert. 2006. Katanin disrupts the microtubule lattice and increases polymer number in *C. elegans* meiosis. *Curr. Biol.* 16:1944–1949. http://dx.doi.org/10.1016/j.cub.2006.08.029

Still, I.H., P. Vince, and J.K. Cowell. 1999. The third member of the transforming acidic coiled coil-containing gene family, TACC3, maps in 4p16, close to translocation breakpoints in multiple myeloma, and is upregulated in various cancer cell lines. *Genomics.* 58:165–170. http://dx.doi.org/10.1006/geno.1999.5829

Sumiyoshi, E., Y. Fukata, S. Namai, and A. Sugimoto. 2015. *Caenorhabditis elegans* Aurora A kinase is required for the formation of spindle microtubules in female meiosis. *Mol. Biol. Cell.* 26:4187–4196. http://dx.doi.org/10.1091/mbc.E15-05-0258

Szollosi, D., P. Calarco, and R.P. Donahue. 1972. Absence of centrioles in the first and second meiotic spindles of mouse oocytes. *J. Cell Sci.* 11:521–541.

Tanenbaum, M.E., and R.H. Medema. 2010. Mechanisms of centrosome separation and bipolar spindle assembly. *Dev. Cell.* 19:797–806. http://dx.doi.org/10.1016/j.devcel.2010.11.011

Toso, A., J.R. Winter, A.J. Garrod, A.C. Amaro, P. Meraldi, and A.D. McAinsh. 2009. Kinetochore-generated pushing forces separate centrosomes during bipolar spindle assembly. *J. Cell Biol.* 184:365–372. http://dx.doi.org/10.1083/jcb.200809055

Tournier, F., E. Karsenti, and M. Bornens. 1989. Parthenogenesis in *Xenopus* eggs injected with centrosomes from synchronized human lymphoid cells. *Dev. Biol.* 136:321–329. http://dx.doi.org/10.1016/0012-1606(89)90259-5

Tsai, M.-Y., C. Wiese, K. Cao, O. Martin, P. Donovan, J. Ruderman, C. Prigent, and Y. Zheng. 2003. A Ran signalling pathway mediated by the mitotic kinase Aurora A in spindle assembly. *Nat. Cell Biol.* 5:242–248. http://dx.doi.org/10.1038/ncb936

Tseng, B.S., L. Tan, T.M. Kapoor, and H. Funabiki. 2010. Dual detection of chromosomes and microtubules by the chromosomal passenger complex drives spindle assembly. *Dev. Cell.* 18:903–912. http://dx.doi.org/10.1016/j.devcel.2010.05.018

Tsou, A.-P., C.-W. Yang, C.-Y.F. Huang, R.C.-T. Yu, Y.-C.G. Lee, C.-W. Chang, B.-R. Chen, Y.-F. Chung, M.-J. Fann, C.-W. Chi, et al. 2003. Identification of a novel cell cycle regulated gene, HURP, overexpressed in human hepatocellular carcinoma. *Oncogene.* 22:298–307. http://dx.doi.org/10.1038/sj.onc.1206129

Uehara, R., R.S. Nozawa, A. Tomioka, S. Petry, R.D. Vale, C. Obuse, and G. Goshima. 2009. The augmin complex plays a critical role in spindle microtubule generation for mitotic progression and cytokinesis in human cells. *Proc. Natl. Acad. Sci. USA.* 106:6998–7003. http://dx.doi.org/10.1073/pnas.0901587106

Walczak, C.E., I. Vernos, T.J. Mitchison, E. Karsenti, and R. Heald. 1998. A model for the proposed roles of different microtubule-based motor proteins in establishing spindle bipolarity. *Curr. Biol.* 8:903–913. http://dx.doi.org/10.1016/S0960-9822(07)00370-3

Wandke, C., M. Barisic, R. Sigl, V. Rauch, F. Wolf, A.C. Amaro, C.H. Tan, A.J. Pereira, U. Kutay, H. Maiato, et al. 2012. Human chromokinesins promote chromosome congression and spindle microtubule dynamics during mitosis. *J. Cell Biol.* 198:847–863. http://dx.doi.org/10.1083/jcb.201110060

Watanabe, Y. 2012. Geometry and force behind kinetochore orientation: Lessons from meiosis. *Nat. Rev. Mol. Cell Biol.* 13:370–382. http://dx.doi.org/10.1038/nrm3349

Wignall, S.M., and A.M. Villeneuve. 2009. Lateral microtubule bundles promote chromosome alignment during acentrosomal oocyte meiosis. *Nat. Cell Biol.* 11:839–844. http://dx.doi.org/10.1038/ncb1891

Wittmann, T., M. Wilm, E. Karsenti, and I. Vernos. 2000. TPX2, A novel *Xenopus* MAP involved in spindle pole organization. *J. Cell Biol.* 149:1405–1418. http://dx.doi.org/10.1083/jcb.149.7.1405

Wollman, R., E.N. Cytrynbaum, J.T. Jones, T. Meyer, J.M. Scholey, and A. Mogilner. 2005. Efficient chromosome capture requires a bias in the 'search-and-capture' process during mitotic-spindle assembly. *Curr. Biol.* 15:828–832. http://dx.doi.org/10.1016/j.cub.2005.03.019

Woodruff, J.B., O. Wueseke, V. Viscardi, J. Mahamid, S.D. Ochoa, J. Bunkenborg, P.O. Widlund, A. Pozniakovsky, E. Zanin, S. Bahmanyar, et al. 2015. Centrosomes. Regulated assembly of a supramolecular centrosome scaffold in vitro. *Science.* 348:808–812. http://dx.doi.org/10.1126/science.aaa3923

Woolley, D.M., and D.W. Fawcett. 1973. The degeneration and disappearance of the centrioles during the development of the rat spermatozoon. *Anat. Rec.* 177:289–301. http://dx.doi.org/10.1002/ar.1091770209

Yan, L.-Y., J.-C. Huang, Z.-Y. Zhu, Z.-L. Lei, L.-H. Shi, C.-L. Nan, Z.-J. Zhao, Y.-C. Ouyang, X.-F. Song, Q.-Y. Sun, and D.-Y. Chen. 2006. NuMA distribution and microtubule configuration in rabbit oocytes and cloned embryos. *Reproduction.* 132:869–876. http://dx.doi.org/10.1530/rep.1.01224

Yoshida, S., M. Kaido, and T.S. Kitajima. 2015. Inherent instability of correct kinetochore-microtubule attachments during meiosis I in oocytes. *Dev. Cell.* 33:589–602. http://dx.doi.org/10.1016/j.devcel.2015.04.020

Chapter 16

Laser Ablation of Microtubule–Chromosome Attachment in Mouse Oocytes

Isma Bennabi and Marion Manil-Ségalen

Abstract

Laser ablation is a powerful tool to study forces within biological systems. This technique has been extensively used to study mitotic spindle formation and chromosome segregation. This chapter describes laser ablation of microtubule–chromosome attachments coupled to fluorescence live microscopy and quantitative analysis of individual chromosome movement after microtubule severing. This method allows to gain insight into the organization and dynamics of the meiotic spindle and chromosomes in metaphase I mouse oocytes.

Key words Laser ablation, Mouse oocyte, Microtubules, Chromosomes, Meiotic spindle

1 Introduction

Meiotic divisions consist of two successive divisions, without DNA replication, which reduce the genetic content by half. These highly asymmetric divisions give rise to a huge haploid cell: the oocyte. During eukaryotic cell division, the spindle organizes chromosome alignment and segregation. The spindle is a complex structure composed of microtubules and associated proteins. Many studies have shed light on the mechanisms of spindle assembly and chromosome segregation in mouse oocytes (for review *see* [1, 2]). The spindle is a highly organized, dense and dynamic microtubule structure, and thus there is a limit into how much of these properties can be resolved by fluorescence microscopy. To get more insight into the organization and dynamics of the cytoskeleton during meiotic divisions, our lab has recently optimized laser ablation in mouse oocytes. Laser ablation techniques consist of using a high intensity laser pulse to severe a selected structure. The system's response to precise

Marie-Hélène Verlhac and Marie-Emilie Terret (eds.), *Mouse Oocyte Development: Methods and Protocols*, Methods in Molecular Biology, vol. 1818, https://doi.org/10.1007/978-1-4939-8603-3_16,
© Springer Science+Business Media, LLC, part of Springer Nature 2018

perturbations reflects the forces at play. Laser ablation has been used in other model systems to study spindle positioning [3–6], spindle assembly and chromosome segregation [7–13].

In this chapter, we describe how we adapted this technique for use in mouse oocytes. In particular, we highlight challenges specific to this model system, which are mostly imposed by the huge cell size (80 μm diameter). We provide a detailed protocol for laser ablation of spindle microtubules coupled to fluorescence live microscopy and quantitative analysis of individual chromosome movement after severing of microtubule–chromosome attachment.

2 Materials

2.1 Oocytes Preparation and Manipulation

1. M2-BSA medium.
2. M2-BSA medium, supplemented with 1 μM Milrinone (Sigma-Aldrich—M4659-10MG).
3. Mineral Oil (Sigma—M8410-1L).
4. Stretched Pasteur glass pipettes.
5. 1 mL syringe + needle.
6. Razor blade.
7. Dissection microscope.
8. Mouth controlled aspiration tube.
9. Coated petri dishes.
10. Cell culture incubator at 37 °C.

2.2 Microinjection

The following cRNA are injected in mouse oocytes as in [14]:

1. cRNA encoding H2B-GFP (*see* **Note 1**) [15].
2. cRNA encoding EB3-GFP [16].

2.3 Oocyte Imaging and Laser Ablation

1. Glass-bottom petri dishes.
2. Pasteur glass pipette.
3. Mineral oil.
4. Immersion oil.
5. Spinning-disc microscope: Leica DMI6000B microscope enclosed in a thermostatic chamber (Life Imaging Service) equipped with a Retiga 3 CCD camera (QImaging) coupled to a Sutter filter wheel (Roper Scientific) and a Yokogawa CSU-X1-M1 spinning disc using a Plan-APO ×40/1.25 NA objective.
6. Laser ablation setup: 355 laser and i-LAS [2] module (Roper Scientific).
7. Metamorph (Molecular Devices).

3 Methods

Keep oocytes at 37 °C during all steps of collection, preparation, and imaging.

3.1 Oocytes Collection and Preparation

1. Collect prophase I-arrested fully grown oocytes from 8- to 12-week-old mice in M2-BSA medium supplemented with 1 μM of milrinone as described previously [17] (*see* **Note 2**).
2. Microinject H2B-GFP (100 ng/μL) and EB3-GFP (100 ng/μL) cRNAs in order to visualize both chromosomes and microtubules in the same channel.
3. Keep microinjected oocytes in M2-BSA medium supplemented with milrinone for 30–60 min to allow cRNA expression (*see* **Note 3**).
4. Wash oocytes by transferring them through five drops of milrinone free M2 medium to allow meiosis resumption.

3.2 Oocytes Preparation for Imaging

To analyze the forces exerted by the microtubules on the chromosomes in the meiotic spindle, laser ablations must be performed when the spindle is fully formed and bipolar with chromosomes attached by kinetochore fibers. This process lasts several hours in mouse oocyte [18–20], and we thus performed the following experiment 6 h after nuclear envelope breakdown (approx. 7.5 h after milrinone washout).

1. Transfer oocytes in a small drop of M2 medium (approx. 5 μL) under oil, in a glass-bottom dish.
2. Several oocytes can be placed in the same drop, but to avoid photodamage and photobleaching, they must be separated by at least 200 μm (*see* **Note 4**).
3. Remove the excess of medium in order to have an almost flat drop. It prevents oocytes from moving under the microscope.

3.3 System Calibration

We recommend calibrating the system before each use to achieve maximum precision.

1. Draw a marker line on the inner bottom of a glass petri dish.
2. Place it under the microscope.
3. Make the focus on the edge of the line.
4. Move to a clean region of the petri dish (no marker, no dust).
5. In the i-LAS [2] module calibration tab set the 355 nm laser to 100%.
6. Using the Metamorph Multidimensional acquisition (MDA) live module (in our case positioned on the excitation laser 491 nm, laser power 0%, Binning 2 (*see* **Note 5**)), determine the top left and the bottom right corners of the field.

7. Launch calibration.
8. Save calibration.
9. To check the calibration, select the On Fly tab in the i-LAS [2] module, set 355 nm laser power to 100%. Select "Point" mode. Open the live acquisition window. Position the red circle somewhere in the imaging field. Click on the image. The laser should appear inside the circle. If not redo calibration (*see* **Note 6**).

3.4 Laser Ablation and Imaging

Before starting the ablation we recommend adjusting the laser 355 nm power so that it is set to the minimal power and number of repetitions to efficiently severe microtubules.

1. Turn on the temperature controller at least 30 min before imaging so that all components adjust to 37 °C.
2. Choose MDA settings before acquisitions (saving file, wavelengths, time interval, z stacks) (*see* **Note 7**). At this stage, chromosomes are very dynamic and oscillate around the metaphase plate at an average speed of 0.5 μm/min [21]. Once the oocyte is correctly positioned, and the ablation zone determined, the ablation has to occur very rapidly. Settings depend on the experiment planed (Table 1).
3. Place the petri dish containing oocytes under the microscope (40× objective in this example (*see* **Note 8**)).
4. Center and make the focus on one oocyte in bright field to avoid photobleaching and photodamage.

Table 1
Laser ablation and Imaging settings used

Laser ablation parameters						Imaging parameters			
355 nm laser power	Ablation shape	ROI thickness	Number of repetions	*Z* thickness	d*Z*	TRANS	491 nm laser power and exposure time	z stacks	d*t*
100%	Line	1	30	10 μm	1 μm	500 ms Only the first time point	30% 500 ms	2 μm × 3	5 s

Summary of the parameters used in the experiment presented in this chapter. Laser 491 nm power and exposure time are adjusted to obtain optimal signal-to-noise ratio. In this experiment, the ablation ROI is a maximum 5 μm length line, cutting a small part of the spindle. We recommend cutting an external part of the spindle. We tried several repetition numbers. Thirty repetitions are ideal to cut the spindle without creating too much photobleaching. We cut on 10 μm thickness to completely detach the chromosome from the microtubules. For the imaging, we decided to do only three z stacks to perform fast acquisitions and allow a 5 s d*t*

5. Observe the spindle and chromosomes with the MDA live module (excitation laser 491 nm, laser power 30%, to observe the GFP signal with an exposure time of 500 ms).
6. To perform the ablation, the spindle must be oriented with its long axis parallel to the observation plane (Fig. 1) (*see* **Note 9**). If not, roll the oocyte by using a closed stretched Pasteur pipette (*see* **Note 10**). Repeat **steps 5** and **6** until the spindle is correctly oriented.
7. Draw the region of interest (ROI; here a line) on a snap image of your oocyte showing microtubules and chromosomes. Two rules must be respected to draw the ROI. The region of ablation (a) must not be too close to the chromosome to avoid photobleaching and (b) must not measure more than one-third of the spindle in width in order to observe concomitantly the behavior of two types of chromosomes (detached or not) within the same spindle. *See* Fig. 2.
8. Upload the ROI on the i-LAS [2] module "targeted laser" tab and set up conditions (*see* Table 1).
9. Fill the z targeted Laser window: *Z* top and bottom, d*Z* and time point of ablation (*see* **Note 11**). Click on the "Setup MDA" button.

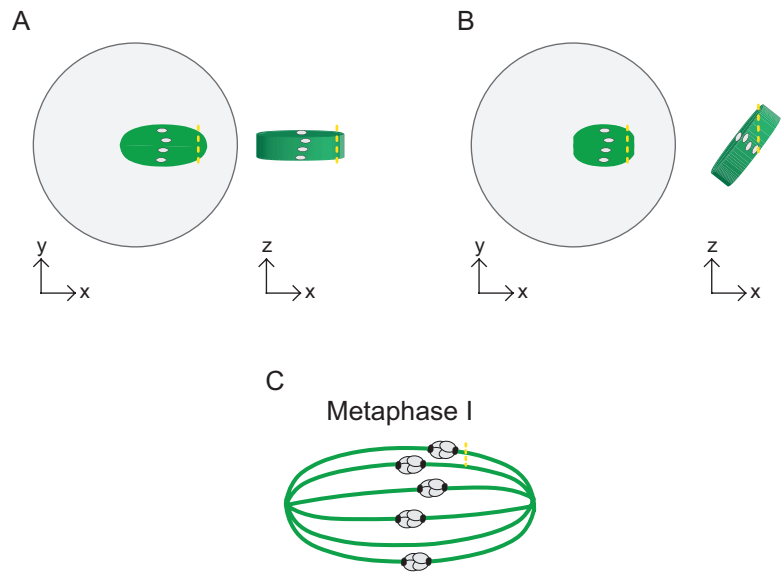

Fig. 1 Laser ablation of spindle microtubules in metaphase I mouse oocytes. (**a**) Laser ablation on a spindle oriented parallel to the observation plane. (**b**) Laser ablation on a spindle tilted relative to the observation plane. In that case laser ablation in depth cannot be precisely directed. (**c**) Laser ablation of microtubule bundles attached to a chromosome. The spindle and microtubules are in green, chromosomes are in grey, kinetochores are in black and the position of the cut is represented by a yellow dotted line

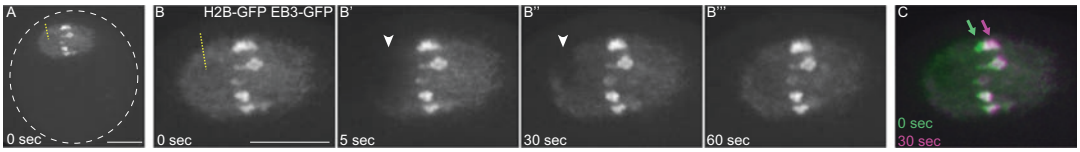

Fig. 2 Example of microtubules laser ablation. Illustrative example of laser ablation of the microtubules connected to one chromosome. (**a**) Image of the entire oocyte before ablation. The contour of the oocyte is highlighted by a dotted white line. The yellow dotted line represents the ablation ROI (**a**, **b**). (**b**–**b**)′″ Higher magnification of the spindle before ablation (**b**), 5 s (**b′**), 30 s (**b″**) and 60 s (**b′″**) after laser ablation. Arrowheads in **b′** and **b″** indicate the photobleached zone close to the laser ablation site. The spindle is fully rebuilt 1 min after ablation (**b′″**). (**c**) Time projection of the spindle. The image taken before ablation is in green and the one taken 30 s after ablation is in magenta. The arrows are showing the position of the chromosome the closest from ablation site before and after ablation. H2B-GFP and EB3-GFP are in grey. Scale bars are 10 μm

10. If everything has been correctly filled in the MDA module, press "Acquire" to start the experiment (live imaging + laser ablation) (Fig. 2).

3.5 Individual Chromosome Movement Analysis

We then analyzed the behavior of chromosomes after laser ablation, which reflects the forces applied on the chromosomes.

Analyses presented here are made using FIJI (LOCI) software, but Active Contour plugin from ICY [22] can also be used.

1. To analyze individual chromosome movements within the spindle, it is important to run the "Correct 3D drift" plugin on the time lapse movies prior any analysis (*see* **Note 12**). To go faster, the plugin can be run on an image sequence cropped around the spindle.
2. Track the chromosome close to the ablation site and 3–5 other chromosomes using the "Manual tracking" plugin. First, enter the properties of your images then track the chromosomes by simply clicking on them. The plugin gives the coordinates of each point, the velocity and the distance between each points and the pixel value (*see* **Note 13**).
3. Calculate "distance to origin" of each point.

   Figure 3 shows the chromosome distance to origin for chromosomes close to the ablated microtubules (Fig. 3, red curve) and for the other chromosomes far from the ablation site (Fig. 3, grey curve). The highest slope difference is during the first 30 s. Movies do not have to last long to be informative. The slope of the curve for the chromosomes close to the ablation site reflects the forces exerted by the microtubules on the chromosomes [9]. The timing of chromosome recapture (Fig. 3) reflects microtubules dynamics.

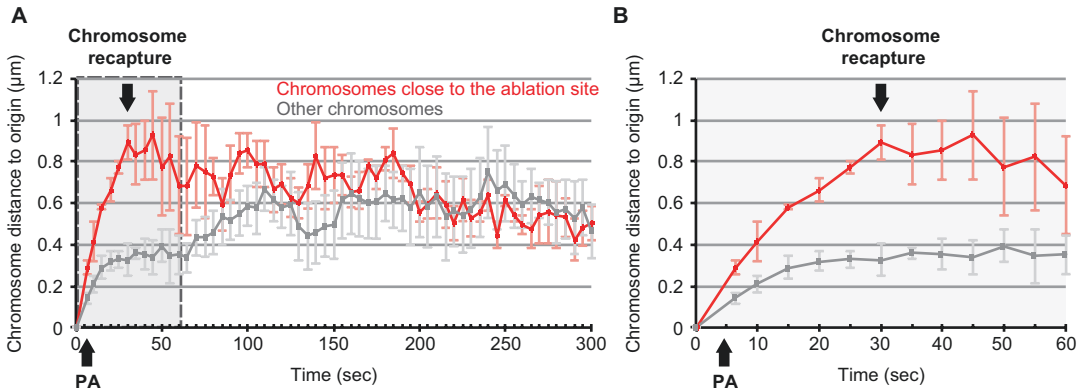

Fig. 3 Analysis of single chromosomes movements after laser ablation. (**a**) Distance of the chromosomes to the position they occupied at $t = 0$. Distances are in µm and time in second. Chromosomes close to the ablation site are represented by the red curve ($n = 3$) and chromosomes located on the opposite side of the metaphase plate by the grey one ($n = 5$). The PA arrow indicates the laser ablation time. The second arrow shows the time at which chromosomes are not moving away from the ablation site anymore indicating that they have been recaptured by microtubules. Error bars are SEM. (**b**) Zoom on the first minute of the experiments

3.6 Conclusion

This chapter presents a method for laser ablation of microtubule–chromosome attachment within metaphase I spindles in mouse oocytes. Because oocytes are extremely big cells (80 µm diameter), we recommend using a system that allows laser ablation in several z stacks. Depending on the system used (laser ablation setup and imaging setup), the cut can be as precise as a single microtubule bundle. In the case of our microtubule–chromosome attachment laser ablation experiments, oocytes divided normally after ablation. Although this method is noninvasive, we recommend monitoring oocytes survival depending on the structure ablated and the size of ablation. Whereas we are presenting only one detailed example, this method can be applied to other cytoskeleton structures in mouse oocytes.

4 Notes

1. We use the Ambion mMessage Machine T3 kit (Invitrogen—AM1348) for in vitro transcription of cRNAs from pRN3 plasmids. cRNAs are purified using Quiagen RNAeasy kit (Quiagen—74104) and then stored at −20 °C.
2. C57BL/6 mouse strain.
3. The expression time should not exceed 2 h in order to prevent microtubules overstabilization and changes in chromosomes structure.
4. Damage can come from the 488 nm laser used during the imaging phase but not from the 355 nm one. Indeed, the 355 nm laser is really focused and does not cause any damage to surrounding oocytes.

5. Calibration is noise-sensitive. Performing it at binning 2 allows an excellent calibration of the system freed from any detection artifact.
6. Before doing laser ablation on biological samples you can test the setup on yellow marker. Using a yellow marker, draw a thick line on the inner bottom of a glass petri dish. Under the microscope, make the focus on the edge of the line. The yellow marker can be observed using the excitation laser 491 nm at 50% laser power with an exposure time of 500 ms. Draw a ROI on the yellow marker. Start ablation. After ablation, the ROI should appear dark.
7. All settings can be adjusted according to experiments. *See* Table 1.
8. In this example, 40× magnification is precise enough to perform ablation of a part of the meiotic spindle. To perform ablation of a smaller structure, higher magnification might be necessary. In this case the laser power should be adjusted.
9. The barrel shape of the spindle must be observed (length aprox. 30 μm), with the two poles at the same focus. If the spindle seems round, it is probably vertically oriented and the oocyte has to be rolled.
10. Although it is quite tricky, this step is crucial. The ablation cannot be precisely directed on a misoriented spindle otherwise its efficiency would be compromised (*see* Fig. 1).
11. The Z targeted journal has been written by Roper in order to perform laser ablations on z stacks.
12. When photobleaching is too extended (e.g., photobleaching of an entire spindle pole), such plugin cannot be used.
13. A correction might be needed because of the imprecision of the imaging system. (The ablation time is not taken into account when the d*t* values are calculated.) Precise image acquisition timing is available in the image information.

References

1. Bennabi I, Terret M-E, Verlhac M-H (2016) Meiotic spindle assembly and chromosome segregation in oocytes. J Cell Biol 215:611–619
2. Dumont J, Desai A (2012) Acentrosomal spindle assembly and chromosome segregation during oocyte meiosis. Trends Cell Biol 22:241–249
3. Bringmann H, Hyman AA (2005) A cytokinesis furrow is positioned by two consecutive signals. Nature 436:731–734
4. Grill SW, Gönczy P, Stelzer EH et al (2001) Polarity controls forces governing asymmetric spindle positioning in the Caenorhabditis elegans embryo. Nature 409:630–633
5. Riche S, Zouak M, Argoul F et al (2013) Evolutionary comparisons reveal a positional switch for spindle pole oscillations in Caenorhabditis embryos. J Cell Biol 201:653–662
6. Tolić-Nørrelykke IM, Sacconi L, Thon G et al (2004) Positioning and elongation of the fission

yeast spindle by microtubule-based pushing. Curr Biol 14:1181–1186
7. Brugués J, Nuzzo V, Mazur E et al (2012) Nucleation and transport organize microtubules in metaphase spindles. Cell 149:554–564
8. Cojoc G, Roscioli E, Zhang L et al (2016) Laser microsurgery reveals conserved viscoelastic behavior of the kinetochore. J Cell Biol 212:767–776
9. Elting MW, Hueschen CL, Udy DB et al (2014) Force on spindle microtubule minus ends moves chromosomes. J Cell Biol 206:245–256
10. Kajtez J, Solomatina A, Novak M et al (2016) Overlap microtubules link sister k-fibres and balance the forces on bi-oriented kinetochores. Nat Commun 7:10298
11. Khodjakov A, La Terra S, Chang F (2004) Laser microsurgery in fission yeast; role of the mitotic spindle midzone in anaphase B. Curr Biol 14:1330–1340
12. Maiato H, Rieder CL, Khodjakov A (2004) Kinetochore-driven formation of kinetochore fibers contributes to spindle assembly during animal mitosis. J Cell Biol 167:831–840
13. Sikirzhytski V, Magidson V, Steinman JB et al (2014) Direct kinetochore-spindle pole connections are not required for chromosome segregation. J Cell Biol 206:231–243
14. Nakagawa S, FitzHarris G (2016) Quantitative microinjection of Morpholino antisense oligonucleotides into mouse oocytes to examine gene function in meiosis-I. Methods Mol Biol Clifton NJ 1457:217–230
15. Chaigne A, Campillo C, Gov NS et al (2015) A narrow window of cortical tension guides asymmetric spindle positioning in the mouse oocyte. Nat Commun 6:6027
16. Breuer M, Kolano A, Kwon M et al (2010) HURP permits MTOC sorting for robust meiotic spindle bipolarity, similar to extra centrosome clustering in cancer cells. J Cell Biol 191:1251–1260
17. Reis A, Chang H-Y, Levasseur M et al (2006) APCcdh1 activity in mouse oocytes prevents entry into the first meiotic division. Nat Cell Biol 8:539–540
18. Dumont J, Petri S, Pellegrin F et al (2007) A centriole- and RanGTP-independent spindle assembly pathway in meiosis I of vertebrate oocytes. J Cell Biol 176:295–305
19. Hached K, Xie SZ, Buffin E et al (2011) Mps1 at kinetochores is essential for female mouse meiosis I. Development 138:2261–2271
20. Schuh M, Ellenberg J (2007) Self-organization of MTOCs replaces centrosome function during acentrosomal spindle assembly in live mouse oocytes. Cell 130:484–498
21. Kitajima TS, Ohsugi M, Ellenberg J (2011) Complete kinetochore tracking reveals error-prone homologous chromosome biorientation in mammalian oocytes. Cell 146:568–581
22. de CF, Dallongeville S, Chenouard N et al (2012) Icy: an open bioimage informatics platform for extended reproducible research. Nat Methods 9:690–696

Résumé

La méiose produit les gamètes haploïdes mâles et femelles. Chez la femme, la méiose est fortement sujette aux erreurs de ségrégation des chromosomes. En effet, au moins 10% des grossesses humaines produisent des embryons aneuploïdes suite à des défauts de séparation des chromosomes qui ont presque toujours lieu dans l'ovocyte. Comprendre l'origine de ces défauts est donc un enjeu sociétal majeur. Durant ma thèse, j'ai étudié l'alignement et la ségrégation des chromosomes dans l'ovocyte de souris sous deux angles différents :

1) Chez les eucaryotes, le fuseau de microtubules est la structure qui gouverne l'alignement puis la séparation des chromosomes. En mitose, le fuseau est assemblé par deux centrosomes contenant des centrioles, constituant les centres organisateurs de microtubules majeurs (MTOCs). Au contraire, les ovocytes sont dépourvus de centrioles, imposant un mode de formation et de positionnement du fuseau méiotique atypique. J'ai utilisé la kinesin-14 HSET comme un outil pour faire passer l'organisation du fuseau ovocytaire d'un mode méiotique à un mode mitotique, ce qui induit des défauts d'alignement des chromosomes. Le mécanisme unique d'assemblage du fuseau méiotique est donc essentiel pour empêcher les défauts d'alignement des chromosomes et la production de gamètes aneuploïdes.

2) En mitose, les centrosomes nucléent aussi les microtubules astraux qui permettent de positionner le fuseau dans la cellule. Les ovocytes étant dépourvus de microtubules astraux, le positionnement de leur fuseau dépend uniquement de l'actine. En particulier, cela repose sur un épaississement cortical d'actine qui ramollit le cortex en diminuant la tension corticale. Nous avons utilisé deux outils différents qui diminuent artificiellement la tension corticale dans les ovocytes de souris. L'alignement des chromosomes est sévèrement altéré dans ces ovocytes extra-mous du fait de dérégulations de la myosine II. En effet, une diminution de l'activité de la myosine II dans les ovocytes extra-mous restore l'alignement des chromosomes. Des dérégulations de la tension corticale pourraient ainsi générer de l'aneuploïdie, contribuant au taux élevé d'aneuploïdie déjà observé dans les gamètes femelles.

Mots Clés

Ovocyte, méiose I, microtubule, assemblage du fuseau de division, alignement et ségrégation des chromosomes, positionnement du fuseau, actine, tension corticale.

Abstract

Meiosis produces male and female haploid gametes. Female meiosis is highly prone to chromosome segregation errors. Indeed, at least 10 % of human pregnancies produce aneuploid embryos, the errors leading to aneuploidy almost always occurring in the oocyte. Understanding the origin of these errors is therefore a major issue. During my PhD, I studied chromosome alignment and segregation in mouse oocytes from two different angles:

1) In eukaryotes, the structure orchestrating chromosome alignment and segregation is the microtubule spindle. Whereas mitotic spindles assemble from two centrosomes that are major microtubule organizing centers (MTOCs) containing centrioles, meiotic spindles in oocytes lack centrioles. Thus, oocytes use alternative ways to assemble and position their spindle. In mouse oocytes, the spindle is not assembled by centrosomes but spindle microtubules are nucleated from multiple acentriolar MTOCs. I used the kinesin-14 HSET as a tool to shift meiotic spindle assembly towards a mitotic mode. This induces severe chromosome misalignment. Thus, the unique mechanism of meiotic spindle assembly is essential to prevent chromosome misalignment and production of aneuploidy gametes.

2) In mitosis, centrosomes nucleate astral microtubules. Oocytes lack astral microtubules and thus meiotic spindle positioning depends only on F-actin. In particular, it relies on the nucleation of a cortical actin thickening leading to a decrease in cortical tension. We used two different tools that nucleate de novo an actin thickening to artificially decrease cortical tension in mouse oocytes, creating extra-soft oocytes. Chromosome alignment is severely impaired in these extra-soft oocytes. It relies on myosin II deregulation since decreasing myosin II activity in extra-soft oocytes rescues chromosome alignment. Aberrant low cortical tension could thus generate aneuploidy in oocytes, contributing to the very high aneuploidy rate measured in female meiosis.

Keywords

Oocyte, meiosis I, microtubule, spindle assembly, chromosome alignment and segregation, spindle positioning, F-actin, cortical tension.